ABSTRACT

Title of Document: APPLICATIONS OF PHOTOINDUCED ELECTRON TRANSFER CHEMISTRY: PHOTOREMOVABLE PROTECTING GROUPS AND CARBON DIOXIDE CONVERSION

Derek Michael Denning, Doctor of Philosophy, 2016

Directed by: Professor Daniel E. Falvey
Department of Chemistry & Biochemistry

Traditional organic chemistry has long been dominated by ground state thermal reactions. The alternative to this is excited state chemistry, which uses light to drive chemical transformations. There is considerable interest in using this clean renewable energy source due to concerns surrounding the combustion byproducts associated with the consumption of fossil fuels. The work presented in this text will focus on the use of light (both ultraviolet and visible) for the following quantitative chemical transformations: (1) the release of compounds containing carboxylic acid and alcohol functional groups and (2) the conversion of carbon dioxide into other useable chemicals.

Chapters 1-3 will introduce and explore the use of photoremovable protecting groups (PPGs) for the spatiotemporal control of molecular concentrations. Two new PPGs are discussed, the 2,2,2-tribromoethoxy group for the protection of carboxylic acids and the 9-phenyl-9-tritylone group for the protection of alcohols. Fundamental interest in the factors that affect C–X bond breaking has driven the work presented in this text for

the release of carboxylic acid substrates. Product analysis from the UV photolysis of 2,2,2-tribromoethyl-(2′-phenylacetate) in various solvents results in the formation of H–atom abstraction products as well as the release of phenylacetic acid. The deprotection of alcohols is realized through the use of UV or visible light photolysis of 9-phenyl-9-tritylone ethers. Central to this study is the use of photoinduced electron transfer chemistry for the generation of ion diradicals capable of undergoing bond-breaking chemistry leading to the release of the alcohol substrates.

Chapters 4 and 5 will explore the use of *N*-heterocyclic carbenes (NHCs) as a catalyst for the photochemical reduction of carbon dioxide. Previous experiments have demonstrated that NHCs can add to CO_2 to form stable zwitterionic species known as *N*-heterocylic-2-carboxylates (NHC–CO_2). Work presented in this text illustrate that the stability of these species is highly dependent on solvent polarity, consistent with a lengthening of the imidazolium to carbon dioxide bond (C_{NHC}–C_{CO2}). Furthermore, these adducts interact with excited state electron donors resulting in the generation of ion diradicals capable of converting carbon dioxide into formic acid.

APPLICATIONS OF PHOTOINDUCED ELECTRON TRANSFER CHEMISTRY: PHOTOREMOVABLE PROTECTING GROUPS AND CARBON DIOXIDE CONVERSION

By

Derek Michael Denning

Dissertation submitted to the Faculty of the Graduate School of the
University of Maryland, College Park, in partial fulfillment
of the requirements for the degree of
Doctor of Philosophy
2016

Advisory Committee:
Professor Daniel Falvey, Chair
Professor Philip DeShong
Professor Neil Blough
Professor Jeffrey Davis
Professor Srinivasa Raghavan (Dean's representative)

DEDICATION

The research presented in this dissertation is dedicated to my family. My mother (Erin), father (Mike) and sister (Kara) have all supported me greatly throughout the years and this work would not have been possible without their support.

ACKNOWLEDGEMENTS

The work presented in this thesis would not have been possible without the assistance of Dr. Falvey over the years. I thank him immensely for the time and knowledgeable oversight that he has been willing to provide me while at the University of Maryland. Throughout the many research struggles that I have encountered, Dr. Falvey always kept a positive attitude and his reminder that “sometimes you have to throw the darts and then draw the target” provided me with the fuel to push on.

I am grateful to my committee members, Dr. Blough, Dr. Davis, Dr. DeShong and Dr. Raghavan for their time and support as well as the many faculty members in the department for mentoring me throughout my teaching here at the university. Specifically, Dr. Montague-Smith for his oversight in the Graduate Assistance in Areas of National Need (GAANN) fellowship from the United States Department of Education as well as Dr. Dixon and Dr. Steffek for their help in becoming an effective teaching assistant.

I am indebted to my current and former colleagues of the Falvey lab for their help with chemistry and all the proofreading I made them do over the years. I also wish to acknowledge them for creating a great working atmosphere and just generally being wonderful people. Specifically Dr. Raffaele Perrotta, Romina Heymann, Steven Wolf, Matthew Thum, and Katie Brennan. A big thanks to the current and former undergraduates that have worked with me over the years, David Kunsberg, Lok-Man Yeung, Ashlee La, Nichole Pedowitz, Allison Kipping, Tara Michael and Kevin Hill-Byrne.

Thank you to the faculty in the analytical services section in the chemistry department, especially Dr. Yue Li, Dr. Yiu-Fai Lam, and Dr. Yinde Wang for keeping the

NMR and mass spectrometry facilities in great condition and running various samples for me. Finally, thank you to all my friends and family for your support through the years. I am very lucky to have such wonderful people in my life.

TABLE OF CONTENTS

LIST OF TABLES

Chapter 2. Photodeprotection of Carboxylic Acids by Direct Irradiation of the 2,2,2-Tribromoethoxy Group

Chapter 3. Photodeprotection of Alcohols Using UV or Visible Light Photoinduced Electron Transfer to 9-Phenyl-9-Tritylone Ethers

Chapter 4. Solvent-Dependent Stability of 1,3-Dimethylimidazolium-2-Carboxylate

Chapter 5. Photochemical Reduction of Carbon Dioxide Using 1,3-Dimethylimidazolylidene

Chapter 6. Supporting Information

LIST OF FIGURES

Chapter 1. Photoremovable Protecting Groups

Chapter 2. Photodeprotection of Carboxylic Acids by Direct Irradiation of the 2,2,2-Tribromoethoxy Group

Chapter 3. Photodeprotection of Alcohols Using UV or Visible Light Photoinduced Electron Transfer to 9-Phenyl-9-Tritylone Ethers

Chapter 4. Solvent-Dependent Stability of 1,3-Dimethylimidazolium-2-Carboxylate

Chapter 5. Photochemical Reduction of Carbon Dioxide Using 1,3-Dimethylimidazolylidene

Chapter 6. Supporting Information

LIST OF SCHEMES

Chapter 1. Photoremovable Protecting Groups

Chapter 2. Photodeprotection of Carboxylic Acids by Direct Irradiation of the 2,2,2-Tribromoethoxy Group

Chapter 3. Photodeprotection of Alcohols Using UV or Visible Light Photoinduced Electron Transfer to 9-Phenyl-9-Tritylone Ethers

Chapter 4. Solvent-Dependent Stability of 1,3-Dimethylimidazolium-2-Carboxylate

Chapter 5. Photochemical Reduction of Carbon Dioxide Using 1,3-Dimethylimidazolylidene

LIST OF ABBREVIATIONS

9,10-DBA	9,10-Dibromoanthracene
AcOH	Acetic acid
ATP	Adenosine triphosphate
ATR	Attenuated total reflectance
B3LYP	Becke, three-parameter, Lee-Yang-Parr functional
BET	Back electron transfer
BDE	Bond dissociation energy
BHT	Butylated hydroxytoluene
BODIPY	Boron-dipyrromethene (fluorescent dyes)
CaH_2	Calcium hydride
CCS	Carbon capture and storage
CCU	Carbon capture and utilization
CH_2Cl_2	Dichloromethane
CH_3CN (MeCN)	Acetonitrile
CH_3OH (MeOH)	Methanol
CIDNP	Chemically induced dynamic nuclear polarization
CIP	Contact ion pair
ClAc	Chloroacetyl group
CO_2	Carbon dioxide
CPCM	Conductor-like polarization continuum model
DART	Direct analysis in real time
DBU	1,8-Diazabicyclo[5.4.0]undec-7-ene
DFT	Density functional theory
DMA	*N,N*-Dimethylaniline
DNA	Deoxyribonucleic acid
E_{00}	Excited state energy
$E_{ox}*$	Excited state oxidation potential
E_{ox}	Oxidation potential
EPR	Electron paramagnetic resonance
E_{red}	Reduction potential
ESI-TOF	Electron spray ionization time of flight
$E_T(30)$	Solvent polarity parameter
EtOH	Ethanol
FID	Flame ionization detection
FT-IR	Fourier transform infrared spectroscopy
GC-MS	Gas chromatography and mass spectrometry
HBr	Hydrobromic acid
HCl	Hydrochloric acid
HPLC	High pressure liquid chromatography
HRMS	High resolution mass spectrometry
IEF-PCM	Integral equation formalism polarizable continuum model
ISC	Intersystem crossing
LED	Light emitting diode
Lev	Levulinyl group

LFP	Laser flash photolysis
$MgSO_4$	Magnesium sulfate
MOF	Metal organic framework
$NaHCO_3$	Sodium bicarbonate
NAP	*N*-Alkylpicolinium group
Nd:YAG	Neodymium-doped yttrium aluminium garnet (laser)
NHC	*N*-Heterocyclic carbene
NHC-CO_2	*N*-Heterocyclic-2-carboxylate
NHE	Normal hydrogen electrode
NMR	Nuclear magnetic resonance
PCM	Polarization continuum model
PET	Photoinduced electron transfer
PMT	Photomultiplier tube
PMB	*p*-Methoxybenzyl group
PPG	Photoremovable protecting group
PTO	Phenyl tritylone group
RTIL	Room temperature ionic liquid
SCE	Saturated calomel electrode
SMD	Solvation model based on density
SSIP	Solvent separated ion pairs
TBAF	Tetrabutyl ammonium fluoride
TBDMS	*tert*-Butyldimethylsiltyl group
TBDPS	*tert*-Butyldiphenyldsilyl group
TEA	Triethylamine
TFA	Trifluoroacetic acid
THF	Tetrahydrofuran
TIPS	Triisopropylsilyl group
TMB	*N,N,N’,N’*-Tetramethylbenzidine
TMS	Trimethylsilyl group
TPA	Triphenylamine
UV	Ultraviolet
Vis	Visible

CHAPTER 1. PHOTOREMOVABLE PROTECTIONG GROUPS

1.1 Introduction to Conventional Protecting Groups

The synthesis of highly complex molecules requires the ability to selectively modify functional groups on a molecular species. While the overall goal of any complicated synthetic endeavor is to minimize the number of reaction steps and maximize yields, it is important to consider the reactivity of the functional groups within a molecule as to not inhibit further reactivity. Thus, deactivation of functional groups is commonly used before performing additional synthetic transformations. Figure 1.1 shows a general example of how this can be achieved. Such directed strategies have made use of protecting groups for the successful lessening of the reactivity for the functional group. To do this, the protecting group is applied to mask its reactivity, allowing the alteration of other moieties on the molecule. Once completed, the protecting group can be removed, rendering the now unblocked functional group able to participate in further chemical modifications.

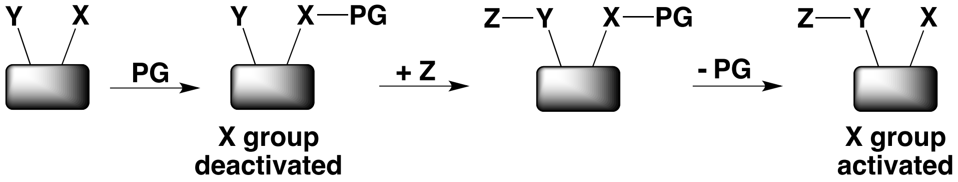

Figure 1.1 Use of a protecting group (PG) to render a substrate “inactive” followed by release from the PG to render the substrate “active.”

An example of this concept is illustrated in Scheme 1.1. Here, the reactive carboxylic acid group in *p*-bromobenzoic acid **1** is deactivated by the formation of an oxazoline **2**. In doing this, the acidic proton of the carboxylic acid is removed allowing the inclusion of strongly basic organometallic reagents that would otherwise be quelled by the reactivity of the carboxylic acid. The protection of the carboxylic acid allows for the formation of a Grignard reagent and subsequent addition to styrene oxide generating **3**. Deprotection of the oxazoline ring is performed under acidic and subsequent basic conditions generating back the carboxylic acid and liberating the new *para*-substituted benzoic acid **4**.[1,2]

Scheme 1.1 The use of a protecting group for a carboxylic acid in organic synthesis.

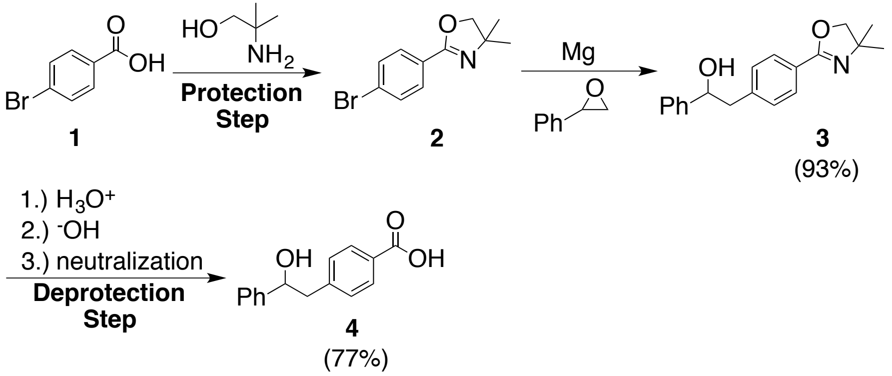

Protecting group chemistry has been such an integral part of an organic chemists toolbox that there have been entire books dedicated to this field.[3] Numerous protecting groups have been developed and successfully applied; however choosing the appropriate blocking group requires careful consideration. Among others, there are four general criteria that a protecting group should follow: (1) The addition of the group should be simple and high yielding; (2) It should remain unreactive throughout the duration of the chemical transformations; (3) The removal of the protecting group is quantitative with the reagents used being unreactive to other sites on the molecule and (4) Byproducts generated in the deprotection reaction should be unreactive and easily removed. Of particular emphasis for the use of protecting groups is the selective deprotection when multiple blocking groups are applied.[4] Thus, two terms used to describe different approaches to this issue are orthogonal stability and modulated lability, illustrated in Figure 1.2.

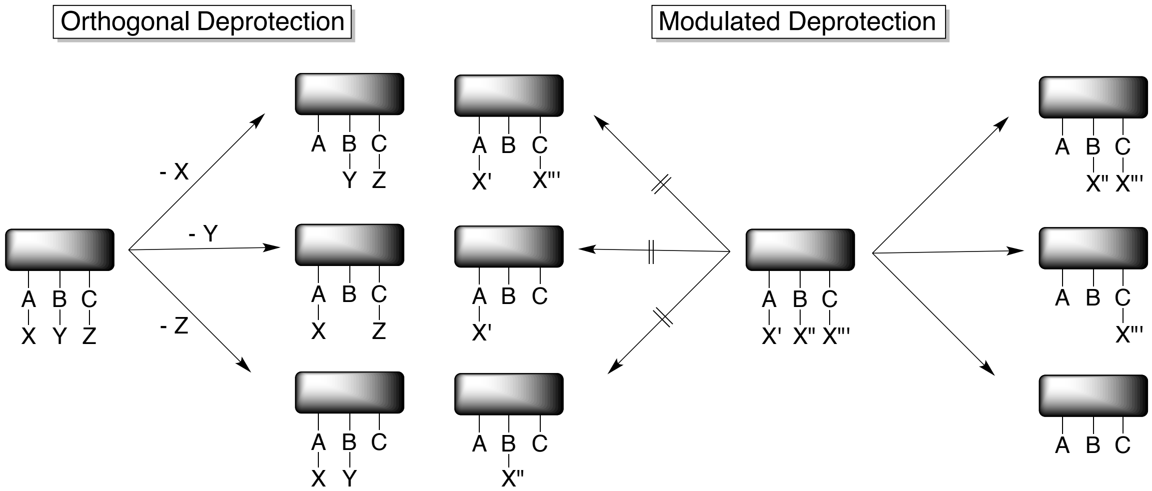

Figure 1.2 The use of orthogonal stability and modulated lability protecting group strategies.

Orthogonal stability describes protecting groups that can be cleaved under different reaction conditions without affecting the other blocking groups. An example of this is the three groups A, B and C that have protecting groups X, Y and Z of which could be removed under acidic, basic and oxidative conditions, respectively. The sensitivity of one group towards a certain chemical environment, leaving the other two groups intact demonstrates orthogonal stability and selective deprotection. In contrast to this is modulated lability where protecting groups are removed under the same reaction conditions but the degree of deprotection is related to the sensitivity of the groups to the removal conditions. While protecting groups X', X" and X"' could be removed under basic conditions, the sensitivity of the groups decrease from X' to X"'. Therefore the removal of X" or X"' cannot be completed without the deprotection of the most labile group, X'.

Successful implementation of the two aforementioned deprotection strategies can be found in the literature. An example of modulated lability is shown in Scheme 1.2, where Danishefsky et al.[5] completed the synthesis of immunosuppressant rapamycin **6** through the deprotection of various silyl ethers. The trimethylsilyl ether (TMS) and *tert*-butyldimethylsiltyl ether (TBDMS) groups on compound **5** are both readily cleaved by the addition of tetrabutylammonium fluoride (TBAF) in the presence of acetic acid (AcOH). The more stable triisopropyl silyl ether (TIPS) can be removed by the addition of HF/pyridine after an oxidation of the secondary alcohol recovered from the cleavage of the TBDMS group and subsequent ring closure.

Scheme 1.2 Modulated deprotection using silyl ethers in the synthesis of Rapamycin.

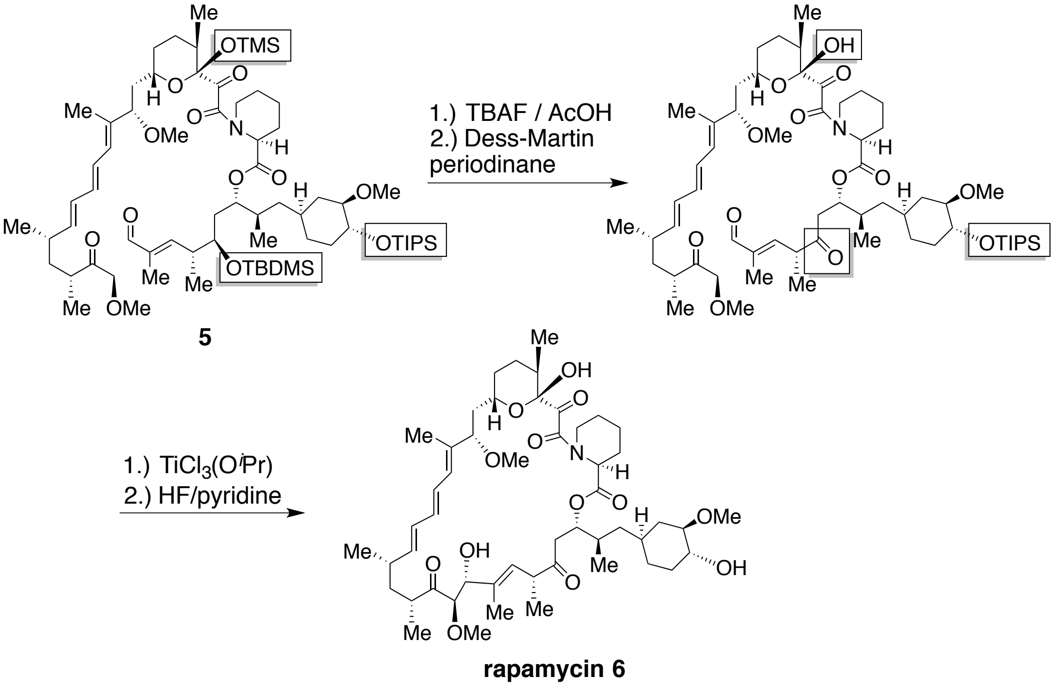

Another example of modulated lability can be found in Scheme 1.3. Here, Ellison and coworkers[6] used the reactivity differences of cyclic and acyclic acetals under acidic conditions. Acyclic acetals are known to revert back to the respective carbonyl species under milder acidic environments in comparison to their cyclic counterparts. Compound **7** was treated with dilute trifluoroacetic acid (TFA), converting the dimethoxy acetal to the aldehyde, leaving the cyclic acetal intact. The authors were then able to modify the deprotected aldehyde leading to the prostaglandin precursor **8**. The variance in reactivity of acetal protecting groups when subjected to acidic environments was successfully applied to the synthesis of a physiologically active lipid precursor.

Scheme 1.3 Selective deprotection of an acyclic acetal in the synthesis of a prostaglandin precursor

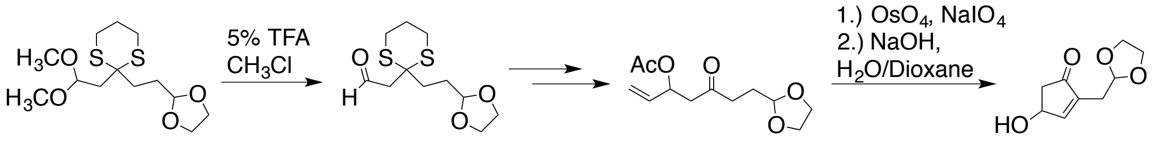

7 **8**

Scheme 1.4 Orthogonal deprotection of a monosaccharide for the synthesis of an oligosaccharide chemical library.

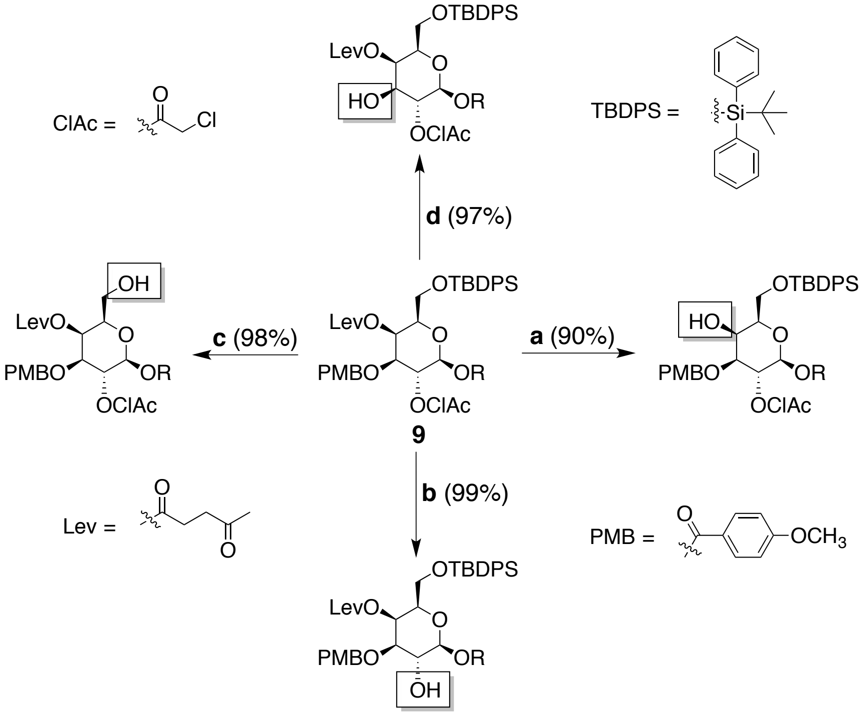

Reagents and conditions: (**a**) NH_2NH_2/AcOH, THF/MeOH (10:1); (**b**) $NaHCO_3$, MeOH/H2O (5:1), 60 °C; (**c**) HF-pyridine, HOAc/THF (1:4); (**d**) trifluoroacetic acid, CH_2Cl_2, -20 °C.

Employment of an orthogonal based deprotection is shown in Scheme 1.4. Monosaccharide building block **9** was synthesized with four different protecting groups, of which can be independently deprotected under different reactions conditions. The chloroacetyl (ClAc), *p*-methoxybenzyl (PMB), levulinyl (Lev) and *tert*-butyldiphenyldsilyl (TBDPS) groups can be deprotected under sodium bicarbonate, TFA, hydrazine and HF/pyridine conditions respectively. Zhang and coworkers[7] were able to use this orthogonal deprotection scheme for the construction of an oligosaccharide library to screen for potential binders to lectins and antibodies.

Selective deprotection in an orthogonal system is not just limited to chemical based strategies. In fact, photochemical orthogonal protecting groups, where specific wavelengths of light can be used to deprotect functional groups have also seen positive response throughout the literature. Though this topic will be discussed in further detail in the following sections, an example of this can be seen in Scheme 1.5. Here, Bochet[8] was able to synthesize a mixed diester **10** having two photochemically active protecting groups, dimethoxybenzoin and an *o*-nitrobenzyl derivative at each terminus of the molecule. Irradiation of this molecule using 254 nm light afforded the deprotection of the *o*-nitrobenzyl group and a 92% yield of the diester **11**. Alternatively, irradiation of **10** at 420 nm afforded cleavage of the dimethoxybenzoin derivative and a 70% yield of diester **12**. This subclass of protecting groups is especially attractive and will drive the narration in the following sections due to the advantages of using light as a chemical reagent.

Scheme 1.5 Wavelength dependent deprotection of an *o*-nitroaryl and dimethoxybenzoin groups.

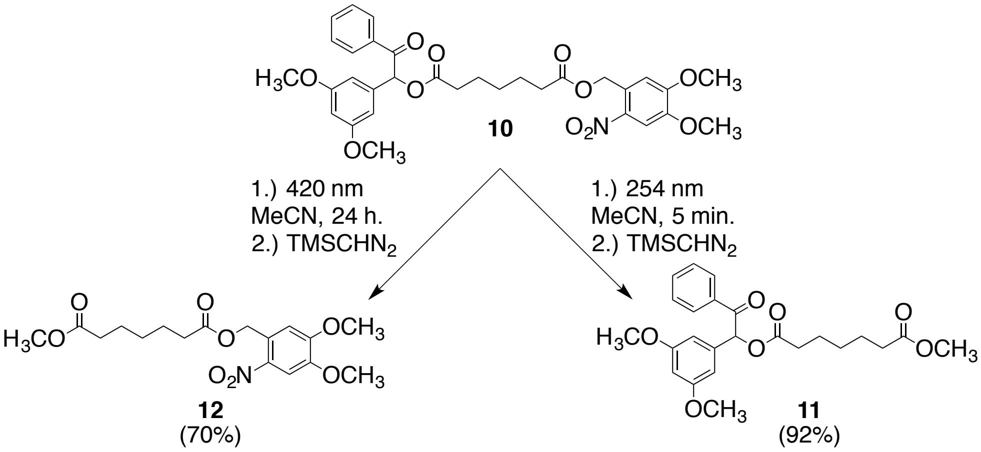

1.2 Photoremovable Protecting Groups

In the preceding section, conventional protecting groups and examples of their use in the literature was presented. These types of protecting groups are removed through the addition of a chemical reagent to a reaction solution such as an acid or a base. Photoremovable protecting groups (PPGs) differ from conventional groups in that they are removed by the addition of light.[9] PPGs have the advantage over conventional protecting groups by providing spatial and temporal control over the deprotection step. Spatial control refers to the location in which the light can be applied and thus unblocking can occur. This can be done broadly by using a flood lamp or site specific by using a focused light source like a laser. The use of masks, to block light from reaching the substrate, can also be used for spatial control and is prominently used in photolithography.[10] Temporal control refers to the precise time in which deprotection can occur, done by turning the lamp source on and off. The addition of an acid or base for the deprotection in conventional protecting groups is much more difficult for such temporal control.

The chemical library of published PPGs has grown rapidly over the past 15 years and has provided chemists many options for the various applications they wish to use it for. When designing a new photoremovable protecting group there are a few criteria to consider that would allow broad usage of the new group.[9,11,12] First, the new protecting group should be sensitive to light and preferably light >300 nm. The lower energy wavelengths help improve the selectivity of the PPG as many molecules contain aromatic rings or carbonyl moieties capable of absorbing light up to 300 nm. Additionally, if the protecting group can absorb into the visible light region this can encourage its use for possible biological applications as it will reduce the need for harmful UV rays that can damage cells and tissue. Second, the PPG should be soluble, stable and unreactive prior to photolysis in the media it is to be used. Third, the byproducts generated post photolysis should be transparent at the wavelength used to initiate deprotection. If there is competing light absorption by the PPG and the undesirable byproducts of the photolysis, this will greatly diminish the efficiency of the deprotection process. Lastly, deprotection should be quantitative with a rapid release rate.

The first successful execution of a photoremovable protecting group came in 1962 when Barltrop and Schofield[13] demonstrated the release of glycine from a benzyloxycarbonyl group upon UV irradiation. The proposed deprotection mechanism is outlined in Scheme 1.6. Benzyloxycarbonyl **13** is irradiated with UV light leading to excited state heterolysis of the benzylic C–O bond generating a benzylic carbocation and a carbamate dianion. Decarboxylation of the latter leads to the free glycine in 75% yield.

Scheme 1.6 Photochemical deprotection of glycine as reported by Barltrop and Schofield.

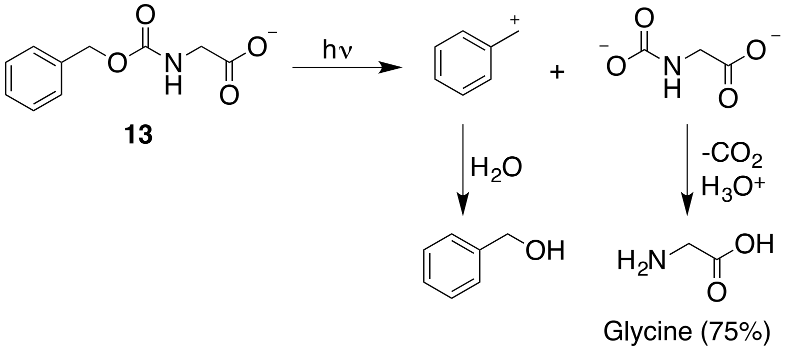

Since their first introduction the 1960's, the number of photoremovable protecting groups has dramatically increased to a level where it would be impractical to discuss them all in depth. However, some of the more foundational PPGs and some recently reported ones that permit visible light deprotection would allow for a better understanding of the mechanistic aspects of photodeprotection and thus will be covered in brief in the following sections. For a more comprehensive review of PPGs and some of their applications, see a recent review from Klán et al.[9]

1.3 *o*-Nitrobenzyl Group

Building upon their seminal work in the photodeprotection of glycine, Barltrop, Plant and Schofield introduced the *o*-nitrobenzyl group.[14] In their initial report they demonstrated the release of benzoic acid from *o*-nitrobenzyl ester **14** (Scheme 1.7, A). The yield afforded from this deprotection system was a measly 17%, though the authors attributed such poor release to the formation of azobenzene **15** from the conversion of photoproduct 2-nitrosobenzaldehyde. The inefficiency of the release is the result of the azobenzene derivative competing for the UV light with the desired *o*-nitrobenzyl protected ester. To circumvent this problem, substitution at the benzylic carbon inhibited the formation of the undesired azobenzene photoproduct and led to enhanced deprotection yields, shown in Scheme 1.7, B with the formation of phenylacetic acid in 87% yield.

Scheme 1.7 *o*-Nitrobenzyl PPG in the deprotection of carboxylic acids.

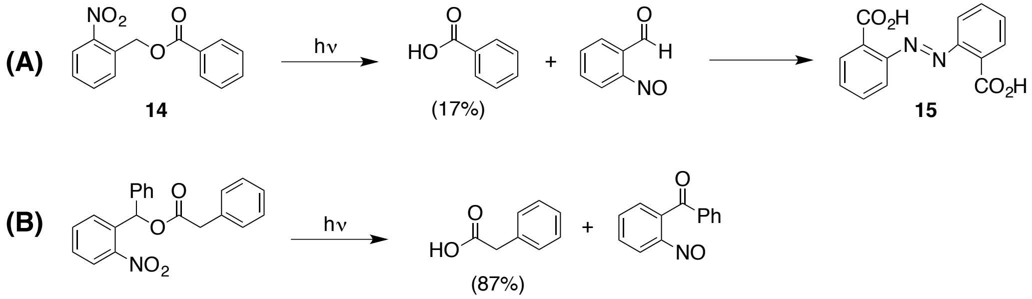

In a subsequent study, Kaplan and coworkers[15] broadened the interest of PPG chemistry when they successfully demonstrated the release of ATP. Introducing the term “caged” ATP to describe the synthesis of bound ATP to a 1-(2-nitrophenyl)ethyl group;

the authors were able to show up to an 80% release of ATP using 340 nm light in under 60 seconds. Denoting it the "uncaging" of ATP, their photolysis reactions were done in an aqueous environment and proceeded with a quantum efficiency of 0.58. Taking this process a step further, the authors were able to demonstrate the utility of this photodeprotection process in a physiological environment. The enzyme responsible for sodium and potassium transport through cell walls (Na,K-ATPase) was used as a model to test for the release of ATP. Caged ATP exhibits no hydrolysis of the terminal phosphate group of ATP. However, when irradiated the ATP is liberated from the *o*-nitrobenzyl group, freeing the terminal phosphate group and activating the Na,K-ATPase enzyme. Hydrolysis of the phosphate group could then be monitored and thus allowing for quantification of the deprotected ATP. The idea that PPGs could help facilitate studies in biological systems, expanded interest outside of traditional synthetic organic chemistry.

Scheme 1.8 Proposed mechanism for the deprotection of the *o*-nitrobenzyl PPG.

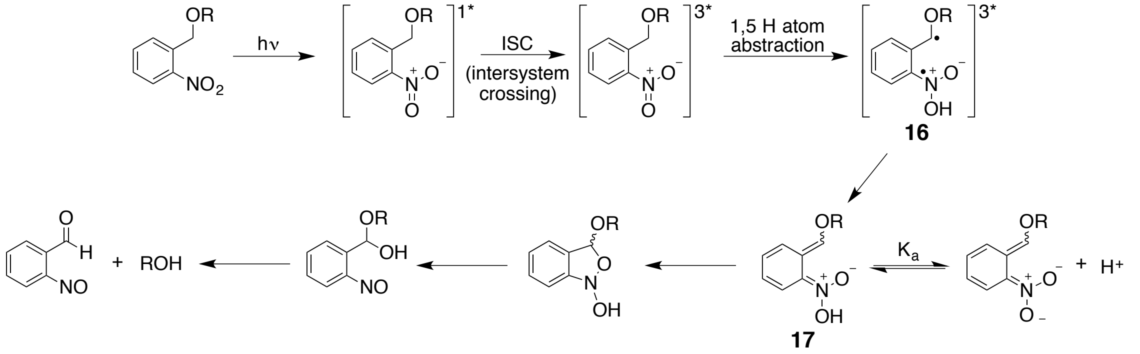

The proposed mechanism for deprotection from the *o*-nitrobenzyl group can be found in Scheme 1.8.[16-18] Excitation of the *o*-nitrobenzyl group affords the excited singlet state, which undergoes intersystem crossing to the longer-lived, lower energy triplet state. 1,5-Intramolecular hydrogen atom transfer generates excited state diradical **16**, leading to the formation of *aci*-nitro intermediate **17** ($\lambda_{max} \approx 400$ nm). These *aci*-nitro intermediates have decay rates of $10^2 – 10^4$ s^{-1} and free the protected group via cyclization of the neutral *aci*-compound and subsequent hydrolysis of the hemiacetal.

Advantages of the *o*-nitrobenzyl PPG include the ease of use, as many *o*-nitrobenzyl derivatives are commercially available and can be easily converted into their respective esters. Deprotection of this group is also favorable as >320 nm light can be used allowing for the use of normal glassware. Disadvantages of this protecting group include the aforementioned photolysis byproducts, which compete for light absorption and can lead to non-productive photochemical processes. The slow release rates from the *o*-nitrobenzyl group due to the rate-determining hydrolysis of the hemi-acetal step can make this group challenging to use for fast biological processes.

1.4 Phenacyl Group

The photochemistry of arylcarbonyl compounds have been extensively studied[19] and seen prominent use as photoremovable protecting groups, in particular the phenacyl group. The synthetic ease, commercial availability and thermal stability make them attractive from a practical standpoint. Fast internal conversion from higher excited singlet states to the S_1 state (~100 – 260 fs),[9,20,21] fast ($>10^{10}$ s^{-1}) intersystem crossing, and high quantum yield (~1 for acetophenone) for triplet formation lends to a longer excited state lifetime than the singlet state allowing for competing photochemical processes other than relaxation back to the ground state.[22-24]

Scheme 1.9 Photodeprotection of phenacyl ester proposed by Sheehan and Umezawa.[25]

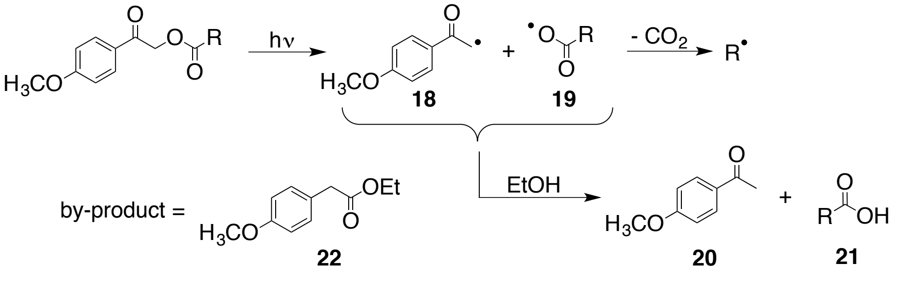

Sheehan and Umezawa demonstrated that the phenacyl group could be used for the photochemical deprotection of carboxylic acids in 1973.[25] UV photolysis of *p*-methoxybenzoate in ethanol afforded benzoic acid in 96% yield. However, the same deprotection was stymied when done in benzene. This, in part led the authors to propose the mechanism shown in Scheme 1.9. Excited state homolysis of the alpha C–O bond leading to the two product radicals **18** and **19**. In the presence of good hydrogen donors like that of 1,4-dioxane and ethanol in comparison to benzene, products **20** and **21** could be afforded. Some earlier studies by Anderson and Reese,[26] while not explicitly studying deprotection of functional groups, looked at the photochemistry of substituted phenacyl chlorides and proposed a "Favorskii-like" rearrangement to help explain byproduct **22**. Subsequent studies by Givens et al.[27] on the photorelease of *p*-methoxybenzoate esters in *tert*-butyl alcohol and methanol confirmed reports by Anderson and Reese on the formation of rearranged esters such as **22**. The authors also noted a solvent isotope effect when the photolyses were carried out in CD_3OD in comparison to CH_3OH and CH_3OD suggesting hydrogen atom transfer was a rate-limiting step. Further evidence for a rearrangement process came from the observation of a lower yield of hydrogen atom abstraction product when *tert*-butyl alcohol was used instead of methanol.

The mechanism of deprotection for *p*-substituted benzoate esters has long perplexed chemists but some transient absorption studies by Givens and coworkers[28,29] in 2008 and further ring size considerations[30] in 2013 helped shed new light on the current understanding of the phenacyl group deprotection. The improved proposed mechanism is outlined in Scheme 1.10. Excitation of **23** lends to the excited singlet state, which undergoes intersystem crossing to the triplet state. Loss of the leaving group and the phenolic hydrogen atom leads to triplet state biradical **24**, which ring closes to the Favorskii spirodiketone intermediate **25**. While there has been no direct spectroscopic evidence supporting the formation of this intermediate, molecular calculations and product analysis support the notion of its presence. Loss of carbon monoxide from the spiro-intermediate gives quinone methide **26**, which has been observed by laser flash photolysis. Subsequent addition of water yields alcohol **27**.

Scheme 1.10 Deprotection of the phenacyl group based on transient absorption analysis.

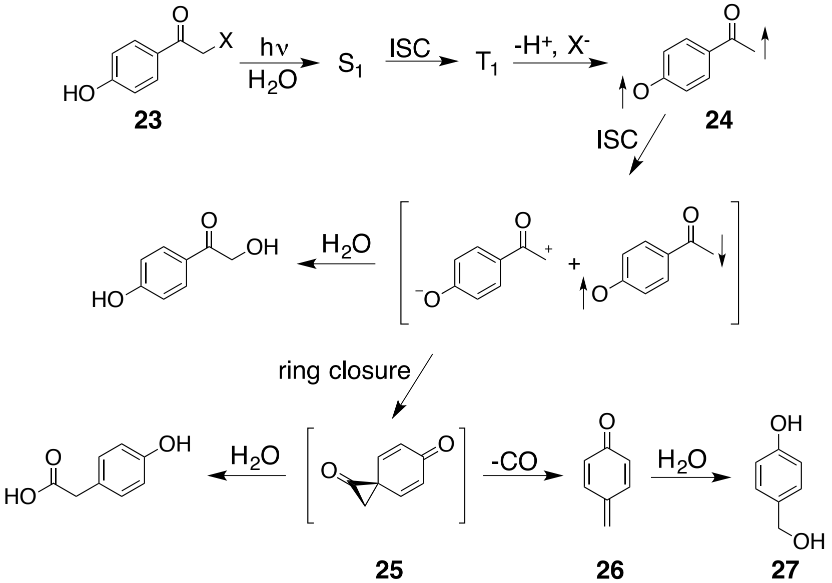

1.5 Coumarinyl Group

Givens and coworkers first introduced the coumarinyl group as a PPG in 1984 in their successful uncaging of phosphate esters.[31] Building upon Zimmerman's "*meta effect"*[32,33] for the photochemistry of arylmethyl groups where electron donating substituents in the *meta* position favor bond heterolysis (Scheme 1.11), the coumarinyl group is an extension of this concept demonstrating benzylic C–O bond heterolysis. Some of the attractive features of this group are the availability to use longer wavelengths (>350 nm) as well as the fast release rates, attaining up to 2 x 10^{10} s^{-1}.[34]

The mechanism for the deprotection of functional groups from the coumarinyl PPG is shown in Scheme 1.11. Photoheterolysis of the benzylic C–O bond arises from the singlet excited state of **28** and competes with non-radiative and fluorescence deactivation pathways. Contact ion pair of the resulting cation and anion can recombine in a non-productive manner, though if solvent separated, solvent and/or another nucleophile can add to the coumarinyl cation and prevent recombination, affording the deprotected functional group. As seen with the *o*-nitrobenzyl and phenacyl protecting groups, weak bases such as carboxylates and phosphates have seen the most use in the literature. Direct release of higher energy products like alcohols and amines can be done, however they are usually employed through a carbonate or carbamate ester linkage. However, because of this, the release is pH dependent and the decarboxylation step can yield slow deprotection times ($k_{\text{-CO2}} = 10^{-3}\ s^{-1}$).[35,36]

Scheme 1.11 Photochemical deprotection of coumarinyl groups.

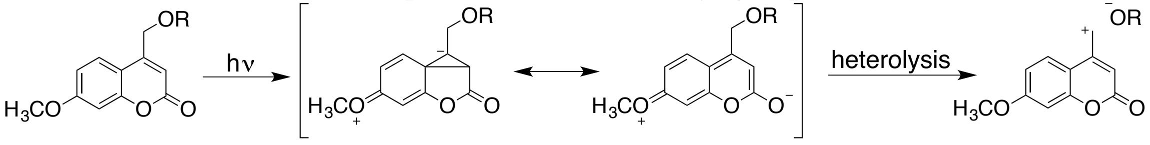

28

Kiso and coworkers[37] reported the photochemical release of paclitaxel (a drug used for the treatment of various cancers) as illustrated in Scheme 1.12. A prodrug of paclitaxel **29**, which has a coumarinyl derivative in conjugation with an amino acid moiety, is irradiated with visible light (430 nm). Deprotection of the caged drug involves the release of the carbamate linker followed by thermal decarboxylation and O–N acyl migration to give paclitaxel **31** in yields that varied between 40–70% (Scheme 1.12). The authors note that the half-life for the intramolecular acyl transfer is 15.1 minutes, a value which should be short enough to prevent diffusion of **30** from the photoirradiated site before the parent drug has been released.

Scheme 1.12 Photochemical release of paclitaxel from a coumarinyl PPG.

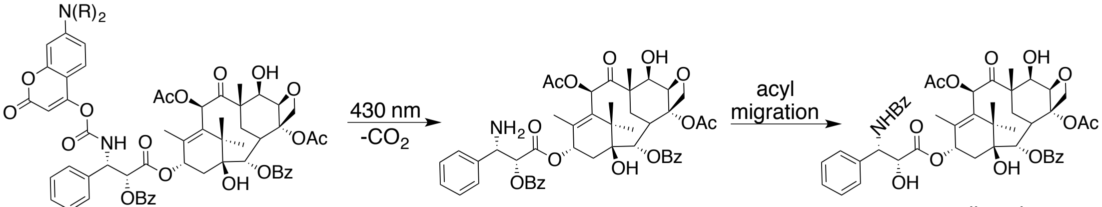

isotaxel

paclitaxel

29 **30** **31**

1.6 Visible Light Absorbing PPGs

In the previous sections three prominent photoremovable protecting groups were discussed. One of the limitations for these groups is that they mostly absorb ultraviolet light (<400 nm), and while this is generally not an issue for laboratories equipped with photolysis apparatuses to accommodate UV irradiation, one of the main goals in using light to drive chemical reactions is to use cheap and widely available visible light for deprotection. Not only can this help reduce the need for costly UV lamp sources, it also helps expand biological applications of the PPG as lower energy wavelengths have a greater ability to penetrate tissue.

Some recent reports of visible light deprotection include a report by Winter and coworkers[38] that use *meso*-substituted BODIPY dyes for the deprotection of acetic acid. The deprotection can occur under green light (>500 nm) and as the authors suggest, proceeds via photoheterolysis of the C–O bond shown in Scheme 1.13. Some of the advantages of this PPG include the facile synthesis, their studied biocompatibility and high extinction coefficients in the visible region. The authors demonstrated the appeal of the BODIPY derived PPG for biological systems by incubating a 2,4-dinitrobenzoic ester with Drosophila S2 cells. Deprotection of 2,4-dinitrobenzoic acid from the BODIPY dye (a known quencher of BODIPY dyes) leads to an increase in the fluorescence intensity of the dye as was monitored in the cells. After 1 hour of continuous 500 nm light 92% of the cells remained viable, in good agreement with the compatibility of this PPG in biological systems.

Scheme 1.13 Visible light deprotection using (A) BODIPY and (B) fluorescein derivatives.

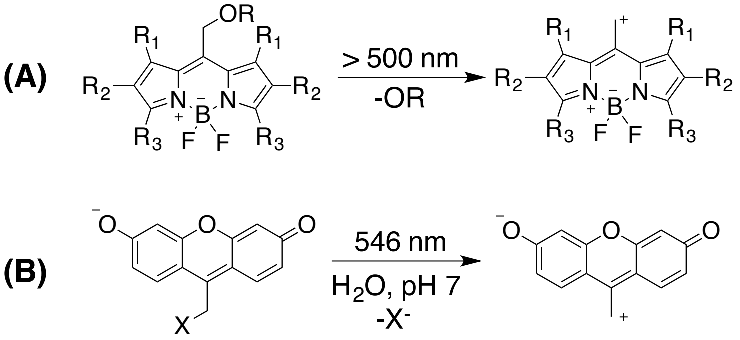

Wirz and coworkers demonstrated similar visible light deprotection using fluorescein analogues as shown in Scheme 1.13.[39] Here, they were able to use green light (λ_{max} = 546 nm) for the release of carboxylates and phosphates of up to 90% yield. Another advantage of this group is the ability to perform the photodeprotection in aqueous phosphate buffer solutions with a pH around 7. However, the multistep synthesis of the analogs (7 steps) and the modest yields (20–25%) of the six-fluorescein derivatives reported by these authors can be viewed as a disadvantage.

Scheme 1.14 The use of near infrared light for the release of caged phenolic compounds

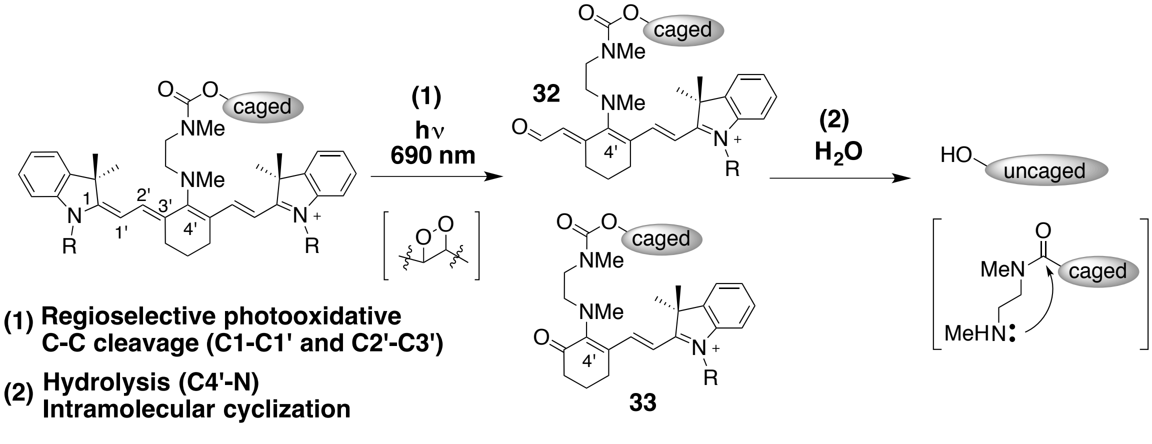

A visible/near IR (690 nm) photochemical uncaging process was recently reported by Schnermann et al.,[40] where small molecule phenolic compounds were released in moderate yields by a photooxidative cleavage and subsequent intramolecular ring cyclization reaction (Scheme 1.14). The protecting group is based upon the C4′-dialkylamine-substituted variant of the heptamethine cyanine fluorophore scaffold where 690 nm irradiation using a commercial LED light source leads to photooxidation of the C1–C1' and C2'–C3' bonds outlined in the scheme above. Formation of compound **32** and **33** undergo hydrolysis of the C4'–N bond and intramolecular cyclization leads to release of the phenolic alcohols. The biocompatibility of this group is promising as deprotection occurs in aqueous media at a pH of 7.5 coupled with the near IR low energy wavelengths. The commercial availability and advantageous cost of LED light sources is an extremely attractive prospect of this protecting group as it allows for wide applicability across research groups. While the deprotection of phenolic derivatives relies on a thermal intramolecular cyclization for release, and thus should provide slow liberation rates, the authors note that the rates are comparable to similar single photon photochemical uncaging methods.

1.7 Conclusions and Research Goals

In this chapter we have introduced what protecting groups are and some of the applications they are used for. Particular emphasis has been placed on photoremovable protecting groups, which use light as a means to uncage/deprotect a functional group (carboxylic acid, phosphoric acid, alcohol, etc.). There are several advantages of PPGs over conventional protecting groups including the spatiotemporal selectivity and the low energy wavelengths that can be used for deprotection. A few widely employed PPGs were discussed including but not limited to the *o*-nitrobenzyl, phenacyl and coumarinyl groups, all of which are primarily used in parallel with UV light (<400) as well as a few visible light absorbing PPGs which could be deprotected using green or near IR light.

Discussed in brief were the mechanisms of deprotection for the aforementioned protecting groups, all of which describe interesting excited state bond breaking and rearrangements leading to the release of the protected substrate. These protecting groups can be described as direct releasable protecting groups, in that the light absorbing chromophore is inherent to the protected substrate. Therefore, the deprotection process primarily follows first order kinetics unless for example a thermal process like solvent hydrolysis is integral in freeing the substrate. Due to this, wavelength tunability for deprotection is limited to chromophore modification. However in doing this, structural modification of the PPG can alter release rates and efficiency. Thus, being able to vary the wavelength used for deprotection while not altering the efficiency of the releasing process is an attractive prospect for photoremovable protecting groups.

In the succeeding chapters and sections, along with direct deprotection, emphasis will be placed on photoinduced electron transfer (PET) chemistry. It will be demonstrated that not only can functional groups be released by UV light using a chromophore fastened to the functional group, but also through using an external donor and/or acceptor for both UV and visible light deprotection systems. This, in principle allows for optimizing both the deprotection and the light absorbing processes allowing for broad spectral PPG use. The discovery of two new photoremovable protecting group will be discussed in the following two chapters.

CHAPTER 2. PHOTODEPROTECTION OF CARBOXYLIC ACIDS BY DIRECT IRRADIATION OF THE 2,2,2-TRIBROMOETHOXY GROUP

2.1 Introduction and Background on the 2,2,2-Trihaloethoxy Group

Organohalogen compounds have attracted considerable interest over the years particularly attributed to the photochemistry of these compounds. Halogenated compounds have been used in refrigerants, flame retardants, pesticides, and other products.[1-3] However, concerns over the environmental degradation pathways of these species have motivated mechanistic studies focused on identifying products resulting from the absorption of ultraviolet light. Organohalides have also been studied for use as free radical photoinitiators[4] as well as photoacid generators.[5-7] Photoinitiators are classified as compounds that, upon absorbing light, produce reactive radical or cationic intermediates capable of initiating a chain polymerization reaction of unsaturated monomers. Among the earliest studied photoinitiators are α-halogenated acetophenones such as 1-chloroacetophenone and desyl chloride that release chlorine atom upon irradiation. McCloskey and Bond demonstrated the use of these halogen containing compounds in the polymerization of vinyl monomers like methyl methacrylate in 1955 (Figure 2.1).[8]

$$\mathrm{R{-}X} \xrightarrow{h\nu} \mathrm{R}^{\bullet} + \mathrm{X}^{\bullet} \ \text{or} \ \mathrm{R}^{+} + \mathrm{X}^{-}$$

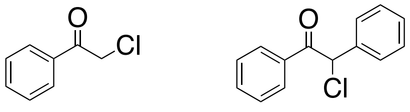

1-chloroacetophenone desyl chloride

Figure 2.1 Formation of reactive radical species upon the absorption of light and two early studied organohalogen photoinitiators.

Photoacid generators have seen use in the production of photoresists that are used industrially for processes like photoengraving and photolithography. Among compounds used are organobrominated species like *trans*-l0,ll-dibromodibenzosuberon **34** as studied by Gannon and McGimpsey.[5] Here, homolysis of a C–Br bond leading to the generation of a bromine atom does not induce polymerization of a monomer, but instead participates in hydrogen atom transfer from a donor in solution generating hydrobromic acid. Unlike dibromoethane which is known to be an efficient photoacid generator, compound **34** is able to absorb light at much higher wavelengths (300–400 nm) lending to its appeal. The mechanism of this process and the formation of short-lived intermediates was probed by laser flash photolysis (LFP). This is a technique that uses spectroscopy in conjunction with a laser pulse to observe short-lived intermediates (this technique will be further assessed in chapter 3). Laser excitation of **34** at 308 nm leads to C–Br homolysis and generation of a bromine atom. Subsequent thermal elimination of another bromine atom leads to conjugated ketone **35** and formation of two equivalents of bromine atoms. The bromine atom can be scavenged by benzene to give a *π*-complex (λ ≈ 560 nm) or bromide in acetonitrile to give bromine radical anion (λ ≈ 360 nm). The generation of HBr can be accomplished at low flux pulsed laser excitation in the presence of a hydrogen atom donor where Br_2 is the major product observed at high flux excitation (Scheme 2.1).

Scheme 2.1 HBr formation from the photolysis of *trans*-l0,ll-dibromodibenzosuberon **34**.

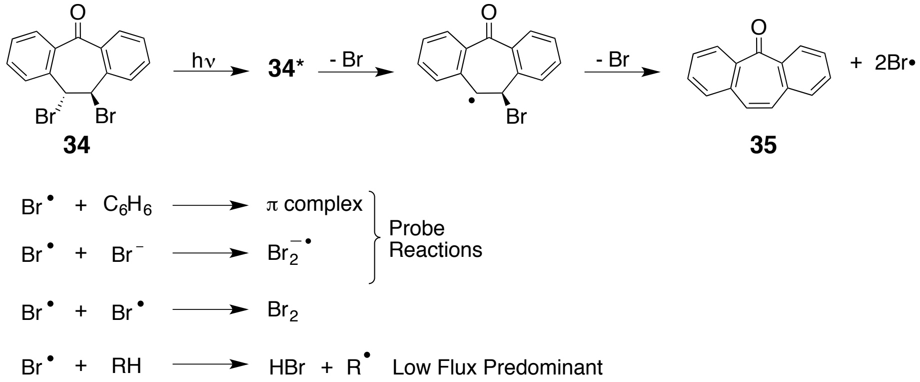

Finally, there is fundamental interest in understanding the factors that influence homolytic vs. heterolytic scission of C–X bonds in the excited state.[9-13] The photochemistry of aryl halides has been well studied, as direct irradiation of aryl chlorides, bromides and iodides leads to the formation of phenyl and halogen radicals via excited state C–X homolysis. Gudmunsdottir and coworkers[10] studied the photolysis of bromophenyl alkyl ketones and found that the excited triplet state undergoes C–Br homolysis with rate constants $\sim 10^8$ s^{-1} at 25 °C. Wender and Jeon[11] have applied this concept by linking 4-bromoacetophenone with a DNA recognition element, polypyrrolecarboxamide. This work reports the use of 4-bromoacetophenone as a DNA cleaving reagent through the generation of reactive phenyl radicals upon the absorption of light. The synthesis of fluorenones has also been reported using C–Br homolysis of 2-bromoarylketones via a Pschorr cyclization reaction subsequent to the absorption of light.[14] In contrast to the above, the photolysis of vinyl halides can result in the formation of vinyl cations through excited state photoheterolysis (Scheme 2.2). Galli and coworkers[9] note structural differences in phenyl versus vinyl cations for the favorable formation of the latter. Stabilizing substituent effects for linear vinyl cations like hyperconjugation of neighboring C–H bonds or π-conjugation effects of aromatic rings are not available in the bent aryl cation leading to primarily C–X homolysis products. Lodder and van Dorp[12] looked that the photoreactivity and selectivity of triaryl vinyl halides and found that the photochemical mechanism for the generation of vinyl cations is a parallel process with radical pair formation, in which the partitioning into radicals and ions occurs in the excited state. The authors note that the selectivity of the photochemically generated vinyl cations to bromide and acetic acid is attributed to the enhanced stability of vinyl cations being more selective towards nucleophilic trapping.

Scheme 2.2 Photochemical generation of vinyl cations (A) and aryl radicals for the synthesis of fluorenones (B).

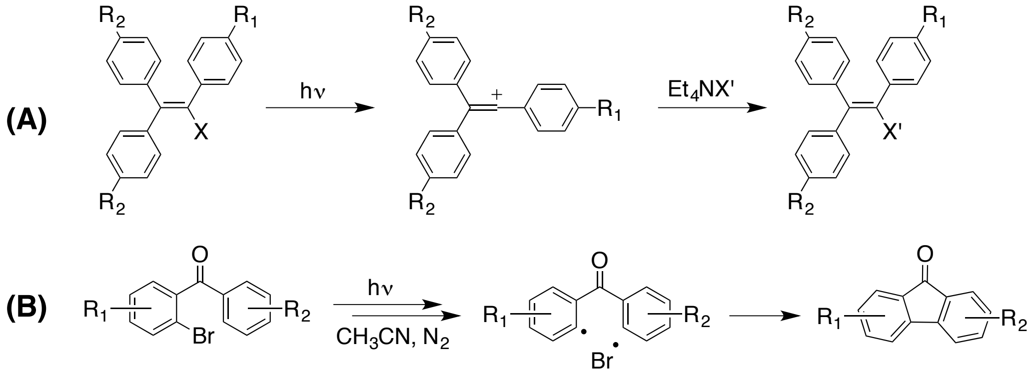

The focus of this chapter is on the photochemical decomposition of the 2,2,2-tribromoethoxy group. This species has seen use as a protecting group for carboxylic acids, alcohols, thiols and amines.[15-18] The tribromo derivative can be removed through electrolysis as demonstrated by Semmelhack and Heinsohn in 1972.[16] The authors report the release of benzoic acid from the tribromo ester in 85% yield with an applied potential of -0.70 V vs. SCE (saturated calomel electrode). Release of benzoic acid was also accomplished from various other chlorinated ethyl derivatives, though at more negative potentials in comparison to the 2,2,2-tribromoethoxy group.

There appears to be few, if any, studies on the photochemistry of the 2,2,2-tribromoethoxy group. However, some reports on related species are relevant to the work presented in this chapter. First, Kropp and coworkers looked at the product distributions from the photolysis of various alkyl monohalides. In general, it was concluded that the initial event upon excitation is C–X bond homolysis. For alkyl iodides in polar protic solvents, it is possible to observe solvolysis products that result from nucleophilic trapping of the corresponding carbenium ion. These products were attributed to an electron transfer process in the geminal radical pair, which in favorable cases predominates over cage escape. For the photolysis of alkyl bromides, a mixture of products arising from both radical and ion intermediate formation was observed.[19-23] Secondly, time-resolved studies on the photolysis of geminal di and tribromides have identified an additional intermediate: the iso di(or tri)-bromomethyl species, wherein one halogen atom dissociates from the carbon atom and recombines to a remaining halogen. This iso species forms within a few picoseconds of photolysis and decays on a subnanosecond time scale by three competing pathways: (1) addition of solvent nucleophiles to form products of OH bond insertion, (2) homolytic dissociation to form radical species and (3) reversion to the starting di or trihalide species (Scheme 2.3).[24-29]

Scheme 2.3 Use of the 2,2,2-tribromoethoxy group as a PPG for the release of benzoic acid by electrolysis (A) and formation of the isotribromomethyl intermediate from C–Br bond scission (B).

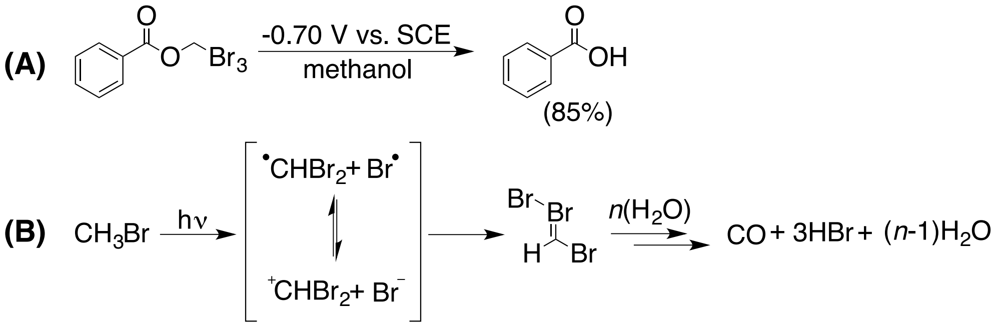

The experiments outlined in the following sections show that, unlike the monobromo species, photolysis of 2,2,2-tribromoethyl-(2′-phenylacetate) **36** can provide clean products that strongly depend on the solvent polarity, nucleophilicity and ability to serve as a hydrogen atom donor. In CH_3CN/H_2O mixtures, photolyses result in the clean formation of a product of hydrolysis. In contrast to this, when good hydrogen atom donors are employed, photolysis of **36** produces excellent yields of mono- and di-dehalogenation products. A mechanism incorporating reversible formation of an isotrihalo intermediate, nucleophilic displacement and competing homolysis reactions is proposed.

2.2 Synthesis and Photophysical Properties

Compound **36** is prepared from commercially available 2,2,2-tribromoethanol and phenylacetyl chloride using standard coupling conditions (Scheme 2.4).[30] The ester is isolated in good yields (~77%) and exhibits an absorption spectrum with a λ_{max} at 210 nm at low concentrations attributed to the $\pi \rightarrow \pi^*$ and weaker $n \rightarrow \sigma^*$ electronic transitions. At preparative photolysis conditions the tail absorption from **36** extends above 300 nm (Figure 2.2) which is attributed to a superposition of the $n \rightarrow \sigma^*$ absorption related to the C–Br bond and the $n \rightarrow \pi^*$ electronic transition.

Scheme 2.4 Synthesis of 2,2,2-tribromoethyl-(2′-phenylacetate) **36** and the major products observed in the photolyses in various solvents.

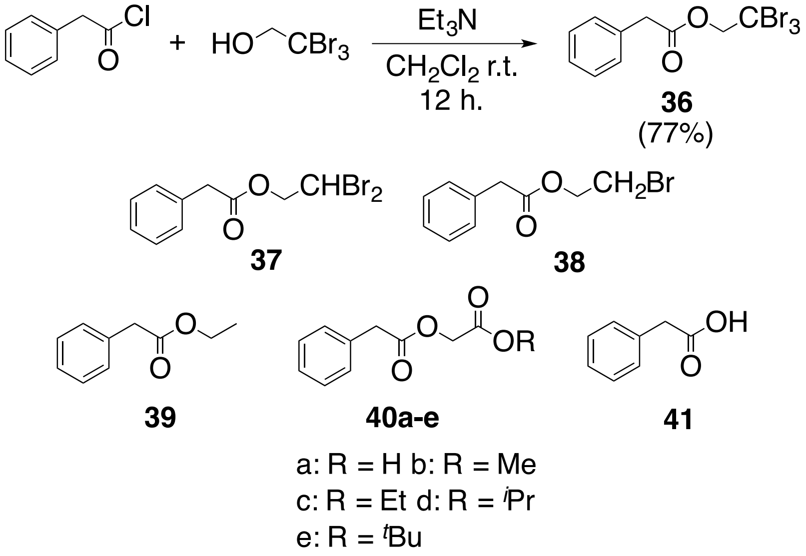

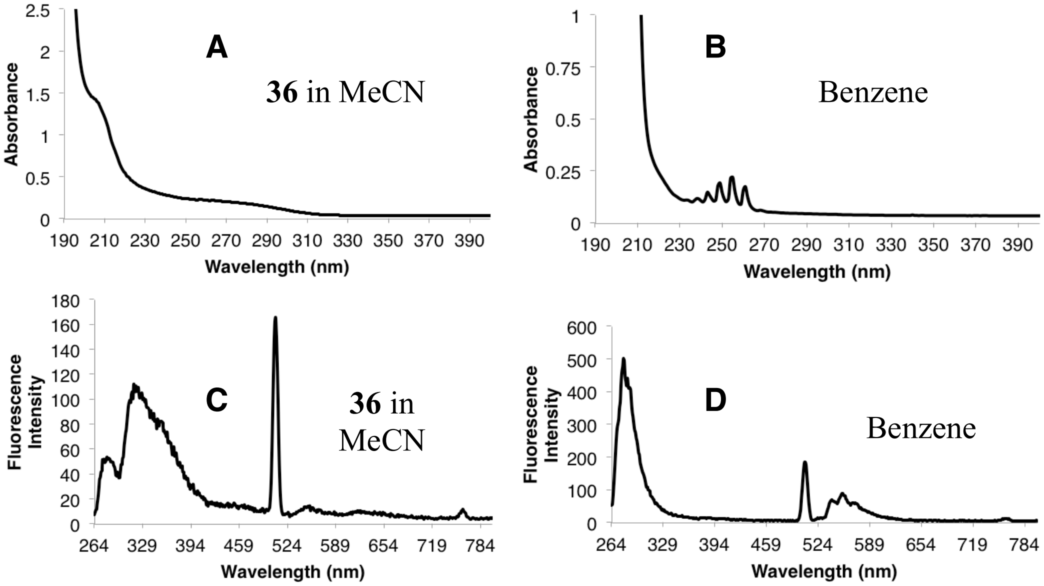

Figure 2.2 Absorption spectrum of (A) 0.1 mM **36** in MeCN and (B) just benzene. Fluorescence spectrum of (C) 0.1 mM **36** in MeCN and (D) just benzene.

Fluorescence of compound **36** was determined to be negligible. Attempts to detect fluorescence in acetonitrile (Figure 2.2) resulted in signals much lower in comparison to that of benzene, which has a fluorescence quantum yield of 0.05.[31] Isolation of the photolysis products was conducted by separatory funnel extraction and column chromatography. Product **40b** was synthesized according to a previously reported procedure using phenylacetic acid, potassium carbonate and methyl bromoacetate.

2.3 Preparative Photolysis and Product Analysis

Ester **36** was dissolved in various solvents in a four sided quartz cuvette, sealed, purged with N_2 and photolyzed at 253.7 nm using an 8-bulb Rayonet photoreactor. Analysis of the crude photoproduct mixtures were conducted by ^{1}H NMR and gas chromatography-mass spectrometry (GS-MS) was used to detect products that were produced in trace amounts. These results are summarized in Table 2.1. It was anticipated that direct photolysis of **36** would result in C–Br bond homolysis generating fragmented radical pairs that could escape the solvent cage and form further radical products. The ensuing dibromo alkyl radical from loss of bromine atom after 253.7 nm photolysis could undergo a variety of radical coupling, hydrogen atom abstraction and/or disproportionation products. Of particular interest is the thinking that this radical might expel a carboxylate ion by way of β-cleavage leading to the formation of phenylacetic acid,[32-34] a pathway for the use of the trihalo group as a photoremovable protecting group for carboxylic acids (Scheme 2.5). As can be seen in Table 2.1, this product does form, though no conditions where this was the sole product were discovered.

Scheme 2.5 Initial proposed pathways for the UV photolysis of **36**.

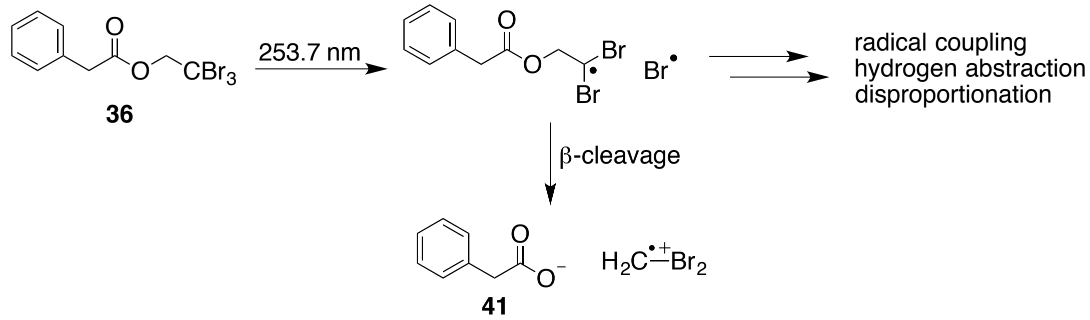

Acetonitrile, being both polar and relatively non-nucleophilic was expected to optimize the release of phenylacetic acid, through stabilization of the dibromo radical intermediate. However, formation of carboxylic acid **40a** was obtained as the major product with small amounts of phenylacetic acid also present. Photolysis in another polar solvent, MeOH, resulted in the formation of two significant products: monodebrominated ester **37** and substitution product **40b**. The major product **37** results from a net reduction

Table 2.1 Product ratios from photolysis of **36** in various solvents as analyzed by ^{1}H NMR.

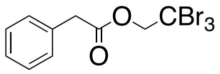

36

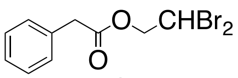

37

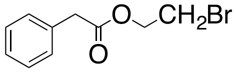

38

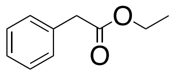

39

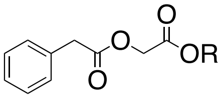

40a-e

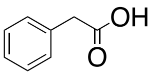

41

a: R = H b: R = Me
c: R = Et d: R = ^{i}Pr
e: R = ^{t}Bu

Solvent	[36] (mM)	Time (min)	36	37	38	39	40a-e	41
MeCN	15.13	60	61.7				31.2 **a**	7.1
MeCN	15.13	120	26.9				62.4 **a**	10.7
MeCN	15.13	180	10.2				75.1 **a**	14.7
MeOH	15.88	30	61.0	22.4			16.6 **b**	
MeOH	15.88	60	3.7	44.9	[a]	[a]	27.9 **b**	23.5
MeCN-d_3	20.12	90	59.9				40.1 **a**	
MeOH-d_4	27.61	90	23.3				76.7 **b**	
MeCN (17% H_2O)	13.80	60	8.6				71.4 **a**	20.0
ethanol	22.70	60	0	[a]	(<45)	55[b]	**c**[a]	
2-propanol	19.87	60	0	[a]	88	12[b]	**d**[a]	[a]
tert-butyl alcohol	16.50	60	4.9	[a]			48.7**a**, **e**[a]	46.4
cyclohexane	13.47	60	0	[c]				
THF (no BHT)	18.54	60	0	[c]				
THF (with BHT)	18.96	30	0	(<100)[d]				

---

[a] minor amounts of this product were detected by GC-MS . [b] based on reported chemical shifts. [c] only product identified by ^{1}H NMR accompanied by numerous unidentified major products. [d] major product identified by ^{1}H NMR accompanied by numerous unidentified minor products.

of the C–Br bond. The latter arises through hydrogen atom transfer from the solvent to the intermediate dibromoalkyl radical. Unlike in acetonitrile, where this radical eliminates the phenylacetoxy ion, the alkyl dibromo radical is apparently able to abstract a hydrogen atom from the solvent. While acetonitrile and methanol have similar bond dissociation energies (96.0 and 96.1 kcal/mol, respectively)[35] previous work has shown that electron-poor radicals react more rapidly with electron-rich C–H bonds in substrates such as methanol compared with electron-deficient C–H bonds in substrates such as acetonitrile.[36,37] This mechanism is supported by a significant kinetic isotope effect. The use of methanol-d_4 suppresses formation of reduction product, and the substitution product, **40b**, is the only species detected by ^{1}H NMR.

Similar C–Br bond reduction is observed in ethanol, a solvent that is a stronger hydrogen atom donor (C–H BDE = 94.8 kcal/mol).[35] However, in this case, the two major products observed were ethyl phenylacetate **39** and 2-bromoethyl-(2′-phenylacetate) **38**. These products presumably result from multiple C–Br bond reductions. Control experiments showed that **39** can also form from Fischer esterification (thermal process) by way of the phenylacetic acid reacting with the solvent where hydrobromic acid (presumed byproduct of C–Br reduction reaction) is added. Thus, there is some uncertainty as to how much of product **39** results from a Fischer esterification pathway as compared to the sequential reduction of **36**. However, the formation of **39** in comparable experiments using isopropyl alcohol suggests that Fischer esterification of phenylacetic acid is only a small contributor to its overall yield. It is unclear why NMR-detectable amounts of the singly reduced species **37** are not observed (trace amounts of this product are detected by GC-MS). One option is that the newly formed 1-

hydroxyethyl radical can further serve as a one-electron reducing agent leading to the formation of acetaldehyde and compound **38**, upon subsequent hydrogen abstraction.

Photolysis of ester **36** in 2-propanol (C–H BDE = 91.0 kcal/mol)[35] garnered results similar to those observed in ethanol. The monobrominated compound is the major component in the photolysis mixture. Seemingly, the isopropyl radical formed from the first hydrogen abstraction can serve as a reducing agent leading to the formation of acetone. Smaller amounts of the completely debrominated product **39** are also detected. In this case, ester **39** is formed through sequential C-Br bond reductions due to the fact that Fischer esterification of phenylacetic acid would lead to isopropyl phenylacetate. GC-MS results show that in fact trace amounts of the isopropyl ester do form, along with minor amounts of substitution product **40d**.

Exclusion of a good hydrogen-donating source, like when *tert*-butyl alcohol is used as the photolysis solvent, affords product distribution lacking reduction products identifiable by ^{1}H NMR. Instead, the major components found were phenylacetic acid and 2-(2′-phenylacetoxy)acetic acid. It would seem that the *tert*-butyl alcohol is too sterically hindered to allow for any substitution product, conceding to the addition of trace amounts of water in the solvent. Trace amounts of the fully reduced ester **39** under these conditions were also confirmed by mass spectrometry. Solvents tested that are less polar and non-nucleophilic, such as cyclohexane and THF, afforded the singly reduced species **37** as the only product detected in the ^{1}H NMR of the crude photolysis mixture. However, these photolyses were not as clean as the experiments mentioned in the previous solvents. The spectra showed that numerous unidentified minor products also accompanied **37**. These products were not afforded in sufficient yield to permit complete isolation and characterization. In contrast, when photolyses were carried out in THF that had 0.025% of the preservative butylated hydroxytoluene (BHT), **37** was the major product observed and preparative quantities could be generated and isolated under these conditions.

2.4 Proposed Photochemical Reaction Pathways

Photolysis of ester **36** at 254 nm in a variety of solvents leads to different product distributions as indicated in Table 2.1. Among these products are solvent and/or water substitution products **40a-e**. The hypothesis for the formation of these products is the trapping of isotribromo intermediate **42** (Scheme 2.6). Reid and coworkers[29] have argued, on the basis of computational studies, that an ion pair ($RCBr_2^{+}\cdots Br^{-}$) is a significant resonance contributor of the isotrihalo species in the condensed phase. Thus, polar protic solvents, like that of water, should be able to stabilize the formation of this intermediate leading to the subsequent substitution product. This is consistent with our findings in that the addition of water or other hydrogen atom bonding reagents to the photolysis mixture increases product distributions consistent with the formation of the isotribomo species. Adding water to the photolysis of ester **36** in acetonitrile led to an increase in the conversion rate of the starting material but did not significantly alter the product outcomes or yield of phenylacetic acid. The proton NMR spectrum of the unpurified photolysis mixture indicates that the two products (**40a** and **41**) form cleanly with negligible byproducts. Interestingly, this photochemical route proved to be a much more feasible method for generating isolable quantities of 2-(2′-phenylacetoxy)acetic acid **40a** than a previously published procedure.[38]

Scheme 2.6 Proposed mechanism for the solvent trapping of isohalo intermediate **42**.

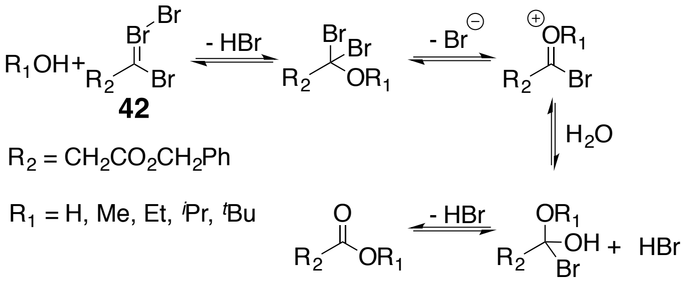

Results in Table 2.1 are consistent with the mechanism proposed in Scheme 2.7. Excited state homolysis of **36** leads to a geminate radical pair partitioning between recombination forming the isotribromo species **42** or cage escape (reversible) forming a dibromoalkyl radial and bromine atom. The isotrihalo intermediate can either isomerize back to the starting material or combine with water or another nucleophile for the formation of **40a-e**. Generation of phenylacetic acid **41** can form through secondary heterolysis of the dibromoalkyl intermediate **37**, though provided its low yields relative to other products, this process is not particularly fast and competes with hydrogen atom abstraction and radical recombination pathways. Recent ultrafast spectroscopic studies on similar systems favor us to consider the isotrihalo species as the key intermediate, though an alternative pathway where electron transfer would result in a carbenium ion as suggested by Kropp et al.[23] (pathway c in Scheme 2.7) cannot be dismissed on the basis of the data presented above from the current study.

Competition between reversion to the starting material (pathway e) and nucleophilic trapping of the solvent or additives (pathway d) is supported by the observation that the photochemical conversion rate increases when water is added to the acetonitrile. An example of this is realized in Table 2.1 when a 60 minute photolysis of ester **36** in nominally dry acetonitrile converts <40% of the starting material compared to >90% in acetonitrile with 17% water. Interestingly the ratio of phenylacetic acid to product **40a** is not significantly affected by the addition of water. This observation implies that the heterolysis step leading to the formation of phenylacetic acid from the dibromoalkyl intermediate (pathway f) is also promoted by the addition of water. This is presumably due to the increasing polarity of the solvent upon the addition of water and thus accelerating the heterolytic bond cleavage (pathway f) to approximately the same extent it accelerates the nucleophilic trapping of **42** leading to **40a** (pathway d).

Scheme 2.7 Proposed reaction pathways for the observed photolysis products of **36**.

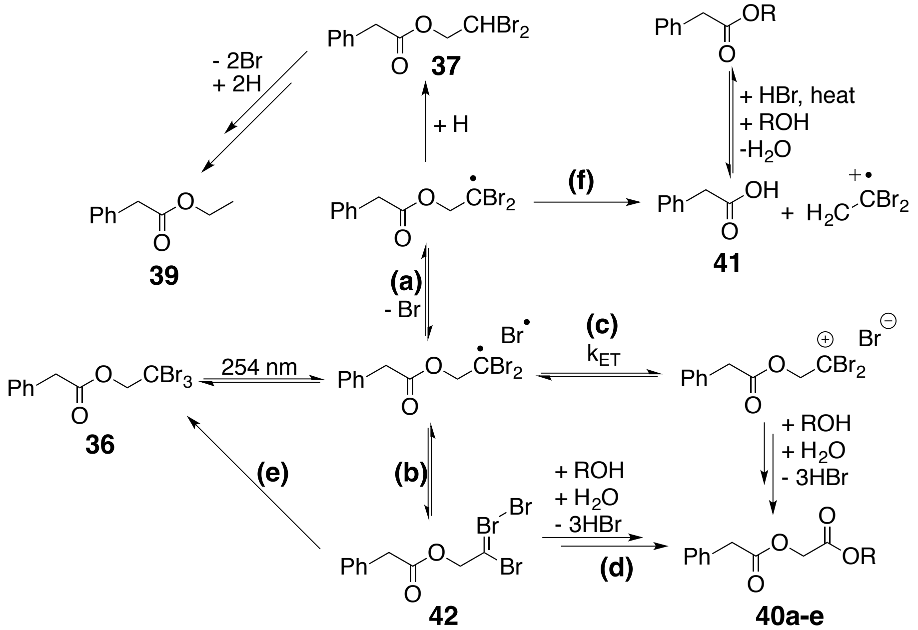

A solvent isotope effect is also notable when comparable runs were carried out in CD_3CN as opposed to CH_3CN. By using the deuterated solvent, only product **40a** is observed, as the formation of the elimination product **41** is below the limit of detection and/or not observed. This is attributed to a kinetic isotope effect on the trapping of the Br atom in the geminate radical pair subsequent to C–Br homolysis. This pair, as alluded to previously, can either recombine to form the isotribromo intermediate **42** or, if free radicals are formed through cage escape or hydrogen atom transfer to the Br atom, through elimination of phenylacetate ion. The deuterated solvent is slower to trap the Br atom (formation of DBr as opposed to HBr), resulting in fewer free radicals and thus low (<5%) yields of **41**.

2.5 Conclusions and Future Research Directions

Direct photolysis of ester **36** at 254 nm results in the formation of a diverse collection of products that are strongly dependent upon the solvent used in the photolysis. The various distributions of products are consistent with the mechanism shown in Scheme 2.5, originating from C–Br homolysis upon the absorption of UV light creating a radical atom pair. The latter can form the isotribromo intermediate **42,** which can be trapped by nucleophiles to form **40a-e** or revert back to the starting material. Alternatively, the radical pair can undergo heterolysis to release phenylacetic acetate ion or undergo a series of reduction steps leading to products **37-39**. The formation of the aforementioned products relies heavily on the solvents ability to serve as a nucleophile or hydrogen atom transfer reagents. For example, when BHT is included in the photolysis mixture it is possible to achieve preparatively useful yields of the monodebrominated product **37**. However, when water is added to the photolysis solution in the absence of a good hydrogen atom donor, it is possible to obtain useful amounts of **40a**, the addition product.

Ideally, the release of the carboxylate ion, in this case phenyl acetate would be a desired pathway for the use of the tribromoethyl group as a photoremovable protecting group. While formed under many different reaction conditions above, we were unable to identify conditions in which it was the sole product. The data presented in the aforementioned sections suggest that the challenge is competing formation of the isotribromo species from the geminate radical pair. This provides an intermediate that is apparently sufficiently long-lived to be trapped by trace amounts of nucleophiles. One potential solution to this problem would be a photochemical electron transfer reaction, which ought to provide the desired radical, accompanied by a bromide ion rather than a bromine atom and possible evasion of the isotribromo intermediate (Scheme 2.8).

Scheme 2.8 Proposed release of phenyl acetate under photoinduced electron transfer conditions.

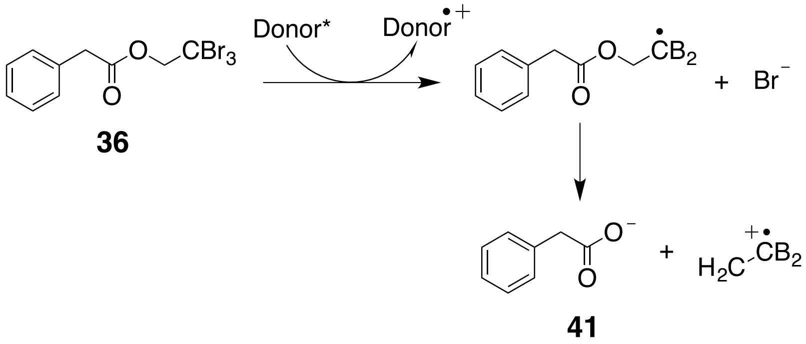

CHAPTER 3. PHOTODEPROTECTION OF ALCOHOLS USING UV OR VISIBLE LIGHT PHOTOINDUCED ELECTRON TRANSFER TO 9-PHENYL-9-TRITYLONE ETHERS

3.1 Introduction and Background on the 9-Phenyl-9-Tritylone Group

In the previous chapter the 2,2,2-tribromoethoxy group was examined for the photochemical deprotection of carboxylic acids by UV irradiation where yields were highly dependent on solvent conditions. While much work has been done on the protection and photorelease of mild leaving groups such as sulfonates, carboxylates and phosphates, less labile leaving groups like alcohols provide fewer options. One approach is to protect the hydroxyl group as a mixed carbonate ester and rely on the spontaneous decarboxylation of the monocarbonic ester for alcohol release.[1-3] Other avenues include photoisomerization and intramolecular cyclization of silyl[4] and cinnamate[5] derivatives, photo-enolization,[6] naphthylenyl derivatives,[7] and the direct photolysis of trityl ethers.[8,9]

This chapter introduces a new photoremovable protecting group, the 9-phenyl-9-tritylone group (PTO). This group can release alcohols in good yields through either direct UV irradiation with a donor, or through a mediated electron transfer pathway using a visible light photocatalyst. There is particular interest in the development of PPGs capable of using visible or near infrared light as was briefly discussed in section 1.6. Low energy wavelengths are particularly important where the hydroxyl group is part of a structure containing other chromophores. For example, 55 (36.7%) of the top 150 small molecule pharmaceutical products (2012 retail sales)[10] contain primary or secondary OH groups. In contrast to this, the carboxyl group, which has garnered significant PPG development, is only observed in 16.7% of that group. Additionally, of the 55 primary and secondary hydroxyl group containing drugs, 49 of them have *α,β*-unsaturated carbonyl moieties or aromatic rings capable of absorbing UV light. Thus, the development of new PPGs for alcohols utilizing low energy light is an important endeavor.

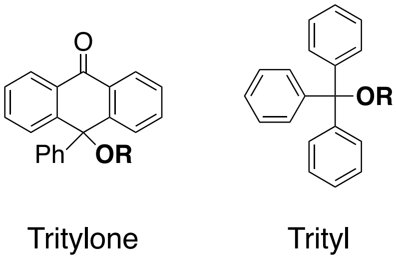

Figure 3.1 The tritylone and trityl protecting groups for alcohols.

Barnett and coworkers[11,12] first introduced the PTO group when they were attempting to find a protecting group for alcohols that was more stable under acidic environments in comparison to the trityl protecting group (Figure 3.1). Similar in structure, trityl derivatives have seen extensive use as protecting groups, especially in peptide synthesis, as they are readily cleaved under acidic conditions with high yields of released substrate.[13-15] In contrast, the PTO group exhibits excellent stability under acidic environments. More importantly, reductive conditions like Wolff–Kishner[12] and electrolysis[16] environments have successfully cleaved the PTO group, but there had been no reports of the photochemistry associated with this protecting group. Thus, in the subsequent sections of this chapter we explore the photochemistry of the PTO moiety and its ability to be photochemically reduced, while reporting yields and conditions for the best release of various primary and secondary alcohols as well as use laser flash photolysis techniques to propose a mechanism of deprotection.

While it was briefly mentioned in Chapter 1, we also re-introduce and go into further details about photoinduced electron transfer (PET) chemistry as it applies to the mechanism of alcohol release from PTO–ethers. PET systems provide a means for decoupling the light-absorbing step from the bond-breaking chemistry allowing for broad spectral response. Successful examples for the deprotection of alcohols include *N*-alkylpicolinium (NAP)[17,18] and phenacyl groups,[19] triplet sensitized nitrophenyl groups,[20] and phenethyl alcohol systems.[21]

3.2 Photoinduced Electron Transfer

When a molecule absorbs a photon an electronic transition occurs from the ground state to an excited state. This newly formed excited state has numerous paths it can take back to the ground state as shown in the Jablonski diagram in Figure 3.2. Upon excitation to a higher excited state, spin is conserved and represented as the singlet state (S_2). Non-radiative internal conversion down to the lowest excited state (S_1) is fast and occurs on a timescale of around 10^{-14} to 10^{-11} seconds, resulting in many photochemical processes deriving from this state. From the lowest excited singlet state, energy can be dissipated to the solvent through another non-radiative process back to the ground state. Alternatively, emission of a lower energy photon can occur in a process known as fluorescence (F), which occurs on a 10^{-9} to 10^{-7} seconds timescale. In certain cases the electron can undergo a spin flip through a process called intersystem crossing (ISC, 10^{-8} to 10^{-3} seconds) to a lower energy triplet state (T_1). The molecule can then relax back to the ground state through a radiative phosphorescence process (P, 10^{-4} to 10^{-1} seconds), a non-radiative process by energy transfer to the solvent/another molecule, or can undergo a chemical reaction. Of particular interest in relation to this chapter are the chemical reactions that occur from the excited state molecule. Such excited state reactions include energy transfer, electron transfer, hydrogen atom transfer and bond-breaking rearrangement chemistry.[22,23]

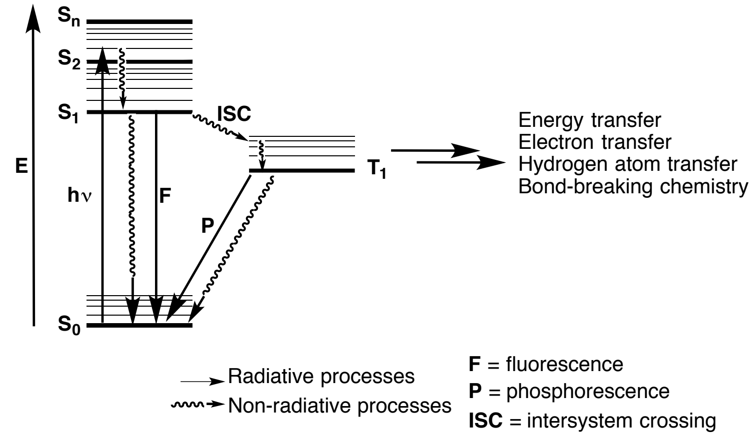

Figure 3.2 Jablonski diagram

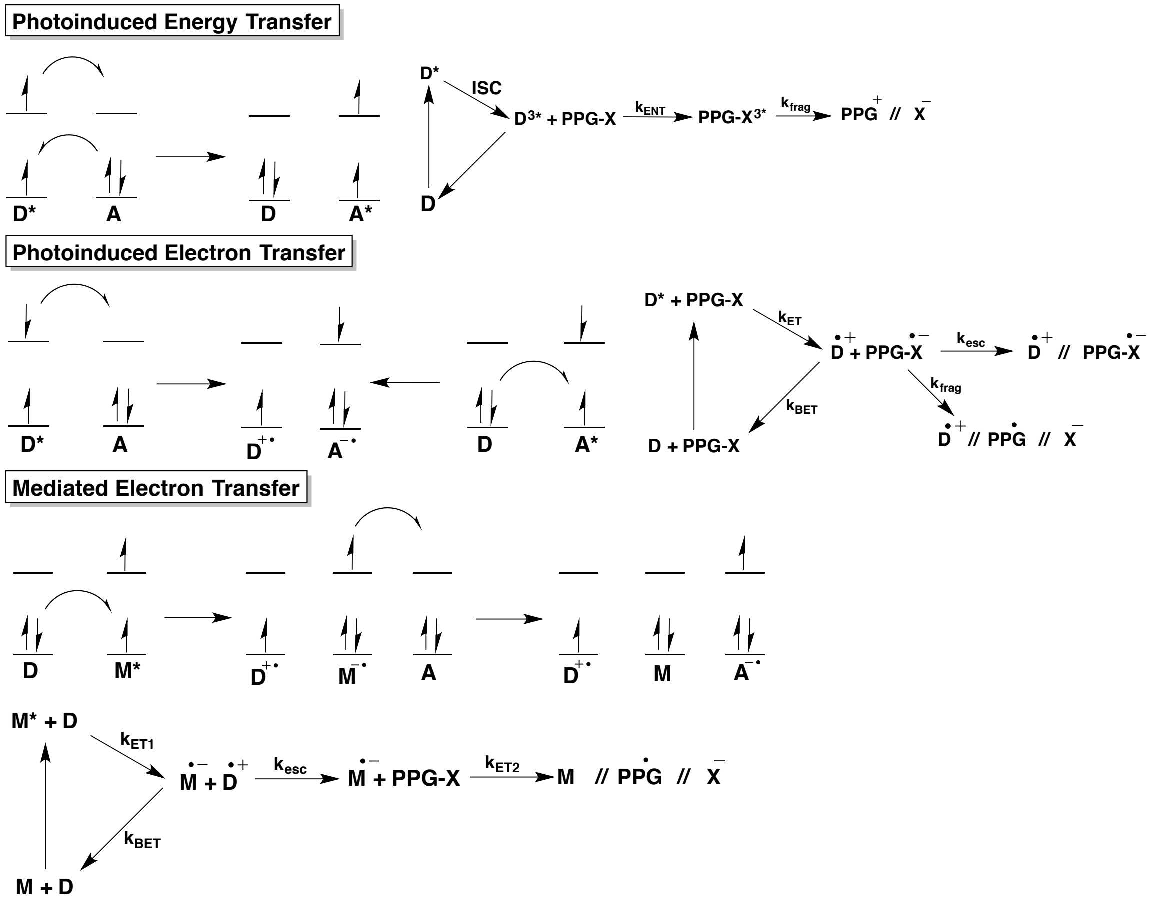

Figure 3.3 Simplified energy diagram for electron movement and application to a PPG in photoinduced energy (top), electron (middle) and mediated (bottom) electron transfer reactions. D = donor, A = acceptor and M = mediator.

Some of the excited state reactions are shown in a simplified energy diagram in Figure 3.3. The first, photoinduced energy transfer, is the reaction of an excited state triplet donor (D*) interacting with an acceptor molecule (A). In this case, electron transfer occurs between the two species, conserving spin, and resulting in the transfer of triplet energy (k_{ENT}) to the acceptor molecule or PPG. An example of this concept used in the deprotection of alcohols is illustrated in Scheme 3.1. Here, acridin-9(10H)-one, labeled as a sensitizer (Sens, i.e. the compound absorbing light energy), is selectively irradiated to generate its triplet excited state. Transfer of triplet energy to an *o*-nitrophenyl protecting group leads to deprotection of the alcohol via C–O bond scission of a carbonate ester linkage followed by thermal decarboxylation.[20]

Scheme 3.1 An example of triplet sensitized deprotection of alcohols.

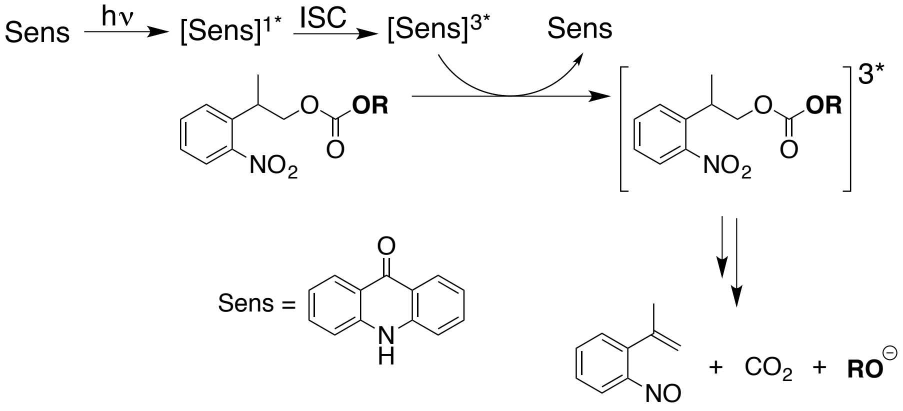

Unlike triplet sensitized photochemical deprotection of functional groups, photoinduced electron transfer (PET) results in the generation of ion radicals by the transfer of an electron from an excited state donor to a ground state acceptor. Alternatively, the same can be accomplished via excitation of the acceptor and subsequent electron transfer from a ground state electron donor (Figure 3.2, middle). The resulting anion radical of the acceptor can undergo bond scission leading to the release of the protected substrate. An example of this reaction can be found in Scheme 3.2. In this instance, *N,N*-dimethylaniline (DMA) is excited and electron transfer occurs from DMA to a phenacyl protected benzoic acid generating the phenacyl anion radical and oxidized

DMA. C–O bond scission from the anion radical leads to deprotection of benzoic acid in 93% yield as analyzed by HPLC.[19,24]

Scheme 3.2 An example of photoinduced electron transfer deprotection of carboxylic acids.

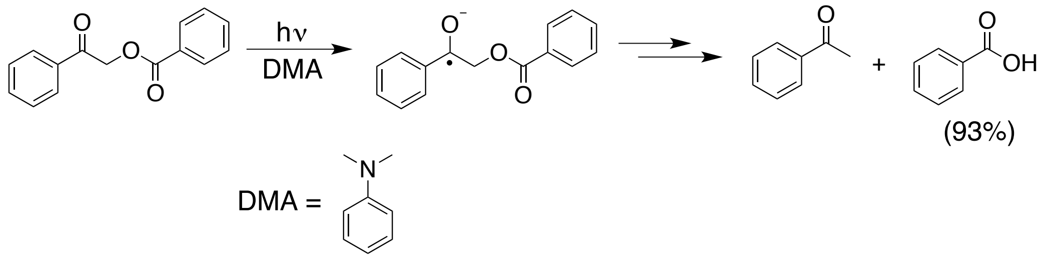

In a mediated electron transfer system, a third component is added to the reaction mixture that absorbs light and acts as a shuttle for the electron to traverse between the donor and acceptor molecules. Here, the donor reduces the excited state of the mediator. The reduced mediator then transfers the electron to the acceptor for ensuing bond breaking chemistry, recycling the mediator in the process. Having a photosensitizer that is recycled in solution allows for sub-stoichiometric amounts of the mediator to be used in the photolysis system, and many examples of this type of system can be found in the literature making use of visible light. An additional benefit of using a mediating electron transfer system is that electron transfer can occur from the donor to an excited triplet state generating a radical ion pair with parallel spins. Due to this, the rate of the non-productive back electron transfer (k_{BET}) is minimized, thus allowing for efficient reduction of the acceptor. An example of this is seen in Scheme 3.3. In this system, benzophenone, which has a high quantum yield for triplet state formation, is used as the mediator. Electron transfer from *N,N*-dimethylaniline generates the anion radical of benzophenone, used to shuttle the electron to the *N*-alkylpicolium ester, leading to the release of phenylacetic acid in high yields.[25] Although this system uses a mediator that absorbs light in the near visible region, a similar type of system can be used for the deprotection of carboxylic acids that make use of a visible light absorbing photocatalyst, $[Ru(bpy)_3Cl_2]$.[18,26] This photocatalyst is also used in the protecting group system described in the following sections.

Scheme 3.3 Use of a mediated electron transfer system for the release of a carboxylic acid.

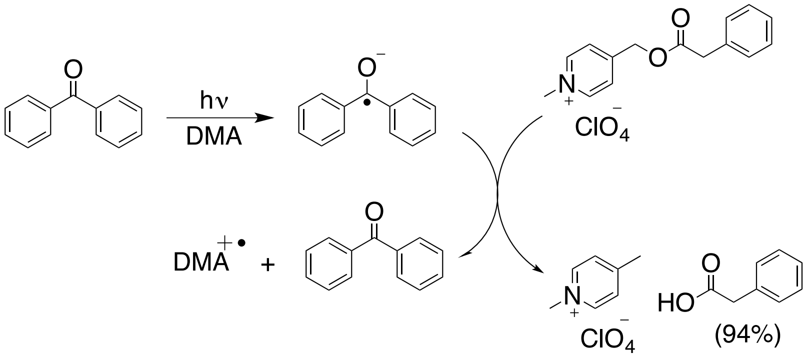

Advancements in analytical techniques in the 1970's and 80's brought electron transfer chemistry to the forefront of investigation due to the direct observation of radical and radical ion intermediates by methods like laser flash photolysis (LFP, discussed in further below), electron spin resonance[27] (EPR) and chemically induced dynamic nuclear polarization (CIDNP).[28] In addition to experimental evidence in support of PET reactions, Rudolph A. Marcus performed seminal work in theoretical considerations of electron transfer processes.[29-31] Beginning in 1956, Marcus predicted a parabolic relationship between the free energy of activation ($\Delta G^{\ddagger}$) and the thermodynamic driving force (ΔG_{ET}) of the electron transfer process between the donor and acceptor molecules. Marcus' theory predicted that the rate of electron transfer would increase as the reaction becomes more exergonic, denoting this the "normal" region, while higher and higher driving forces were predicted to decrease the rate of electron transfer leading to an "inverted" region. A graphic depicting this idea is illustrated in Figure 3.4. In the diagram below the donor and acceptor molecules are represented as potential energy surfaces. Starting at the top left (A), the exergonicity of the electron transfer process increases in subsequent diagrams. Both (B) and (C) represent exergonic electron transfer processes with decreasing free energy of the reaction. However, in diagram (C), the increased exergonicity of this reaction leads to an increase in the activation barrier and a slower electron transfer rate as predicted in Marcus' "inverted" region.

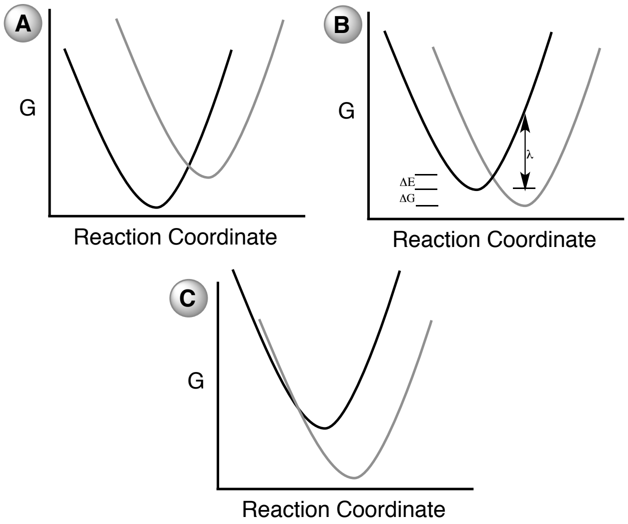

Figure 3.4 Potential energy well diagrams for an endergonic (A), exergonic (B) and inverted region (C) electron transfer processes.

Early attempts to experimentally observe the inverted region was met with disappointment, as increasing the exergonicity of an electron transfer reaction did not result in a decrease in the rate of transfer. For example, in 1970 Rehm and Weller studied the fluorescence quenching rates of various electron donor and acceptor molecules. No experimental results corroborated the proposed inverted region, as electron transfer rate constants at high exergonicity were deemed diffusion-controlled. However, from the work of Rehm and Weller,[32,33] it was determined that the feasibility of a bimolecular electron transfer process could be predicted from equation 1. The driving force for an electron transfer process (ΔG_{ET}, kcal/mol) was found to depend on the ground state oxidation potential of the donor (E_{ox}) and the ground state reduction potential of the acceptor (E_{red}) measured in volts. Also considered is the excited state energy of the electron donor (E_{00}) in kcal/mol and a fourth term that accounts for a correction for the desolvation and attraction of the ion pair, though in polar solvents like MeCN and MeOH this term is generally accepted as negligible.

$$\textbf{(Eq 1.)} \qquad \Delta G_{ET} \approx 23.06(E_{ox} - E_{red}) - E_{00} - (q^2/R\varepsilon)$$

It was not until some 30 years after Marcus proposed his theory on electron transfer that evidence surfaced in support of an inverted electron transfer region. In 1984 Miller and coworkers[34] published a report of measured electron transfer rates from a series of donor-acceptor molecules linked by a rigid saturated hydrocarbon spacer, the steroidal 5α-androstane skeleton shown in Figure 3.5. In keeping the electron transfer distance fixed, the authors measured the intramolecular transfer rate constants and plotted them against the driving force of the reaction. As the free energy of the reaction increased, the authors noted that a decrease in electron transfer rate constants was observed from the biphenyl electron donor to chlorinated quinones as the acceptor. This was regarded as the first unambiguous report in support of the Marcus inverted region. Previous reports that attempted to observe the inverted region in non-linked systems failed due to the fact that intermolecular electron transfer reactions are diffusion limited. In fact, a report in 2001 by Gopidas et al.[35] looked at the free energy dependence of electron transfer processes in molecules with hydrogen bonding (carboxylic acids) to assess the role of diffusion in concealing the inverted region. What the authors found was that intermolecular electron transfer between two molecules is diffusion controlled and follows Rehm-Weller behavior, where the rate of electron transfer increases as the driving force of the reaction increases and reaches a maximum where further exergonicity of the reaction will not lead to increased electron transfer rates. On the other hand, unimolecular electron transfer processes follow Marcus behavior where the rate increases with increasing driving force of the reaction, reaches a maximum and further exergonicity leads to a decrease in observed charge transfer rates. Regardless, equation 1 is very useful for determining the driving force of bimolecular electron transfer reactions.

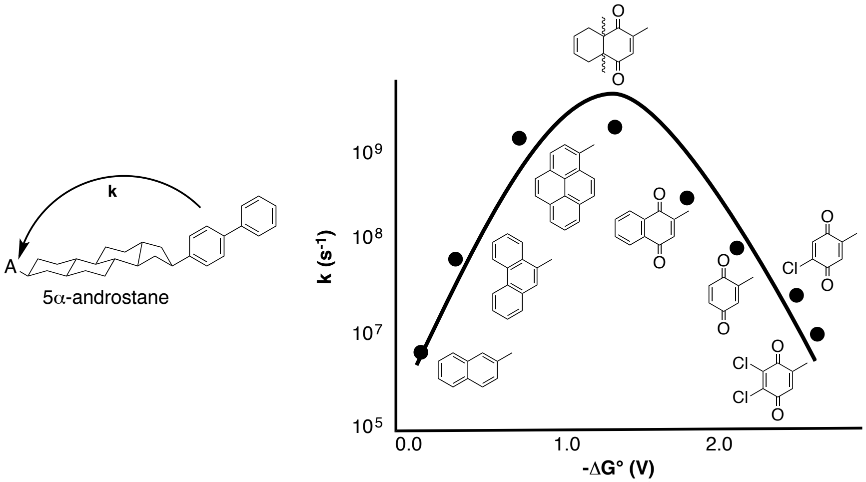

Figure 3.5 General reproduction of results from Miller et al.[34] Evidence of Marcus “inverted” region using a rigid spacer.

While the importance of distance dependence in electron transfer reactions, particularly unimolecular processes have been established, another important consideration for these reactions is solvent polarity. Polar solvents like that of methanol help stabilize the radical ions formed while non-polar solvents destabilize ion formation. This is particularly important when further chemistry is desired after the electron transfer process. Polar solvents help favor solvent separated ion pairs (SSIP) reducing the possibility of the non-productive back electron transfer process (Figure 3.6). Alternatively, non-polar solvents favor contact ion-pairs (CIP) that exist in the same solvent shell allowing back electron transfer to compete with other desired photochemical processes.[36-38] Unlike electron transfer reactions, energy transfer is less dependent on the solvent polarity as charged ions are not produced. Only an induced dipole moment from the transfer of triplet energy is produced and thus solvent polarity does not play a large role in stabilizing the short-lived intermediate.

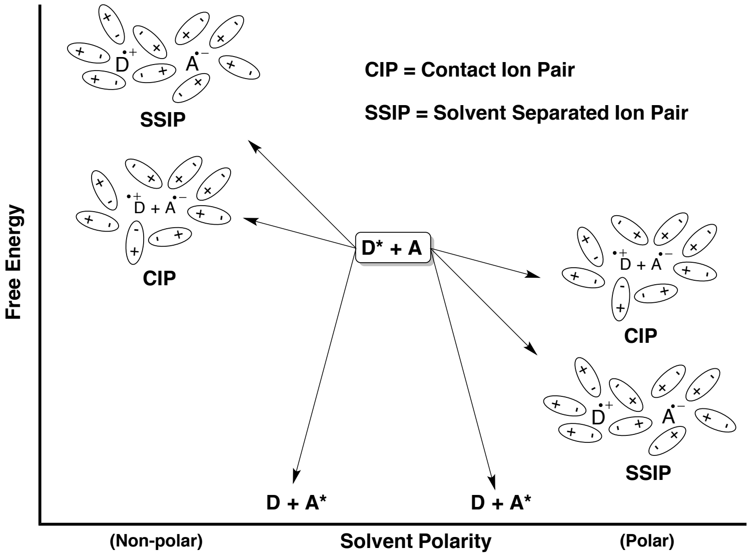

Figure 3.6 The effect of solvent polarity on electron and energy transfer.

3.3 Synthesis and Properties of PTO–ethers

The synthesis of PTO–ethers can be completed in two steps and is outlined in Scheme 3.4. Commercially available 9-phenylanthrancene is oxidized using sodium dichromate dihydrate under an acidic environment (acetic acid) generating 9-hydroxy-9-phenyltritylone **43**. Following acid-catalyzed condensation of **43** and the azeotropic removal of water yielded seven PTO–ethers **44-50**. The synthesis of ethers using primary alcohols gave the best yields with secondary alcohols being less reactive and providing smaller yields. Consistent with the attempts of previous studies,[11] we found it difficult in the preparation of ethers using tertiary and phenolic alcohols with the former providing dehydration compounds as the major products.

Scheme 3.4 Synthesis and scope of PTO-ethers.

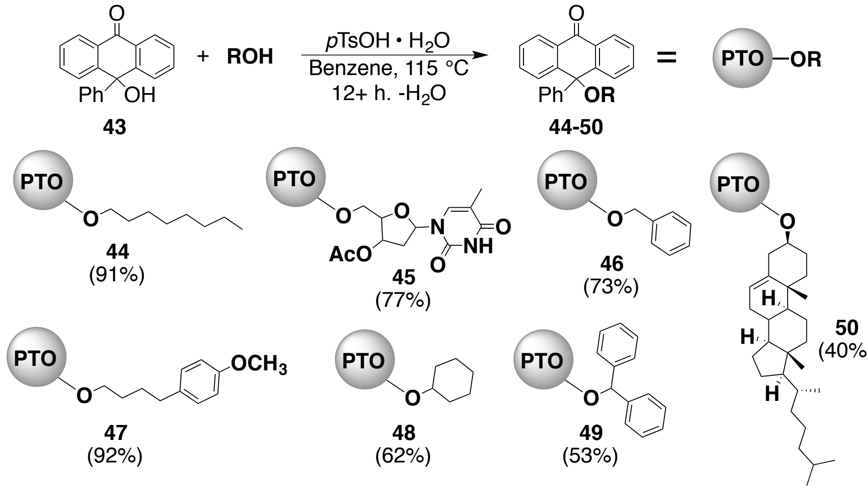

The UV-Vis absorption spectrum of octyl ether **44** is shown in Figure 3.7. At low concentrations this compound has at $\lambda_{max} \approx 275$ nm, while at higher concentrations the absorbance tails to ca. 400 nm and thus would not be suitable for the direct release of alcohols using visible light (>400 nm). As was previously mentioned, PTO–ethers release alcohols under electrolysis conditions and have reported ground state reduction potentials (E_{red}) of -1.30 to -1.36 V (vs. Ag/AgCl).[16] To determine the feasibility of photoinduced electron transfer chemistry to occur from an external amine donor to the excited state PTO–ether, the free energy change for electron transfer was calculated using the Weller equation introduced in the previous section (Eq. 1). Using the ground state oxidation potential (E_{ox}) of triethylamine (TEA, +1.15 V vs. SCE)[39] and the excited triplet state energy (E_{00}) of structurally comparable benzophenone (69.2 kcal/mol)[40] it was predicted that this electron transfer process would be exergonic by about 13 kcal/mol. It was further anticipated that the resulting radical anion would undergo bond-breaking leading to the deprotection and recovery of the alcohol.

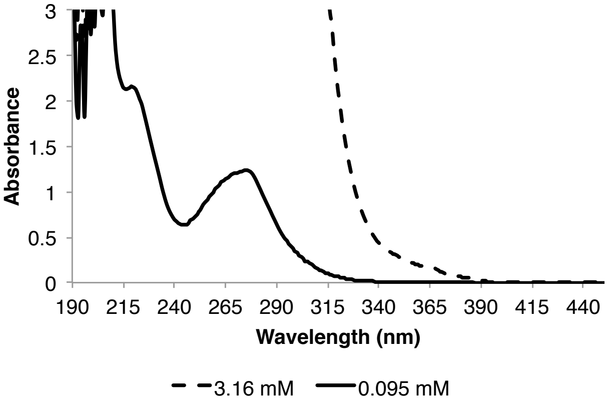

Figure 3.7 UV-Vis spectrum of octyl ether **44** in methanol.

3.4 Photodeprotection Using UV Light

Preparative photolyses of the seven PTO–ethers in methanol and mixtures of methanol/1,4-dioxane were conducted with a 350 nm 12-bulb, 32-watt rayonet reactor. Analyses of the deprotected alcohols were done using gas chromatography (except ether **45** where HPLC was used) and yield is reported against a calibration curve performed for each released alcohol. A typical time course for these photolyses can be seen in Figure 3.8 and the results of the remaining ethers can be found in Table 3.1: 3'-O-acetylthymidine, benzyl alcohol, cyclohexanol, benzhydrol and cholesterol were all released in satisfactory yields. Interestingly, ether **47** exhibited the poorest release of alcohol. In this case the readily oxidized anisyl group can act as an electron donor, competing with TEA for the reduction of the triplet state PTO chromophore and reducing the yield of 4-(4'-methyoxyphenyl)-1-butanol. In fact, when a similar photolysis is conducted under visible light deprotection conditions (discussed in further detail in the next section) the yield of alcohol increases to 66%. This supports the notion that intramolecular photoinduced electron transfer is acting as a non-productive photochemical pathway resulting in a reduced yield of this alcohol as reported in Table 3.1.

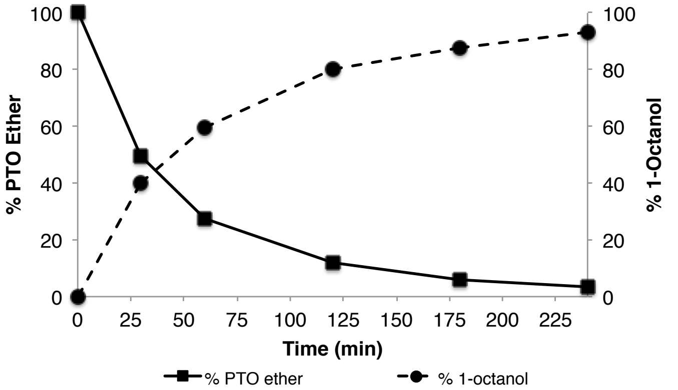

Figure 3.8 Time course photolysis of **44** (13.3 mM) and TEA (28.7 mM) at 350 nm. Conversion of **44** and yield of 1-octanol represented as a percent.

Table 3.1 Yield of released alcohols following 240 minutes of 350 nm irradiation as analyzed by gas chromatography.

Ether	[Ether] mM	[TEA] mM	Solvent(s)[b]	% Yield[c]
44	11.4	21.5	MeOH	91.0 ± 1.8
45[a]	2.80	5.38	MeOH	82.3 ± 1.6
46	8.99	26.9	MeOH/1,4-Dioxane (25%)	92.2 ± 1.6
47	11.8	21.5	MeOH/1,4-Dioxane (12.5%)	31.6 ± 0.6
48	11.9	21.5	MeOH/1,4-Dioxane (12.5%)	82.3 ± 3.6
49	7.24	17.9	MeOH/1,4-Dioxane (25%)	63.7 ± 1.7
50	5.75	17.9	MeOH/1,4-Dioxane (25%)	77.4 ± 5.1

[a] 25 minute photolysis. Analyzed by HPLC. [b] 1,4-dioxane added to help solubilize ether at concentrations used. [c] photolysis reactions were performed in triplicate under anaerobic conditions.

As shown in Figure 3.8, the release of 1-octanol is nearly quantitative after 4 hours in the presence of TEA. In order to gain better insight into the effect solvation and donors may play in this photochemical deprotection, octyl ether **44** was photolyzed under a myriad of different reaction conditions. It is important to note that the results outlined in Table 3.2 represent photolyses carried out at modest conversion of the starting ether (~70% under standard conditions) so that changes in yields or photolysis rates would be more apparent. All of the yields are reported in triplicate and are relative to the conditions that garnered the best release shown in the first entry.

Table 3.2 Relative yields of 1-octanol in the 60-minute photolysis at 350 nm of **44** and a donor in various solvents.

[44] mM	Donor	[Donor] mM	Solvent	Relative Yield[c]
11.3	TEA	28.7	MeOH	1.00 ± 0.030
11.3	TEA	14.3	MeOH	0.98 ± 0.020
11.3	TEA	5.65	MeOH	0.84 ± 0.054
10.4[a]	TEA	27.0	MeOH	0.38 ± 0.0064
10.4[b]	DMA	28.4	MeOH	0.40 ± 0.0081
10.4	DBU	29.5	MeOH	0.64 ± 0.033
10.4	Anisole	27.3	MeOH	0.79 ± 0.066
10.8	TEA	28.7	1,4-Dioxane	0.63 ± 0.017
11.0	TPA	28.7	1,4-Dioxane	0.37 ± 0.023
11.8	TEA	28.7	MeCN	0.98 ± 0.098
10.9	TEA	28.7	Benzene	0.52 ± 0.016
10.0	TEA	32.6	*tert*-BuOH	0.59 ± 0.014

[a] purged with O_2. [b] average of 2 runs, peaks of donor and ROH not well resolved.
[c] photolysis reactions were performed in triplicate under anaerobic conditions and yields reported are relative to entry 1.

Table 3.2 illustrates the results of one hour photolyses of octyl ether **44** under various electron transfer conditions. The best yields are acquired in polar solvents and increasing the concentration of the donor above ca. 15 mM had no significant effect on the yield or efficiency. Two aryl amine donors were probed, *N,N*-dimethylamine (DMA) and *N,N,N'*-triphenylamine (TPA) and both resulted in lower yields. We attribute these lower yields, as is with anisole, to competing light absorption in the 300–380 nm range (Figure 3.9) between the PTO–ether and the aryl amine. While excited state aryl amines should be able to reduce the PTO–ether, under these conditions it would be expected to be of lower efficiency due to the short singlet lifetime of the donors. A bridgehead amine, 1,8-diazabicyclo[5.4.0]undec-7-ene (DBU), was also examined to determine the importance of secondary proton transfers from the oxidized donor. The bicyclic structure of this amine prevents proton transfer from the cation radical and the lower yield reported in Table 3.2 suggests that this process may play a role in secondary proton transfer to the PTO group and/or the released alkoxide anion. Finally, product yields can be inhibited from the addition of a triplet state quencher. Purging the photolysis solution with O_2 results in a lower efficiency of the deprotection process and this is attributed to the competition of the PET process and excited state triplet quenching with ground state oxygen. This will be elaborated on further in section 3.6 covering laser spectroscopy studies.

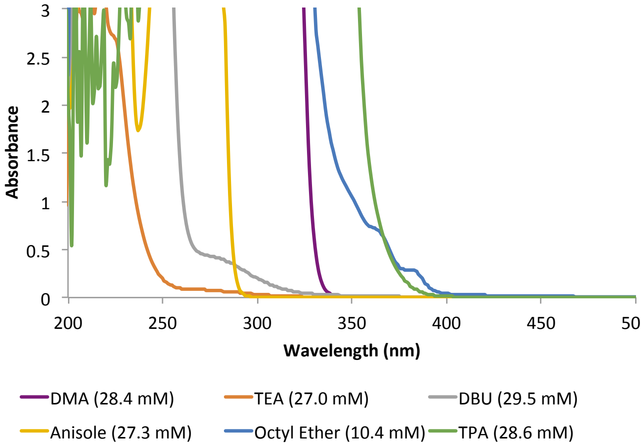

Figure 3.9 Absorption spectra of PTO-ether **44** and various donors at concentrations used in the preparative photolysis results witnessed in Tables 3.1 and 3.2.

3.5 Photodeprotection Using Visible Light

In the previous section it was demonstrated that alcohol release could be cleanly afforded under UV irradiation in the presence of an external donor. This suggests that reduction of the PTO group to the anion radical intermediate is sufficient to provide C–O bond scission for deprotection. Thus, it was postulated that this photochemical process could be initiated with visible light using a mediated electron transfer process as outlined in Scheme 3.5. Therefore, instead of using UV light to direct excite the PTO group, *fac*-(tris-(2,2'-phenylpyridine))iridium(III) (Figure 3.10), commonly referred to as *fac*-Ir(ppy)$_3$ is used as a visible light absorbing photocatalyst. The following photolysis experiments were conducted using a 1-watt, 447 nm, CW diode laser or a 16-bulb, 419 nm, 35-watt rayonet reactor. As seen in Figure 3.11, in the presence of TEA, a photolysis mixture of octyl ether **44** and *fac*-Ir(ppy)$_3$ results in the formation of 1-octanol in ca. 50% yield after 12 hours of irradiation using the 419 nm Rayonet reactor. The same deprotection yield can be realized using the 447 nm laser with photolysis time decreasing to 150 minutes. Here, excitation of *fac*-Ir(ppy)$_3$ followed by electron transfer from TEA generates a strong reducing reagent (Ir(III)/Ir(II) = -2.19 V vs. SCE)[41] that is able to transfer an electron from Ir^{2+} to the PTO chromophore.

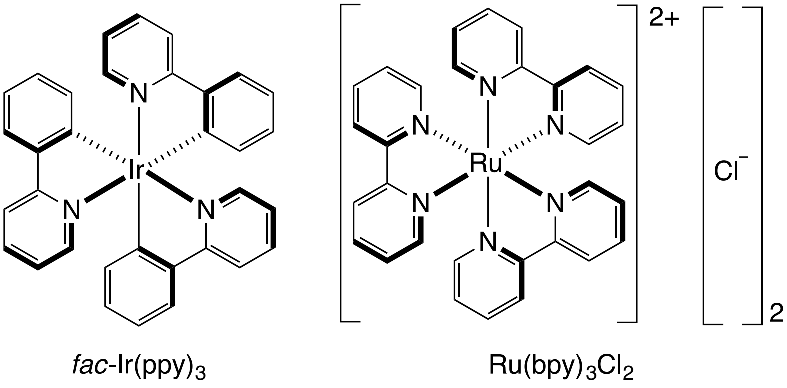

Figure 3.10 Visible light photocatalysts used in the deprotection of alcohols from PTO–ethers.

Without the presence of a donor the reaction should still be able to proceed as the excited state of *fac*-Ir(ppy)$_3$ is a fairly strong reducing agent as well ((Ir(IV)/Ir(III)*) = -1.73 V vs. SCE)[41], having demonstrated that it can reduce alkyl halides to initiate free radical reactions, it should be able to reduce the ground state PTO chromophore ($E_{red} \approx$ -

1.30 V vs. Ag/AgCl)[16]. As shown in Figure 3.11, irradiation of the photocatalyst in the presence of octyl ether **44** without the presence of TEA did not result in the formation of 1-octanol or any noticeable conversion of the starting ether as measured by gas chromatography. However, provided the sub-stoichiometric amount of photocatalyst relative to the PTO–ether (~200 µM : ~10 mM respectively) the formation of any 1-octanol is presumably below the detection limit. While reports of iridium photocatalysts have demonstrated their use in both oxidative and reductive quenching mechanisms, it is unclear at this time whether our current system falls into the former or the latter given that both the excited state of *fac*-Ir(ppy)$_3$ and the reduced form of the photocatalyst should be able to transfer an electron to the PTO–ethers. Regardless, the need for the inclusion of TEA in the photolysis solution for the regeneration of the photocatalyst or the mediated electron transfer process is apparent. A proposed mechanism for visible light mediated deprotection can be found in section 3.7.

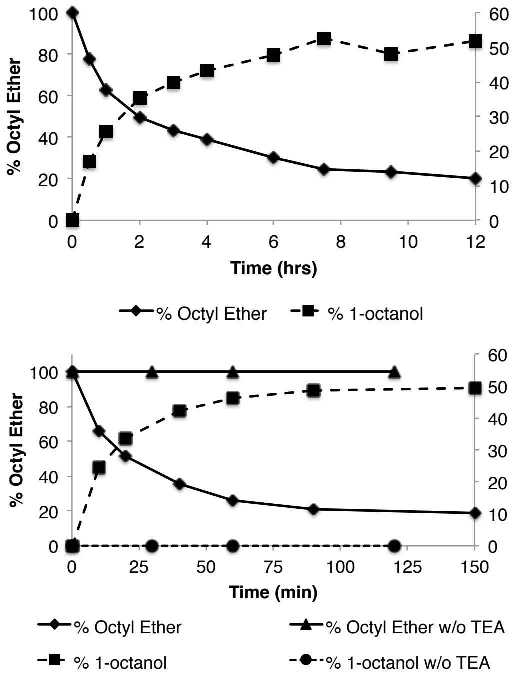

Figure 3.11 Photolysis of octyl ether **44** (~10 mM), TEA (~93 mM) and *fac*-Ir(ppy)$_3$ (~200 µM) using 419 nm rayonet reactor (top) and 447 nm laser (bottom).

Visible light deprotection of octyl ether **44** was also performed using the well studied and popular photocatalyst tris(bipyridine)ruthenium(II) chloride, commonly referred to by its shorthand notation $[Ru(bpy)_3]Cl_2$. While the excited state of $[Ru(bpy)_3]Cl_2$ (Ru(III)/R(II)* = -0.81 V vs. SCE) is not sufficient to reduce the PTO–ethers, formation of the stronger reducing agent (Ru^+) via electron transfer from TEA (Ru(I)/R(II) = -1.33 V vs. SCE) should be able to mediate an electron transfer to ethers **44-50**.[42] The results summarized in Figure 3.12 are consistent with this proposal as a solution containing $[Ru(bpy)_3]Cl_2$, 3'-O-acetylthymidine PTO–ether **45**, and TEA was irradiated using the same 447 nm light source as noted above and the released nucleoside was produced in a similarly moderate yield of ~42% yield with nearly quantitative conversion of the starting ether. As is consistent with above, control photolyses on solutions lacking either the photocatalyst or TEA showed no discernable conversion of the PTO–ether or yield of alcohol. The red-shifted absorbance spectrum of $[Ru(bpy)_3]Cl_2$ in comparison to *fac*-$Ir(ppy)_3$ allowed for monitoring the photocatalyst during the photolysis reaction. Over the course of the reaction a decrease in the absorption spectrum associated with the $[Ru(bpy)_3]Cl_2$ photocatalyst could be observed suggesting degradation of the species. Thus, this degradation of the photocatalyst could explain why only moderate yields of alcohol could be obtained under both the visible light conditions stated above.

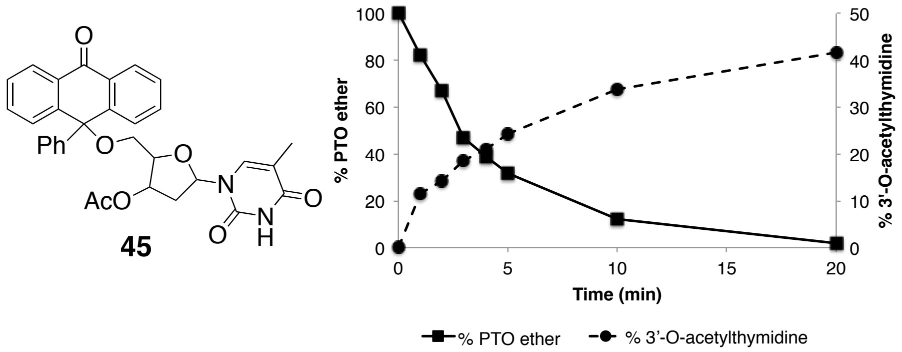

Figure 3.12 Photolysis of nucleoside ether **45** (0.832 mM), TEA (0.108 mM) and $[Ru(bpy)_3]Cl_2$ (2.11 mM) using 447 nm laser. Analysis by HPLC.

3.6 Laser Flash Photolysis Studies

Laser flash photolysis (LFP) is a technique that allows for the observation of transient intermediates that have lifetimes longer than the duration of the laser pulse.[43,44] This technique is especially useful for the characterization of short-lived excited state and radical ion intermediates. This method was used to probe for such intermediates in the UV deprotection of PTO–ethers in the presence of TEA. The results, as well as a proposed mechanism will be discussed below, but first a description of how the following experiments were conducted by LFP will be discussed.

The following LFP results were acquired using a laser set up as outline in Figure 3.13. The excitation source used is a neodymium-doped yttrium aluminum garnet ($Nd:Y_3Al_5O_{12}$, Nd:YAG) laser with an excitation wavelength of 355 nm and a pulse width of 4–6 nanoseconds. The probe beam, which provides a continuous broad spectrum of light and used to generate the absorption spectrum of transient intermediates, is a 350 W xenon-arc lamp. A shutter is placed in front of the probe beam to control the light output before and after the laser pulse in order to minimize sample decomposition from excessive exposure to the light source. This beam is focused by the passage through two lenses before exposure to the monochromator when the signal is amplified by a PMT, detected by the oscilloscope and converted to an output spectrum by computer software. To minimize light scattering from the laser to the monochromator, the probe and laser beam are set up for perpendicular analysis of the sample. Finally, a cylindrical lens is used in front of the cuvette sample to help distribute the laser beam evenly across the front of the cuvette sample, the purpose of which is to prevent re-excitation of the excited state compound in solution.

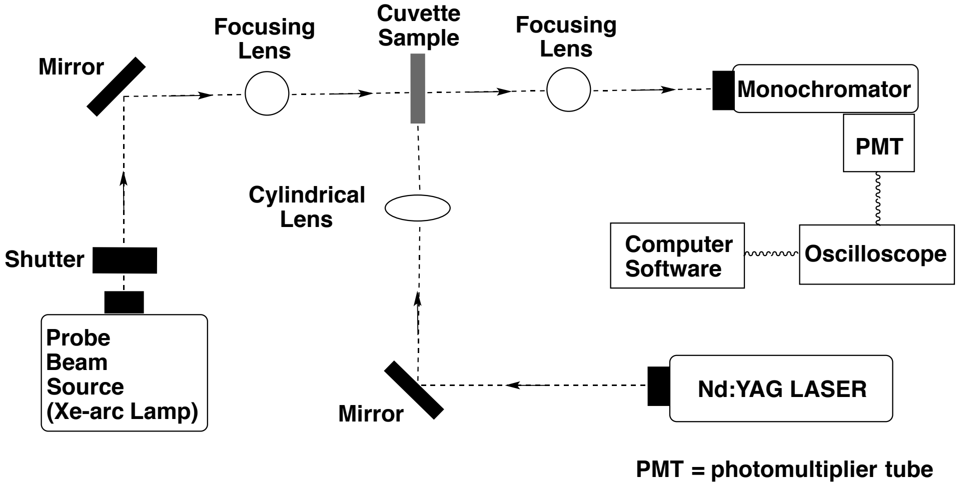

Figure 3.13 Laser flash photolysis apparatus layout.

Transient spectra like those shown in Figures 3.14-16 are a result of changes in voltage over time as monitored by the oscilloscope after the laser pulse generated by a specific probe wavelength, to which is then converted to change in optical density (ΔOD). A positive optical density refers to an absorbance increase from the ground state absorbing species and formation of a transient species, while a negative optical density refers to a decrease in the ground state absorbing species. Waveforms collected at various wavelengths are used to generate a transient absorption spectrum. These spectra can then be compared to previous literature results and short-lived intermediates can be identified in the photolysis solution. Measuring the decay kinetics for each waveform at a specific wavelength provides insight into the lifetime of the transient and whether the rate can be affected by external quenchers like electron donors or acceptors and triplet state quenchers like ground state oxygen.

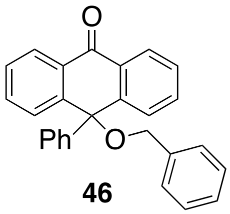

46

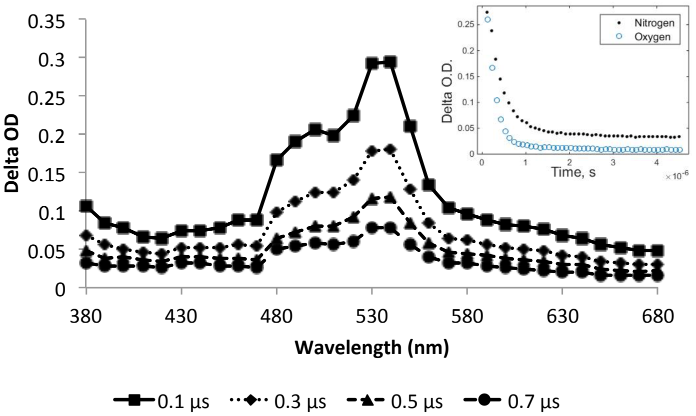

Figure 3.14 Transient absorption spectrum of benzyl ether **46** in benzene with decay profile monitored at 530 nm under N_2 and O_2.

Figure 3.14 displays the transient absorption spectrum at various times following pulsed laser excitation of benzyl ether **46**. The experiment was conducted in neat benzene, which is considered to be an inert solvent with hydrogen atom transfer from the solvent to aryl carbonyl compounds being a minor pathway in structurally similar compounds like benzophenone.[45,46] Under these conditions a short-lived band with λ_{max} = 540 nm appears immediately following the nanosecond laser pulse. This species decays in a first-order manner with a rate constant of 2.63×10^6 s^{-1} and is quenched upon the addition of oxygen, yielding an increased decay rate constant of 4.87×10^6 s^{-1}. The transient species observed under these conditions looks and behaves similar to the structurally comparable excited triplet state of benzophenone.[47] Therefore, it was expected that the observed transient under these conditions is the triplet state of the PTO group.

When a similar experiment is conducted with the inclusion of TEA as an electron donor, two new transient species are formed. Shown in Figure 3.15 is the transient absorption spectrum of ether **46** following laser pulsed excitation at 350 nm in acetonitrile. One of the new species is a broad band with an indistinct peak around 620 nm while the other is a sharper feature at 530 nm. The broad band decays rapidly, leaving the longer-lived 530 nm transient. The transient intermediate responsible for the broad band at 620 nm decays in a bi-exponential manner, a rapid phase of 4.03 x 10^5 s^{-1} and a slower phase of 4.75 x 10^4 s^{-1}. This behavior is characteristic of what has been observed for benzophenone in the presence of amine donors.[48,49] In that instance, the anion radical decays by protonation forming the neutral ketyl radical with a transient absorption maximum around 530 nm. Based on this precedence we attributed the broad band at 620 nm to the PTO anion radical **51** and the 530 nm peak to the neutral ketyl radical intermediate **52**. Though the 530 nm peak overlaps significantly with the signal assigned to the PTO triplet state, the two can be readily distinguished by their lifetimes, the latter having the faster decay rate.

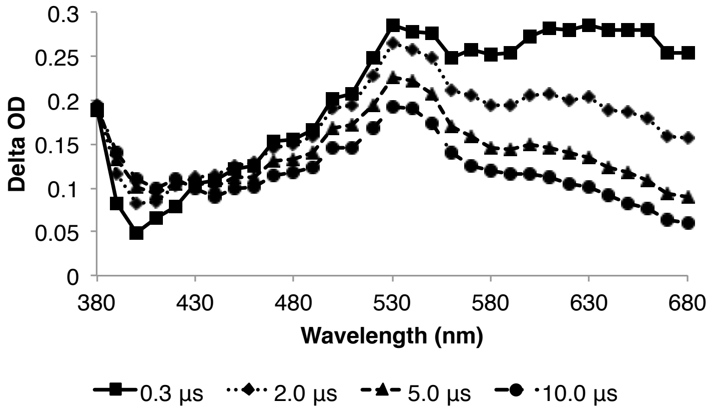

Figure 3.15 Transient absorption spectrum of benzyl ether **46** in MeCN with TEA under N_2.

Following the decay of the broad band at 620 nm and subsequent 530 nm peak assigned to the ketyl radical, additional transient absorptions in the 370–420 and 470–520 nm regions can be observed (Figure 3.16). These persist, without detectable decay for

>0.5 ms following the laser pulse. Long-lived radicals in similar structure to the tritylonyl radical **53** predicted to form in the proposed photochemical release of alcohols from the PTO group are known to have characteristic sharp peaks ca. 360 nm[50,51] consistent with what is observed in Figure 3.16. Additionally, the signals at 360, 440 and 540 nm see an increase in the decay kinetics when the sample is exposed to oxygen suggesting that the intermediate(s) associated with these peaks are not consistent with the formation of a tritylonyl cation.

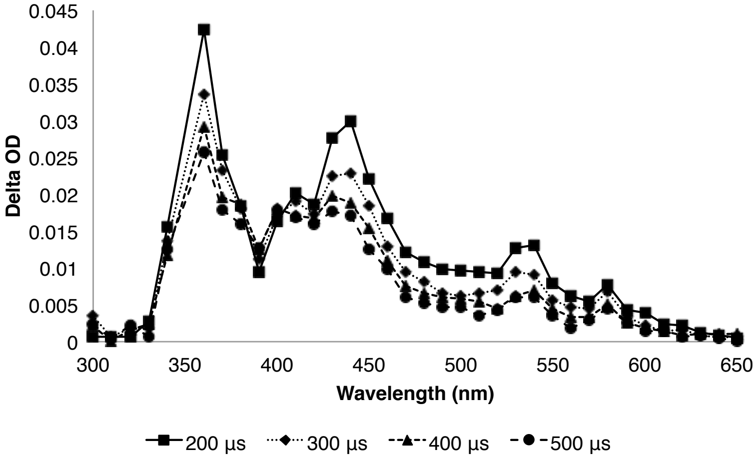

Figure 3.16 Transient absorption spectrum of benzyl ether **46** in MeCN with TEA under N_2 at long time scales.

3.7 Proposed Mechanism of Release

The experiments described above provide support for the proposed mechanism outlined in Scheme 3.5. Under direct excitation (350 nm) of the PTO–ether in the presence of electron donors, the excited triplet state of the PTO chromophore is reduced to the anion radical intermediate **51**, while protonation of this species leads to ketyl radical **52**. The latter results in release of the alcohol on a timescale of ca. 20 microseconds. Deprotection using visible light (419 or 447 nm) occurs through the use of an excited state photocatalyst. Here, the same radical anion and ketyl intermediates are presumed to form, though this comes from mediated electron transfer by the reduced excited state photocatalyst or from direct electron transfer from excited state *fac*-Ir(ppy)$_3$. Several details of the mechanism such as whether the C–O bond scission releases the alkoxide or if it is coupled to a proton transfer and whether it is released via the ketyl radical or anion radical have not been established at this time.

Scheme 3.5 Proposed mechanism for the release of alcohols under (a) direct UV irradiation, (b) oxidative and (c) reductive visible light irradiation.

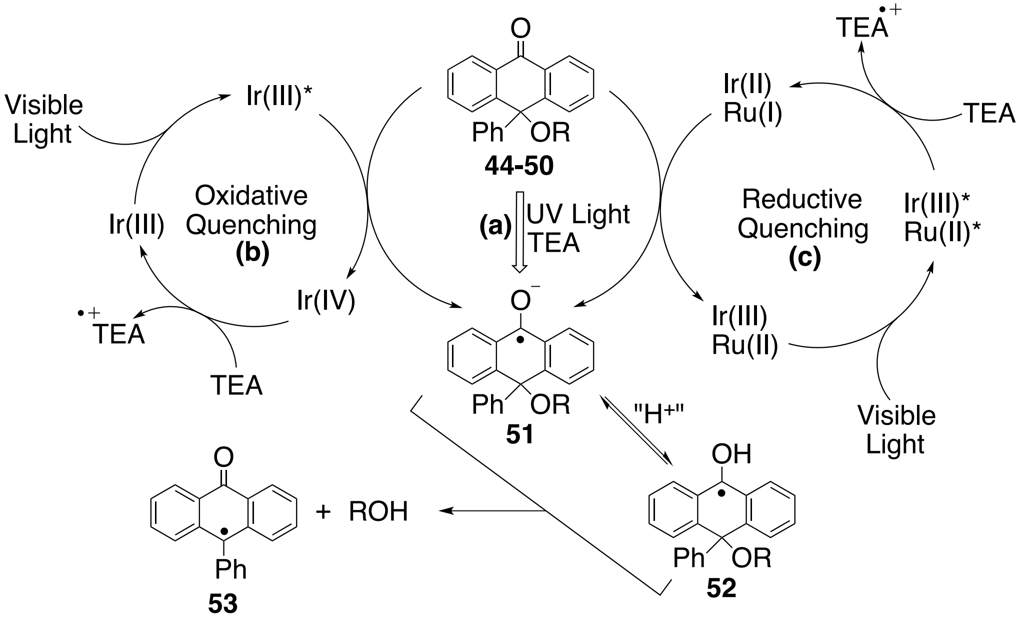

3.8 Conclusions and Future Research Directions

In this chapter a new photoremovable protecting group for primary and secondary alcohols was introduced. While previous studies have looked at the use of the PTO group for the deprotection of alcohols through chemical and electrolytic methods, the above experiments have established some of the photochemistry associated with this protecting group. Synthesis of protected alcohols is carried out in a facile one step acid catalyzed condensation reaction and subsequent release of the alcohols can be afforded using either UV or visible light in good yields. Laser flash photolysis results aided in the proposal of a release mechanism in which both an anion radical and ketyl radical intermediate were established. Further long-lived intermediates are consistent with a stable tritylonyl radical intermediate, though future work should be done to clearly establish this photochemical by-product.

Much work in the literature has been done on the deprotection of alcohols via a carbonate ester linker that lead to slower deprotection times. In this system proposed above, the direct release of alcohols is done without such a linker leading to faster release times (~20 microseconds). Future work on the visible light deprotection of alcohols is currently under investigation through the use of a charge transfer complex system. A charge transfer complex is when charge is transferred between two entities that are part of a larger molecule. This process results in a red shifted absorbance spectrum as opposed to if the two entities were independently studied. Recently, this has been demonstrated by the deprotection of carboxylic acids from *N*-alkylpicolinium idodide esters.[52] Such a system would allow for visible light deprotection of alcohols in a more controlled unimolecular process and may lead to even faster deprotection rates.

Scheme 3.6 Synthesis of 9-hydroxyphenyl-9-tritylone ether **54**

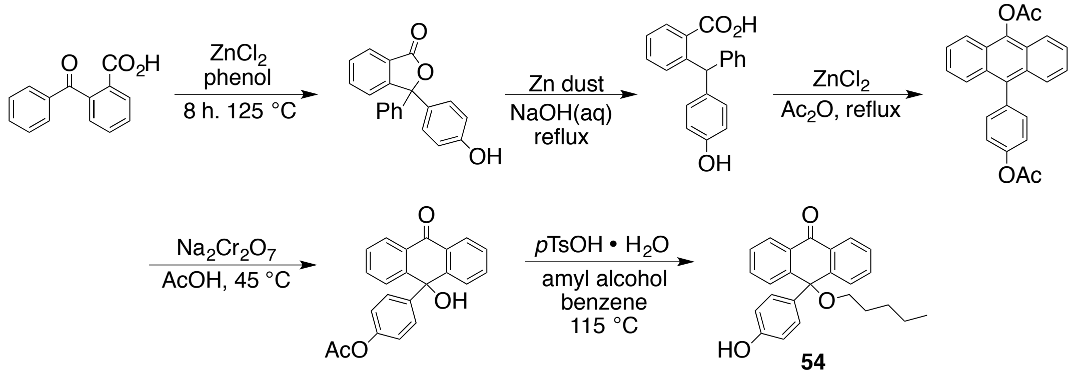

The synthesis of compound **54** is shown in Scheme 3.6. It was postulated that the deprotonation of the phenolic hydroxyl group would serve two purposes. First, it may aid in the application for the release of alcohols in aqueous media and second, the formation of a charge transfer complex would allow for direct deprotection at wavelengths >400 nm. While initial studies indicate that the amyl ether **54** is not soluble in a pH > 7 solution, solvation in 1,4-dioxane with subsequent addition of alkaline water cause the solution to go from clear to yellow, in which a new absorbance band occurs at >400 nm (Figure 3.17). Additionally, the formation of this new band does not result in the release of amyl alcohol as monitored by ^{1}H NMR. However, extended photolysis of this solution (8+ hrs, 350 nm) resulted in minimal release of the alcohol supporting evidence for an inefficient photochemical deprotection process. One such problem with the system could be a small amount of triplet formation if intramolecular electron transfer competes efficiently. Thus, the resulting singlet state could relax back to the ground state efficiently, essentially creating heat in the process. Further work will be done to characterize intermediates by LFP in an attempt to improve the deprotection yield. LFP studies will also be conducted in the mediated electron transfer mechanism using the aforementioned visible light absorbing photocatalysts in an attempt to improve upon the reported ~50% yield of deprotection. Characterization data and synthetic improvements will also be made on ether **54**.

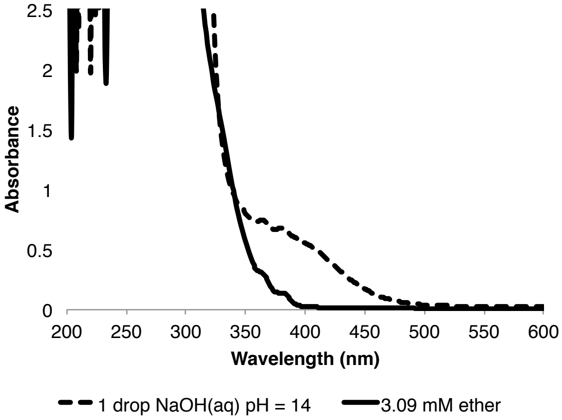

Figure 3.17 UV-Vis spectrum of ether **54** in 1,4-dioxane with and without the addition of aqueous NaOH.

CHAPTER 4. SOLVENT-DEPENDENT STABILITY OF 1,3-DIMETHYLIMIDAZOLIUM-2-CARBOXYLATE

4.1 Introduction to Carbon Dioxide Capture and Storage

Rising atmospheric levels of carbon dioxide due to anthropogenic activity is motivating concerns about raising the global temperature leading to climate change. Approximately 80% of global CO_2 emissions comes from the combustion of coal, oil and natural gas which has lead to an atmospheric concentration of ca. 400 ppm, a 24% increase since the Mauna Loa observatory in Hawaii starting recording CO_2 levels in 1958 (Figure 4.1).[1-3] In order to slow the rate of CO_2 addition to the earth's atmosphere, an ideal solution would be to transition from a global combustion society to one that meets its energy demands from a renewable and clean energy source. However, to do so would require massive changes to the way the world's economy is conducted, and thus current efforts have focused on ways to prevent CO_2 release into the atmosphere from combustion sources.

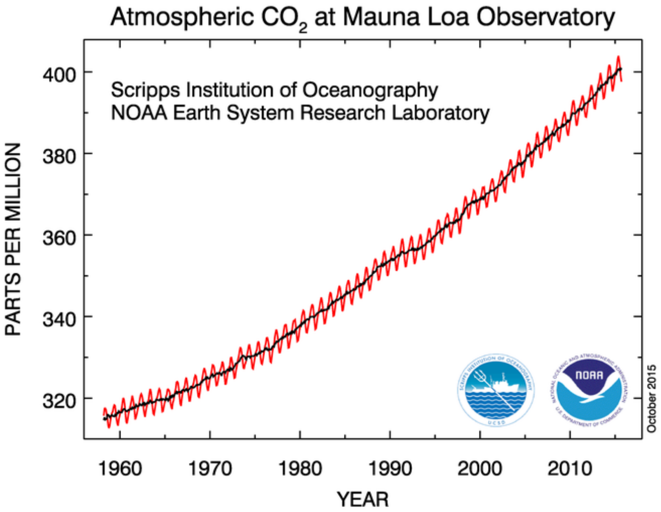

Figure 4.1 Carbon dioxide atmospheric levels as recorded at Mauna Loa, Hawaii.[2,3]

One strategy, known as carbon capture and storage/sequestration (CCS)[4,5] entails developing materials that can efficiently and selectively bind to CO_2. The bound carbon dioxide can then be stored long term or, ideally the binding process would be reversible, allowing CO_2 to be used in further chemical processes as a renewable C_1 carbon source. The development of new sequestration materials and techniques has grown considerably over the past 14 years. A simple SciFinder® search for "carbon dioxide capture" is shown in Figure 4.2. From only 3 reported hits in 2000, to almost 800 reported hits in 2014, new advancements are being rapidly researched on CO_2 mitigation to counteract this growing global concern.

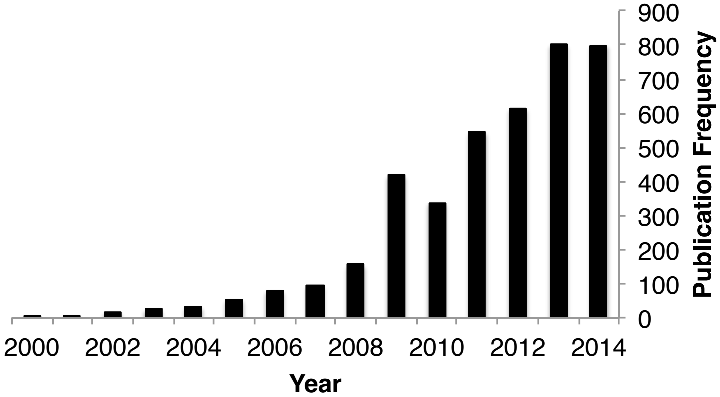

Figure 4.2 Scifinder® search results for "carbon dioxide capture" listed from 2000-2014.

One of the most commonly used capture systems is the use of aqueous alkanolamine solutions.[6-8] Here, the nucleophilic nitrogen atom adds to CO_2 generating carbamates, or in the case of tertiary amines with the addition of water, bicarbonate (Figure 4.3). The strong orbital interaction between the new carbon-nitrogen bond leads to strong binding to CO_2. The reverse reaction, release of carbon dioxide, is done by heating the solutions to elevated temperatures resulting in a significant energy barrier if there is desire to recover the captured CO_2.

A capture and storage technique that is gaining significant attention in the literature is the use of metal organic frameworks (MOFs).[9,10] A general scheme for how this system works is also depicted in Figure 4.3. MOFs are porous solid structures that consist of metal-based joints connected through organic linking groups to generate three-dimensional structures. The interesting aspect of MOFs is the greatly increased surface area for applications in gas storage. Additionally, they can be tuned to selectively bind CO_2[11] much better than alkanolamine capture systems. For instance, in the generic example below a flow of CO_2 and H_2 is passed through a metal organic framework where the CO_2 is selectively retained while the hydrogen gas passes straight through. The applicability of MOFs for use in the manufacturing industry is currently a strong topic of interest.

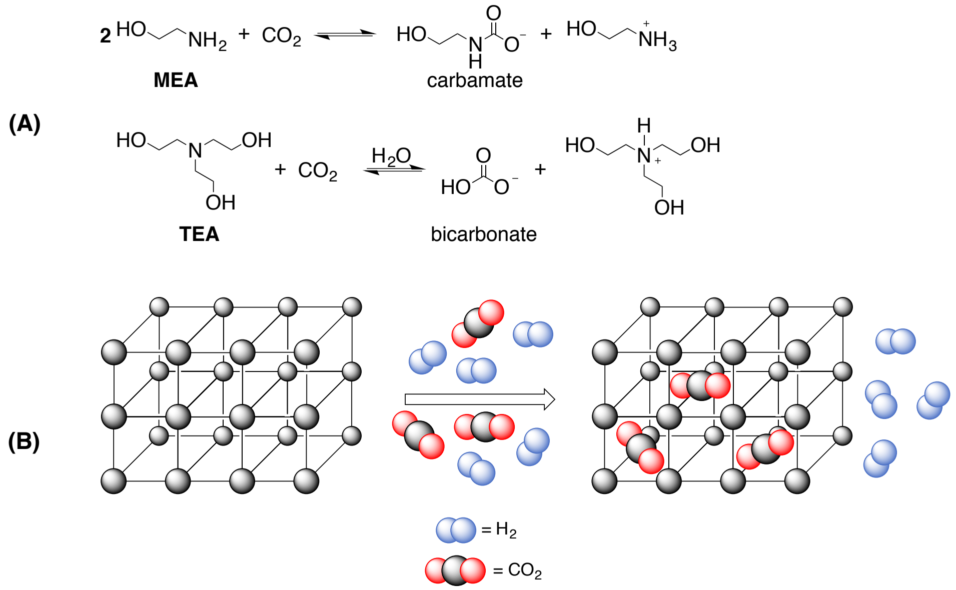

Figure 4.3 The use of (A) aqueous alkanolamine solutions and (B) metal organic frameworks for the capture of CO_2.

Frustrated Lewis pairs[12-14] and ionic liquids[15] are two other CO_2 capture and storage techniques garnering significant attention in the literature. The former are Lewis acid and base compounds that are sterically shielded from joining together to form a zwitterionic adduct. However, this steric bulk allows the activation of small molecules like CO_2. The electronegative oxygen atom binds to the Lewis acid while the more electropositive carbon is bound to the Lewis base. Mömming and coworkers[13] were able to demonstrate this concept with the use of sterically hindered phosphines and boranes as shown in Scheme 4.1. Here, the *tert*-butyl groups on the phosphine and the pentafluoro aromatic rings on the borane hinder the reactivity of this acid-base pair with each other. However, when CO_2 is added to the mixture, compound **55** was formed from the addition of the frustrated pairs to carbon dioxide. This can also be accomplished via an intramolecular cyclized addition to CO_2 to form compound **56**. More importantly though is that this process is reversible as either heating the bimolecular addition to CO_2 or cooling the unimolecular addition to CO_2 results in the generation of the starting materials.

Room temperature ionic liquids (RTILs)[15] are another interesting capture system. RTILs are classified as organic salts that are molten under ambient conditions whose properties differ from traditional organic solvents. Ionic liquids are non-volatile, thermally stable and have enhanced solubility properties for gases, particularly carbon dioxide over customary solvents. Many efforts for CO_2 capture make use of imidazolium based ionic liquids. These imidazolium salts are nitrogen containing 5 membered heterocycles with varying alkyl chains substituted on the nitrogen atoms. The counter ions for these imidazolium cations are typically weakly coordinating species like hexafluorophosphate ($^-PF_6$), tetrafluoroborate ($^-BF_4$) and bistriflimide ($^-N(CF_3SO_2)_2$). The enhanced solubility of gases like CO_2 in ionic liquids[16,17] is attributed, among others, to the increased viscosity of the solvent and the binding effects of the fluorine atoms of the counter ion to carbon dioxide. Davis and coworkers[18] took this a step further by combining RTILs and amine CO_2 capturing processes. This helped provide selectivity for CO_2 uptake in the ionic liquid and was able to demonstrate a 100-fold increase in the amount of dissolved carbon dioxide when compared to some traditional ionic liquids. A representation of this ionic liquid is shown below in Scheme 4.1.

Scheme 4.1 Use of frustrated Lewis acid base pairs (A) and ionic liquids (B) for the capture of CO_2.

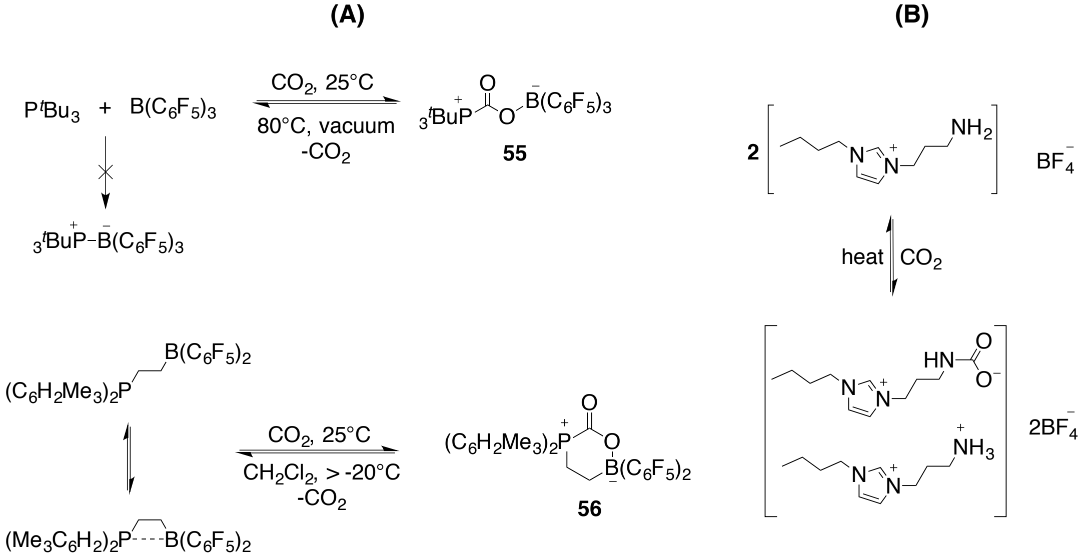

The concern of increasing levels of carbon dioxide in the earth's atmosphere is fueling the development of new chemistries that can effectively capture and store this greenhouse gas. Examples described above illustrate the enhanced solubility of this gas in ionic liquids, selective binding in metal organic frameworks and reversible formation of carbamates with CO_2 addition. In the next section, a reactive intermediate known as an *N*-heterocyclic carbene (NHC) is defined, in which was found to add to carbon dioxide to form stable compounds. We further explore NHCs ability to bind to CO_2 under various solvent conditions and assess its ability to act as an efficient carbon capture and storage method.

4.2 *N*-Heterocyclic Carbenes

Carbenes are divalent carbon centered reactive intermediates that can exist in two possible electronic states. The first, called the singlet state, is classified as having paired electron spins in an empty *p*-orbital on the divalent carbon. The second, called the triplet state, is where the electron spins are parallel to one another, unpaired, occupying orthogonal *p*-orbitals on the divalent carbon (Figure 4.4).[19,20] The preference for an electronic state can be tailored depending upon the substitution around the carbon center.[21] The addition of bulky substituents causes the carbene to adopt a more linear orientation resulting in more *p* character in the occupied sp^2 orbital. The increasing degeneracy of the orbitals favors formation of the lower energy triplet state. Less bulky or strained substituents like the cyclopropyl carbene in Figure 4.5 favor the singlet by 12.9 kcal/mol[22] while the bulky di-*tert*-butyl carbene is 5.2 kcal/mol[22,23] in favor of the triplet state.

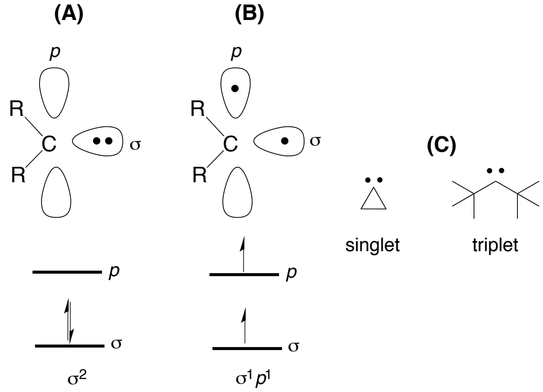

Figure 4.4 Electronic structures of carbenes (A) singlet, (B) triplet and an example of each type of carbene (C).

Electronic effects deriving from substitution around the carbene center can also have a profound effect on the electronic configuration of the carbene. Replacing alkyl substituents with π-electron donating groups (NH_2, OCH_3, etc.) has a destabilizing effect on the triplet state of the carbene. This results from electron-electron repulsion of the lone pair electrons on the substituents and the partially filled *p*-orbital of the carbene center. Thus, with electron donating substituents the singlet state electronic structure is favored. The opposite can be observed when π-electron withdrawing substituents are flanking the carbene center. Here, the *p*-orbital energy is lowered resulting in the formation of the favored triplet state.[24] Carbenes were once thought of as too reactive to isolate under ambient conditions, and could only be observed using techniques like low temperature EPR[24-26] or laser flash photolysis studies.[24,27,28] However, the development and understanding of the electronic and steric stabilization of carbenes lead to the isolation of the first air stable carbene reported in 1991 by Arduengo et al.[29] (Figure 4.5). Here, 1,3-diadamantylimidazolium chloride was treated with sodium or potassium hydride leading to the deprotonation in the 2 position generating the carbene. Both steric, in the form of the large adamantly groups and electronic, from the flanking nitrogen atoms in the imidazolium ring aided in the stabilization of the carbene. In fact, some 20 years prior, Wanzlick et al.[30,31] demonstrated that imidazolium salts could be deprotonated in the presence of a strong base though they were unable to obtain a pure stable carbene. The carbene reported by Arduengo fueled further studies of these new stable carbenes known as *N*-heterocylic carbenes (NHCs).

NHCs are carbenes containing one or more heteroatoms, typically including one nitrogen atom in the ring structure. The heteroatoms, nitrogen in the case shown in Figure 4.5 provide a "push-pull" effect on the stabilization of the NHC. The electronegative heteroatom inductively withdraws electron density from the carbene center lowering the energy of the filled sp^2 orbital. This is combined with the "pushing" effect of the lone pair electrons overlapping with the *p*-orbital favoring formation of the singlet carbene.[32]

While the bulky substituents on the nitrogen centers provide kinetic stability from the dimerization of two NHCs, further reports provided evidence to suggest that electronic factors play a greater role in *N*-heterocyclic carbenes inherent stability.[33,34]

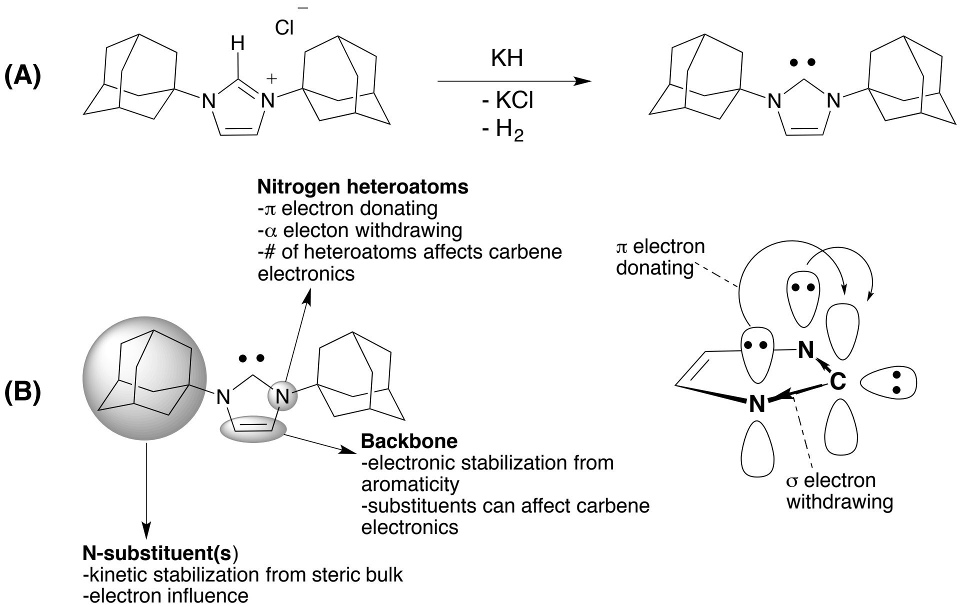

Figure 4.5 Formation of (A) the first stable crystalline carbene and (B) the electronic and steric factors for the stability of NHCs.

The most common way for the formation of NHCs is through the deprotonation of the C_2 hydrogen using a strong base ($pKa \approx 20–28$)[35,36] as shown in Figure 4.5. Not only is this a simple one step process but also many heterocyclic cations are commercially available. The synthesis of these NHC precursors can be accomplished through the condensation reaction of oxalaldehyde and formaldehyde with primary amines to generate both symmetrical and unsymmetrical imidazolium salts (Scheme 4.2) depending on the ratio of amine used. The synthesis of imidazolium cations can also be performed using imidazole as a nucleophile for the reaction with alkyl halides as well as the generation of NHCs through desulfurization of thiourea derivatives.[37,38]

Scheme 4.2 The synthesis of symmetrical (A), unsymmetrical (B) imidazolium salts and the desulfurization to form NHCs (C).

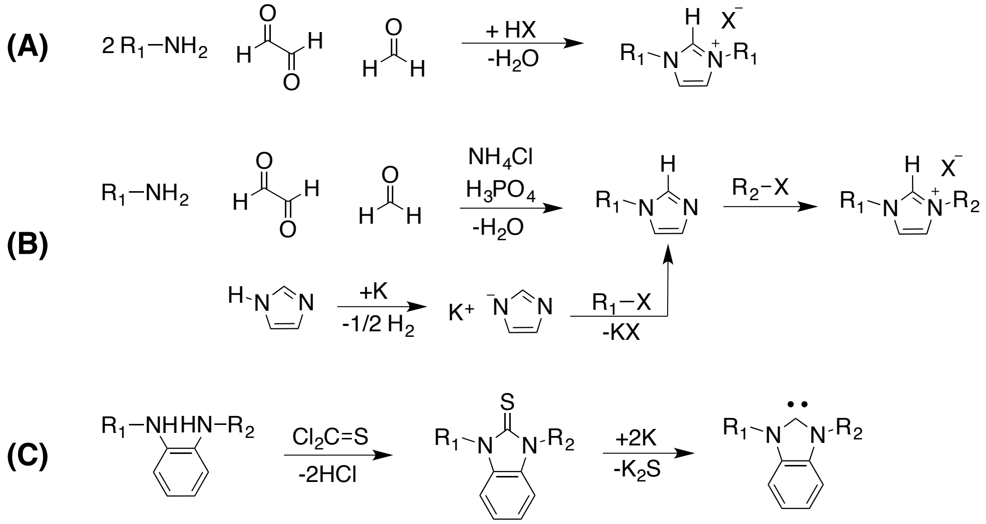

Due to the their formal *sp*^{2} character and lone pair electrons, NHCs have found applications using their singlet nucleophilic properties. This enhanced sigma donation has made NHCs widely used as ligands for transition metal catalysts.[39] For example, Chauvin, Grubbs and Schrock were awarded the Nobel Prize in chemistry in 2005 for their work in metathesis reactions that included the 2nd generation Grubbs catalyst containing an NHC.[40] They have also seen wide use as organocatalysts[41] for reactions like the benzoin condensation[42-44] and Stetter[42,45,46] reactions. Additional reports have used NHCs for transesterification/acylation reactions, Claisen rearrangements,[47] conjugate addition of alcohols,[48] and the ring opening polymerization of cyclic esters.[49] NHCs can also be used to coordinate to *p*-block elements for either stabilization or activation of molecules.[50,51] For example, NHCs can be used in conjunction with sterically hindered boranes in frustrated Lewis pair chemistry as discussed in section 4.1.[12-14] The splitting of dihydrogen as an example has been accomplished in this way. In the next section the coordination of an NHC to carbon dioxide will be discussed and experimental results look at the stability of these species.

4.3 1,3-Dialkylimidazolium-2-Carboxylates

As discussed in section 4.2, NHCs are strong sigma donors and can act as nucleophiles in the presence of electrophilic compounds. Of particular importance in this chapter is the addition of NHCs to carbon dioxide generating imidazolium-2-carboxylates. The first report of an isolation and characterization of a NHC–CO_2 came in 1999 when Kuhn and coworkers reported the successful addition of 1,3-diisopropyl-4,5-dimethylimidazolylidene to carbon dioxide generating 1,3-diisopropyl-4,5-dimethylimidazolium-2-carboxylate (Scheme 4.3).[52] These zwitterionic species have characteristic IR stretching frequencies in the mid to low 1600 cm^{-1} region corresponding to the carbonyl stretch of the CO_2 moiety.

Scheme 4.3 Addition of CO_2 to an NHC (left) and methylimidazole reacting with dimethylcarbonate (right) to generate an imidzolium-2-carboxylates.

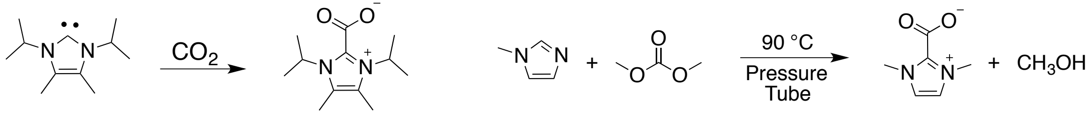

The synthesis of these species is typically performed from a starting imidazolium salt, many of which are commercially available. As alluded to previously, deprotonation at the C_2 position using a strong base leads to the NHC, with subsequent addition to carbon dioxide generating the NHC–CO_2. The challenge in the synthesis of these species is driven by the need for moisture-free conditions. The basicity of NHCs, as discussed in section 4.2, means that the addition of water or other protic species will lead to protonation rather than addition to CO_2. Holbrey et al. reported an alternative to this synthetic route in 2003 for the unexpected synthesis of 1,3-dimethylimidazolium-2-carboxylate from 1-methylimidazole and dimethylcarbonate (Scheme 4.3).[53] This reaction proceeds in a heated pressure tube, and while low to moderate yields were recovered, the synthetic process is simple, derived from cheap commercially available starting materials, provides minimal by-products and requires simple purification to obtain the pure compound. For these reasons, the focus of this chapter is on the study of 1,3-dimethylimidazolium-2-carboxylate **57**.

Since the first report of these adducts some 16 years ago, the chemistry associated with these species is rapidly expanding. Some prominent studies on these species demonstrate their use as CO_2 transfer reagents[54-57] and precursors for NHCs used in the synthesis of carbonates[58,59] and transition metal ligands.[60-62] Additionally, there have been some experimental[63,64] and computational[65] mechanistic studies performed on these species, particularly with respect to substituent effects on the imidazolium ring and its relation to the binding energy to carbon dioxide. Louie et al. showed that increasing the steric bulk of the groups bound to the nitrogen atoms leads to a lower temperature required for decarboxylation as measured by thermogravimetric analysis. Electronic effects were also found to control stability as electron-donating groups on the imidazolium ring resulted in an increased decarboxylation temperature.[66] These results were corroborated with some density functional theory (DFT) calculations performed on a variety of NHC–CO_2 in the gas phase.[65]

Imidazolium-2-carboxylates are generally poorly solubilized in organic media such as tetrahydrofuran (THF), acetonitrile and dichloromethane. Improvements on the solubility in non-polar solvents like THF can be achieved through the incorporation of hydrophobic salts such as tetraphenylborate salts.[67] In contrast to this, 1,3-dimethylimidazolium-2-carboxylate exhibits enhanced solubility in water. Though it is clear that the NHC carboxylation is a reversible process, there is some uncertainty regarding the stability of these species under various solvent conditions. For example, Crabtree and coworkers[61] report full characterization of these adducts in aqueous media but Taton et al.[63] report fast conversion of NHC–CO_2 to its corresponding imidazolium cation and hydrogen carbonate in organic solvents upon the addition of water. Thus, in order for possible future applications of NHCs as a carbon capture and storage technique, it would be important to understand the stability of these species in mixed solvent systems as it relates to the binding of carbon dioxide. In the next section, the stability of 1,3-dimethylimidazolium-2-carboxylate will be addressed under various mixed solvent systems in an attempt to understand factors leading to the instability of these adducts.

4.4 Kinetic Studies on the Decomposition of NHC–CO_2 in Solvent Mixtures

Compound **57** is indefinitely stable in H_2O and nominally dry MeCN, though decomposes in mixtures of the two. As can be seen in Figure 4.7, this compound exhibits a λ_{max} ca. 227 nm in acetonitrile with 10% v/v H_2O. Over the duration of approximately 210 minutes, this compound cleanly converts to imidazolium ion **58** with an isosbestic point and λ_{max} ca. 211 nm. The decay of **57**, monitored at 240 nm fits to an apparent first order rate law and is illustrated in Figure 4.6.

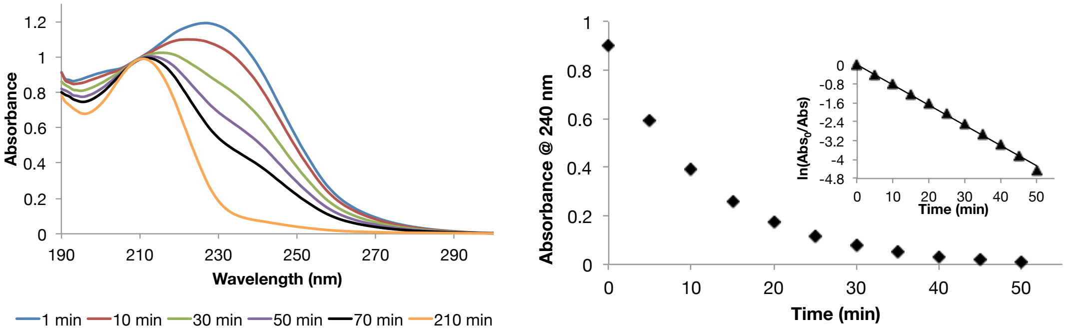

Figure 4.6 UV−Vis absorption spectrum at varying times following addition of **57** to CH_3CN with 10% H_2O (left). Time-dependent decomposition of **57** in 5% H_2O in MeCN monitored at 240 nm with the first-order rate plot (right).

This same process can be observed by ^1H NMR by monitoring the singlet corresponding to the two hydrogen atoms on the backbone of the imidazolium ring (Figure 4.7). An increase in a singlet resonance slightly downfield from **57** is observed for the formation of the imidazolium cation when done in mixtures of D_2O/CD_3CN. Under many different conditions monitored by UV-Vis, the decay of **57** follows apparent first order kinetics, though for comparison purposes rate constants of decomposition reported in this section and following sections were determined by the initial rate method. The rate constants displayed in the Table 4.1 were determined by monitoring the change in absorbance at 240 nm in mixtures of water and acetonitrile, 1,4-dioxane or methanol.

Figure 4.7 Decomposition of **57** in mixtures of $MeCN/H_2O$ as monitored by ^1H NMR.

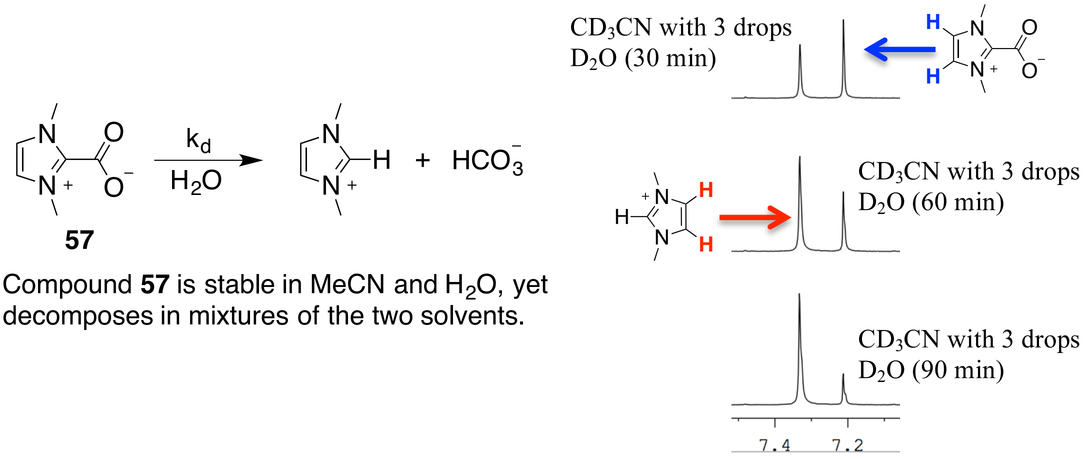

Compound **57** is stable in MeCN and H_2O, yet decomposes in mixtures of the two solvents.

Table 4.1 Decomposition rate constants (s^{-1}) for **57** in various solvent mixtures.

% H_2O	1,4-Dioxane	Acetonitrile	Methanol
3.0	$(3.32 \pm 0.09) \times 10^{-2}$	$(3.67 \pm 0.83) \times 10^{-3}$	$(1.37 \pm 0.25) \times 10^{-4}$
5.0	$(2.18 \pm 0.12) \times 10^{-2}$	$(1.04 \pm 0.25) \times 10^{-3}$	$(8.84 \pm 0.45) \times 10^{-5}$
10.0	$(3.12 \pm 0.24) \times 10^{-3}$	$(2.48 \pm 0.30) \times 10^{-4}$	$(4.00 \pm 0.42) \times 10^{-5}$
15.0	$(6.83 \pm 0.13) \times 10^{-4}$	$(9.00 \pm 0.57) \times 10^{-5}$	$(1.33 \pm 0.72) \times 10^{-5}$
20.0	$(2.57 \pm 0.17) \times 10^{-4}$	$(4.43 \pm 0.31) \times 10^{-5}$	$(6.22 \pm 0.67) \times 10^{-6}$

As can be seen in Table 4.1, increasing amounts of water in the organic solvents leads to slower decomposition rate constants. Mixtures of 1,4-dioxane/H_2O show the fastest decomposition rate constants with minimal variation above 10% H_2O, while the slowest rates can be found in mixtures of methanol and water. Thus the rate of decomposition depends upon the polarity of the solvents as more polar solvent mixtures of methanol/water stabilize **57** to a greater degree than 1,4-dioxane/water mixtures. While the data presented in Table 4.1 illustrate a clear trend for the increasing stability of **57** in more polar media, it was still unclear as to why such stability was also observed in neat acetonitrile, a solvent inherently less polar than water. In the following section, experiments are discussed in favor of a proposed mechanism of decomposition for **57**, supporting the stability of this adduct in neat acetonitrile.

4.5 Decomposition Pathway of NHC–CO_2

The decomposition of **57** leads to 1,3-dimethylimidazolium cation through the loss of CO_2 and the addition of a proton. Therefore, one possible pathway considered for the decomposition of NHC–CO_2 is a concerted decarboxylation/protonation process. This pathway would be dependent upon the strength and concentration of the proton donor in solution. In contrast to this decomposition pathway is a stepwise decarboxylation and subsequent protonation step (Scheme 4.4). This process would be expected to exhibit decomposition rates independent of the concentration or strength of the proton source. In that case, decomposition in acetonitrile would be expected to be faster than what is observed in acetonitrile/water mixtures due to the reduced solvent polarity. Additionally, the decomposition of **57** would show dependency on the amount of water or proton source in solution at low concentrations. At higher concentrations of water, the bulk polarity of the solvent would cause the rate-limiting step to be the initial decarboxylation of **57** due to the stabilizing affects of the polar solvent as observed in the rate constants provided in Table 4.1. The two decomposition processes that were considered are illustrated in Scheme 4.4 and the following four experiments provide support in favor of a stepwise decarboxylation and protonation pathway for the decomposition of imidazolium-2-carboxylates.

Scheme 4.4 Possible mechanisms for the decomposition of **57** in binary solvent mixtures.

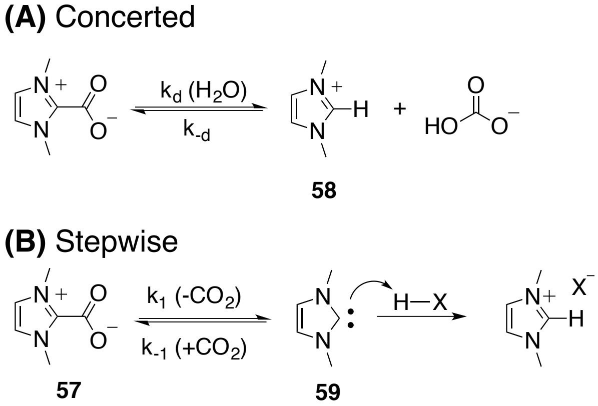
(A) Concerted

(B) Stepwise

The first experiment is exchange of isotopically labeled CO_2 into **57**. As displayed in Figure 4.8, solutions of **57** in CD_3CN were saturated with natural abundance CO_2 and isotopically labeled $^{13}CO_2$. These solutions were subjected to ^{13}C NMR and analyzed for a peak increase corresponding to the carboxylate carbon atom. As can be seen, the peak at ca. 156 ppm is attributed to the carboxylate moiety and a significant increase in the signal can be observed in spectrum (b), the solution purged with $^{13}CO_2$. This result confirms the exchange of labeled CO_2 into compound **57** and is consistent with a stepwise and reversible decomposition pathway.

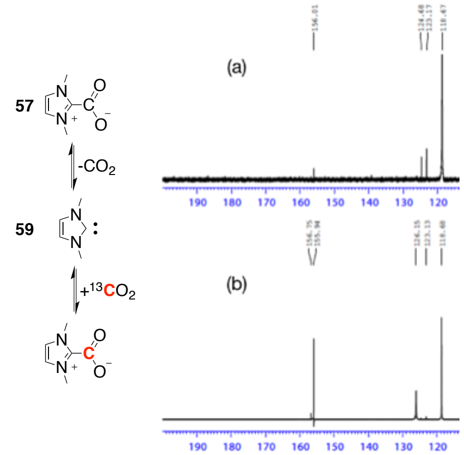

Figure 4.8 ^{13}C NMR spectra from **57** dissolved in CD_3CN after purging with (a) unlabeled CO_2 and (b) ^{13}C-labeled CO_2.

Table 4.2 Decomposition rate constants (s^{-1}) for **57** in various solvent mixtures purged with CO_2.

% H_2O	1,4-Dioxane	Acetonitrile	Methanol
5.0	$(1.94 \pm 0.07) \times 10^{-2}$	$(8.14 \pm 0.23) \times 10^{-4}$	$(6.60 \pm 0.20) \times 10^{-5}$
5.0[a]	$(2.18 \pm 0.12) \times 10^{-2}$	$(1.04 \pm 0.25) \times 10^{-3}$	$(8.84 \pm 0.45) \times 10^{-5}$
10.0	$(2.05 \pm 0.15) \times 10^{-3}$	$(1.87 \pm 0.05) \times 10^{-4}$	$(3.03 \pm 0.38) \times 10^{-5}$
10.0[a]	$(3.12 \pm 0.24) \times 10^{-3}$	$(2.48 \pm 0.30) \times 10^{-4}$	$(4.00 \pm 0.42) \times 10^{-5}$
15.0	$(6.31 \pm 0.50) \times 10^{-4}$	$(8.16 \pm 0.51) \times 10^{-5}$	$(1.28 \pm 0.12) \times 10^{-5}$
15.0[a]	$(6.83 \pm 0.13) \times 10^{-4}$	$(9.00 \pm 0.57) \times 10^{-5}$	$(1.33 \pm 0.72) \times 10^{-5}$

[a] values in red are reproduced from Table 4.1 in sample that were not purged with CO_2.

The second experiment was designed to probe whether increasing the concentration of CO_2 in solution could inhibit the decomposition of **57**. Specifically, solutions of **57** were purged with carbon dioxide and their decomposition was monitored by UV-Vis in a similar fashion as described above. The rate constants displayed in Table 4.2 were compared with those in Table 4.1. In each organic/water mixture from 5–10%, there was a consistent but modest decrease in the rate constants for the solutions purged with CO_2. Mechanism (A) in Scheme 4.4 would not show a dependency on the concentration of CO_2 in solution for the initial rate constants experimentally determined and thus provides additional evidence in support of the reversible step-wise pathway.

Irreversible decarboxylation and protonation of **57** would be expected to show identical decomposition rate constants whether the polar component is H_2O or D_2O. However, in a concerted decarboxylation/protonation decomposition process, a primary kinetic isotope effect should be observed. The reversible step-wise decomposition pathway would be expected to show an isotope effect at low water concentrations where proton/deuterium transfer from the solvent is rate limiting, while at high water concentrations where decarboxylation is rate-limiting the isotope should reduce to almost non-existent. This is what is observed for **57** when comparing decomposition rates in mixtures of 1,4-dioxane/H_2O and 1,4-dioxane/D_2O. Illustrated in Table 4.3 are the rate constants for decomposition using D_2O. Here, a k_H/k_D of 1.33 is observed at low H_2O/D_2O concentrations (5%) where decarboxylation is rate-limiting and this diminishes to 1.08 at 20% H_2O/D_2O in 1,4-dioxane.

Table 4.3 Decomposition rate constants (s^{-1}) for **57** in 1,4-dioxane/D_2O solvent mixtures.

% H_2O/D_2O	**1,4-Dioxane**[a]	**1,4-Dioxane**[b]	**k_H/k_D**
5.0	$(2.18 \pm 0.12) \times 10^{-2}$	$(1.64 \pm 0.65) \times 10^{-2}$	1.33
10.0	$(3.12 \pm 0.24) \times 10^{-3}$	$(2.41 \pm 0.05) \times 10^{-3}$	1.29
15.0	$(6.83 \pm 0.13) \times 10^{-4}$	$(5.90 \pm 0.03) \times 10^{-4}$	1.16
20.0	$(2.57 \pm 0.17) \times 10^{-4}$	$(2.37 \pm 0.04) \times 10^{-4}$	1.08

[a] values represent using H_2O. [b] values represent using D_2O.

Lastly, partial decay of **57** can be observed in nominally anhydrous acetonitrile. A dilute solution of **57** was prepared in CH_3CN that was distilled from CaH_2 and the UV-Vis absorption at 240 nm was monitored over time. What can be observed in Figure 4.9 is an initial decomposition of **57** over the first 4 hours, which then appears to have little or no decay over the final 9 hours. This behavior is consistent with a step-wise decarboxylation/protonation pathway. Completely anhydrous CH_3CN is difficult to obtain and thus in the first 4 hours of this experiment trace amounts of H_2O in the solution is being consumed by protonation of carbene **59** after decarboxylation. Once the water is consumed the carbene is formed reversibly and there is minimal change in the concentration of **57**. Slow decomposition of **57** over the latter 9 hours in the experiment could be attributed to deprotonation of acetonitrile as Louie and coworkers have reported a similar process with a related carbene.[67]

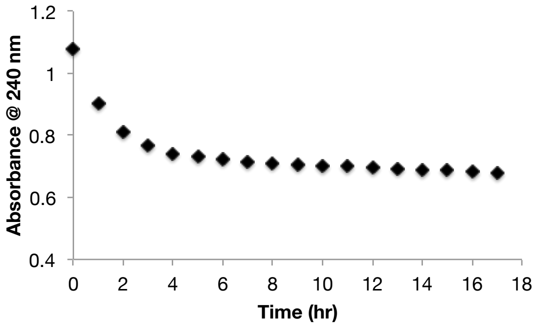

Figure 4.9 Time dependence stability of **57** (240 nm) in nominally dry CH_3CN.

The experiments described above provide evidence in support of a reversible stepwise decarboxylation and protonation decomposition pathway in aqueous binary solvent mixtures. In mixtures of low water and high organic solvent, the rate-limiting step is protonation of the carbene intermediate forming 1,3-dimethylimidazolium cation. In mixtures of higher water concentrations the rate-limiting step is decarboxylation of the imidazolium-2-carboxylate to the neutral carbene (Scheme 4.5). This helps explain the stability of **57** in aprotic media like acetonitrile, but it does not establish a clear understanding as to the stability of **57** in water and more generally, polar solvents. The next section describes computational and experimental results probing the geometric parameters of **57** that are affected by changing the solvent polarity.

(A) Low Water Concentration

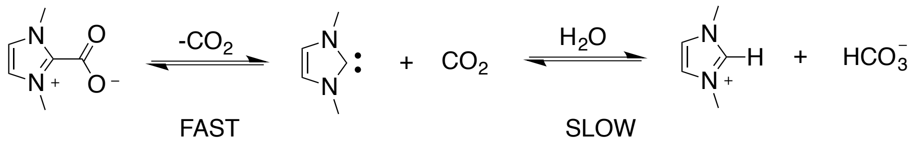

(B) High Water Concentration

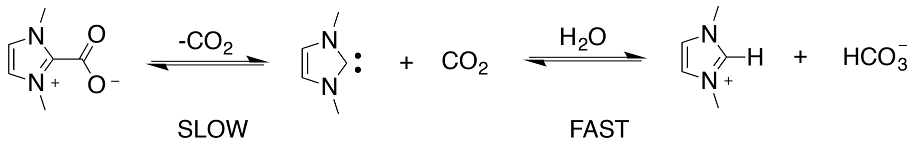

Scheme 4.5 Summary of the stability of **57** in solution of low and high water concentrations.

4.6 Computational Results, Eyring Analysis and Salt Decomposition

Upon establishing the stepwise decomposition pathway of **57**, several density functional theory (DFT) calculations were done to probe the geometric parameters and free energy of **57** in the gas phase and under several solvent conditions. For gas phase calculations, the geometry of **57** was optimized at the B3LYP/6-31G(d,p) level[68,69] and stationary points were identified as local minima or transition states by analysis of the calculated vibrational frequencies. In general, these calculations gave three stationary points: minima corresponding to structure **57**, a weakly bound molecular complex consisting of carbene **59** and CO_2 as well as a transition state connecting these two minima. The electrostatic potential maps for the previously stated structures are illustrated in Figure 4.10.

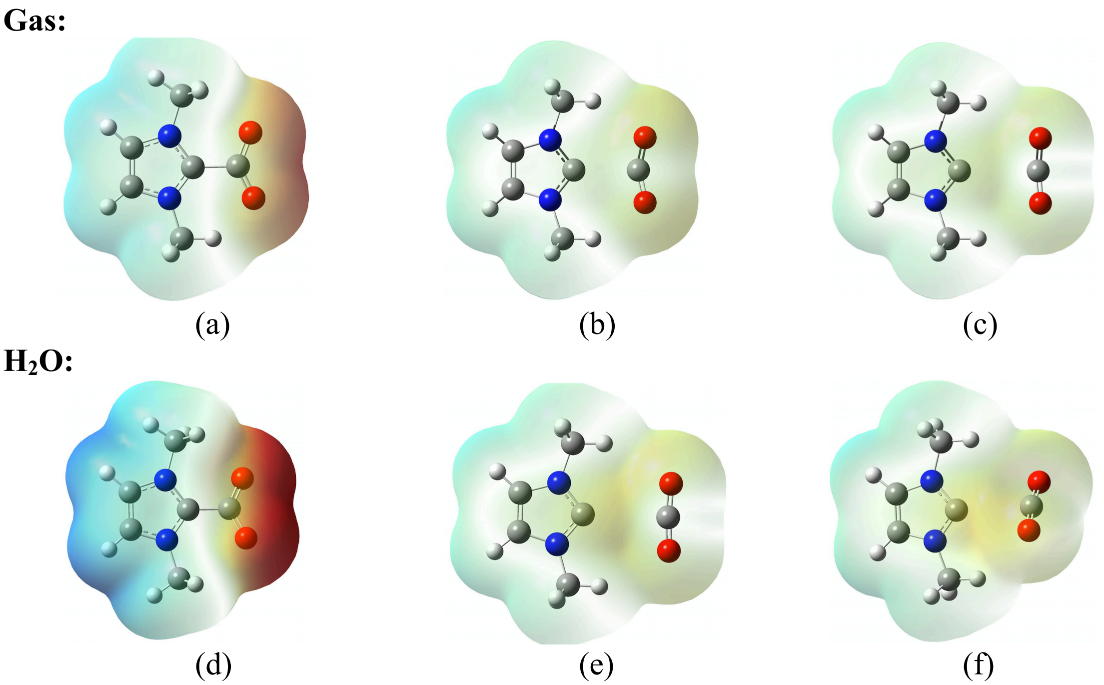

Figure 4.10 Structures derived from DFT optimizations on **57** (a,d), transition state (b,e), and **59**/CO_2 (c,f) in the gas phase (a-c) and water (d-f), as simulated using the SMD implicit solvation model. The shaded isosurfaces are representations of the molecular electrostatic potential, where dark blue denotes positive charge (+0.092) and dark red denotes negative charge (-0.092).

Absent a solvation model, these calculations show an elongated C_{NHC}–C_{CO2} carbon-carbon bond for **57** with a distance of 1.579 Å, which is ca. 3.8 kcal/mol below the complex. The corresponding transition state shows a low barrier of ca. 6.4 kcal/mol. Since it has already been well established that solvation plays a large role in the stability of **57**, it was important to identify an experimental standard that could be used to validate possible theoretical treatments of solvation models. Therefore the Gibbs free energy barrier for decomposition ($\Delta G^{\ddagger}$) of **57** was experimentally determined by fitting the temperature dependence of the decomposition rate (k_d) constants for **57** in H_2O to the Eyring equation (equation 2). The constants k_b, h, and R are the Boltzmann, Planck, and the gas constant respectively. For our purposes the transmission coefficient, κ, was assumed to be 1. Through the analysis of the experimental results illustrated in Figure

4.11, the Gibbs free energy barrier for decomposition was found to be 24.9 ± 0.28 kcal/mol. This barrier was compared to the calculated results by modeling **57**, the **59**/CO_2 complex and the transition state using various implicit solvation models. The results of these calculations are outlined in Table 4.4. The SMD implicit solvation model developed by Truhlar and Cramer[70] agreed nicely with experimental results as it predicted a barrier of 25.1 kcal/mol. Other models, like the IEF-PCM algorithm (the default model in the Gaussian 09 software) faired far worse with almost a 10 kcal/mol difference between computational and experimental results. Therefore, the SMD solvation model was used for the computational studies described below.

(Eq 2.) $$k_d = \frac{\kappa k_b T}{h} exp^{\left[\Delta G^{\ddagger}/_{RT}\right]}$$

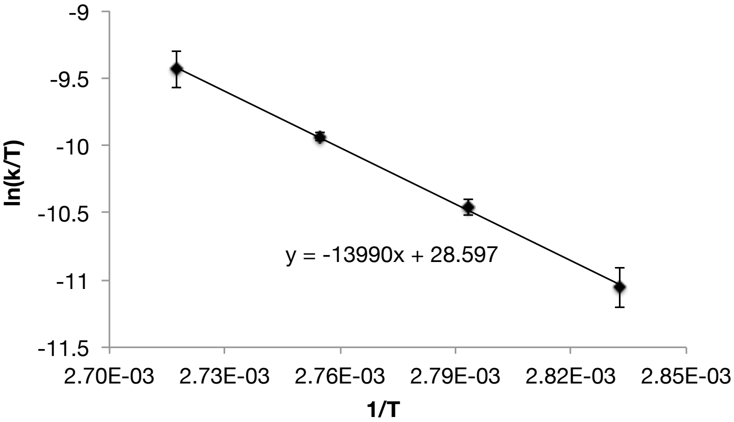

Figure 4.11 Eyring analysis of the temperature dependence (T, in K) for the decomposition rate constants for **57** (k, in s^{-1}) in H_2O.

Selected geometric parameters, dissociation free energies (ΔG^0 defined as the difference between **57** and the **59**/CO_2 complex), and activation free energies ($\Delta G^{\ddagger}$) predicted for **57** in various solvents calculated using B3LYP/6-31G(d,p)/SMD are listed in Table 4.4. Consistent with experimental data, there is a significant dependence upon solvent polarity. For example, the free energy of activation increases approximately 20 kcal/mol in going from the gas to water phases. As can be seen in Figure 4.12, there is a linear dependency between the solvent polarity and the barrier to decomposition.

Table 4.4 Comparison of computed Gibbs free energy barriers for decarboxylation of **57** using various implicit solvation models and experiment.

Model/Expt	$\Delta G^{\ddagger}$ (kcal/mol)
SMD[a]	25.1
CPCM[b]	16.1
IEF-PCM[c]	16.0
PCM[d]	16.0
Expt.	24.9 ± 0.28

[a] Ref 70. [b] Ref 71, 72. [c] Ref 73. [d] Ref 74, 75.

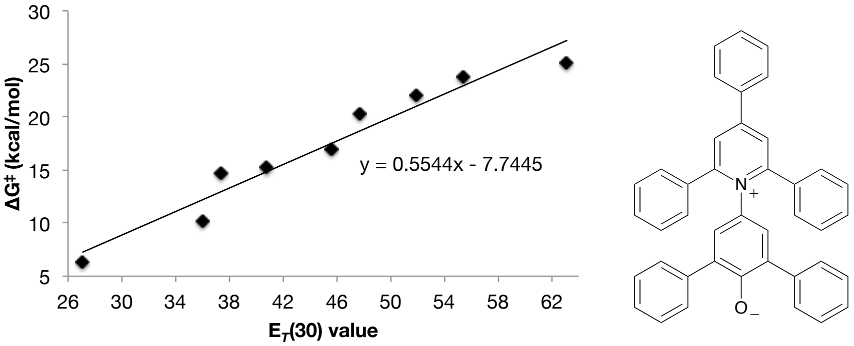

Figure 4.12 Linear free energy relationship between the calculated $\Delta G^{\ddagger}$ and Reichardt's $E_T(30)$ solvation parameter. $E_T(30)$ dye is represented on the right.

To do this, a clear definition of solvent polarity must be established. Thus, the calculated $\Delta G^{\ddagger}$ was plotted against Reichardt's $E_T(30)$ solvation parameter.[76,77] In this system, solvent polarity is defined by the shift in λ_{max} of the $E_T(30)$ dye (Figure 4.12) in different solvents. Here, water is given a solvent polarity value of 63.1 and the gas phase assigned 27.1. Seven different solvents were modeled between the gas and water phase of varying $E_T(30)$ values and the C_{NHC}–C_{CO2} bond is reflected in the change in length of the corresponding bond distance, which diminishes from 1.576 Å in the gas phase to 1.522 Å in aqueous solution. Interestingly, the dipole moment of **57** is predicted to increase, despite the shorter bond distance. It is also notable that the transition state C_{NHC}–C_{CO2} bond distances (C_{NHC}–$C_{CO2}^{\ddagger}$) tend to increase with increasing solvent polarity. This trend mirrors the product-like transition states associated with these increasingly endergonic reactions as would be expected on the basis of the Hammond postulate.

Table 4.5 Selected geometric parameters, dipole moments (D), and free energies, computed for **57** using the B3LYP/6-31G(d,p) and the SMD implicit solvation model.

Solvent	$E_T(30)$ value	C_{NHC} -C_{CO2} (Å)	CO_2 ∠ (°)	D	$\Delta G^{\ddagger}$ (kcal/mol)	C_{NHC}-C_{CO2} ‡ (Å)	ΔG^0 (kcal/mol)	$D^{\ddagger}$
Gas	27.1	1.576	133.7	9.13	6.37	2.310	3.83	5.14
1,4-Dioxane	36.0	1.568	132.0	10.3	10.2	2.438	9.26	5.17
THF	37.4	1.554	132.0	11.2	14.7	2.495	13.0	5.40
CH_2Cl_2	40.7	1.555	130.7	11.6	15.3	2.519	13.9	5.33
MeCN	45.6	1.541	131.1	12.0	17.0	2.513	14.7	5.57
1-Decanol	47.7	1.538	129.9	12.3	20.3	2.591	19.4	5.06
EtOH	51.9	1.528	129.5	13.0	22.0	2.551	21.0	5.54
MeOH	55.4	1.530	129.1	13.1	23.8	2.592	22.2	5.36
H_2O	63.1	1.522	128.8	13.4	25.1	2.792	24.4	4.59

The effect of increasing solvent polarity with respect to **57** is to favor a shorter, stronger and more polarized bond. As previously stated, this can be observed in the electrostatic potential maps in Figure 4.10. The greater charge density in water as compared to the gas phase is evident by the color saturation in the molecule where more positive character (blue) is located on the imidazolium ring and more negative character (red) is localized on the CO_2 moiety. Thus, it appears that C_{NHC}–C_{CO2} bond formation is accompanied by increasing charge transfer to the CO_2 group.

Table 4.6 Selected geometric parameters computed for **57** with cations using B3LYP/6-31G(d,p) and the SMD implicit solvation model.

Cation	C_{NHC}-C_{CO2} (Å)	CO_2 ∠ (°)
Li^+	1.508	125.8
Na^+	1.501	125.8
K^+	1.511	127.5
Mg^{2+}	1.473	120.4

Increasing the negative charge density on the CO_2 group leads to the formation of a shorter and stronger C_{NHC}–C_{CO2} bond and therefore the binding of a Lewis acid to the carboxylate group should slow the decomposition of **57**. To see if Lewis acids like metal cations would result in a decrease in the C_{NHC}–C_{CO2} bond length due to the binding to the carboxylate group, DFT calculations were performed and the results are shown in Table 4.6. In comparison to the calculations in Table 4.5 for **57** in H_2O without any metal cation, there is a substantial reduction in the C_{NHC}–C_{CO2} bond length when the carboxylate group is bound to a Lewis acid. The most considerable decrease was with magnesium dication giving a bond distance of 1.473 Å, while the alkali metals Li^+, Na^+ and K^+ all had similar bond length reductions.

The computational results outlined in Table 4.6 suggest that metal cations should slow the decomposition of **57** through the binding to the carboxylate moiety. To test this, initial rates of decomposition were obtained in mixtures of 1,4-dioxane/H_2O using various chloride salts in combination with the NHC–CO_2. The increased concentration of chloride salts necessitated higher water concentrations but a similar trend could be observed as seen in Table 4.7, that is, with higher water concentrations a slower initial decomposition rate is observed. Additionally, a decrease in rate could be observed in the 20% H_2O experiments when comparing the addition of salts versus no salts. The size of the cation (Li^+, Na^+, K^+) seemed to have little effect on the decomposition rate, which mirrors computational results that showed there was little change in the calculated C_{NHC}–C_{CO2} bond length for those ions. The effect of a counter ion however did have considerable effect on the decomposition rate as a 22% decrease in the rate could be observed with Li^+ at 20% H_2O in comparison to no added salt. This decrease was intensified when a more electropositive cation (Mg^{2+}) was used, as a 39% reduction in the decomposition of **57** was observed at 20% H_2O solutions.

Table 4.7 Initial decomposition rates (s^{-1}) of **57** in 1,4-dioxane/H_2O mixtures with chloride salts.[a]

% H_2O	**Li^+**	**Na^+**	**K^+**	**Mg^{2+}**
20.0[b]	$(2.01 \pm 0.09) \times 10^{-4}$	$(2.04 \pm 0.15) \times 10^{-4}$	$(2.00 \pm 0.04) \times 10^{-4}$	$(1.59 \pm 0.06) \times 10^{-4}$
25.0	$(9.26 \pm 0.76) \times 10^{-5}$	$(9.49 \pm 0.38) \times 10^{-5}$	$(8.66 \pm 0.32) \times 10^{-5}$	$(8.00 \pm 0.43) \times 10^{-5}$
30.0	$(4.60 \pm 0.28) \times 10^{-5}$	$(4.85 \pm 0.73) \times 10^{-5}$	$(4.51 \pm 0.37) \times 10^{-5}$	$(3.67 \pm 0.26) \times 10^{-5}$

[a] [LiCl] = 40.0 mM, [NaCl] = 40.4 mM, [KCl] = 39.8 mM, [$MgCl_2$] = 39.9 mM. [b] $(2.57 \pm 0.17) \times 10^{-4}$ was obtained in 20% H_2O in 1,4-dioxane with no metal cation from Table 4.1.

4.7 Conclusions and Future Research Directions

The experimental and computational results outlined in the preceding sections demonstrate that solvent polarity has a convincing effect on the stability of imidazolium-2-carboxylates. Evidence in support of this is provided by a decreasing decomposition rate constant for **57** in higher water concentrations of binary solvent mixtures as well as the calculated Gibbs free energy for binding of CO_2 to carbene **59** which goes from 4 kcal/mol in the gas phase to 24 kcal/mol in water. Charge transfer accompanies bond formation between NHCs and CO_2 from the carbene to the carboxylate substituent. Non-polar solvents favor longer and weaker C_{NHC}–C_{CO2} bonds while more polar solvents favor shorter and stronger C_{NHC}–C_{CO2} bonds.

The ability to modulate the binding affinity for carbon dioxide is an important goal for CO_2 capture and storage strategies. Not only is it important for the material to be able to selectively bind to carbon dioxide, but also if there is interest in reusing the CO_2 in a chemical process, it is equally important to be able to easily remove the greenhouse gas from its captor. The degree to which solvent polarity drastically affects the binding strength of NHCs to CO_2 affords the opportunity to probe further possibilities of this capture strategy.

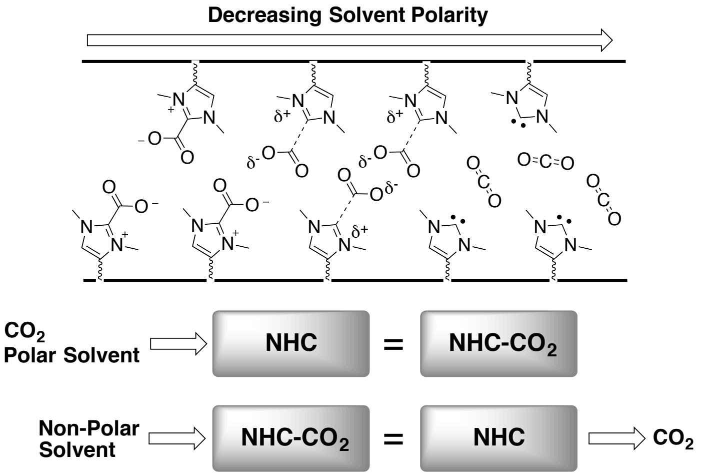

Figure 4.13 Depiction of using NHCs bound to solid support for the use of CO_2 capture and storage system.

As discussed in section 4.1, a commonly used carbon capture and storage strategy is the use of aqueous amines for the formation of carbamates. While a reversible process, carbamates must be heated to high temperatures in order to release carbon dioxide. In the system discussed in this chapter, simply changing the solvent polarity can enact this reversibility. An example of how this may be used is illustrated in Figure 4.13. A system in which NHC's are bound to a solid support where CO_2 dissolved in a polar solvent could be flowed in, affording the formation of imidazolium-2-carboxylates. A subsequent gradual decrease in the solvent polarity would lead to decarboxylation and release of carbon dioxide. Unlike that of carbamates, no heating would be required for the release of the bound CO_2.

In an attempt to identify NHCs that would be ideal for the binding to CO_2, 26 different zwitterions (mostly imidazolium-2-carboxylates) were computationally modeled and specifically probed for the C_{NHC}–C_{CO2} bond length. The sum of electronic and thermal free energies were acquired in five different media (gas, 1,4-dioxane, acetonitrile, methanol and water) of varying $E_T(30)$ values using the SMD implicit solvation model to observe how the bond lengths differ in changing solvent polarity. While it is important for the bond distance to vary greatly in going from 1,4-dioxane to water, it is equally important that the neutral NHC not be protonated in a protic environment and thus eliminating further binding to CO_2. Since the previously alluded to experimental barrier to decarboxylation agreed nicely with the B3LYP/6-31G(d,p) computational result, the NHC–CO_2 outlined in Figure 4.14 were modeled in the same way.

The C_{NHC}–C_{CO2} bond lengths for the 26 zwitterions are outlined in Table 4.8. Not surprisingly, lower $E_T(30)$ values for gas and 1,4-dioxane result in longer bond lengths while both methanol and water lead to shorter bond lengths. From these results it appears that both electronic and steric effects factor into the bond distance. An example of this can be seen in comparing **57** and **63** in water. While methyl groups lead to a bond length of 1.522 angstroms, the addition of *tert*-butyl substituents results in a 1.538 angstrom bond length. In contrast, keeping the methyl substituents consistent and adding electron withdrawing groups on the imidazolium backbone as seen in compound **80** leads to a longer bond length of 1.542 angstroms. NHC–CO_2 **74** has a large difference in bond length going from 1.583 in 1,4-dioxane to 1.537 angstroms in water. These oxazolium zwitterions might present a promising alternative to imidazolium derived CO_2 capture systems as it still binds tightly in water but should decompose faster in non-polar solvents. Coupled with a decreased pKa for oxazolium salts, research in this area may lead to water soluble NHCs that are able to reversibly bind to CO_2 without the non-productive protonation step. Additionally, there appears to be a correlation between the calculated C_{NHC}–C_{CO2} bond length and activation energy required for decarboxylation as show in Figure 4.15. The barriers of nine different NHC–CO_2 of varying bond lengths were modeled against the activation energy required for decomposition in the gas phase. Thus, bond length of the NHC–CO_2 seems to be a reasonable approximation for how tightly the CO_2 is bound to the NHC and represents a promising quick computational result for future studies in this area to validate whether certain NHC–CO_2 are sensible CO_2 capture reagents.

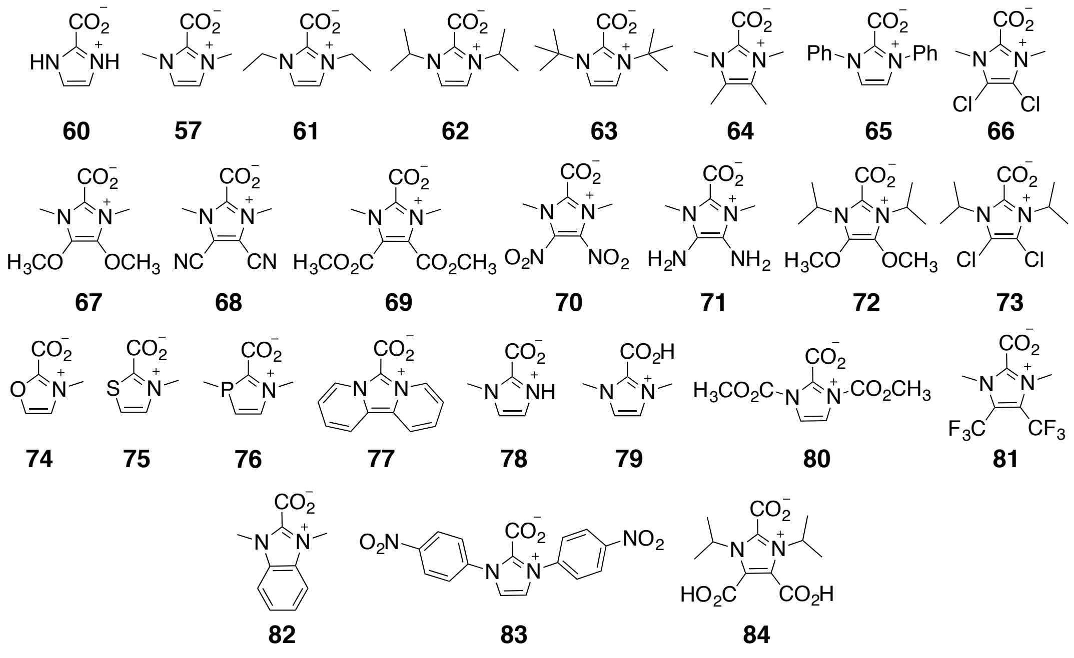

Figure 4.14 Computationally modeled NHC–CO_2

Table 4.8 DFT-B3LYP/6-31G(d,p) calculated C_{NHC}–C_{CO2} bond lengths (Å) using the SMD implicit solvation model

NHC–CO_2	**Gas**	**1,4-Dioxane**	**Acetonitrile**	**MeOH**	**Water**
60	1.552	1.544	1.533	1.518	1.515
57	1.576	1.568	1.541	1.530	1.522
61	1.570	1.559	1.544	1.529	1.526
62	1.569	1.562	1.549	1.531	1.529
63	1.564	1.553	1.554	1.540	1.538
64	1.581	1.566	1.550	1.528	1.525
65	1.568	1.562	1.553	1.541	1.539
66	1.598	1.580	1.562	1.542	1.538
67	1.579	1.566	1.548	1.523	1.520
68	1.604	1.586	1.564	1.542	1.539
69	1.592	1.574	1.559	1.540	1.537
70	1.615	1.592	1.568	1.550	1.546
71	1.579	1.563	1.547	1.528	1.523
72	1.579	1.568	1.553	1.534	1.532
73	1.590	1.576	1.562	1.544	1.541
74	1.613	1.583	1.560	1.540	1.537
75	1.585	1.569	1.555	1.542	1.539
76	1.565	1.553	1.541	1.527	1.526
77	1.553	1.541	1.524	1.505	1.501
78	1.567	1.556	1.542	1.527	1.524
79	1.503	1.497	1.492	1.490	1.488
80	1.590	1.581	1.568	1.553	1.549
81	1.592	1.576	1.561	1.546	1.542

82	1.582	1.568	1.553	1.537	1.532
83	1.570	1.565	1.558	1.545	1.542
84	1.584	1.570	1.558	1.543	1.540

As the search for new carbon dioxide capture and storage systems continues, *N*-heterocyclic carbenes remain an intriguing option due to the large variance in stability of these adducts in binary solvent mixtures. While the primary goal remains developing efficient CO_2 capture and storage reagents to prevent increased levels of this greenhouse gas in the earth's atmosphere, an ideal situation would envision using CO_2 as a renewable carbon source for the production of other chemicals and/or fuels. To do this, it would require a system that is equally efficient in removing carbon dioxide from the capture reagent. While many techniques require high-energy inputs to accomplish this, the system described above simply requires modulating solvent polarity. In the next chapter, the use of these NHCs as catalysts for the transformation of carbon dioxide into other chemicals will be discussed.

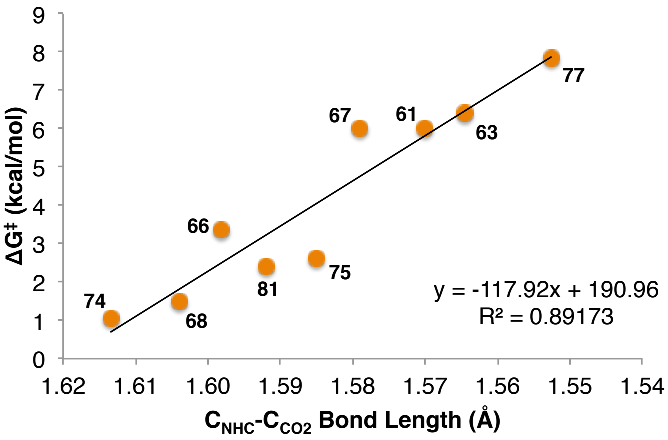

Figure 4.15 Correlation of C_{NHC}–C_{CO2} bond length and the free energy barrier to decarboxylation for select NHC–CO_2 in the gas phase

CHAPTER 5. PHOTOCHEMICAL REDUCTION OF CARBON DIOXIDE USING 1,3-DIMETHYLIMIDAZOLYLIDENE

5.1 Introduction to Carbon Dioxide Capture and Utilization

The previous chapter introduced chemical techniques that are used for carbon dioxide capture and storage/sequestration (CCS) systems. While efforts to improve CO_2 selectivity in these capture methods is a topic of current interest, there is also much desire to be able to use CO_2 as a renewable carbon source. The increasing consumption of global fuel reservoirs is driving current efforts to not only capture, but recycle, carbon dioxide as a source of providing new chemicals and/or fuels (carbon capture and utilization, CCU).[1-3] Carbon dioxide, existing as the most oxidized form of carbon, is thermodynamically and kinetically stable, meaning that a large amount of energy is required to transform it into other chemicals like formaldehyde, formic acid and methanol.

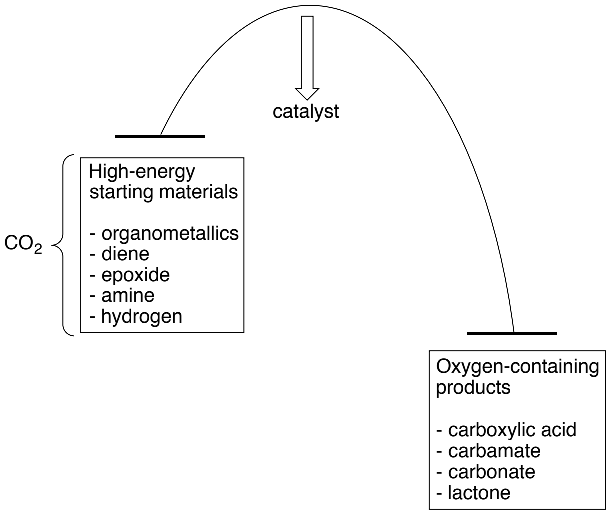

Figure 5.1 Conversion of carbon dioxide using high-energy starting materials.

Thus, there are four main approaches taken to convert carbon dioxide into other useful chemicals: (1) using high-energy starting materials like organometallics, small membered rings and dienes (Figure 5.1), (2) target oxygen-containing lower energy products like carboxylic acids, (3) employing Le Chatelier's Principle to drive off unwanted side products and shift the equilibrium towards the CO_2 containing products, and (4) by using an external energy source like light or electricity to drive CO_2 to new products.[4]

Scheme 5.1 Transformation of CO_2 (A) using metal catalysts and (B) organic nucleophiles.

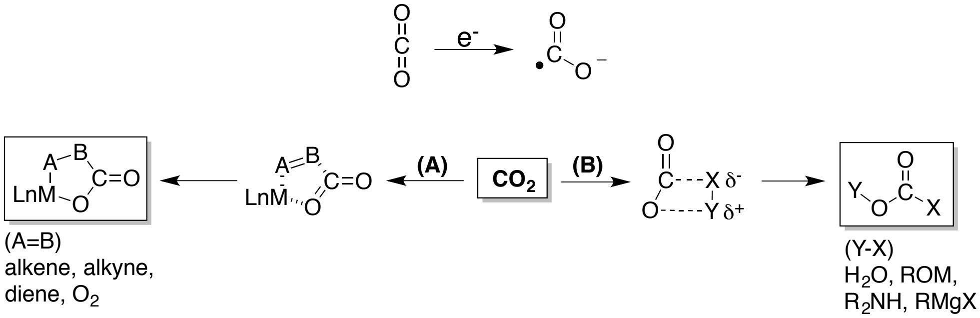

The large amount of energy required to transform carbon dioxide is derived from the reorganizational energy in going from linear CO_2 to bent CO_2 anion radical assuming the one electron reduction from an external donor. To aid this process, a catalyst is employed to facilitate this bending towards products and thus reduce the kinetic barrier making CO_2 conversion more favorable. By utilizing the dipole moment in the C=O double bonds, the binding of a catalyst is typically performed in one of two ways (Scheme 5.1).[4] The first can be made via the electropositive carbon center through the addition of organic nucleophiles, establishing the desired bent geometry. The other is through the use of transition metal catalysts, which can coordinate to the electronegative oxygen atoms with additional binding to the carbon center from the ligands attached to the metal center. The use of these catalysts has seen tremendous attention in the electrochemical reduction of CO_2 to small molecules like that mentioned above.[3,5-8] While the one electron reduction of CO_2 is largely unfavorable owing to a ground state reduction potential of -1.90 V vs. normal hydrogen electrode (NHE),[9] CO_2 reduction is thermodynamically driven by multi-electron proton assisted steps, as more stable products are formed (Scheme 5.2).

Scheme 5.2 Single and multi-electron proton assisted reduction of carbon dioxide (vs. NHE).

$$CO_2 + 2e^- + 2H^+ \rightarrow CO + H_2O \ (E^0 = -0.53 \text{ V})$$
$$CO_2 + 2e^- + 2H^+ \rightarrow HCO_2H \ (E^0 = -0.61 \text{ V})$$
$$CO_2 + 4e^- + 4H^+ \rightarrow HCHO + H_2O \ (E^0 = -0.48 \text{ V})$$
$$CO_2 + 6e^- + 6H^+ \rightarrow CH_3OH + H_2O \ (E^0 = -0.38 \text{ V})$$
$$CO_2 + 8e^- + 8H^+ \rightarrow CH_4 + 2H_2O \ (E^0 = -0.24 \text{ V})$$
$$CO_2 + e^- \rightarrow CO_2^{\bullet -} \ (E^0 = -1.90 \text{ V})$$

Current attempts at using CO_2 for chemical processes include the synthesis of cyclic carbonates/carbamates,[10] chemical hydrogenation,[11] the carboxylation of olefins,[12] methylation of amines[13] and formation of amides.[14] An example of an industrial scale CO_2 conversion process is the formation of aromatic hydroxy acids through the treatment of a metal phenolate reacting with CO_2.[15,16] The process, dubbed the Kolbe–Schmitt reaction,[17] is a chemical process for utilizing carbon dioxide in the synthesis of salicylic acid, a precursor used in the synthesis of aspirin. However, one general problem with the aforementioned CO_2 conversion methods is that a net reversal of the combustion processes that produce carbon dioxide would require energy inputs that are independent of the combustion process. One such energy input, solar energy, has motivated the search for photochemical based methods for CO_2 conversion. Approaches under current study include transition metal photocatalysts,[18-21] semiconducting layered double hydroxide catalysts,[22,23] and solar driven photoelectrochemical cells.[24-26] The use of organic photochemical and electrochemical catalysts[27,28] for both capture and reduction, albeit less readily reported, has also been performed which include high-energy radical anion aromatics,[29-31] tetraalkylamonium[32] and pyridinium ions.[33]

The Bocarsly[34,35] and MacDonnell[33] groups have performed recent work in using organocatalysts for the electrochemical or photochemical reduction of CO_2. This chemistry is tailored around using pyridinium catalysts to convert carbon dioxide into formic acid and methanol. The binding of the pyridinium ion to CO_2 makes it easier to be electrochemically reduced and enables the use of excited state photocatalysts that don't require a UV light source to initiate the reduction process. This is evident in the work done in the MacDonnell group where the reduction of CO_2 was undertaken using a ruthenium based visible light absorbing photocatalyst in conjunction with the pyridinium ion (Scheme 5.3).

Scheme 5.3 The use of pyridinium ions for the visible light photochemical reduction of CO_2.

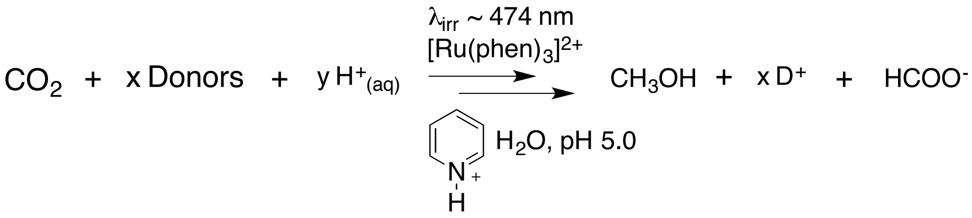

The work described above is in contrast to that reported in the 90's by Yanagida and coworkers[30,31] who used excited state oligo(*p*-phenylenes) with triethylamine to reduce carbon dioxide in non-aqueous solvents generating formate ion and to a much lesser degree, carbon monoxide and hydrogen gas. As shown in Scheme 5.4, UV light is used to excite *p*-terphenyl, which is reduced upon one electron reduction from TEA. The resulting *p*-terphenyl radical anion, a strong reducing reagent (-2.63 V vs. SCE), is able to shuttle the electron to carbon dioxide generating CO_2 anion radical leading to the products stated above. In this system, there is no evident pre-binding or activation of carbon dioxide, but instead high-energy anion intermediates are generated using UV light to directly reduce carbon dioxide.

Scheme 5.4 Photochemical reduction of CO_2 using *p*-terphenyl with triethylamine.

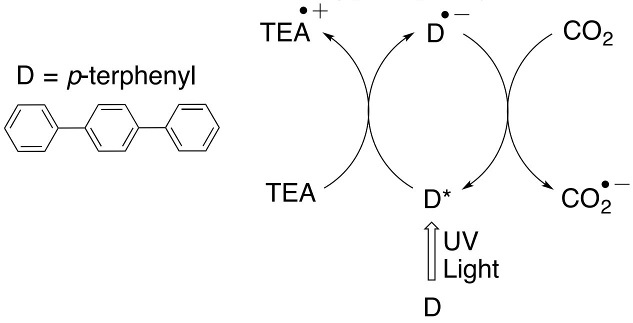

In the following sections, a new photochemical process for the reduction of CO_2 into formate using UVA light (350 nm) is introduced. However, unlike in the oligo(*p*-phenylenes) system, pre-binding of CO_2 to the catalyst allows for the use of lower energy excited state oxidation potential electron donors. Below, NHCs are investigated for their ability to be used as organocatalysts in the photochemical reduction of carbon dioxide. Specifically, evidence for the one electron reduction of imidazolium-2-carboxylates is reported and more importantly is that the resulting radical ions lead to the generation of formate (Scheme 5.5).

Scheme 5.5 General depiction of the photochemical reduction of NHC–CO_2 for the generation of formate ion.

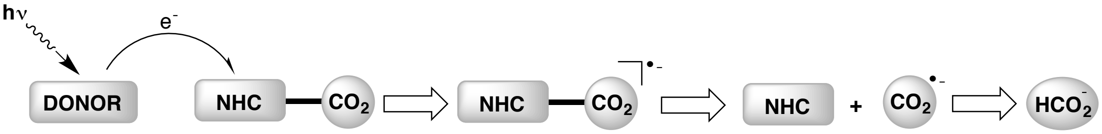

5.2 CO_2 Utilization by 1,3-Dialkylimidazolium-2-Carboxylates

As mentioned in the previous chapter, new chemistries associated with imidazolium-2-carboxylates are a current topic of interest. With respect to CO_2 conversion is the ability of these adducts to act as carbon dioxide transfer reagents for the synthesis of carbonates and carboxylic acids.[36,37] Sorrentino and Tommasi have demonstrated carbon dioxide transfer from NHC–CO_2 to methanol and benzaldehyde. In both these cases, carbonate esters were obtained in moderate yields. Additional work has been done with compounds containing α-proton available compounds like acetone, cyclohexanone and benzylcyanide. Here, the acidity of these α-protons in conjunction with the basicity of the free NHC allowed for carboxylation at these positions to their respective carboxylates. Ikariya and coworkers[38] demonstrated the formation of cyclic carbonates through the use of imidazolium-2-carboxylates by using propargylic alcohols. These reactions were carried out at 100 °C at 10.0 MPa for 15 hours, and resulted in the formation of cyclic carbonates with yields >80% (Scheme 5.6).

Scheme 5.6 Utilization of carbon dioxide using imidazolium-2-carboxylates in the synthesis of cyclic carbonates (A) and carboxylates (B).

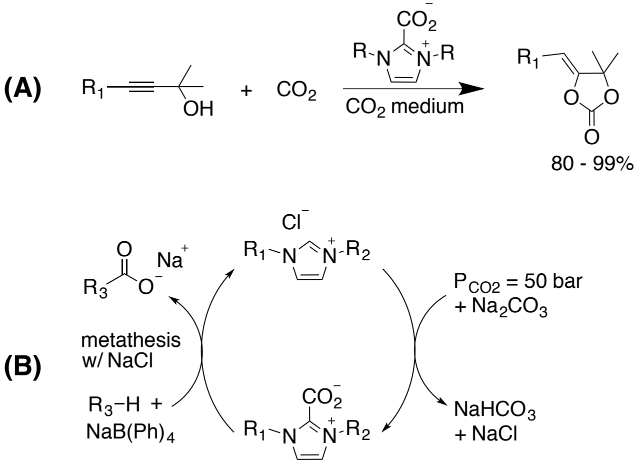

R_3H = acetophenone (77.3 %), cyclohexane (62.2%), benzylcyanide (60.0%).
percentages represent carboxylate yields.

A seminal report by Ying and coworkers[39] found that imidazolium-2-carboxylates could be used to facilitate the chemical reduction of CO_2 with the use of silanes. As the authors note, a typical reaction consisted of 1,3-bis(2,4,6-trimethylphenyl)imidazolium-2-carboxylate dissolved in DMF with a balloon filled with CO_2 equipped to continuously add the gas to the mixture. To this, diphenylsilane was added as the reducing reagent and was fully consumed in 6 hours at room temperature as monitored by GC. A mixture of silyl containing intermediates were identified, but of interest was the final methoxide products $Ph_2Si\text{-}(OMe)_2$ and $(Ph_2(MeO)SiO\text{-})_n$. Treatment of this mixture with two equivalents of NaOH/H_2O led to methanol being obtained as the major product, in upwards of 90% yield (based upon the silane).

Koval et al.[40] has reported the electrochemical reduction of carbon dioxide using NHCs. Here, the authors use 1,3-bis(2,6-diisopropylphenyl)imidazolium-2-carboxylates as a way to pre-activate carbon dioxide along with added $[Ni(cyclam)]^{2+}$, a well studied electrocatalyst for CO_2, in a saturated trifluoroethanol solution for the conversion of CO_2 to methane. Labeling studies suggest that the reduced carbon dioxide derives from the NHC–CO_2 adduct, while the proton source for reduction stems from the trifluoroethanol solvent. The samples were subjected to a potential of -1.5 V vs. Ag/$AgNO_3$ with faradaic efficiencies ca. 93% (Scheme 5.7).

Scheme 5.7 The use of NHC–CO_2 for the chemical (A) and electrochemical reduction (B) of CO_2 to methanol and methane.

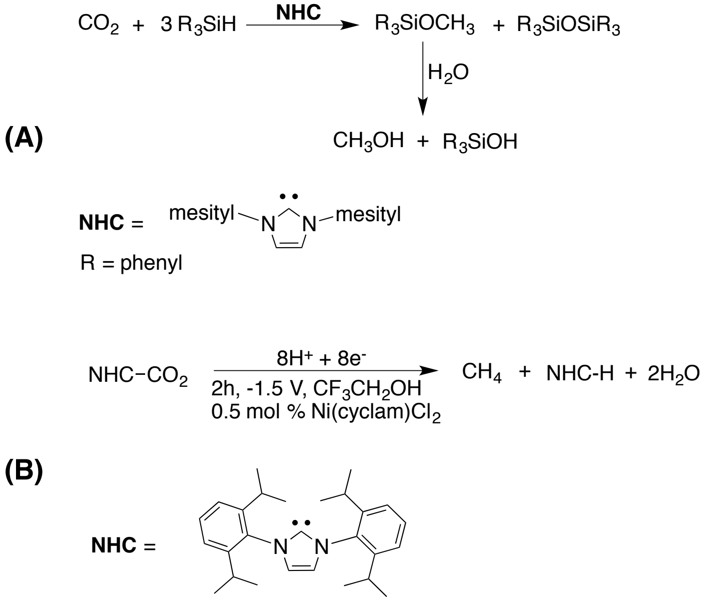

The aforementioned literature examples demonstrate the diverse use of imidazolium-2-carboxylates in the net conversion of CO_2 into reduction products like carboxylates, methanol and methane. In the next section we explore the excited state chemistry of electron donors in the presence of **57**, the imidazolium-2-carboxylate compound introduced in Chapter 4 to see if this an interaction with excited state donors results in the conversion of CO_2 into stable reduction products.

5.3 Fluorescence Quenching Studies

The first step in the photochemical process is the one electron reduction of **57** from an excited state sensitizer. To test this, a series of fluorescence quenching experiments were conducted. As illustrated in Figure 5.2, increasing concentrations of **57** decreases the fluorescence intensity of *N,N,N'N'*-tetramethylbenzidine (TMB), an excited state electron donor, demonstrating that there is an interaction between the excited state of TMB and the ground state of **57**. Stern–Volmer analysis of the quenching data is provided in the insert in Figure 5.2 and yields a fast and efficient quenching rate constant (k_q) of 3.55×10^9 $M^{-1}s^{-1}$. Table 5.1 summarizes the quenching results of various excited state electron donors in solvent mixtures of sufficiently high water concentrations as to ensure the stability of **57**, which was discussed in the previous chapter. Also provided in Table 5.1 is the calculated free energy of the electron transfer process using equation 1 (Chapter 3). Although we were unable to measure the E_{red} for **57** electrochemically, structurally similar imidazolium cations have been reported to be reduced around -1.8 V vs. SCE[41] and thus this value was used to calculate the driving force for this electron transfer step.

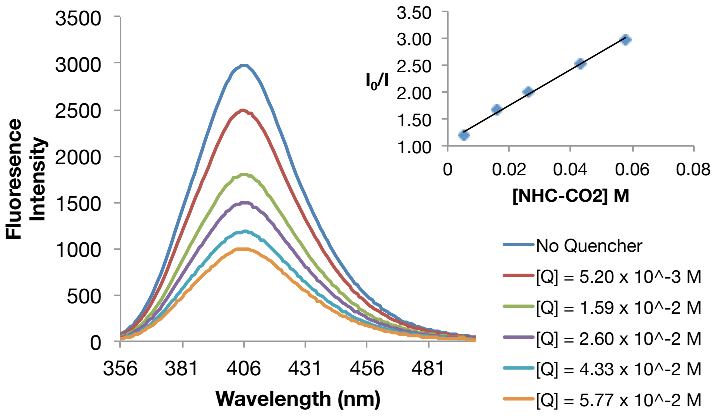

Figure 5.2 Fluorescence quenching analysis of TMB with **57** in 60% H_2O in 1,4-dioxane with the corresponding Stern−Volmer plot (λ_{ex} = 346 nm, λ_{em} = 405 nm).

Changing the water concentration (40–70%) had little, if any, effect on the rate of quenching but there is good agreement with the excited state oxidation potential (E_{ox}*) of the donor and the quenching rate constant (k_q). For example, *N*-methylcarbazole, a very good excited state electron donor exhibits a quenching rate constant more than 100 times faster than 9,10-dibromoanthracene, which could not be effectively quantified at the concentrations of quencher used. This is also in good agreement with the predicted free energy of the electron transfer process as *N*-methylcarbazole is predicted to be ca. 17 kcal/mol exergonic while 9,10-dibromoanthracene is slightly endergonic. While it is established that there is an interaction between the excited state of various donors and ground state NHC–CO_2, the following section of results was conducted in order to see if this interaction led to the generation of radical ions capable of further bond-breaking chemistry.

Table 5.1 Fluorescence quenching results of sensitizers and **57** in 1,4-dioxane/H_2O mixtures.

Sensitizer	E_{ox} (V)[a]	E_{00} (kcal/mol)[a]	E_{ox}^* (V)[d]	% H_2O	k_q ($M^{-1}s^{-1}$)	ΔG_{ET} (kcal/mol)
TMB	0.43	83.0[b]	-3.17	40.0	3.51×10^9	-31.6
TMB	0.43	83.0	-3.17	50.0	4.46×10^9	-31.6
TMB	0.43	83.0	-3.17	60.0	3.55×10^9	-31.6
TMB	0.43	83.0	-3.17	70.0	2.74×10^9	-31.6
N-methylcarbazole	1.03[c]	82.9	-2.56	50.0	1.03×10^9	-17.6
2-aminoanthracene	0.44	63.1	-2.30	50.0	5.70×10^8	-11.4
anthracene	1.09	76.2	-2.21	50.0	3.32×10^8	-9.56
phenanthrene	1.50	82.5	-2.08	50.0	1.30×10^7	-6.40
9,10-dibromoanthracene	1.28[c]	70.5	-1.78	50.0	$< 10^7$	+0.52

[a] ref 42. [b] ref 43. [c] ref 44. [d] $E_{ox}^* = E_{ox} - E_{00}$

5.4 Laser Flash Photolysis Results

To test if the interaction between the excited state donor and **57** resulted in electron transfer chemistry, and thus the generation of ion radical pairs, laser flash photolysis experiments were conducted on TMB and *N*-methylcarbazole using **57** as the quencher. Illustrated in Figure 5.3 is the transient spectrum resulting from pulsed laser excitation (355 nm, 7 ns, 10−30 mJ/pulse) of TMB and *N*-methylcarbazole in a mixture of 40% H_2O in 1,4-dioxane. Excitation of only the amine donors resulted in excited state triplet spectra. The signals are significantly quenched in the presence of oxygen when the solutions are subjected to air-equilibrated conditions.

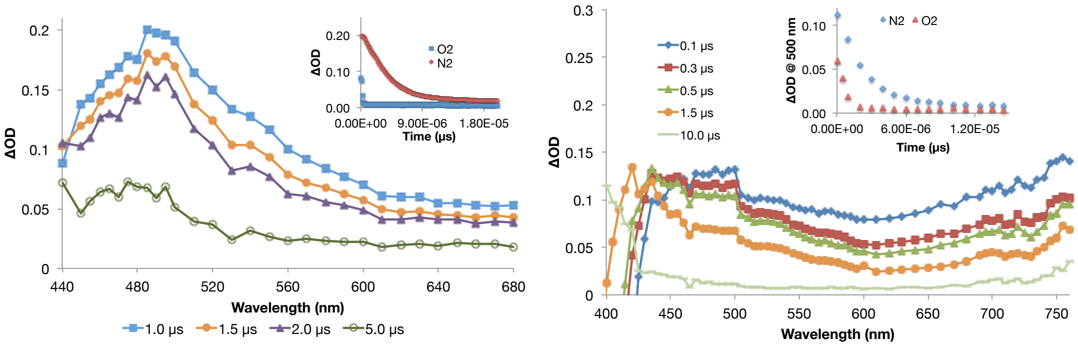

Figure 5.3 (Left) Transient absorption spectrum of 1.60 mM TMB with no quencher. Oxygen quenching monitored at 480 nm (insert). (Right) Transient absorption spectrum of 2.58 mM *N*-methylcarbazole. Both samples were done in 40% H_2O in 1,4-dioxane.

When **57** is included into the solutions the triplet spectra are replaced with longer-lived species (Figure 5.4). These are assigned to the TMB and *N*-methylcarbazole cation radicals, $\lambda_{max} \approx 480$ nm for TMB and $\lambda_{max} \approx 400$ and 780 nm for *N*-methylcarbazole as signals above 780 nm were difficult to acquire. While the TMB triplet state and cation radical have overlapping absorption bands, they are distinguished by their kinetic behavior: the triplet state is short lived and quenched by the addition of O_2, while the cation radical is much longer-lived (τ >17.7 μs) and the addition of O_2 does not affect the decay of the transient signal. Both the triplet and radical cation spectra obtained for TMB and *N*-methylcarbazole are consistent with previous reports.[45-47] Thus, the laser flash photolysis results are consistent with photoinduced electron transfer from an excited state donor to NHC–CO_2. In order to see if the radical ions, particularly the imidazolium-2-carboxylate radical anion undergoes further bond breaking chemistry, preparative photolysis experiments were conducted to analyze for CO_2 reduction products.

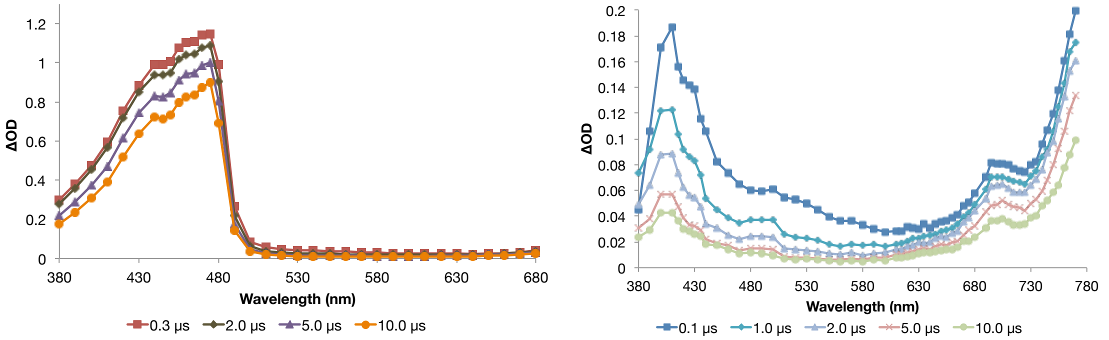

Figure 5.4 Transient absorption spectrum of 1.23 mM TMB with 0.142 M **57** (Left). Transient absorption spectrum of 2.58 mM *N*-methylcarbazole with 0.343 M **57** (Right). Both samples were done in 40% H_2O in 1,4-dioxane.

5.5 Preparative Photolysis Results

Detection of products arising from CO_2 reduction was performed using ^{1}H NMR. Specifically, solutions of TMB and **57** were degassed with N_2 and irradiated using a Rayonet reactor (8 bulb, 32 watt, 350 nm) for one hour. The solvent was then removed under reduced pressure and the photolysis products were re-dissolved in D_2O with fumaric acid acting as the internal standard. The slurry solution was filtered so that only water-soluble products were analyzed in an attempt to minimize competing NMR peaks in the analysis. The CO_2 reduction product, formate ion **85** was detected by its resonance at 8.45 ppm along with imidazolium cation **58** resulting from the protonation of NHC **59** in aqueous environments. The formation of **58** was verified by the addition of independently synthesized 1,3-dimethylimidazolium cation which led to an increase in the singlet at 7.35 ppm. Figure 5.5 illustrates the time course of formate production as measured against fumaric acid, the internal standard used for quantification of formate ion, which has a singlet appearing at ca. 6.50 ppm.

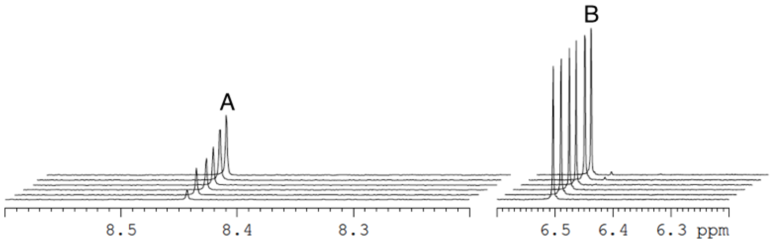

Figure 5.5 Photolysis time course of formate production (4.39 mM **57**, 10.2 mM TMB in 5.0% H_2O in 1,4-dioxane at 350 nm). ^1H NMR showing the increase in formate (A) over photolysis time (0, 15, 30, 45, 60, 90 min, front to back) and fumaric acid as the internal standard (B).

Further verification of formate production is provided from the colorimetric detection procedure reported by Sleat and Mah[48] where formate reacts with acetamide, citric acid, 2-propanol, acetic anhydride and sodium acetate to generate a peak at 510 nm. As shown in Figure 5.6, an increase in absorbance is observed for the three samples run in triplicate under UV irradiation compared to the three dark control samples. A calibration curve for formate using this technique afforded yields of 34.5 ± 3.59% for the one-hour photolyses and 7.25 ± 4.51% for the dark control. A small percentage (~5-15%) of formate can be observed for all the non-irradiated samples analyzed by ^1H NMR and the colorimetric assay. We attribute this to possible thermal electron transfer in the workup conditions subsequent to photolysis but did not investigate this further. An additional product that may arise from this photolysis reaction is oxalate **86**, which is ^1H NMR silent and thus would not be observed under the conditions used for analysis of formate. Therefore, product mixtures were also analyzed by high-pressure liquid chromatography (HPLC). Photolysis mixtures of TMB and **57** in 10% water and 1,4-dioxane provided low concentrations of oxalate (<6%). Increasing the alkalinity of the photolysis solution led to a slight increase in the amount of oxalate that was observed and thus is not considered a major product in this photochemical process.

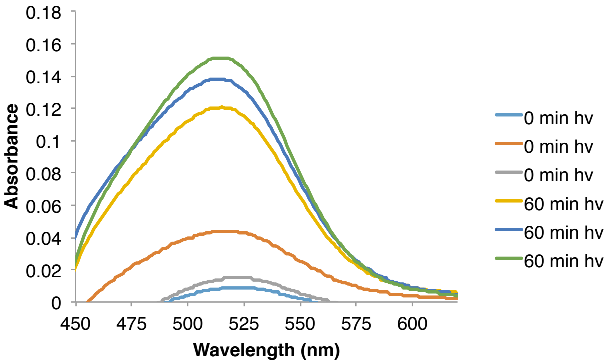

Figure 5.6 Colorimetric detection of formate ion at 510 nm in 60-minute photolyses and dark control solutions.

Yields of formate, which were measured at nearly complete conversions of **57**, are listed in Table 5.2. The maximum amount of formate under these conditions was ca. 47%. Increasing the TMB concentration from 10 to 20 mM, and changing the aqueous component from 3 to 10% had insignificant effects on the overall yield of formate. As was stated in chapter 4, NHC–CO_2 **57** is thermodynamically stable in high aqueous environments. However, the photolysis experiments outlined in Table 5.2 were done at lower concentrations of water (≤10%) to ensure solubility of the donors at the concentrations that were used. Moderately lower yields of formate (<30%) were observed when the organic component was changed from 1,4-dioxane to the more polar acetonitrile, and when 9,10-dibromoanthracene was used as the excited state donor. The latter is a much weaker excited state donor than TMB and the fluorescence quenching studies outlined in section 5.3 demonstrate that it is less reactive. In the absence of a donor, small amounts of formate can be observed. This yield is attributed to thermal electron transfer or excitation due to the tailing absorption of **57** at the UV irradiation output of the lamp. While this process was not investigated in depth, as was stated above, the small amounts of formate could also be derived from the elevated temperatures and reduced pressure used in the workup procedure illustrated in the experimental section.

Table 5.2 Photolysis results (60 minutes) of **57** and sensitizer (Sens) in mixtures of an organic solvent and H_2O as analyzed by ^1H NMR.

Sens	[Sens] mM	[57] mM	Organic	% H_2O	% Yield Formate[d]
TMB	10.2	5.59	1,4-dioxane	3.0	38.1 ± 4.29
TMB	10.2	5.59	1,4-dioxane	5.0	42.4 ± 4.23
TMB	10.2	5.59	1,4-dioxane	10.0	43.4 ± 2.10
TMB	0.00	5.59	1,4-dioxane	5.0	18.8 ± 2.84
TMB	20.2	5.59	1,4-dioxane	5.0	42.5 ± 3.33
TMB[a]	7.60	0.00	1,4-dioxane	5.4	<10.0
TMB[b]	9.45	0.00	1,4-dioxane	5.0	<10.0
TMB[c]	9.45	5.59	1,4-dioxane	5.0	47.3 ± 5.89
TMB	10.1	4.39	MeCN	1.0	13.4 ± 2.56
TMB	10.1	4.39	MeCN	5.0	15.9 ± 3.10
ANT	10.1	5.59	1,4-dioxane	5.0	41.4 ± 5.02
9,10-DBA	9.83	5.59	1,4-dioxane	5.0	29.8 ± 0.93

[a] 24.2 mM 1,3-dimethylimidazolium tetrafluoroborate solution saturated with CO_2 (90 min photolysis). [b] Solution saturated with CO_2. [c] 10% v/v 1,4-cyclohexadiene (average of 2 samples). [d] Yields presented represent high conversion of **57**.

The importance of complex **57** for the photochemical generation of formate was also investigated and verified by three experiments. First, a solution of TMB saturated with CO_2 was irradiated at 350 nm to ensure that formate production was not the result of direct reduction of carbon dioxide from excited state TMB. Second, a solution of 1,3-dimethylimidazolium tetrafluoroborate and TMB was saturated with CO_2 and irradiated without the presence of **57**. This was performed to provide evidence in support for the importance of the NHC–CO_2 adduct and that formate production was not the result of mediated electron transfer from excited state TMB to CO_2 via the imidazolium cation, which has been reported for structurally similar imidazolium based ionic liquids.[49-51] Finally, fluorescence quenching experiments were conducted on TMB using HCO_3^- as the quencher, a product arising from the thermal decomposition of **57**. No significant quenching could be observed at bicarbonate concentration levels well exceeding amounts that would be produced in the photolysis experiments outlined in Table 5.1. Combined with no detectable amounts of formate in the photolysis experiments, the formation of the imidazolium-2-carboxylate adduct for the photochemical generation of formate is apparent.

5.6 Proposed Photochemical Mechanism

The experiments described above are summarized in the proposed photochemical mechanism in Scheme 5.8. Electron transfer from excited state singlet of TMB (Sens*) to **57** generates anion radical **87**. Homolytic cleavage of C_{NHC}–C_{CO2} of the anion radical leads CO_2 anion radical **88** and NHC **59**. The latter is expected to protonate in aqueous media giving 1,3-dimethylimidazolium cation **58**. It is assumed that 1 equivalent (at a minimum) of TMB is consumed in each photochemical reaction. However, the large excess of TMB used and the diversity of stable products expected from its cation radical[52,53] made its consumption difficult to quantify. Conversion of carbon dioxide anion radical to formate requires a hydrogen atom transfer or a second reduction step. While in principle hydrogen atom transfer could occur from the solvent, donor or additives, two observations suggest that this process does not contribute in a major way.

First, adding a strong hydrogen atom donor (1,4-cyclohexadiene, 1.06 M) had only a negligible effect on the yield of formate. Hydrogen atom transfer could also occur from the methyl groups of the TMB cation radical. Such reactions are known to occur, producing the corresponding iminium ion,[54] which would hydrolyze to form *N,N,N'*-trimethylbenzidine. In fact, trace amounts of this byproduct are seen in the mass spectrum of the photoproduct mixtures (m/z = 227 ESI(+)-MS). However, replacing TMB with anthracene (which does not have available hydrogen atoms) has only a negligible effect on formate production, suggesting that H-atom transfer from the donor is at best a minor pathway in the photochemical generation of formate ion. Additionally, the C–H bond dissociation energy for 1,4-dioxane is 96.0 kcal/mol, only slightly lower than the C–H dissociation energy for formic acid (96.6 kcal/mol),[55] implying that while hydrogen atom transfer from dioxane to CO_2 anion radical is feasible, the process is expected to be fairly slow.

Scheme 5.8 Proposed mechanism for the photochemical generation of formate ion.

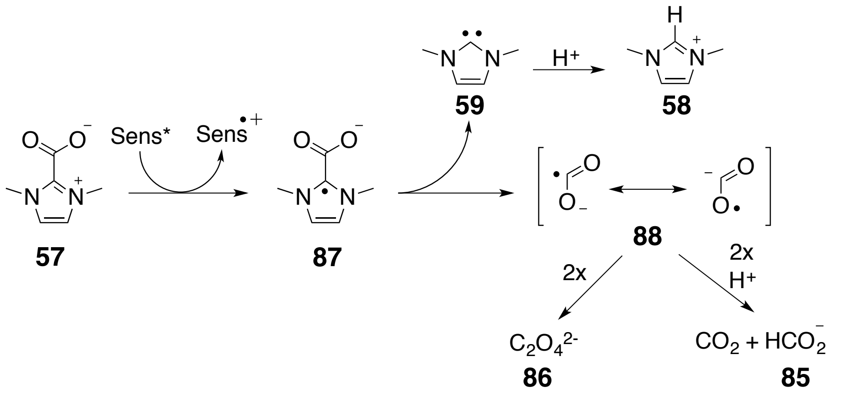

The considerations outlined above suggest that the most likely source of additional reducing equivalents is from disproportionation of $CO_2^{\bullet -}$ and/or its conjugate acid, $HOCO^{\bullet}$. While the electrochemical reduction of carbon dioxide in neat polar aprotic organic solvents like acetonitrile has been reported to yield oxalate as a major product, pulse radiolysis experiments of Flyunt et al.[56] have shown that $CO_2^{\bullet -}$ decays with a bimolecular rate constant that is near diffusion limited in aqueous media. The products of this process are CO_2 and HCO_2^- formed from a net disproportionation or dimerization of

CO_2 anion radical to form oxalate. Dimerization predominates at high pH, however under lower pH conditions where $HOCO^•$ can exist, disproportionation products are favored. In the photolysis experiments stated above, the predominantly organic and thus less polar solvent conditions favor the formation of $HOCO^•$ leading to the generation of CO_2 and formate.

5.7 Conclusions and Future Research Directions

In summary, the results described in this chapter demonstrate that excited state donors can enact the one electron reduction of imidazolium-2-carboxylates. Further, this reduction results in the formation of ion radical pairs capable of undergoing further bond breaking chemistry. In the case of the NHC–CO_2 anion radical, the result of this is the formation of formate anion, a reduction product of carbon dioxide. This is presumably accomplished via a net disproportionation of two CO_2 anion radical intermediates providing the desired formate and an equivalent of unwanted carbon dioxide. Due to this, the photochemical pathway is limited to a maximum theoretical yield of formate to <50% under single turnover conditions. Therefore, future development of NHCs being used for the photochemical reduction of carbon dioxide should strive for a truly catalytic system as outlined in Scheme 5.9.

The challenge with the system described above is that the conjugate acid of 1,3-dimethylimidazolylidene has a pKa exceeding that of water and thus is protonated under aqueous conditions. In order to prevent this from occurring, the use of aprotic solvents and/or carbenes that would be stable under protic environments is necessary. This is a double-edged sword though, because lowering the pKa of the NHC precursor means a decrease in the nucleophilic properties of the free carbene. Thus, binding to carbon dioxide would be reduced and directly impact the photochemical reduction of CO_2. The challenge is finding the "goldilocks" binding of the NHC to carbon dioxide where the NHC would be stable in the solvent environment. Too tight of binding could result in no homolytic cleavage of the anion radical **87** while too loose of binding means that the photochemical reduction step of NHC–CO_2 would presumably be an inherently slow process.

Scheme 5.9 An ideal catalytic cycle for the photochemical reduction of CO_2 using NHCs.

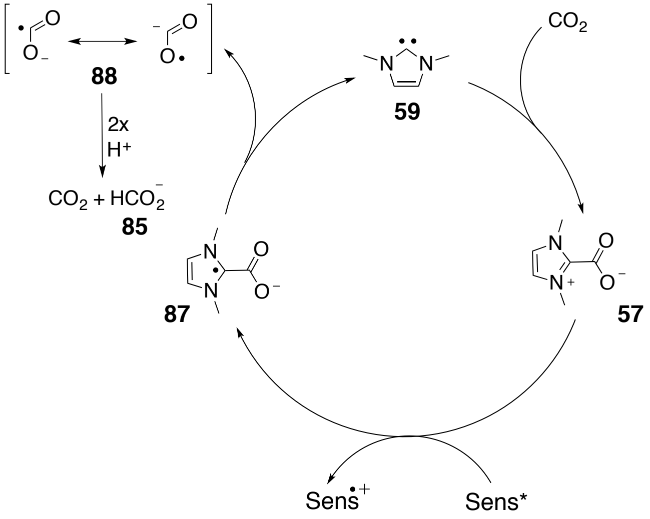

The advantage of this system is the variety of parameters that can be adjusted to modify the stability of the NHC–CO_2. In chapter 4 we saw that the changing of the solvent polarity lead to wide variations in the stability of **57**. This polarity change led to elongated or shortened C_{NHC}–C_{CO2} bond lengths in direct relation to the decomposition rate of **57**. Additionally, changing both steric and electronic effects of the NHC can have major influences on the binding strength to carbon dioxide. As was stated in chapter 4 we have already begun a computational investigation for potential NHCs that could participate in a truly catalytic photochemical system. The first step is to identify bond lengths that would ensure binding of carbon dioxide. For example, it is understood that

1,3-dimethylimidazolium-2-carboxylate **57** is stable and binds CO_2 extremely well in aqueous environments. The calculated C_{NHC}–C_{CO2} bond length is ca. 1.521 angstroms using the SMD implicit solvation model. However, **57** will decompose quickly when 1,4-dioxane is introduced as a co-solvent at high concentrations, the bond length computationally increasing to 1.553 angstroms in the nonpolar media. Therefore targeting a binding catalyst with a computed bond length within this range would be a logical place to begin. Once NHCs that fall within this bond distance are identified, calculations or experimentally determined pKa values will be assessed to ensure their stability in protic environments and thus help favor additional turnover conditions. In addition to these calculations, DFT calculations will be performed to estimate the barrier to bond dissociation of the anion radical into the respective NHC and CO_2 anion radical. This will provide further evidence in support of whether or not this photochemical process will be feasible. Taking all the aforementioned parameters into consideration, it could be possible to find an ideal situation in which the photochemical reduction of CO_2 using NHCs proceeds with much greater efficiency.

CHAPTER 6. SUPPORTING INFORMATION

6.1 General Methods and Materials

All chemicals and solvents were purchased from commercial suppliers and unless otherwise stated were used without further purification. In general, HPLC grade solvents were used in photolysis reactions which were stored in amber bottles with 4 angstrom molecular sieves and purged with nitrogen prior to use. Acetonitrile and dichloromethane were distilled from calcium hydride prior to use. Anhydrous inhibitor free tetrahydrofuran (Sigma-Aldrich, ≥99.9%) and spectroscopic grade 1,4-dioxane (Acros, 99.9+%) was also used for photolysis reactions. Synthesis reactions and photolyses were performed in oven dried (~370 °C) round bottom flasks or four sided quartz cuvettes capped with a septum and purged with nitrogen in both the solution and head space of the flask/cuvette.

All NMR experiments (^{1}H and ^{13}C) were conducted on a Bruker 400 MHz instrument. All signals are referenced to the solvent peak and the splitting is represented by (s = singlet, d = doublet, t = triplet, q = quartet, sep = septet, dd = doublet of doublets, dt = doublet of triplets and m = multiplet or not well resolved peaks). ^{13}C experiments were conducted under broadband proton decoupled conditions resulting in all the signals appearing as singlets and referenced to the solvent peak.

Photolysis reactions were performed using a RPR-100 Rayonet reactor (16-bulb, 35 watt, ~33 °C operating temperature, 350/419 nm) or a RMR-600 Rayonet reactor (8-bulb, 32 watt, ~37 °C operating temperature, 253.7/350 nm) supplied by Southern New England Ultraviolet. A 1-watt, 447 nm laser provided by Laserglow Technologies was also used for select photolyses below.

Gas chromatography analysis was done using a Shimadzu GC-17A, containing a RTX-5 stationary phase column (length = 15 m, inner diameter (i.d.) = 0.25 mm, film thickness = 0.25 μm), equipped with a FID detection system, and using the following method specifications: equipped with a FID detection system, and using the following method specifications: column temperature = 60 °C, injection temperature = 280 °C, and detector temperature = 300 °C, with a temperature/pressure profile for injection of: 67 kPa, 3.0 minutes, 3.9 mL/minute, 98 kPa, 9.0 minutes, column of: 60 °C, 3 minutes, 30 mL/minute, 300 °C, 9.0 minutes, injector pressure of 60 kPa, total flow of 31 mL/min., column flow of 1.45 mL/min., and a linear velocity of 39.1 cm/s.

UV-Vis data was collected on a Shimadzu UV-1800 spectrometer using UVProbe 2.43 software. Samples were scanned from 800 nm to 190 nm using a fast scanning speed and a sampling interval (nm) of 1.0. Each sample was pre-blanked with the solvent of choice used in solvating the compound(s). ATR FT-IR data was collected using a Thermo Nicolet 670 FT-IR with an OMNIC software package. The samples were performed neat (liquid, oil, solid) using the air from the room as the blank and either 32 or 64 scans were acquired for each sample.

Mass spectra data was acquired on a JEOL AccuTOF-CS using ESI-TOF or DART (Direct Analysis in Real Time) or a JEOL JMS-700 MStation coupled with an Agilent 6890N GC system. Fluorescence quenching experiments were conducted on a Hitachi F-4500 fluorescence spectrophotometer and laser studies were conducted using a Nd:YAG laser (355 nm output) supplied by Continuum with pulses 4-6 ns in duration as the excitation source. The probe beam that was used was a 350 W Xenon arc lamp.

Specific details about the experimental processes and/or techniques can be found under the desired sections provided below.

6.2 Chapter 2 Experimental Results

A. General Photolysis Procedure

Photolysis experiments were performed in a capped, four sided quartz cuvette purged with nitrogen gas for 15 and 3 minutes for the solution and headspace respectively. Isolation reactions were carried out in a capped 120 mL quartz test tube that was purged with nitrogen gas for a minimum of 20 and 10 minutes for the solution and headspace respectively. Reactions were conducted on an 8-bulb Rayonet reactor using 253.7 nm light bulbs. After the allotted amount of photolysis time, the mixture was transferred to a vial and the solvent was removed under reduced pressure. The unpurified products were dissolved in $CDCl_3$ and subjected to ^{1}H NMR analysis.

B. Synthesis of 2,2,2-Tribromoethyl-(2′-phenylacetate) (36)

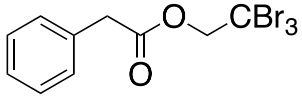

2,2,2-Tribromoethanol (2.00 g, 7.07 mmol), triethylamine (1.97 mL, 14.1 mmol), phenylacetyl chloride (1.87 mL, 14.1 mmol), and distilled CH_2Cl_2 (30 mL) were stirred at room temperature overnight. After 12 hours a GC trace of the mixture confirmed consumption of the starting material. The reaction mixture was transferred to a 125 mL separatory funnel and the organic layer was washed with deionized H_2O (3 x 50 mL) and cold (on ice) 1 M HCl (3 x 50 mL). The organic layer was dried over $MgSO_4$, filtered, and concentrated under reduced pressure to afford orange watery oil. Purification of the ester was done by flash column chromatography with 1:1 hexanes/CH_2Cl_2 as the eluent. The ester was obtained as a very faint peach colored watery oil (2.19 g, 77.0%). ^{1}H (400 MHz, $CDCl_3$): δ 7.32 (m, 5H), 4.94 (s, 2H), 3.79 (s, 2H). ^{13}C (400 MHz, CD_3CN): δ 171.3, 135.1, 131.0, 129.9, 128.6, 77.9, 41.7, 37.1. FT-IR (ATR): neat, 1748.19 cm^{-1}. HRMS (ESI-TOF) m/z: $[M]^+$ calculated for $C_{10}H_9Br_3O_2$ 400.8211; found 400.8214.

C. Isolation of 2,2-Dibromoethyl-(2′-phenylacetate) (37)

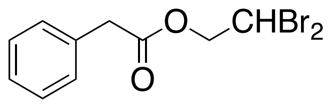

Compound **36** (98.3 mg, 0.245 mmol) was added to a 120 mL quartz test tube with 30 mL of THF containing 0.025% butylated hydroxyl toluene (BHT). The solution was irradiated for 90 minutes and the solvent was removed under reduced pressure. A ^{1}H NMR of the crude photolysis mixture confirmed the loss of the starting material and the formation of **37**. The crude product was transferred to a 125 mL separatory funnel with 30 mL of CH_2Cl_2. The organic layer was washed with deionized water (3 x 30 mL) and a saturated $NaHCO_3$ solution (2 x 30 mL), dried over $MgSO_4$, filtered, and concentrated under reduced pressure. The still crude mixture by ^{1}H NMR proved difficult to purify, but was accomplished by flash column chromatography using a gradient of 95:5, hexanes/ethyl acetate followed by 90:10, hexanes/ethyl acetate as the eluent. Ester **37** was obtained as a watery clear oil (7.70 mg, 9.75%). ^{1}H NMR (400 MHz, $CDCl_3$): δ 7.33 (m, 5H), 5.70 (t, 1H, J = 6.4 Hz), 4.58 (d, 2H, J = 6.4 Hz), 3.71 (s, 2H) ^{13}C (400 MHz, CD_3CN): δ 171.9, 135.3, 130.9, 129.9, 128.5, 70.6, 42.0, 41.6. FT-IR (ATR): neat, 1740.82 cm^{-1}. HRMS (ESI-TOF) m/z: $[M]^+$ calculated for $C_{10}H_{10}Br_2O_2$ 322.9106; found 322.9116.

D. Isolation of 2-Bromoethyl-(2′-phenylacetate) (38)

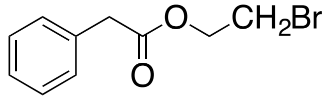

Compound **36** (73.7 mg, 0.184 mmol) was added to a 120 mL quartz test tube with 30 mL of 2-propanol. The solution was irradiated for 90 minutes and the solvent was removed under reduced pressure. A ^{1}H

NMR of the crude photolysis mixture confirmed the loss of starting material and the formation of **38**. The crude mixture proved difficult to purify but was accomplished by flash column chromatography using a gradient of 95:5, hexanes/ethyl acetate followed by 90:10, hexanes/ethyl acetate as the eluent. The remaining product appeared as a clear watery oil (4.90 mg, 11.0%). ^{1}H NMR (400 MHz, $CDCl_3$): δ 7.30 (m, 5H), 4.42 (t, 2H, J = 6.0 Hz), 3.68 (s, 2H), 3.51 (t, 2 H, J = 6.0 Hz). ^{13}C (400 MHz, $CDCl_3$): δ 171.3, 133.8, 129.5, 128.8, 127.4, 64.3, 41.3, 28.7. FTIR (ATR): neat, 1735.81 cm^{-1}. HRMS (ESI-TOF) m/z: $[M]^+$ calculated for $C_{10}H_{11}BrO_2$ 243.0021; found 243.0033.

E. Isolation of 2-(2′-Phenylacetoxy)acetic acid (40a)

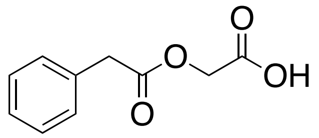

Compound **36** was added to a 120 mL quartz test tube with 40 mL of acetonitrile. The reaction was monitored by ^{1}H NMR until the loss of starting material could be confirmed. The solvent was removed under reduced pressure, and the resulting product was characterized. ^{1}H (400 MHz, $CDCl_3$): δ 7.32 (m, 5 H), 4.68 (s, 2H), 3.76 (s, 2H). ^{13}C (400 MHz, CD_3CN): δ 172.3, 169.7, 135.3, 130.7, 129.7, 128.3, 61.9, 41.2. FT-IR (ATR): CH_3CN subtracted: 3235.00 cm^{-1}, 1745.39 cm^{-1}, 1655.18 cm^{-1}. HRMS (ESI-TOF) m/z: $[M]^-$ calculated for $C_{10}H_9O_4$ 194.0535; found 194.0503.

F. Synthesis of 2-Methoxy-2-oxoethyl-(2′-phenylacetate) (40b)[1]

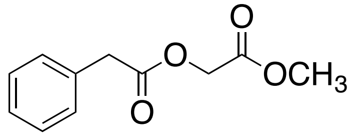

Phenylacetic acid (3.03 g, 22.2 mmol), potassium carbonate (2.80 g, 20.2 mmol), methyl bromoacetate (2.30 mL, 24.3 mmol), and acetone (30 mL) were added to a flask equipped with a condenser. The mixture was heated under reflux (70 ± 5 °C) for 5 hours with stirring. The reaction mixture went from chalky white to clear upon prolonged heating. After 5 hours, the reaction was concentrated under reduced pressure and the contents were transferred to a 125 mL separatory funnel using 50 mL of deionized H_2O. The aqueous layer was extracted with 150 mL of diethyl ether. The organic layer was dried over Na_2SO_4, filtered, and concentrated under reduced pressure to yield a clear watery oil (4.22 g, 91.1%). ^{1}H (400 MHz, $CDCl_3$): δ7.32 (m, 5H), 4.63 (s, 2H), 3.746 (s, 2H), 3.740 (s, 3H). ^{13}C (400 MHz, CD_3CN): δ 172.4, 169.6, 135.4, 130.7, 129.8, 128.4, 62.2, 53.1, 41.4. FT-IR (ATR): neat, 1740.97 cm^{-1}. HRMS (ESI-TOF) m/z: $[M]^+$ calculated for $C_{11}H_{12}O_4$ 209.0814; found 209.0803.

G. ^{1}H NMR of Selected Photolysis Reactions

The following ^{1}H NMR spectra are from the photolysis reactions presented in Table 2.1. The solvents of the photolysis mixtures were removed under pressure and the unpurified products were dissolved in $CDCl_3$. Product ratios were determined by integration of the methylene (R_2CH_2) protons for the following compounds at the corresponding chemical shifts.

Figure 6.1 ^{1}H NMR spectra (below) of the photolysis of **36** in various solvents at 253.7 nm

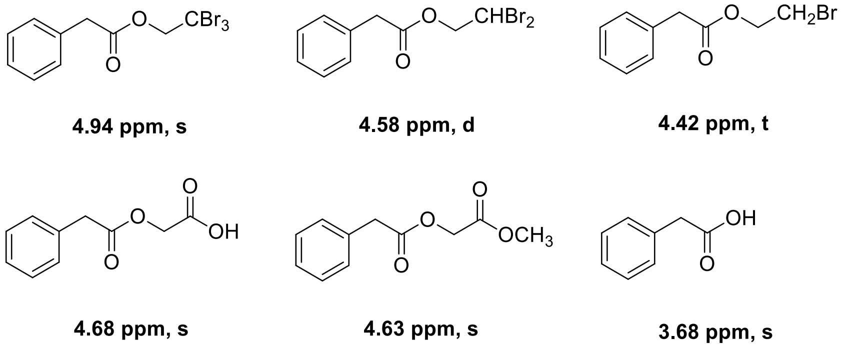

4.94 ppm, s

4.58 ppm, d

4.42 ppm, t

4.68 ppm, s

4.63 ppm, s

3.68 ppm, s

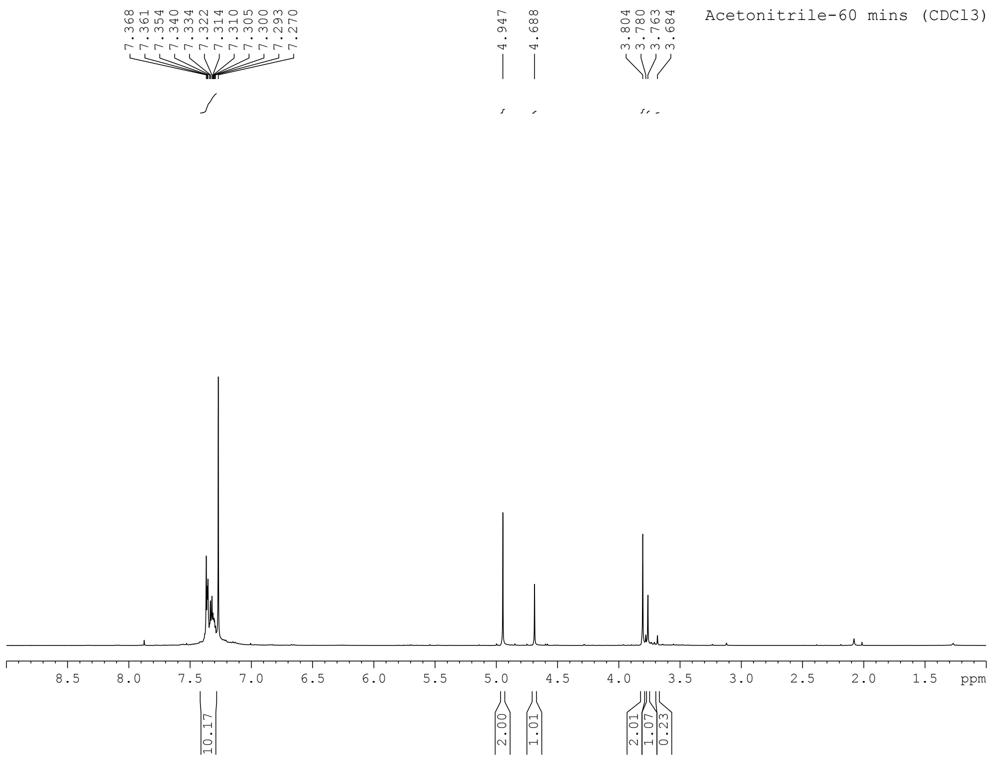

Photolysis of **36** (15.2 mM) in acetonitrile 60 minutes ($CDCl_3$).

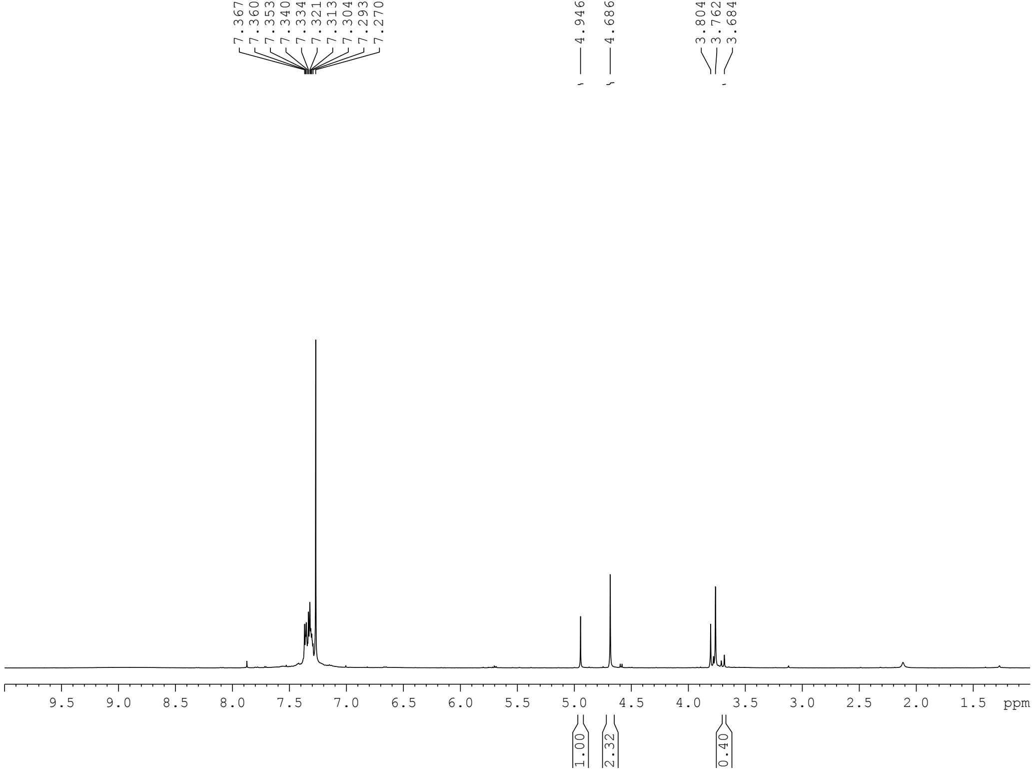

Photolysis of **36** (15.2 mM) in acetonitrile 120 minutes ($CDCl_3$).

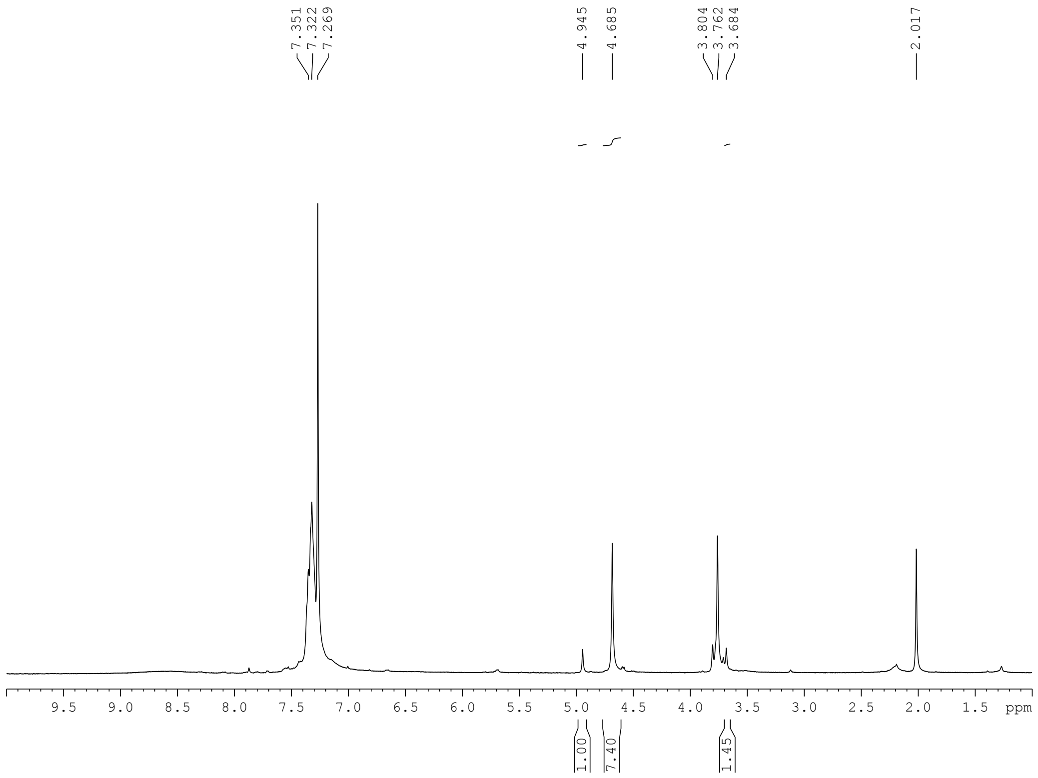

Photolysis of **36** (15.2 mM) in acetonitrile 180 minutes ($CDCl_3$).

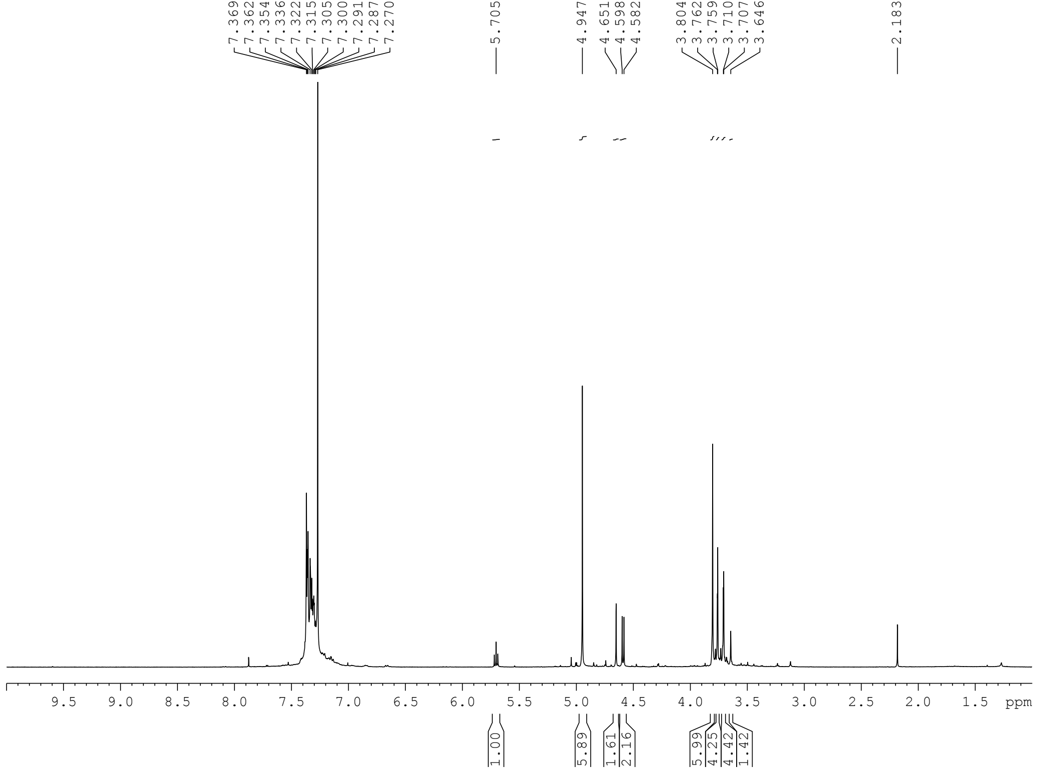

Photolysis of **36** (15.9 mM) in methanol 30 minutes ($CDCl_3$).

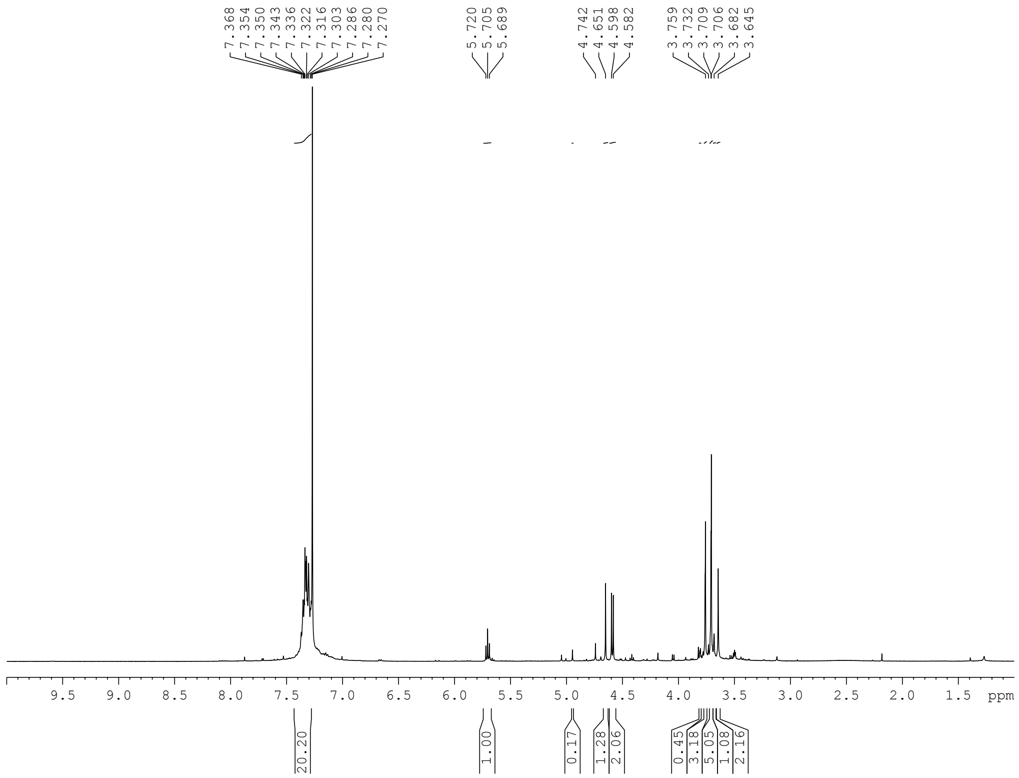

Photolysis of **36** (15.9 mM) in methanol 60 minutes ($CDCl_3$).

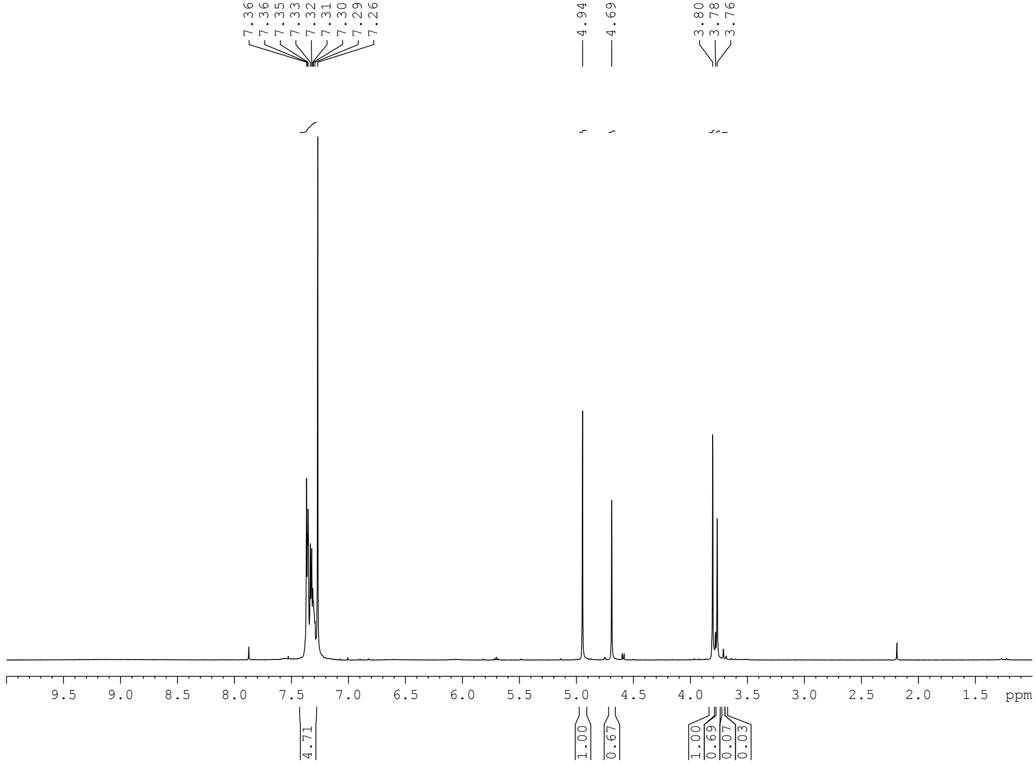

Photolysis of **36** (20.1 mM) in acetonitrile-d_3 90 minutes ($CDCl_3$).

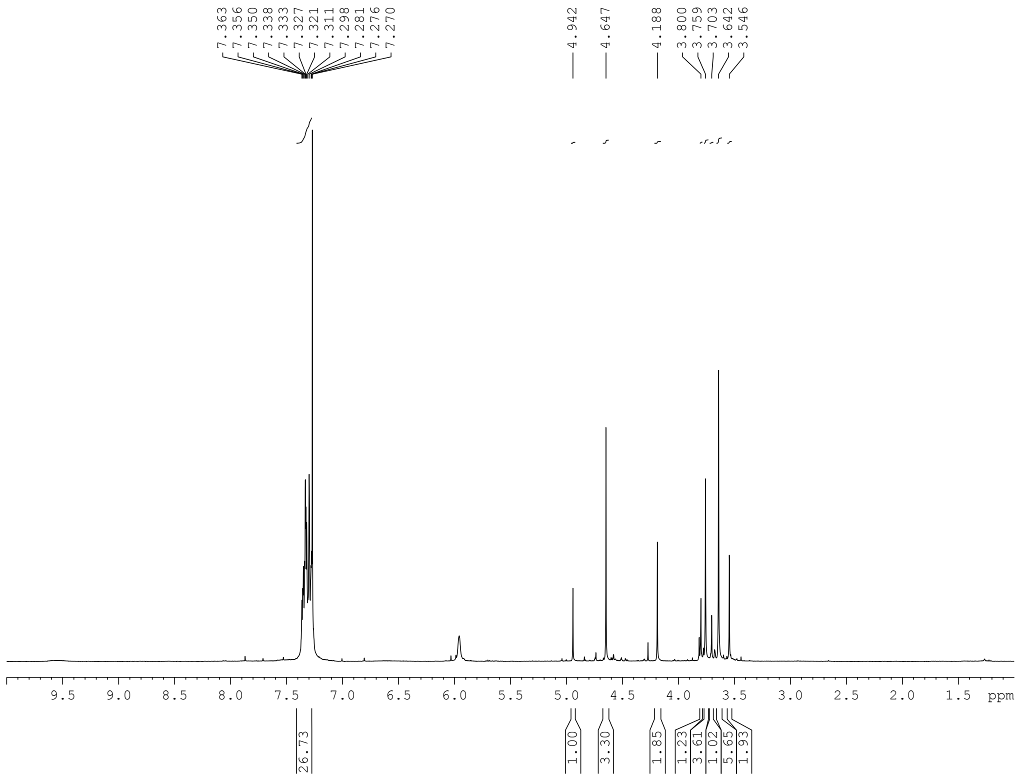

Photolysis of **36** (27.6 mM) in methanol-d$_4$ 90 minutes (CDCl$_3$).

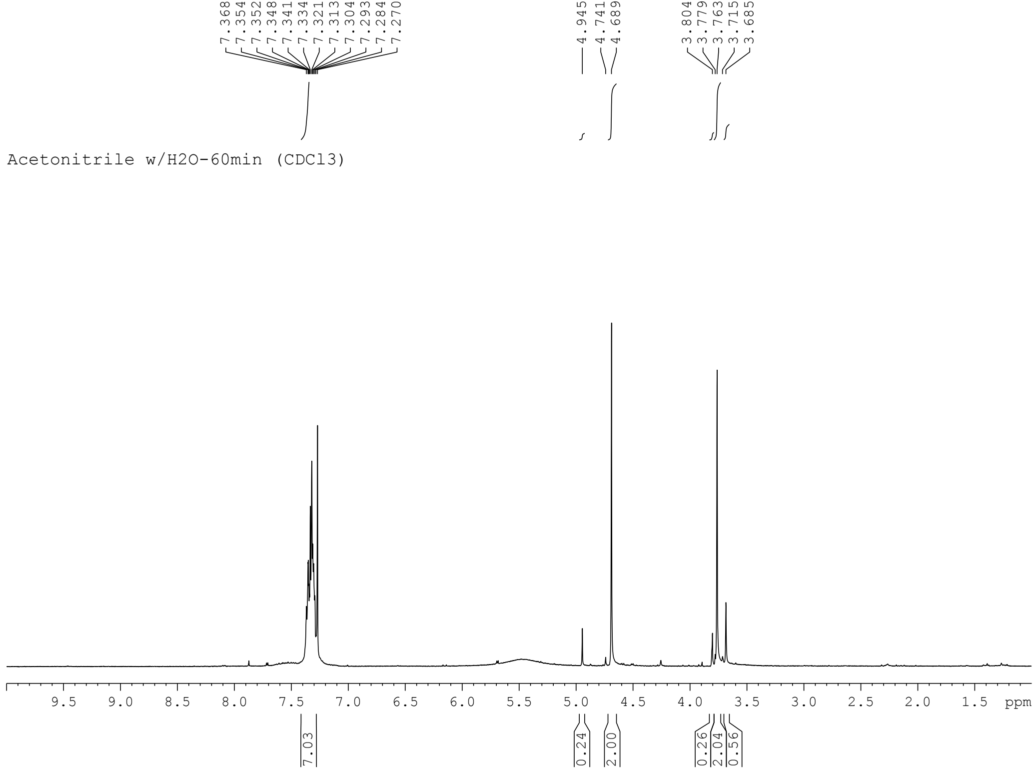

Photolysis of **36** (13.8 mM) in acetonitrile w/added H$_2$O 60 minutes (CDCl$_3$).

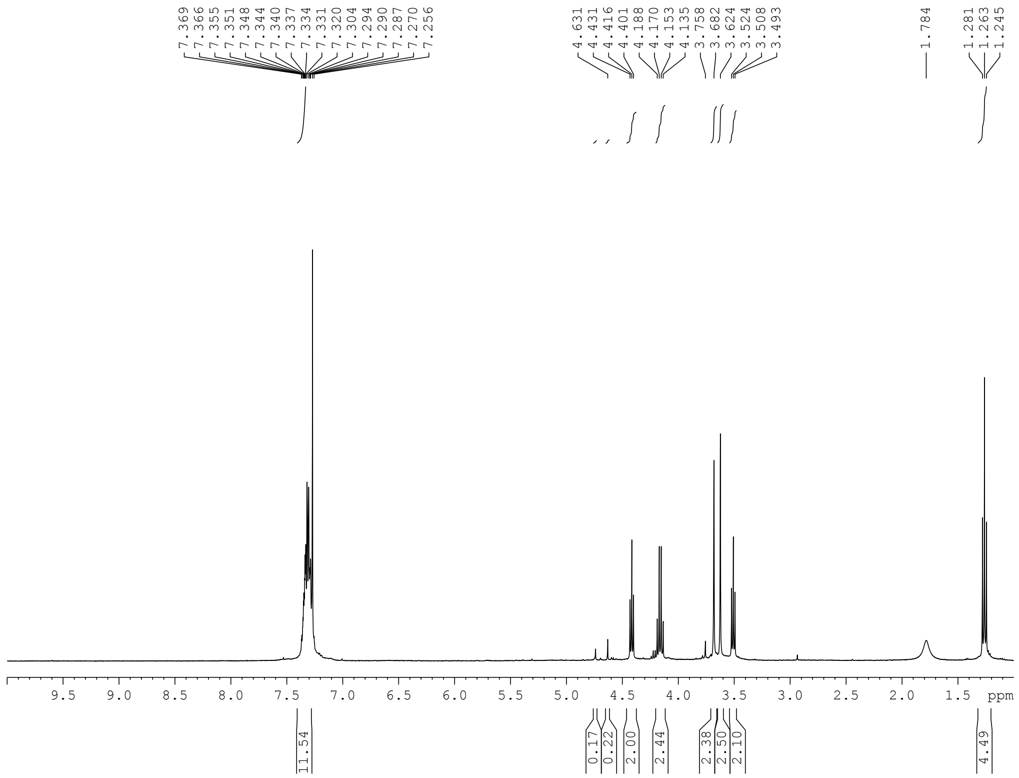

Photolysis of **36** (22.7 mM) in ethanol 60 minutes ($CDCl_3$).

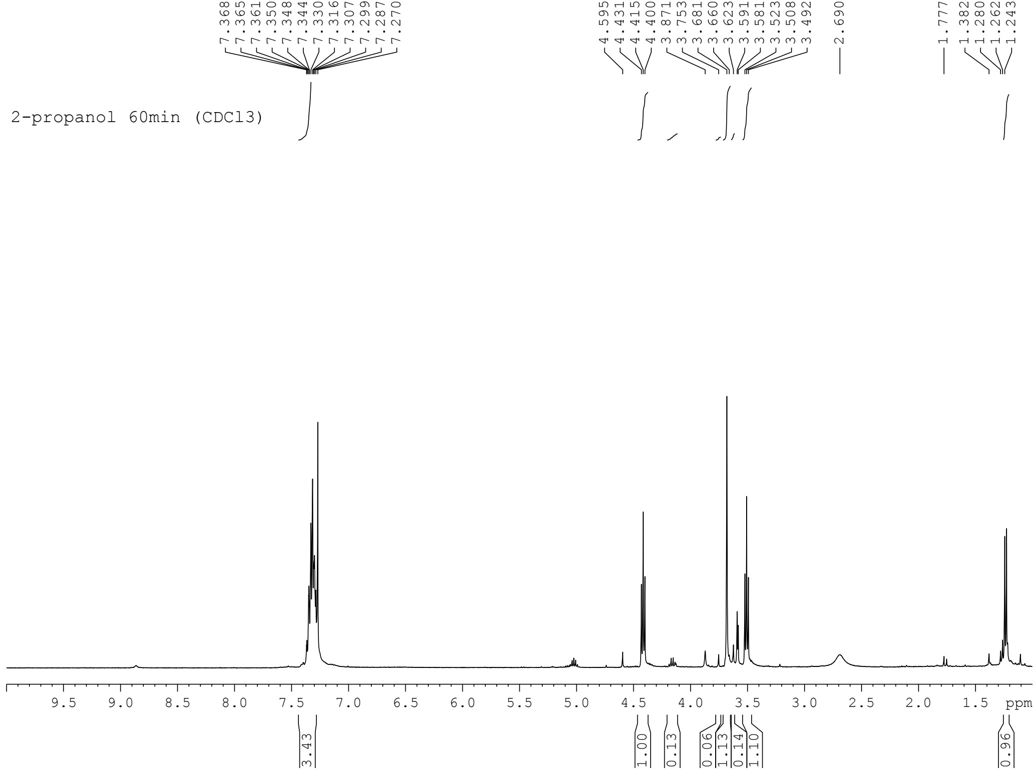

Photolysis of **36** (19.9 mM) in 2-propanol 60 minutes ($CDCl_3$).

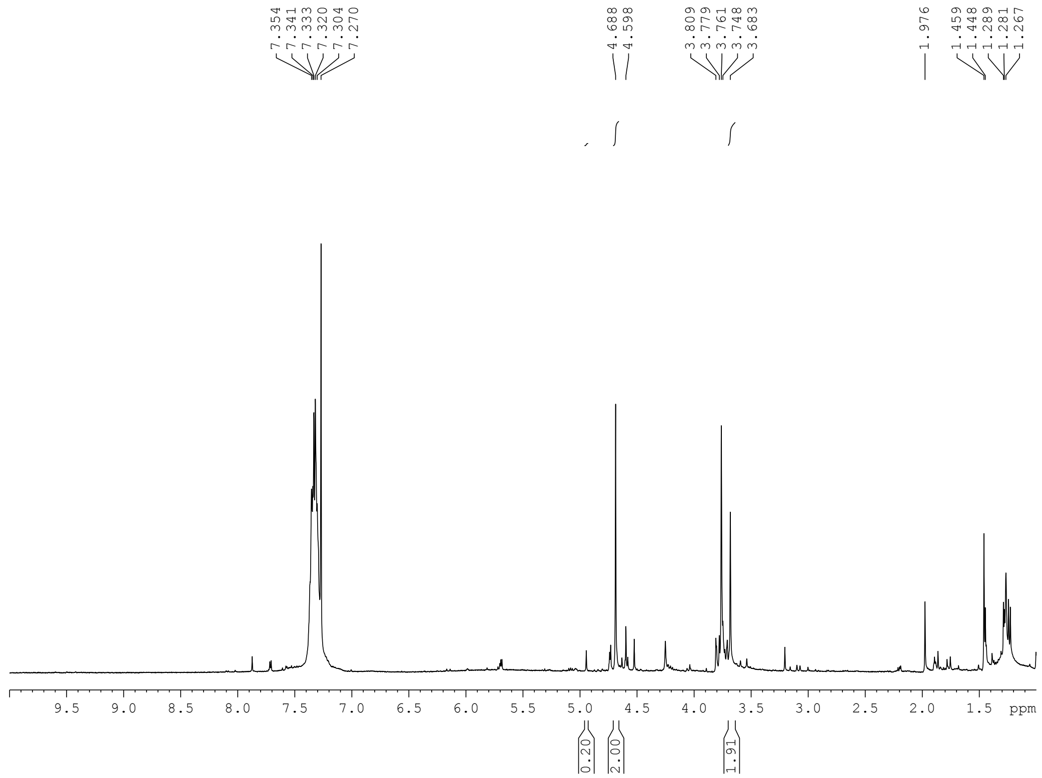

Photolysis of **36** (16.5 mM) in *tert*-butyl alcohol 60 minutes ($CDCl_3$).

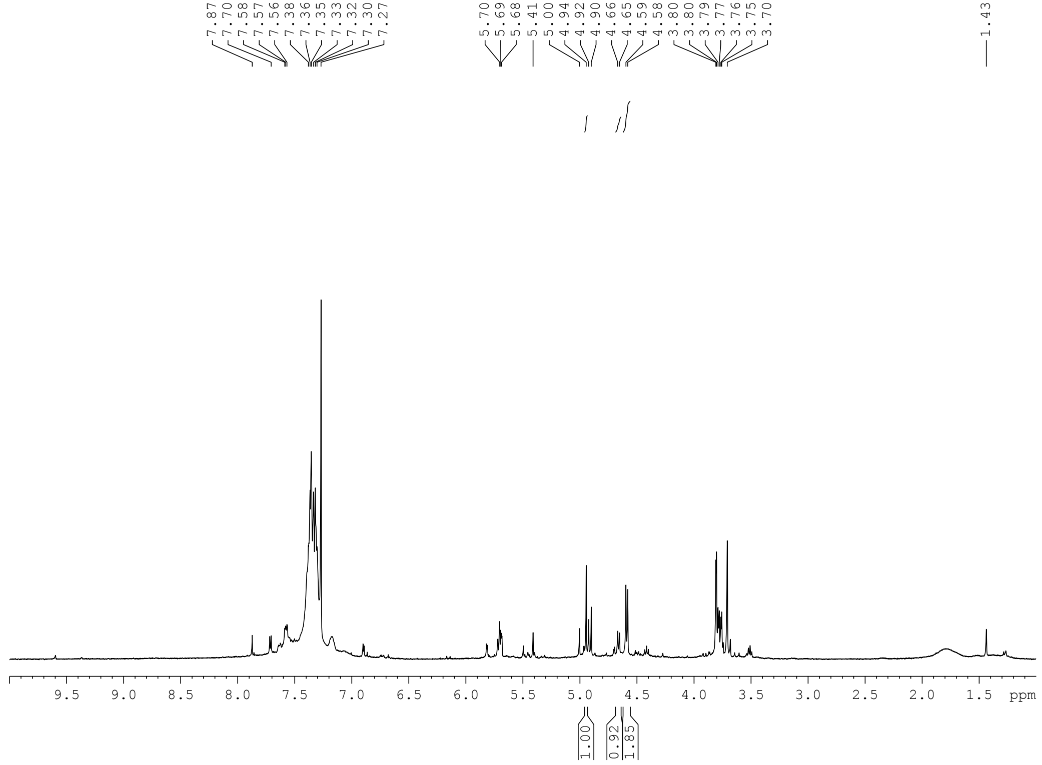

Photolysis of **36** (13.5 mM) in cyclohexane 60 minutes ($CDCl_3$).

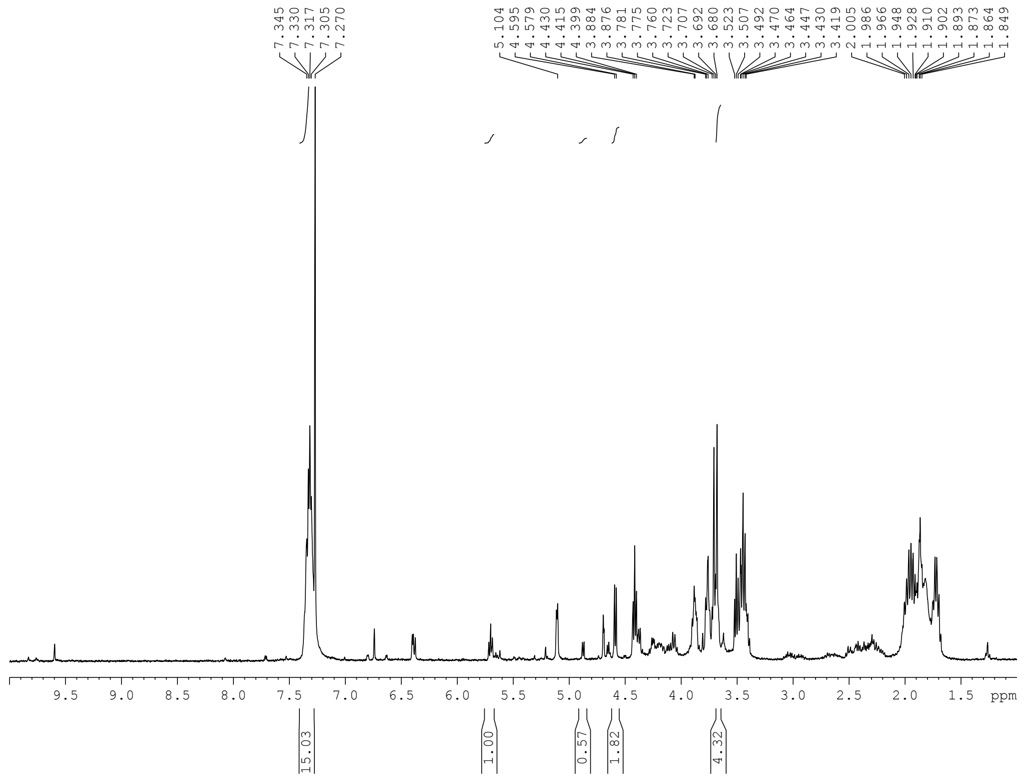
Photolysis of **36** (18.5 mM) in THF no BHT 60 minutes ($CDCl_3$).

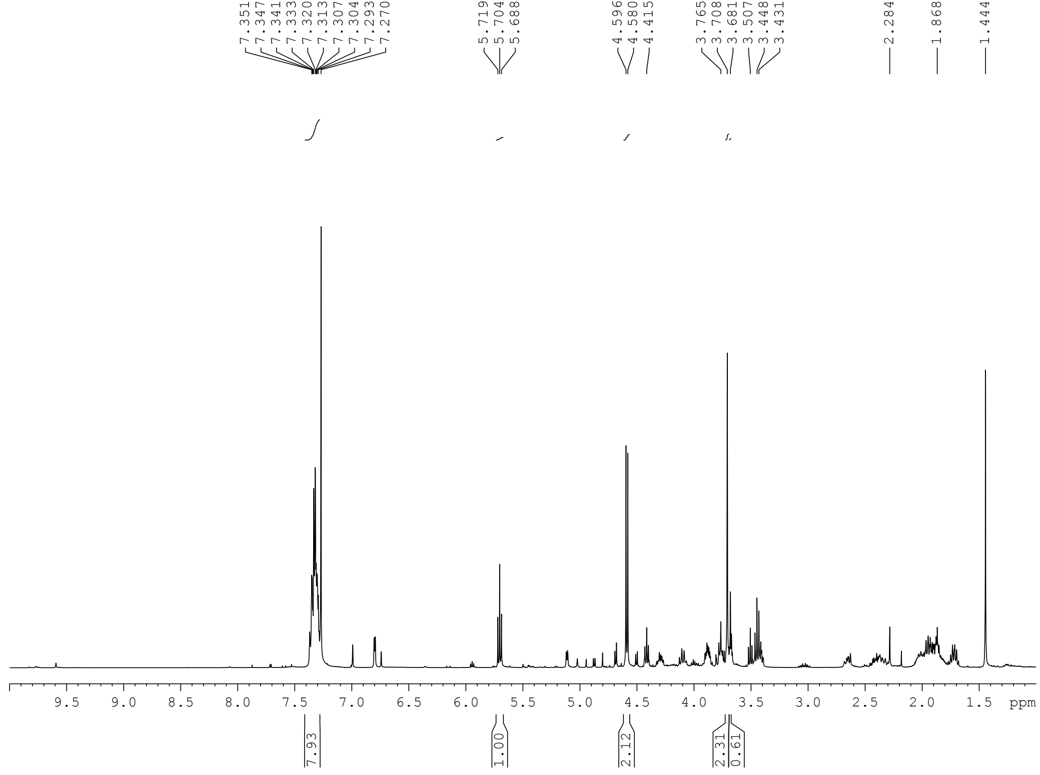
Photolysis of **36** (19.0 mM) in THF w/BHT 30 minutes ($CDCl_3$).

H. HPLC and MS Confirmation of Glycolic Ester 40b and Acid 40a

The following HPLC results were conducted on a Shimadzu Prominence LC-20AT instrument. The stationary phase is a Luna 5 µm C_{18}(2) 100 Å column (dimensions 250 x 4.6 mm) provided by Phenomenex. The mobile phase was a 60:40 mixture of MeOH:H_2O at a flow rate of 1.0 mL/min. Detection was carried out at 254 nm with a cell temperature of 40 °C.

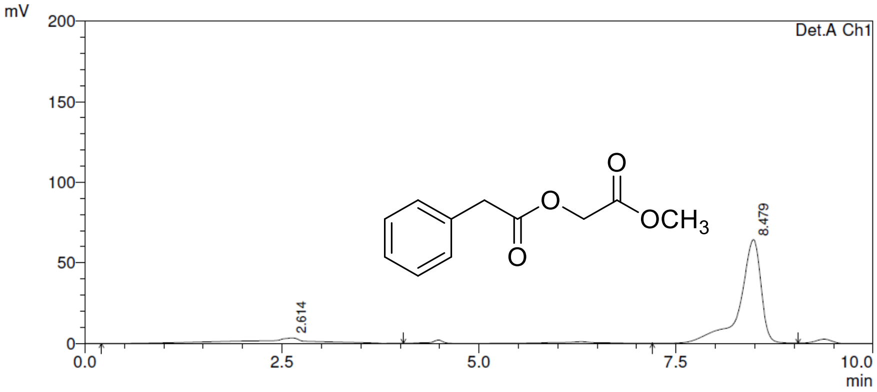

Figure 6.2 HPLC chromatogram of compound **40b**.

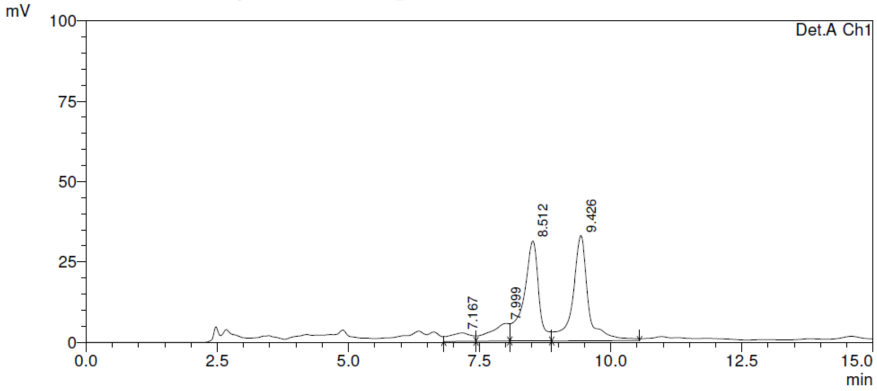

Figure 6.3 HPLC chromatogram after 60 minute photolysis of **36** in methanol.

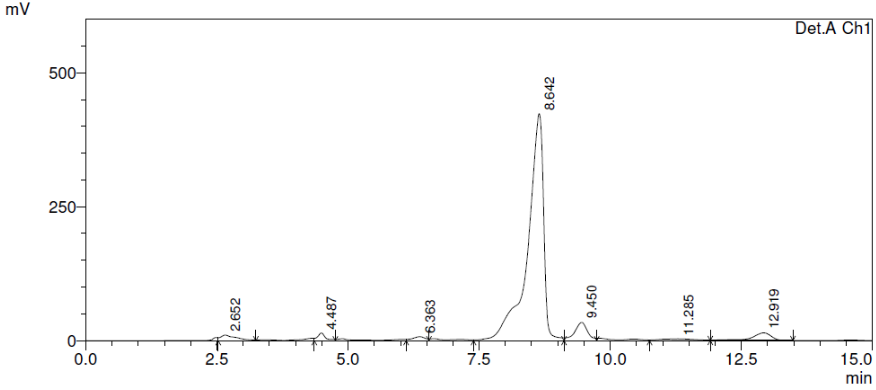

Figure 6.4 HPLC chromatogram of a **36** photolysis spiked with compound **40b**.

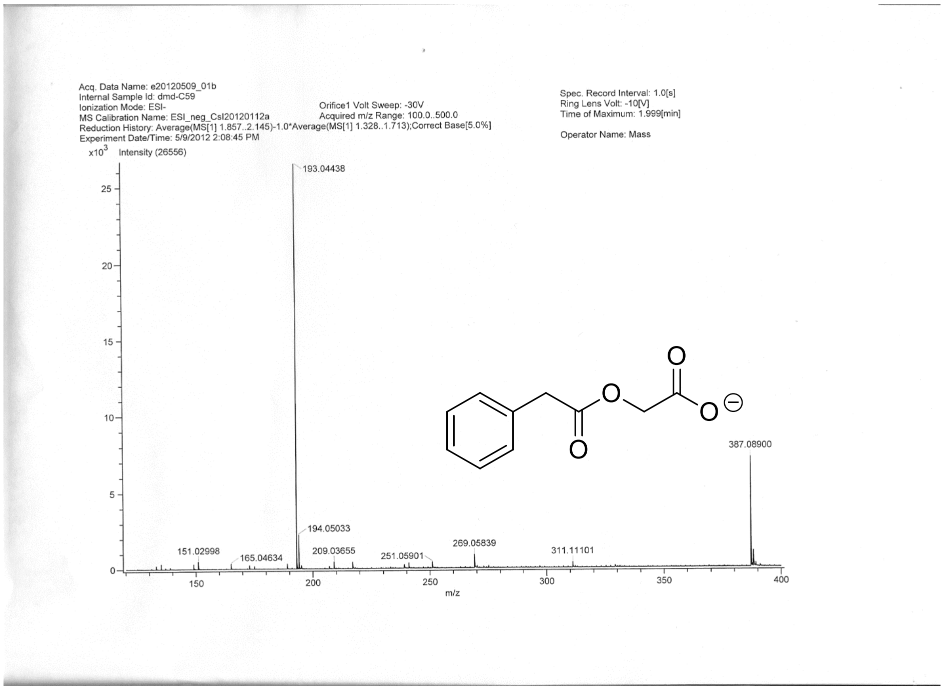

Acq. Data Name: e20120509_01b
Internal Sample Id: dmd-C59
Ionization Mode: ESI-
MS Calibration Name: ESI_neg_CsI20120112a
Orifice1 Volt Sweep: -30V
Acquired m/z Range: 100.0..500.0
Reduction History: Average(MS[1] 1.857..2.145)-1.0*Average(MS[1] 1.328..1.713);Correct Base[5.0%]
Experiment Date/Time: 5/9/2012 2:08:45 PM
Spec. Record Interval: 1.0[s]
Ring Lens Volt: -10[V]
Time of Maximum: 1.999[min]
Operator Name: Mass

Figure 6.5 MS confirmation of **40a** in photolysis reaction of **36** performed in *tert*-butyl alcohol.

I. GC-MS Photolysis Results of 36 in Various Alcoholic Solvents

The following photolysis experiments were conducted under conditions previously stated and analyzed by GC-MS. The photolysis solvents were evaporated and dissolved in MeCN without purification. Analysis was done on a JEOL JMS-700 MStation coupled with an Agilent 6890N GC system. Identifiable molecular ion peaks **(M+)** are matched to the presumed molecular structure where appropriate.

Figure 6.6 GC-MS results of the 253.7 nm photolysis of **36** in (A) methanol (9.38 mM), (B) ethanol (15.47 mM), (C) 2-propanol (11.3 mM) and (D) *tert*-butyl alcohol (11.2 mM).

(A) methanol

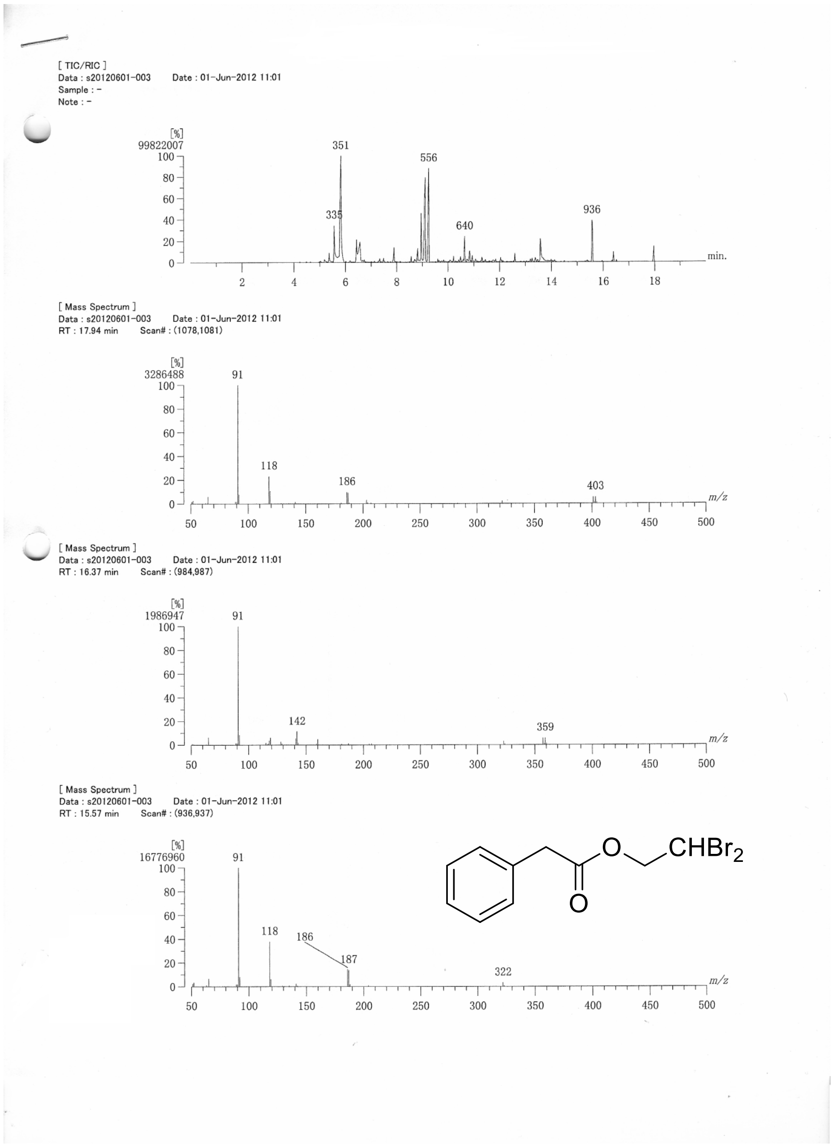

[TIC/RIC]
Data : s20120601-003 Date : 01-Jun-2012 11:01
Sample : -
Note : -

[Mass Spectrum]
Data : s20120601-003 Date : 01-Jun-2012 11:01
RT : 17.94 min Scan# : (1078,1081)

[Mass Spectrum]
Data : s20120601-003 Date : 01-Jun-2012 11:01
RT : 16.37 min Scan# : (984,987)

[Mass Spectrum]
Data : s20120601-003 Date : 01-Jun-2012 11:01
RT : 15.57 min Scan# : (936,937)

[Mass Spectrum]
Data : s20120601-003 Date : 01-Jun-2012 11:01
RT : 10.63 min Scan# : (639,641)

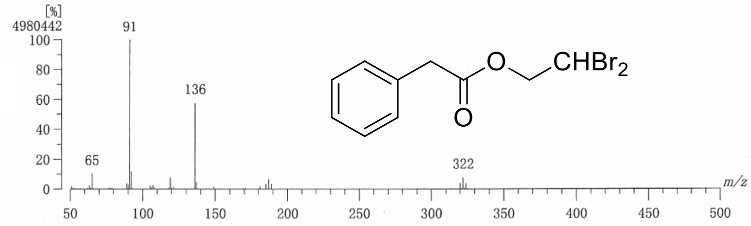

[Mass Spectrum]
Data : s20120601-003 Date : 01-Jun-2012 11:01
RT : 10.46 min Scan# : (629,631)

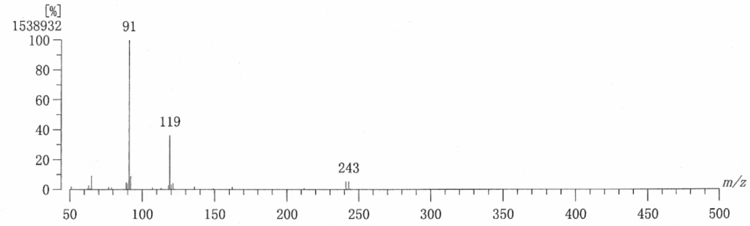

[Mass Spectrum]
Data : s20120601-003 Date : 01-Jun-2012 11:01
RT : 9.21 min Scan# : (554,557)

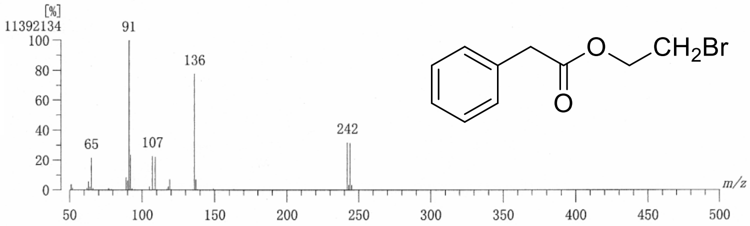

[Mass Spectrum]
Data : s20120601-003 Date : 01-Jun-2012 11:01
RT : 9.06 min Scan# : (545,548)

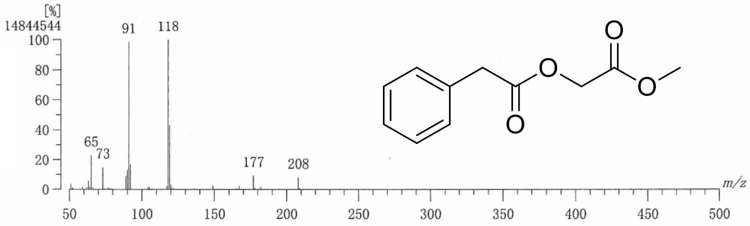

[Mass Spectrum]
Data : s20120601-003 Date : 01-Jun-2012 11:01
RT : 8.93 min Scan# : (537,540)

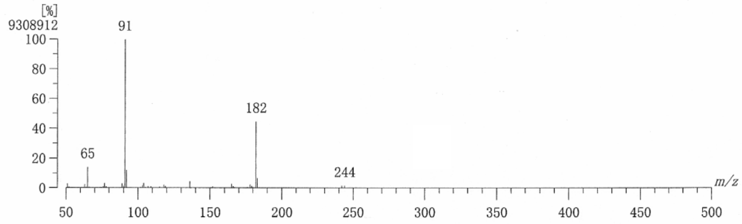

[Mass Spectrum]
Data : s20120601-003 Date : 01-Jun-2012 11:01
RT : 8.79 min Scan# : (529,531)

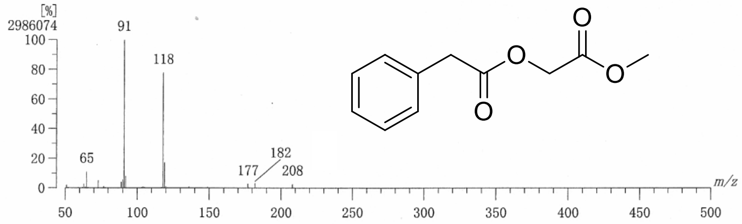

[Mass Spectrum]
Data : s20120601-003 Date : 01-Jun-2012 11:01
RT : 7.88 min Scan# : (474,475)

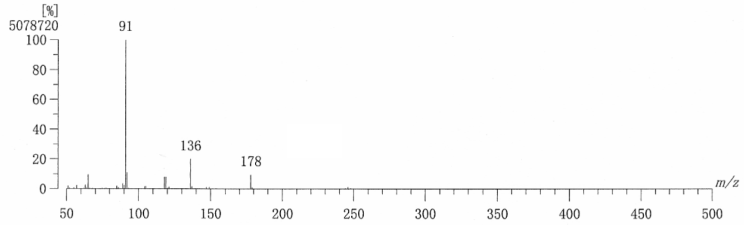

[Mass Spectrum]
Data : s20120601-003 Date : 01-Jun-2012 11:01
RT : 6.41 min Scan# : (386,397)

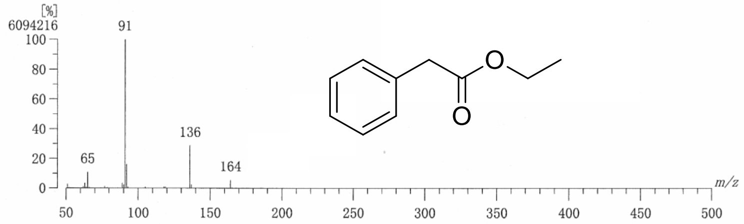

[Mass Spectrum]
Data : s20120601-003   Date : 01-Jun-2012 11:01
RT : 5.78 min   Scan# : (348,352)

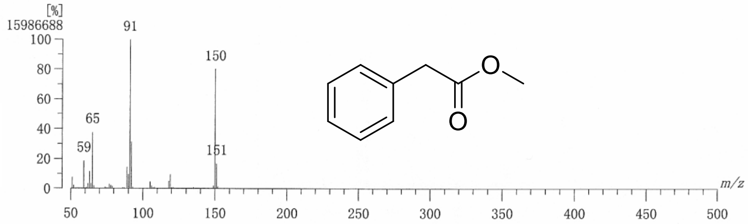

[Mass Spectrum]
Data : s20120601-003   Date : 01-Jun-2012 11:01
RT : 5.55 min   Scan# : (334,336)

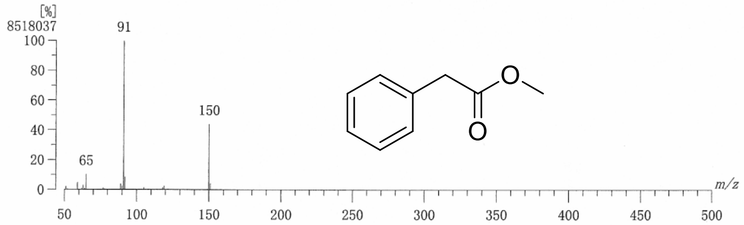

(B) ethanol

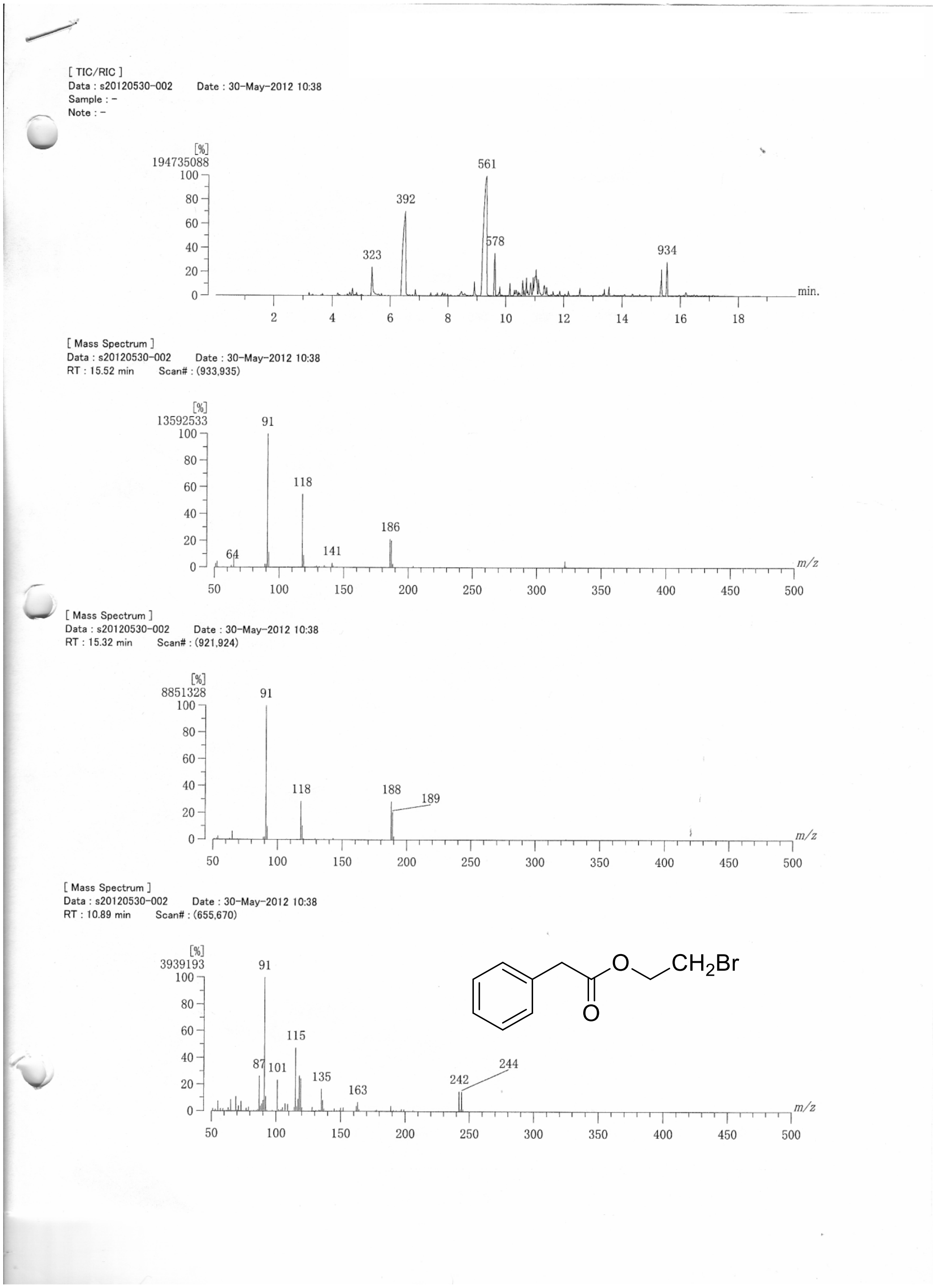

[TIC/RIC]
Data : s20120530-002 Date : 30-May-2012 10:38
Sample : -
Note : -

[Mass Spectrum]
Data : s20120530-002 Date : 30-May-2012 10:38
RT : 15.52 min Scan# : (933,935)

[Mass Spectrum]
Data : s20120530-002 Date : 30-May-2012 10:38
RT : 15.32 min Scan# : (921,924)

[Mass Spectrum]
Data : s20120530-002 Date : 30-May-2012 10:38
RT : 10.89 min Scan# : (655,670)

[Mass Spectrum]
Data : s20120530-002 Date : 30-May-2012 10:38
RT : 9.58 min Scan# : (576,579)

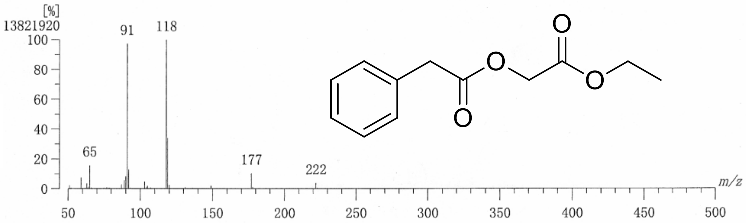

[Mass Spectrum]
Data : s20120530-002 Date : 30-May-2012 10:38
RT : 9.14 min Scan# : (550,562)

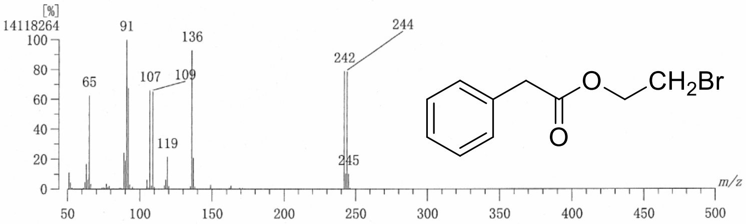

[Mass Spectrum]
Data : s20120530-002 Date : 30-May-2012 10:38
RT : 6.40 min Scan# : (385,393)-k(431)[k=1.0]

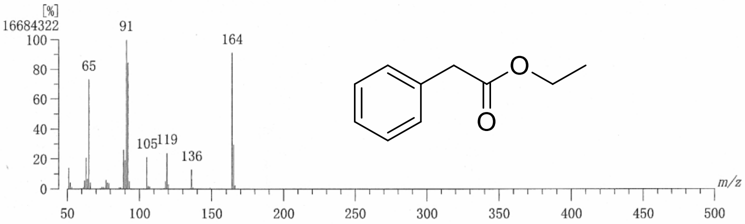

[Mass Spectrum]
Data : s20120530-002 Date : 30-May-2012 10:38
RT : 5.33 min Scan# : (321,325)-k(353)[k=1.0]

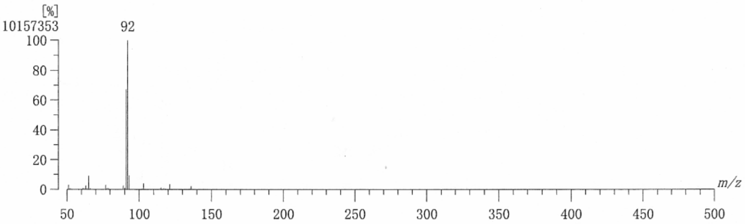

(C) 2-propanol

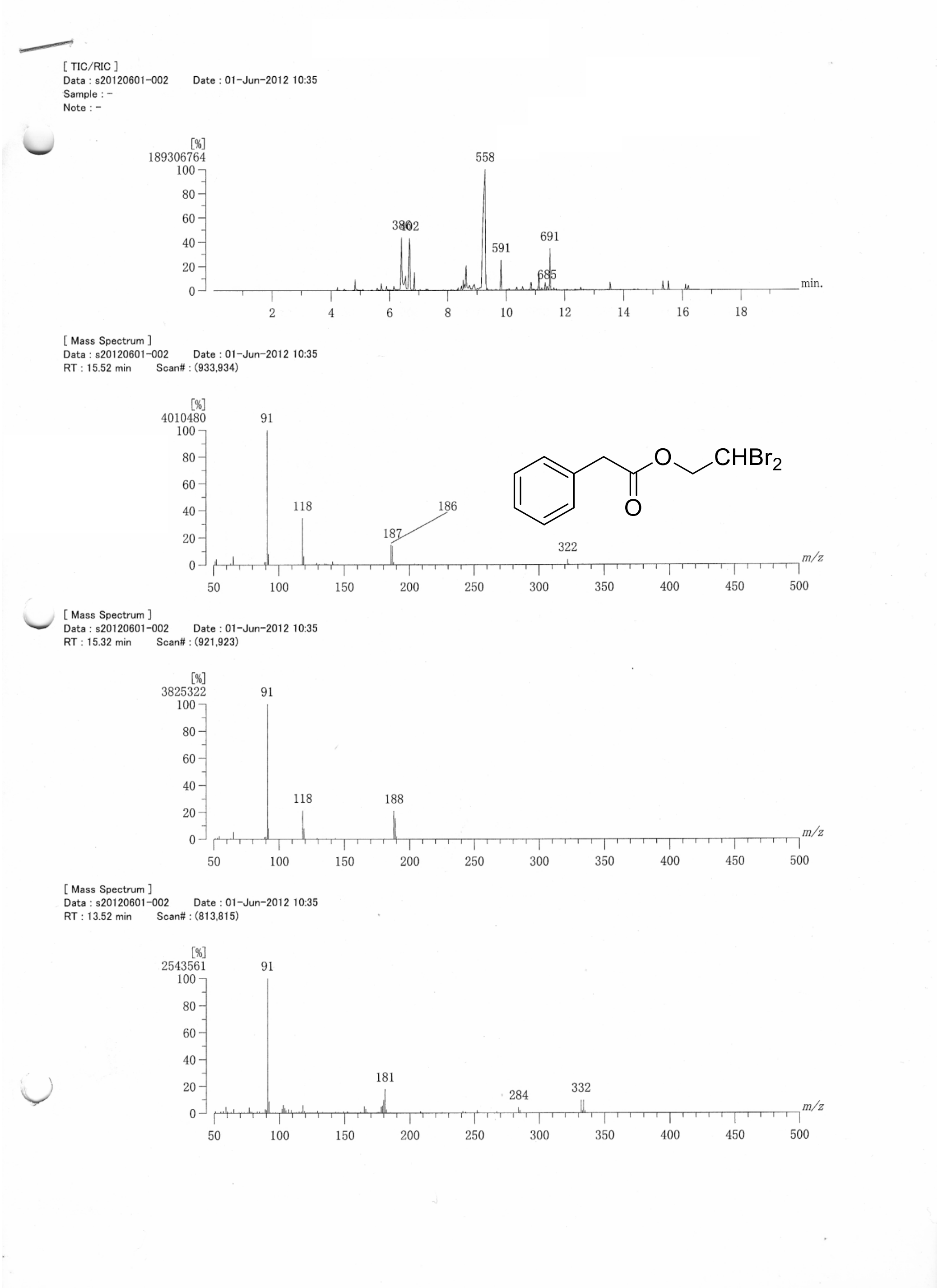

[TIC/RIC]
Data : s20120601-002 Date : 01-Jun-2012 10:35
Sample : -
Note : -

[Mass Spectrum]
Data : s20120601-002 Date : 01-Jun-2012 10:35
RT : 15.52 min Scan# : (933,934)

[Mass Spectrum]
Data : s20120601-002 Date : 01-Jun-2012 10:35
RT : 15.32 min Scan# : (921,923)

[Mass Spectrum]
Data : s20120601-002 Date : 01-Jun-2012 10:35
RT : 13.52 min Scan# : (813,815)

[Mass Spectrum]
Data : s20120601-002 Date : 01-Jun-2012 10:35
RT : 11.48 min Scan# : (690,692)

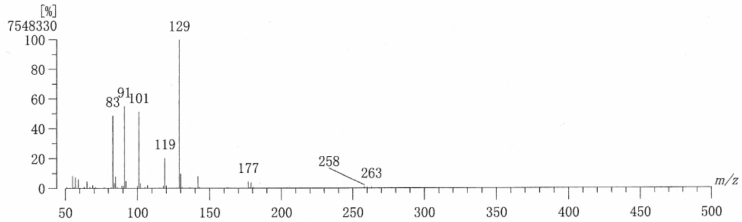

[Mass Spectrum]
Data : s20120601-002 Date : 01-Jun-2012 10:35
RT : 11.09 min Scan# : (667,669)

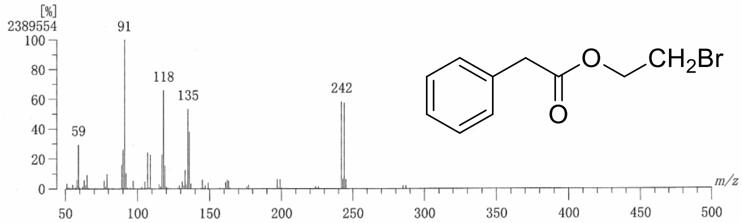

[Mass Spectrum]
Data : s20120601-002 Date : 01-Jun-2012 10:35
RT : 10.83 min Scan# : (651,653)

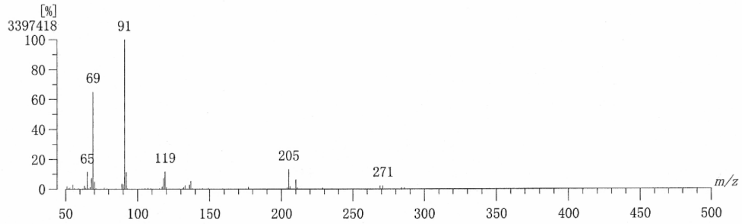

[Mass Spectrum]
Data : s20120601-002 Date : 01-Jun-2012 10:35
RT : 9.81 min Scan# : (590,592)

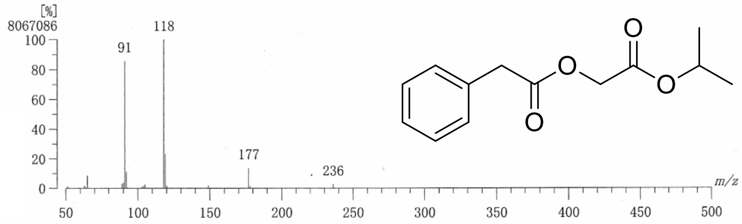

[Mass Spectrum]
Data : s20120601-002 Date : 01-Jun-2012 10:35
RT : 9.16 min Scan# : (551,559)

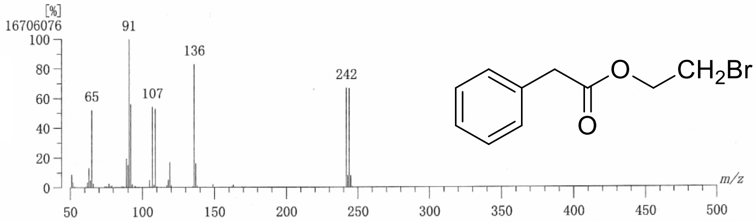

[Mass Spectrum]
Data : s20120601-002 Date : 01-Jun-2012 10:35
RT : 8.53 min Scan# : (513,520)

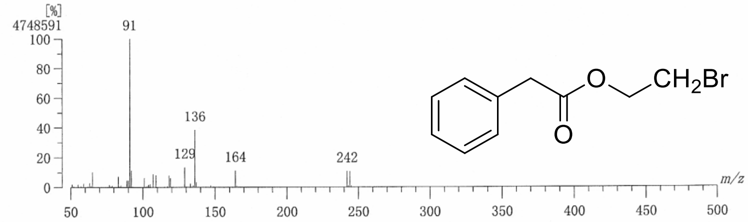

[Mass Spectrum]
Data : s20120601-002 Date : 01-Jun-2012 10:35
RT : 6.83 min Scan# : (411,413)

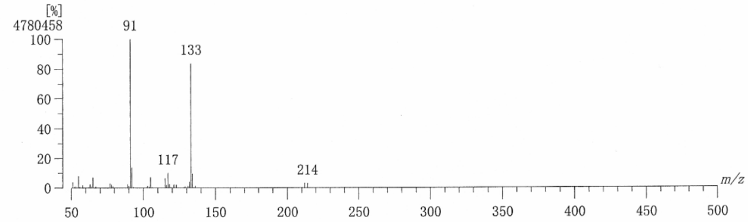

[Mass Spectrum]
Data : s20120601-002 Date : 01-Jun-2012 10:35
RT : 6.65 min Scan# : (400,403)

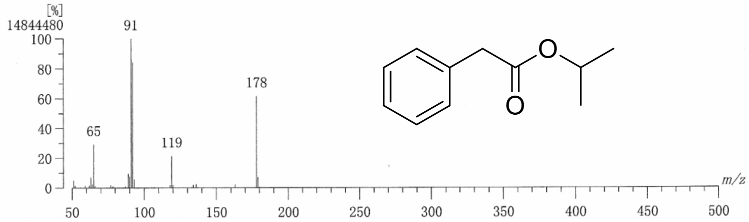

[Mass Spectrum]
Data : s20120601-002 Date : 01-Jun-2012 10:35
RT : 6.51 min Scan# : (392,395)

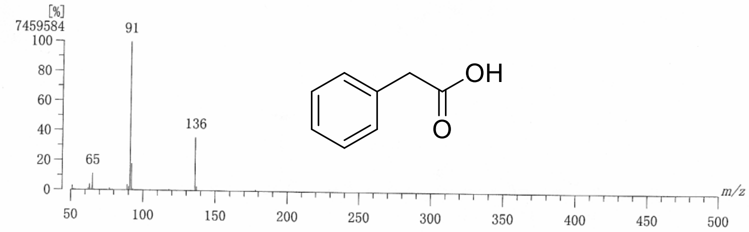

[Mass Spectrum]
Data : s20120601-002 Date : 01-Jun-2012 10:35
RT : 6.38 min Scan# : (384,387)

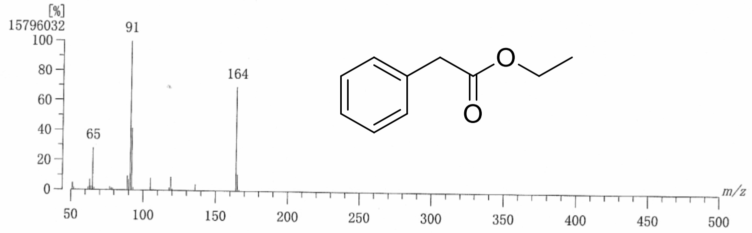

(D) *tert*-butyl alcohol

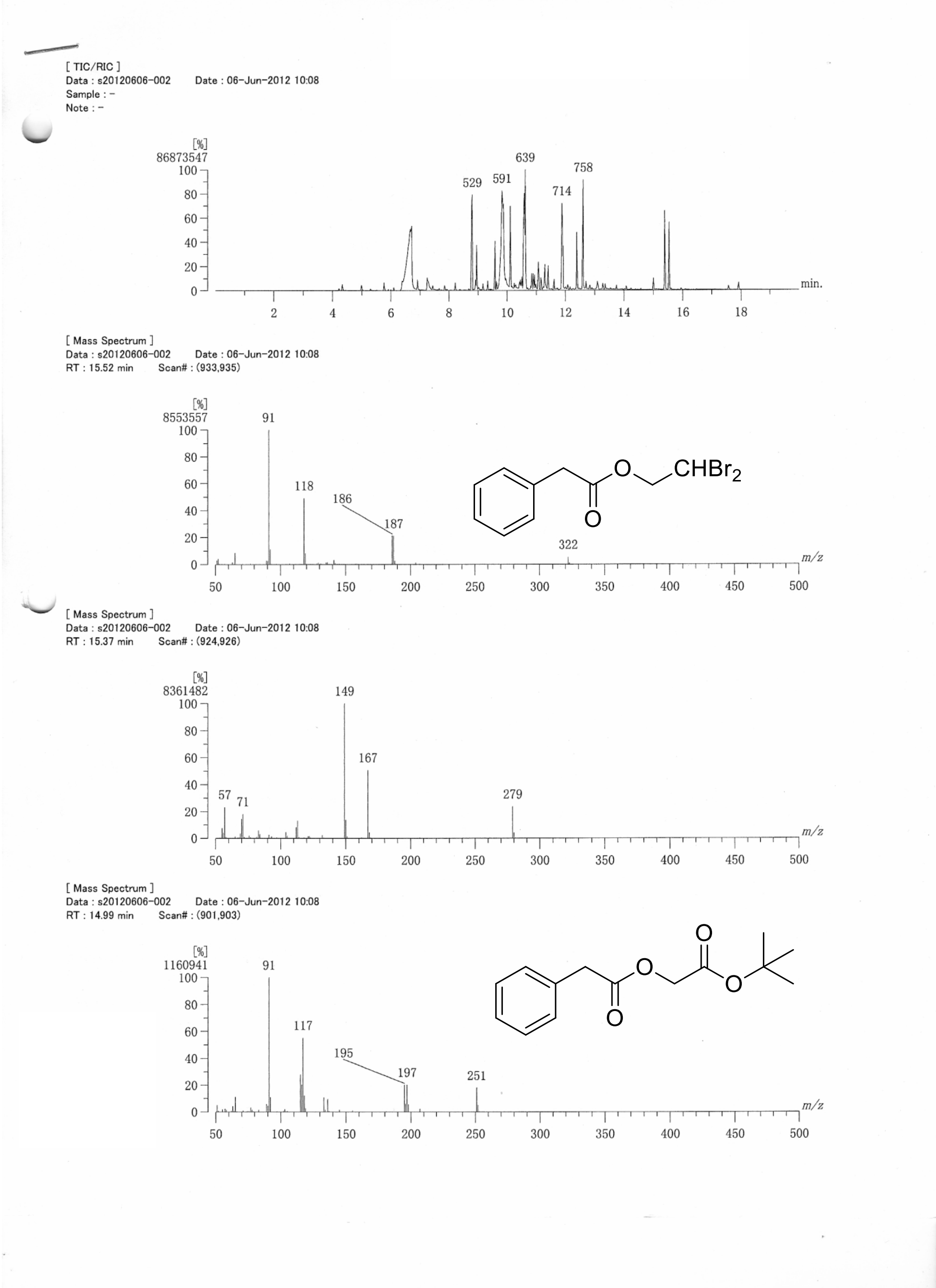

[TIC/RIC]
Data : s20120606-002 Date : 06-Jun-2012 10:08
Sample : –
Note : –

[Mass Spectrum]
Data : s20120606-002 Date : 06-Jun-2012 10:08
RT : 15.52 min Scan# : (933,935)

[Mass Spectrum]
Data : s20120606-002 Date : 06-Jun-2012 10:08
RT : 15.37 min Scan# : (924,926)

[Mass Spectrum]
Data : s20120606-002 Date : 06-Jun-2012 10:08
RT : 14.99 min Scan# : (901,903)

[Mass Spectrum]
Data : s20120606-002 Date : 06-Jun-2012 10:08
RT : 12.59 min Scan# : (757,759)

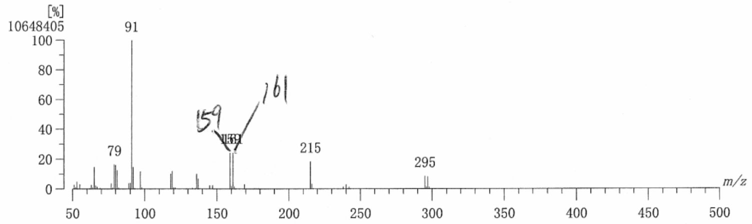

[Mass Spectrum]
Data : s20120606-002 Date : 06-Jun-2012 10:08
RT : 12.37 min Scan# : (744,746)

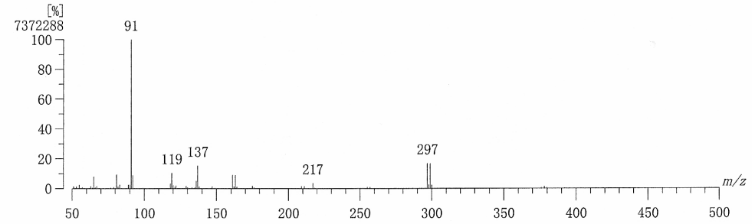

[Mass Spectrum]
Data : s20120606-002 Date : 06-Jun-2012 10:08
RT : 11.86 min Scan# : (713,717)

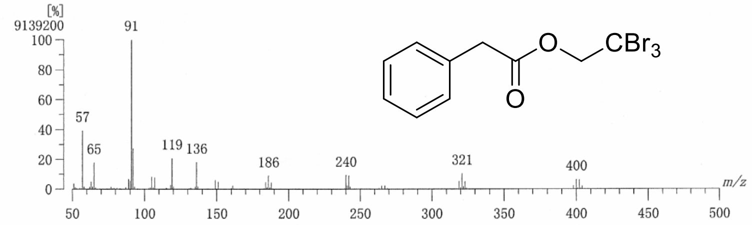

[Mass Spectrum]
Data : s20120606-002 Date : 06-Jun-2012 10:08
RT : 11.06 min Scan# : (665,667)

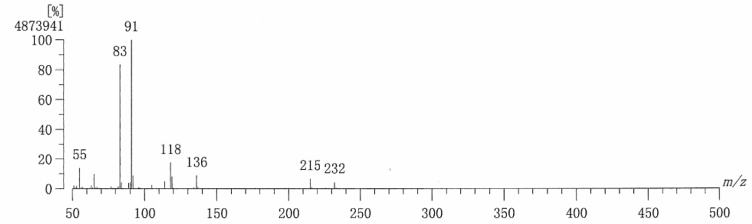

[Mass Spectrum]
Data : s20120606-002 Date : 06-Jun-2012 10:08
RT : 10.54 min Scan# : (634,640)

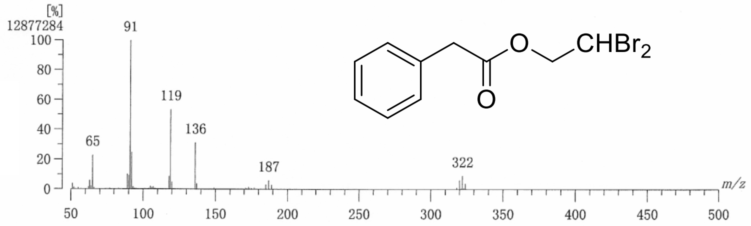

[Mass Spectrum]
Data : s20120606-002 Date : 06-Jun-2012 10:08
RT : 10.09 min Scan# : (607,610)

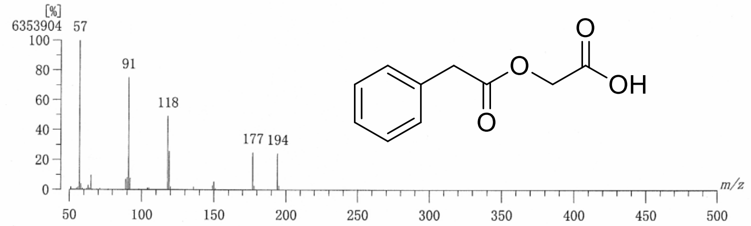

[Mass Spectrum]
Data : s20120606-002 Date : 06-Jun-2012 10:08
RT : 9.74 min Scan# : (586,596)

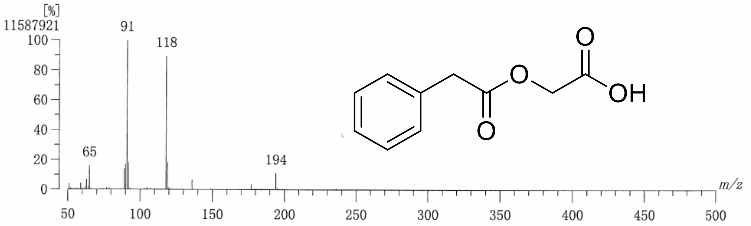

[Mass Spectrum]
Data : s20120606-002 Date : 06-Jun-2012 10:08
RT : 8.91 min Scan# : (536,540)

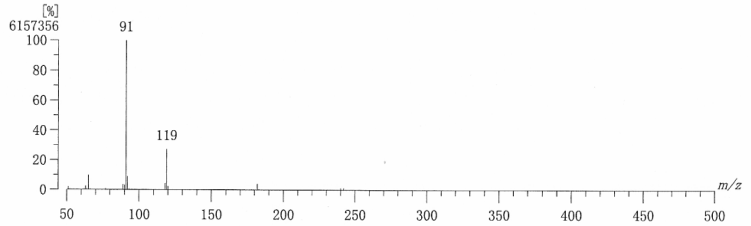

[Mass Spectrum]
Data : s20120606-002 Date : 06-Jun-2012 10:08
RT : 8.76 min Scan# : (527,529)

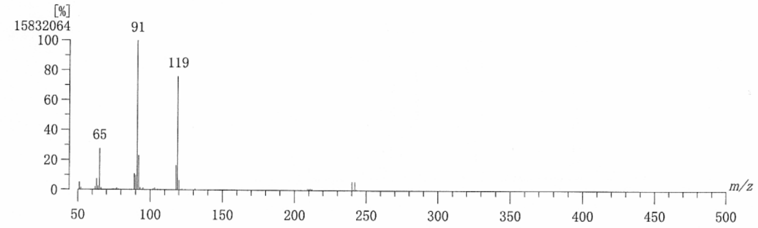

[Mass Spectrum]
Data : s20120606-002 Date : 06-Jun-2012 10:08
RT : 6.38 min Scan# : (384,405)

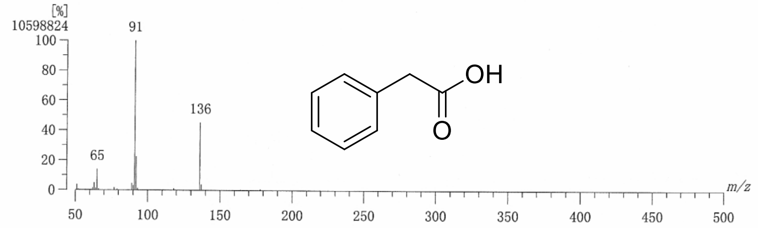

6.3 Chapter 3 Experimental Results

A. Synthesis of Tritylone Ethers

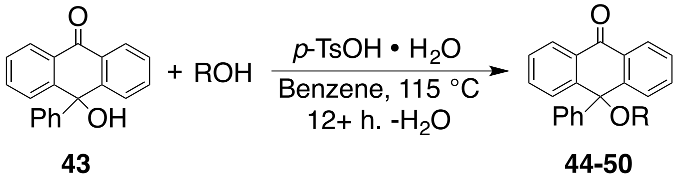

The following general procedure was used for the synthesis of ethers **44-50**. More specific details can be found under the corresponding ether. Tritylone alcohol **43**, *p*-toluenesulfonic acid monohydrate (*p*-TsOH•H_2O) and the alcohol of choice are added to benzene in an oven dried round bottom flask with a stir bar. The solution is heated while stirring at 115 °C under reflux equipped with a Dean–Stark trap for the removal of water. The reaction can be monitored by the disappearance of **43** via gas chromatography, and all the syntheses listed below were heated for 12+ hours. Upon completion of the reaction, the solution was left to cool to room temperature and the solvent was removed under reduced pressure with heating. The resulting black solid was purified using flash column chromatography with silica gel and a mobile phase of petroleum ether/diethyl ether unless otherwise noted.

9-hydroxy-9-phenylanthrone (43)

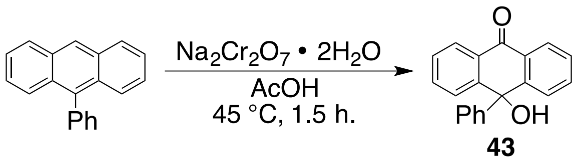

To an oven dried 50 mL round bottom flask with a stir bar, 9-phenylanthracene (2.3065 g, 9.07 mmol) was added to approximately 30 mL of glacial acetic acid. To the slurry solution, sodium dichromate dihydrate (3.9610 g, 13.3 mmol) was added and placed in an oil bath where it was heated at 45 °C for 90 minutes with stirring. Soon after the addition of sodium dichromate the solution goes from a tan/brownish color to dark green. After the allotted time, the solution was poured into 100 mL of deionized water and vacuum filtered. The white/off white powder is washed with generous portions of deionized water and placed under vacuum to dry (2.5433g, 97.9%). If necessary the white powder can be recrystallized from hexanes/ethyl acetate. GC R_T of tritylone alcohol is 14.1 minutes. ^{1}H NMR (400 MHz, $CDCl_3$) δ = 8.31-8.29 (dd, *J* = 1.2, 6.8 Hz, 2H), 7.65-7.56 (m, 4H), 7.48-7.44 (m, 2H), 7.38-7.35 (m, 2H), 7.26-7.22 (m, 2H), 7.18 (m, 1H), 2.84 (s, 1H). ^{13}C NMR (400 MHz, $CDCl_3$) δ = 183.90, 147.89, 146.11, 134.34, 130.04, 128.61, 128.56, 128.48, 127.16, 127.08, 125.63, 73.34. m.p. = 215-217 °C. HRMS (ESI-TOF) Calculated for $C_{20}H_{14}O_2$ $[M+H]^+$: 287.1072, Found: 287.1055. FT-IR (ATR): neat, 3405.35, 1738.24, 1650.83, 1599.61 cm^{-1}.

9-octoxy-9-phenylanthrone (44)

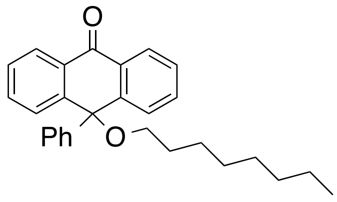

Tritylone alcohol (1.242 g, 4.34 mmol), *p*-TsOH•H_2O (60.2 mg, 0.316 mmol) and 1-octanol (0.684 mL, 4.33 mmol) was added to 80 mL of benzene in a 100 mL round bottom flask. Purified to white crystals with mobile phase of (1:9 ether:petroleum ether) to give (1.5690 g, 90.8%) of ether. GC R_T of octyl ether is 16.7 minutes. ^{1}H NMR (400 MHz, C_6D_6) δ = 8.64-8.62 (dd, *J* = 1.6, 6.2 Hz, 2H), 7.50-7.46 (m, 4H), 7.06-6.97 (m, 6H), 6.91-6.87 (m, 1H), 2.98 (t, *J* = 6.3 Hz, 2H), 1.53-1.46 (m, 2H), 1.28-1.20 (m, 10H), 0.916 (t, *J* = 6.9 Hz, 3H). ^{13}C NMR (400 MHz, $CDCl_3$) δ = 183.84, 146.83, 145.85, 134.13, 131.86, 128.84, 128.42, 128.22, 127.17, 126.79, 125.92, 77.99, 63.77, 32.06, 30.17, 29.57, 29.46, 26.46, 22.87, 14.32. m.p. = 42-43 °C. HRMS (ESI-TOF) Calculated for $C_{28}H_{30}O_2$ $[M+H]^+$: 399.2324, Found: 399.2305. FT-IR (ATR): neat, 2929.24, 2854.98, 1738.38, 1663.93, 1599.67 cm^{-1}.

9-(3’-O-acetoxythymidine)-9-phenylanthrone (45)

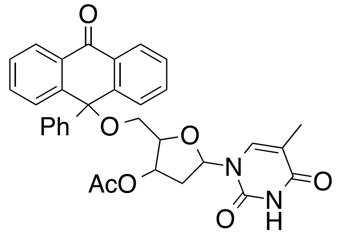

Tritylone alcohol (0.1847 g, 0.645 mmol), *p*-TsOH•H_2O (22.4 mg, 0.118 mmol) and 3’-O-acetoxythymidine (0.2047 g, 0.720 mmol) was added to 30 mL of benzene in a 50 mL round bottom flask. Purified to white crystals with a mobile phase of ethyl acetate to give (0.2733 g, 76.7%) of ether ^{1}H NMR (400 MHz, $CDCl_3$) δ = 8.93 (s, 1H), 8.42-8.40 (dd, *J* = 1.3, 6.5 Hz, 1H), 8.37-8.35 (dd, *J* = 1.2, 6.7 Hz, 1H), 7.70, (d, *J* = 1.2 Hz, 1H), 7.63-7.47 (m, 5H), 7.40-7.38 (m, 1H), 7.29-7.27 (m, 2H *partly buried under solvent peak), 7.26-7.16 (m, 3H), 6.43 (m, 1H), 5.43, (m, 1H), 4.08 (q, *J* = 2.5 Hz, 1H), 3.44-3.29 (ABX, *J* = 2.8, 7.6 Hz, 2H), 2.59-2.45 (m, 2H), 2.08 (s, 3H), 1.68 (d, *J* = 0.96 Hz, 3H). ^{13}C NMR (400 MHz, $CDCl_3$) δ = 183.14, 170.53, 163.50, 150.38, 146.05, 144.15, 143.86, 135.16, 134.58, 132.26, 131.68, 129.06, 128.91, 128.82, 128.54, 128.23, 127.68, 127.63, 127.58, 125.62, 111.88, 84.65, 83.57, 79.17, 74.80, 63.81, 38.35, 21.16, 12.36 (3 peaks not accounted for and could be overlapping with previous peaks). m.p. = 219-221 °C. HRMS (ESI-TOF) Calculated for $C_{32}H_{29}N_2O_7$ $[M+NH_4]^+$: 570.2240, Found: 570.2233. FT-IR (ATR): neat, 3067.15, 1738.23, 1687.43, 1663.28, 1599.78 cm^{-1}.

9-benzyloxy-9-phenylanthrone (46)

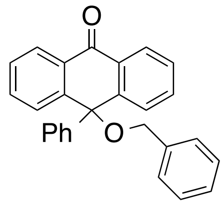

Tritylone alcohol (0.5850 g, 2.04 mmol), *p*-TsOH•H_2O (45.7 mg, 0.240 mmol) and benzyl alcohol (0.320 mL, 3.08 mmol) was added to 60 mL of benzene in a 100 mL round bottom flask. Purified to white crystals with mobile phase of (1:9 ether:petroleum ether) to give (0.5650 g, 73.5%) of ether. GC R_T of benzyl ether is 17.7 minutes. ^{1}H NMR (400 MHz, C_6D_6) δ = 8.65-8.63 (m, 2H), 7.51-7.45 (m, 4H), 7.22-7.19 (m, 3H), 7.12-7.10 (m, 1H), 7.04-6.93 (m, 6H), 6.89-6.87 (m, 1H), 4.03 (s, 1H). ^{13}C NMR (400 MHz, $CDCl_3$) δ = 183.70, 146.44, 145.27, 138.56, 134.40, 131.92, 128.88, 128.55, 128.53, 128.51, 127.70, 127.51, 127.35, 126.96, 125.96, 78.58, 65.97. m.p. = 144-146 °C. HRMS (ESI-TOF) Calculated for $C_{27}H_{20}O_2$ $[M+H]^+$: 377.1542, Found: 377.1545. FT-IR (ATR): neat, 3031.93, 2871.04, 1738.15, 1659.64, 1599.59 cm^{-1}.

9-(4-(4'-methyoxyphenyl)-1-butoxy)-9-phenylanthrone (47)

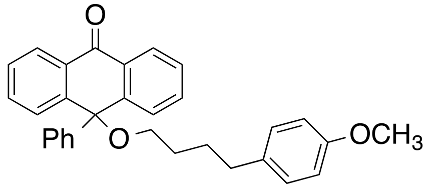

Tritylone alcohol (0.1897 g, 0.663 mmol), *p*-TsOH•H_2O (20.7 mg, 0.109 mmol) and 4-(4'-methyoxyphenyl)-1-butanol (0.130 mL, 0.752 mmol) was added to 30 mL of benzene in a 50 mL round bottom flask. Purified to white crystals with mobile phase of (1:9 ether:petroleum ether) to give (0.2733 g, 92.0%) of ether. GC R_T of ether is 16.6 minutes ^{1}H NMR (400 MHz, C_6D_6) δ = 8.64-8.61 (dd, *J* = 1.5, 6.0 Hz, 2H), 7.46-7.43 (m, 4H), 7.04-6.94 (m, 8H), 6.90-6.88 (m, 1H), 6.82-6.79 (m, 2H), 3.35 (t, *J* = 6.2 Hz, 2H), 2.39 (t, *J* = 7.4, 2H), 1.60-1.46 (m, 4H). ^{13}C NMR (400 MHz, $CDCl_3$) δ = 183.78, 157.93, 146.74, 145.74, 134.64, 134.17, 131.86, 129.46, 128.82, 128.43, 128.26, 127.19, 126.82, 125.89, 113.92, 78.02, 63.48, 55.46, 34.87, 29.67, 28.42. m.p. = 117-118 °C. HRMS (ESI-TOF) Calculated for $C_{31}H_{28}O_3$ $[M+H]^+$: 449.2117, Found: 449.2111. FT-IR (ATR): neat, 2935.00, 2867.45, 1738.38, 1655.71, 1598.49 cm^{-1}.

9-cyclohexoxy-9-phenylanthrone (48)

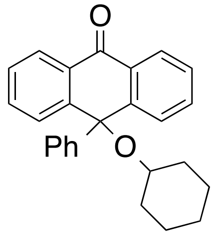

Tritylone alcohol (0.3175 g, 1.11 mmol), *p*-TsOH•H_2O (36.7 mg, 0.193 mmol) and cyclohexanol (0.17 mL, 1.63 mmol) was added to 40 mL of benzene in a 100 mL round bottom flask. Purified to white crystals with mobile phase of (1:9 ether:petroleum ether) to give

(0.2529 g, 61.8%) of ether. GC R_T of ether is 15.8 minutes. ^{1}H NMR (400 MHz, C_6D_6) δ = 8.62-8.60 (m, 2H), 7.48-7.41 (m, 4H), 7.04-6.96 (m, 7H), 3.35-3.30 (m, 1H), 1.53-1.47 (m, 2H), 1.26-1.21 (m, 4H), 1.11-1.06 (m, 2H), 0.842-0.809 (m, 2H). ^{13}C NMR (400 MHz, $CDCl_3$) δ = 183.88, 147.62, 146.50, 133.59, 131.45, 130.75, 128.30, 128.23, 126.83, 126.73, 126.23, 77.58, 73.10, 34.02, 25.73, 24.12. m.p. = 172-175 °C. HRMS (ESI-TOF) Calculated for $C_{26}H_{24}O_2$ $[M+H]^+$: 369.1855, Found: 369.1858. FT-IR (ATR): neat, 2923.45, 2867.45, 1738.44, 1663.62, 1599.92 cm^{-1}.

9-benzhydryloxy-9-phenylanthrone (49)

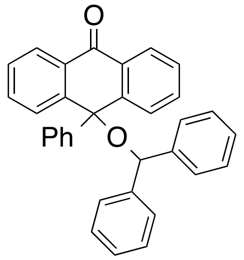

Tritylone alcohol (0.2180 g, 0.761 mmol), *p*-TsOH•H_2O (30.3 mg, 0.159 mmol) and benzhydrol (0.1502 g, 0.815 mmol) was added to 30 mL of benzene in a 50 mL round bottom flask. Purified to white crystals with mobile phase of (1:9 ether:petroleum ether) to give (0.1819 g, 52.8%) of ether. GC R_T of benzhydrol ether is 17.9 minutes ^{1}H NMR (400 MHz, $CDCl_3$) δ = 8.29-8.27 (dd, *J* = 0.96, 7.6 Hz, 2H), 7.52-7.50 (m, 2H), 7.32-7.30 (m, 4H), 7.21-7.04 (m, 15H), 5.16 (s, 1H). ^{13}C NMR (400 MHz, $CDCl_3$) δ = 183.73, 147.10, 144.81, 143.30, 133.38, 131.51, 130.93, 128.48, 128.29, 128.10, 127.06, 127.00, 126.95, 126.61, 126.24, 79.32, 79.28. m.p. = 148-150 °C. HRMS (ESI-TOF) Calculated for $C_{33}H_{24}O_2$ $[M+H]^+$: 453.1855, Found: 453.1851. FT-IR (ATR): neat, 3026.22, 1738.33, 1662.50, 1599.97 cm^{-1}.

9-cholesteroxy-9-phenylanthrone (50)

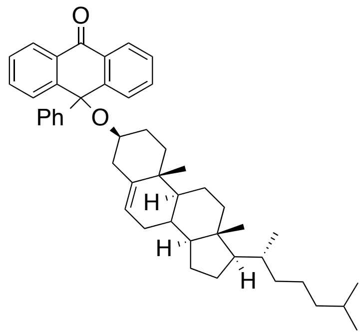

Tritylone alcohol (0.2400 g, 0.838 mmol), *p*-TsOH•H_2O (30.7 mg, 0.161 mmol) and cholesterol (0.4973 g, 1.29 mmol) was added to 50 mL of benzene in a 100 mL round bottom flask. Purified clearish/white crystals by recrystallization from hexanes/ethyl acetate to give (0.2177 g, 39.7%) of ether. A prior column using 1:10 ether:petroleum ether did not completely purify the product ether. Ether did not elute via GC in 20 minutes. ^{1}H NMR (400 MHz, C_6D_6) δ = 8.61-8.58 (dt, *J* = 1.9, 7.6 Hz), 7.52-7.47 (m, 4H), 7.08-6.96 (m, 7H), 5.04 (d, *J* = 5.1 Hz, 1H), 3.35 (sep, 1H), 2.55-2.49 (m, 1H), 1.97-1.94 (m, 2H), 1.81-1.78 (m, 2H), 1.63-1.17 (m, 16H), 1.08-0.911 (m, 16H), 0.828-0.754 (m, 1H), 0.618-0.543 (m, 4H), 0.485-0.401 (m, 1H). ^{13}C NMR (400 MHz, $CDCl_3$) δ = 183.79, 147.36, 146.55, 146.38, 140.94, 133.60, 133.59, 131.40, 131.35, 130.72, 130.65, 128.31, 128.24, 126.90, 126.86, 126.76, 126.19, 121.61, 77.61, 75.18, 56.82, 56.21, 50.03, 42.44, 41.03, 39.86, 39.71, 37.42, 36.50, 36.36, 35.94, 31.95, 30.36, 28.38, 28.20, 24.43, 23.97, 23.02, 22.76, 21.09, 19.43, 18.89, 12.00 (4 peaks not accounted for and could be overlapping with previously mentioned peaks). m.p. = 199-201 °C. HRMS (ESI-TOF) Calculated for $C_{47}H_{58}O_2$ $[M+H]^+$: 655.4515, Found: 655.4522. FT-IR (ATR): neat, 2933.86, 2866.04, 1668.78, 1601.31 cm^{-1}.

B. Gas Chromatography Analysis of Deprotected Alcohols

Ethers **44** and **46-50** were analyzed for the deprotection of the corresponding alcohol by gas chromatography. For each alcohol a calibration curve was performed and an example of this can be seen below for 1-octanol. Also shown below are representative GC chromatograms for the ethers previously mentioned. Ether **45** was analyzed by HPLC. 3'-O-acetylthymidine was detected at 260 nm using a Shimadzu LC-20AT with an SPD-20AV detector and 20 microliter injection loop. An Eclipse Plus C18, 5 micrometer, 4.6 x 155 mm column was used. A flow rate of 0.8 mL/min with 75%

methanol and 25% water. Integration of the alcohol peak was done from ~1.6 to 2.8 minutes.

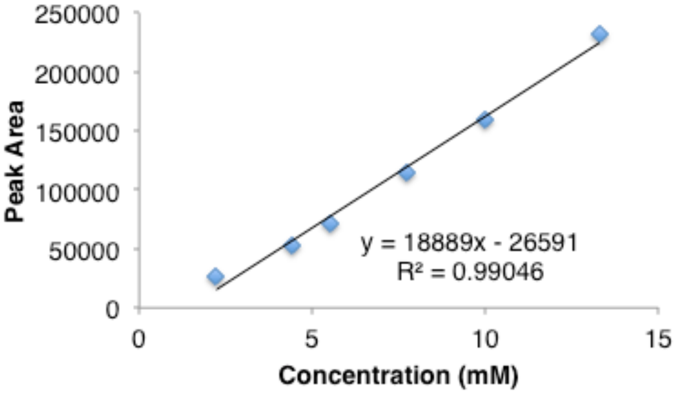

Figure 6.7 GC calibration curve for 1-octanol

Figure 6.8 Representative GC chromatograms (below) for the photolysis of tritylone ethers.

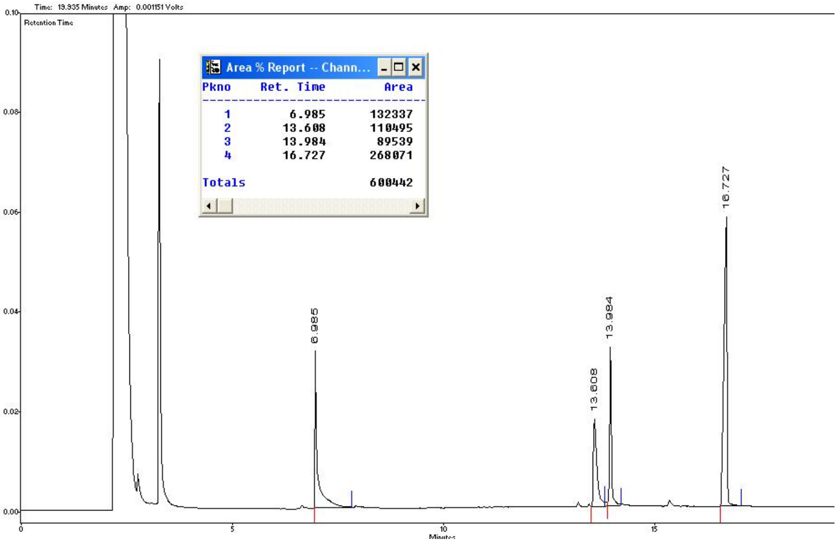

```
Pkno    Ret. Time        Area
-------------------------------
   1        6.985      132337
   2       13.608      110495
   3       13.984       89539
   4       16.727      268071

Totals                 600442
```

Representative GC chromatogram for the photolysis of octyl ether **44** (11.3 mM) and triethylamine (28.7 mM) for 60 minutes at 350 nm. Peak ~7 minutes is attributed to 1-octanol and the peak ~16.7 minutes is attributed to the tritylone ether starting material.

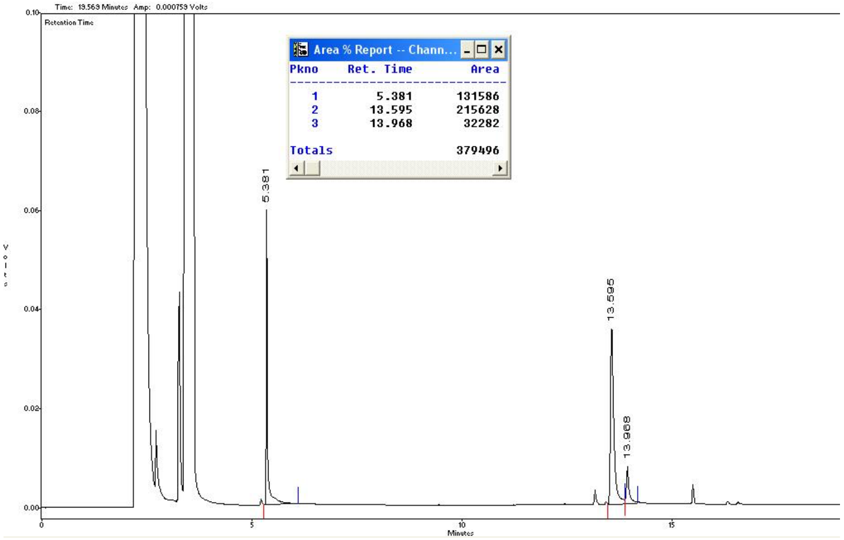

```
Area % Report -- Chann...
Pkno    Ret. Time        Area
------------------------------
   1        5.381      131586
   2       13.595      215628
   3       13.968       32282

Totals                 379496
```

Representative GC chromatogram for the photolysis of cyclohexyl ether **48** (11.9 mM) and triethylamine (21.5 mM) for 240 minutes at 350 nm. Peak ~5.4 minutes is attributed to cyclohexanol and the peak ~15.5 minutes is attributed to the tritylone ether starting material.

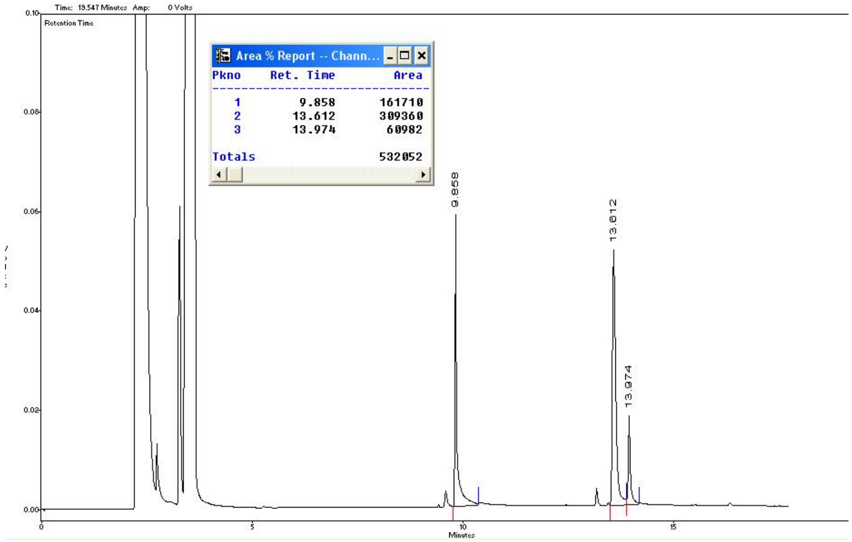

```
Area % Report -- Chann...
Pkno    Ret. Time        Area
------------------------------
   1        9.858      161710
   2       13.612      309360
   3       13.974       60982

Totals                 532052
```

Representative GC chromatogram for the photolysis of 4-(4’-methyoxyphenyl)-1-butanol ether **47** (11.8 mM) and triethylamine (21.5 mM) for 240 minutes at 350 nm. Peak ~9.8 minutes is attributed to 4-(4’-methyoxyphenyl)-1-butanol and the starting ether peak is not visible.

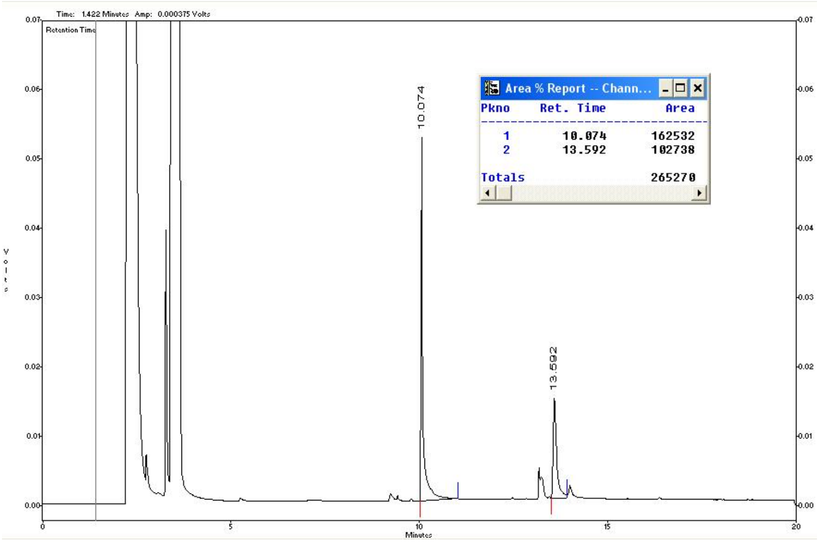

```
Pkno     Ret. Time          Area
--------------------------------
   1       10.074         162532
   2       13.592         102738

Totals                    265270
```

Representative GC chromatogram for the photolysis of benzhydrol ether **49** (7.24 mM) and triethylamine (17.9 mM) for 240 minutes at 350 nm. Peak ~10 minutes is attributed to benzhydrol and the starting ether peak is not visible.

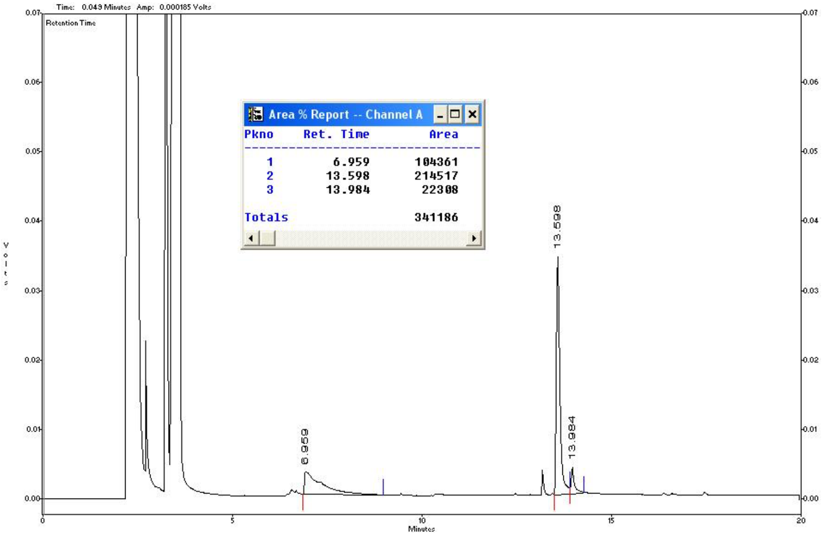

```
Pkno     Ret. Time          Area
--------------------------------
   1        6.959         104361
   2       13.598         214517
   3       13.984          22308

Totals                    341186
```

Representative GC chromatogram for the photolysis of benzyl ether **46** (8.99 mM) and triethylamine (26.9 mM) for 240 minutes at 350 nm. Peak ~7 minutes is attributed to benzyl alcohol and the starting ether peak is not visible.

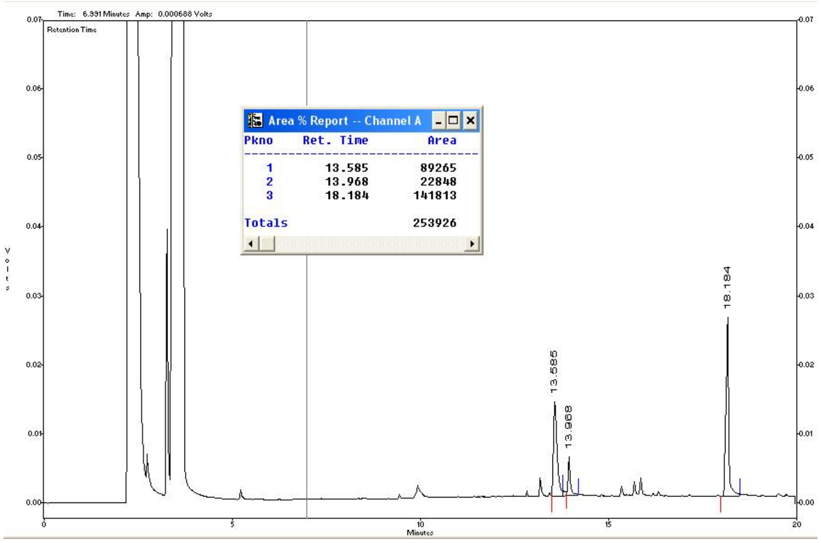

```
Pkno    Ret. Time        Area
--------------------------------
  1       13.585        89265
  2       13.968        22848
  3       18.184       141813

Totals                 253926
```

Representative GC chromatogram for the photolysis of cholesterol ether **50** (5.75 mM) and triethylamine (17.9 mM) for 240 minutes at 350 nm. Peak ~18.1 minutes is attributed to cholesterol and the starting ether peak is not visible.

C. Laser Flash Photolysis Results

The following laser studies used the benzyl tritylone ether **46** and were conducted using a Nd:YAG laser (355 nm output) supplied by Continuum with pulses 4–6 ns in duration as the excitation source. The probe beam that was used was a 350 W Xenon arc lamp that passed through a monochromator to a PMT detector. The solvents used were supplied from commercial sources and used without any purification. Solutions were purged with N_2, both in the solution (minimum of 10 minutes) and the headspace (minimum of 3 minutes). For O_2 quenching, the septum was removed and exposed to the air for 20 minutes then shaken slightly. The following kinetic decay curves were fitted using MATLAB software. All laser studies were conducted with an ether concentration range of 5 to 8 mM, which corresponds to an absorbance of 0.397 to 0.867 at 355 nm for 4.97 mM and 8.02 mM respectively. For the benzyl ether **46**, 5% 1,4-dioxane was used to aid in the solubility of the ether in methanol.

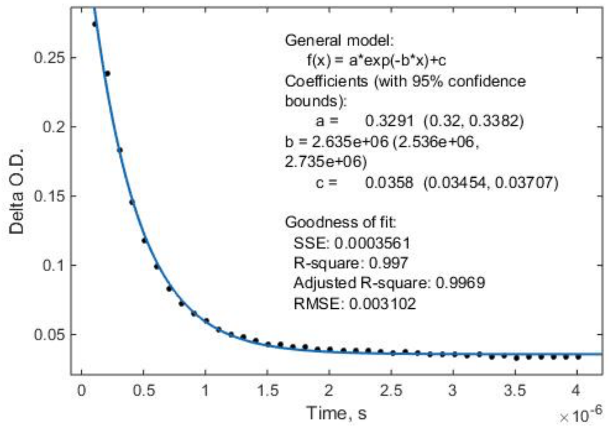

Figure 6.9 Kinetic decay curve of benzyl ether **46** in benzene without donor monitored at 530 nm under N_2.

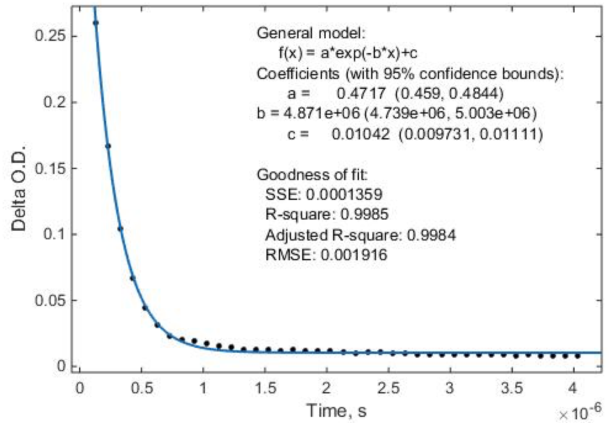

Figure 6.10 Kinetic decay curve of benzyl ether **46** in benzene without donor monitored at 530 nm under O_2.

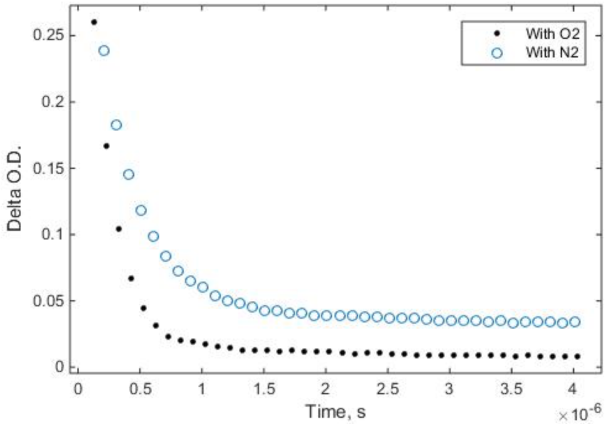

Figure 6.11 Decay curves of benzyl ether **46** in benzene without donor monitored at 530 nm under N_2 and O_2 plotted together.

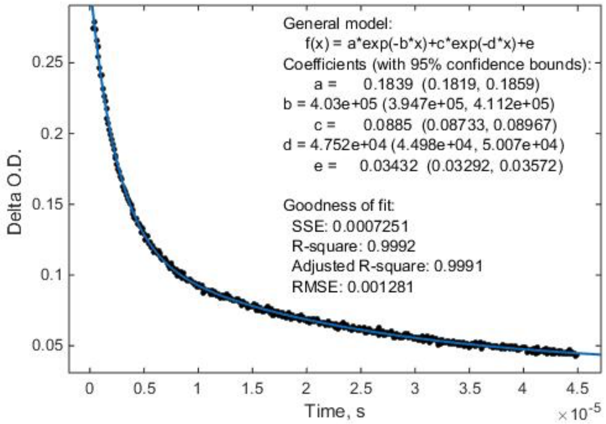

Figure 6.12 Kinetic decay curve of benzyl ether **46** in acetonitrile with triethylamine monitored at 620 nm under N_2.

D. Visible Light Release of Alcohols

Photolysis on ether **44** was conducted using a 1-watt, 447 nm laser provided by Laserglow Technologies and using a 35-watt, 419 nm maximum output, 16 bulb rayonet reactor supplied by Southern New England Rayonet company. The sample was prepared in a 4-sided, 1 cm quartz cuvette capped with a septum and purged with N_2. The sample using the 447 nm laser was placed in a temperature controlled cuvette holder at 20 °C and stirring occurred while being irradiated, while the sample irradiated on the rayonet was not stirred or cooled (temperature reaches approximately 35 degrees Celsius). Approximately, 200 microliter aliquots were taken out of the photolysis solutions at designated times and subjected to gas chromatography for analysis.

For the 447 nm photolysis: [Octyl Ether **44**] = 9.94 mM, [TEA] = 93.2 mM

For the 419 nm photolysis: [Octyl Ether **44**] = 10.3 mM, [TEA] = 93.2 mM

For the 447 nm photolysis control (NO DONOR): [Octyl Ether **44**] = 10.2 mM

The photocatalyst described below is difficult to solubilize in solvents like acetonitrile and methanol. Therefore, for the photolysis reactions consisted of an unknown amount of photocatalyst that was solubilized in acetonitrile (essentially saturated to maximize visible light absorption) and transferred to dissolve ether **44** and TEA. The absorbance of the photolysis solutions measured at 419 nm was 1.298. Based on the diluted absorbance spectrum below (Abs @ 419 nm = 0.122 for 0.022 mM) we estimate the concentration of *fac*-Ir(ppy)$_3$ used in the photolysis mixtures at 0.234 mM (~200 μM).

Spectroscopic and electrochemical properties of *fac*-Ir(ppy)$_3$[2]

Absorption λ_{max} = 375 nm, ε (10^3 $M^{-1}cm^{-1}$) = 7.2

Emission λ_{max} = 494 (at 77K, in alcoholic solvent), ϕ = 0.38, τ (μs) = 1.9

$E^{00,d}$ (eV) = 2.50, $Ir^{IV/III}$ (V) = + 0.77, $Ir^{III/II}$ (V) = - 2.19.

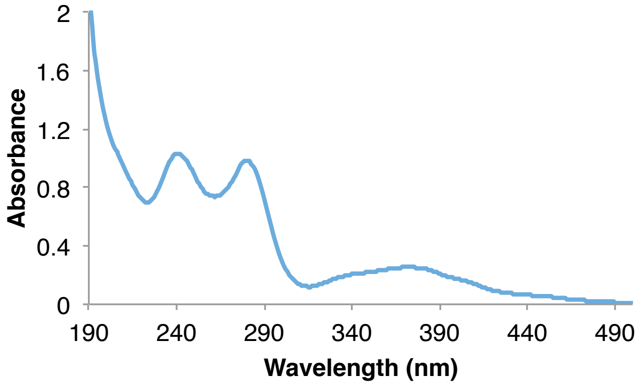

Figure 6.13 Absorbance spectrum of *fac*-Ir(ppy)$_3$ (0.022 mM) solution in acetonitrile.

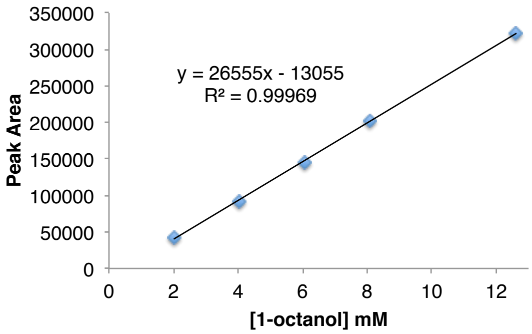

Figure 6.14 GC calibration curve for visible light release of 1-octanol.

Figure 6.15 Representative GC chromatograms (below) for the visible light deprotection of octyl ether **44**.

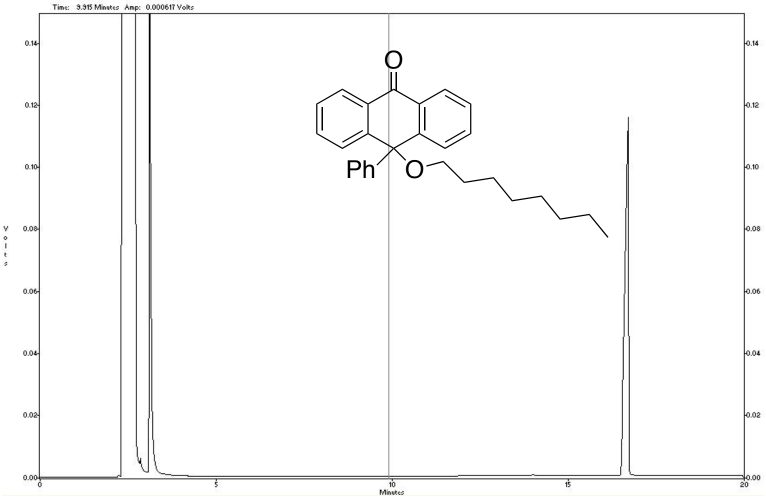

Irradiation using 419 nm rayonet. Time = 0 mins (no irradiation). Peak represents octyl ether **44**.

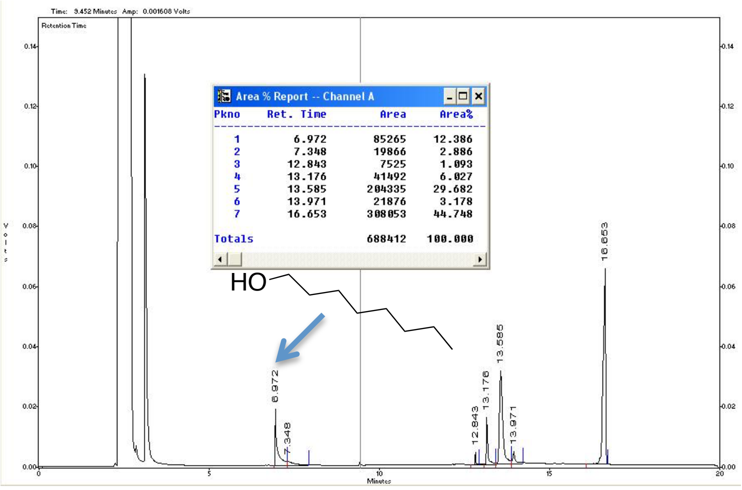

```
Pkno     Ret. Time          Area      Area%
--------------------------------------------
   1         6.972         85265     12.386
   2         7.348         19866      2.886
   3        12.843          7525      1.093
   4        13.176         41492      6.027
   5        13.585        204335     29.682
   6        13.971         21876      3.178
   7        16.653        308053     44.748

Totals                    688412    100.000
```

Irradiation using 419 nm rayonet. Time = 4 hours. Peak at 7 minutes represents 1-octanol release.

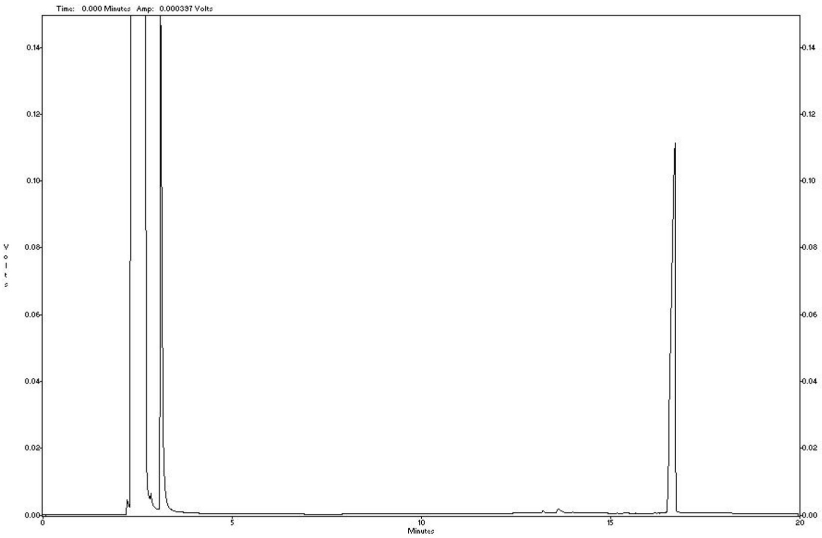

Irradiation using 447 nm laser. Time = 0 mins (no irradiation). Peak represents octyl ether **44**.

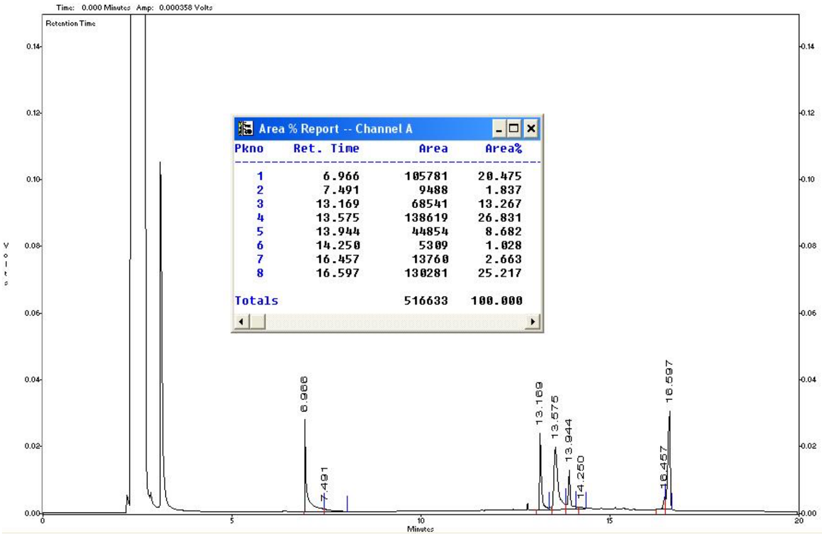

```
Pkno   Ret. Time       Area     Area%
--------------------------------------

  1       6.966      105781    20.475
  2       7.491        9488     1.837
  3      13.169       68541    13.267
  4      13.575      138619    26.831
  5      13.944       44854     8.682
  6      14.250        5309     1.028
  7      16.457       13760     2.663
  8      16.597      130281    25.217

Totals               516633   100.000
```

Irradiation using 447 nm. Time = 90 mins. Peak at 7 minutes represents 1-octanol release.

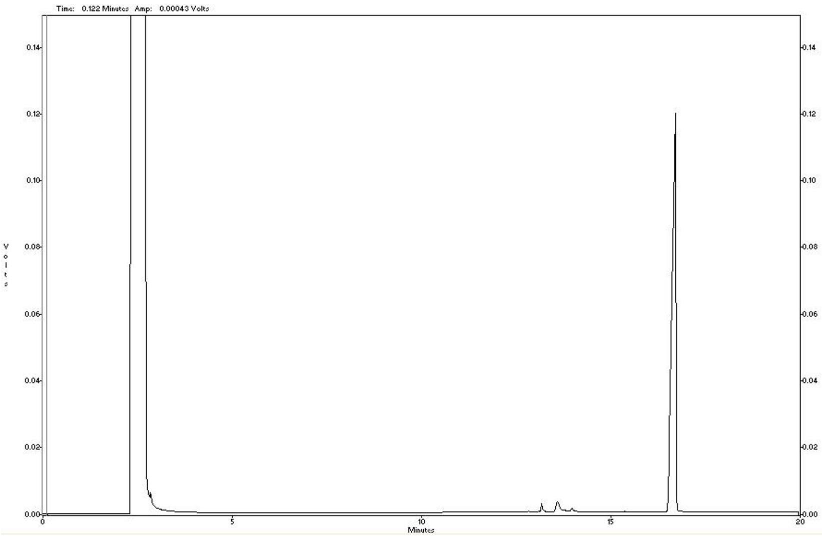

Irradiation using 447 nm. Time = 0 mins. NO DONOR used in this photolysis. Peak above represents octyl ether **44**.

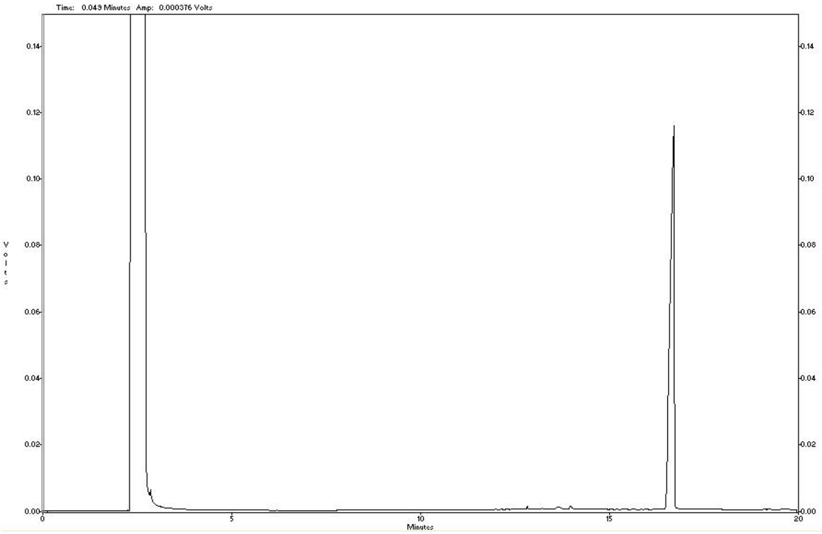

Irradiation using 447 nm. Time = 2 hours. NO DONOR used in the photolysis. Peak above represents octyl ether **44**. No decomposition of starting material or release of 1-octanol.

Photolysis on ether **45** was conducted using a 1-watt, 447 nm laser provided by Laserglow Technologies. The sample was prepared in a 4-sided, 1 cm quartz cuvette capped with a septum and purged with N_2. The sample was placed in a temperature controlled cuvette holder at 20 °C and stirring occurred while being irradiated. Approximately, 100 microliter aliquots were taken out of the photolysis solution at designated times and subjected to HPLC for analysis. Conditions for analysis and operation were as follows: A Shimadzu LC-20AT with an SPD-20AV detector and 20 microliter injection loop was used. An Eclipse Plus C18, 5 micrometer, 4.6 x 155 mm column was used. A flow rate of 1.0 mL/min with an initial ratio of 55% water and 45% methanol that linearly decreased the water and increased the methanol to where at 20 minutes it was 100% methanol. Elution of ether **45** came at ~14.4 minutes, tris(bipyridine)ruthenium(II) chloride at ~1.5 minutes and the deprotected 3'-O-acetylthymidine at ~2.5 minutes. A calibration curve for the alcohol was used to quantify the amount of deprotection. Detection occurred at 260 nm.

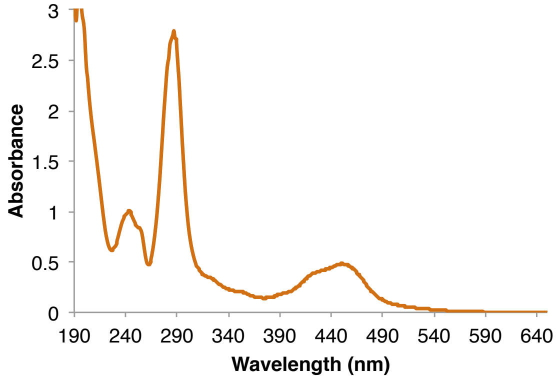

Figure 6.16 Absorbance spectrum of Ru(bpy)$_3$Cl$_2$ (0.035 mM) in acetonitrile.

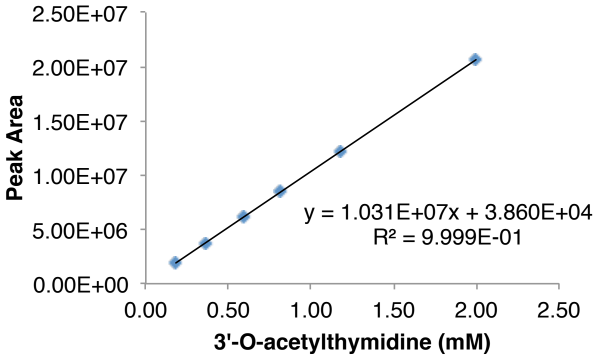

Figure 6.17 Calibration curve for 3'-O-acetylthymidine (deprotected alcohol).

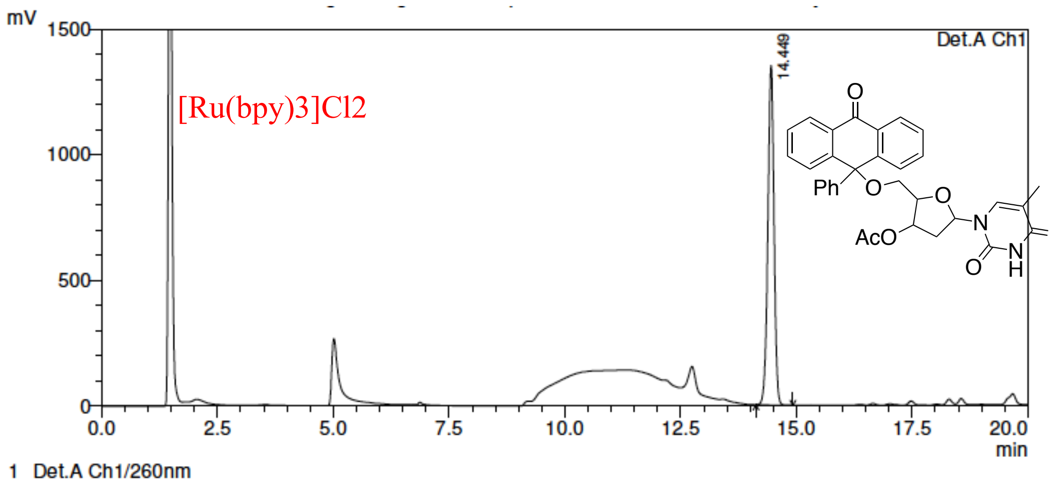

PeakTable

Detector A Ch1 260nm

Peak#	Ret. Time	Area	Height	Area %	Height %
1	14.449	12448708	1349620	100.000	100.000
Total		12448708	1349620	100.000	100.000

Figure 6.18 HPLC chromatogram of ether **45** (0.832 mM), triethylamine (0.108 M) and tris(bipyridine)ruthenium(II) chloride (2.11 mM) at t = 0 minutes.

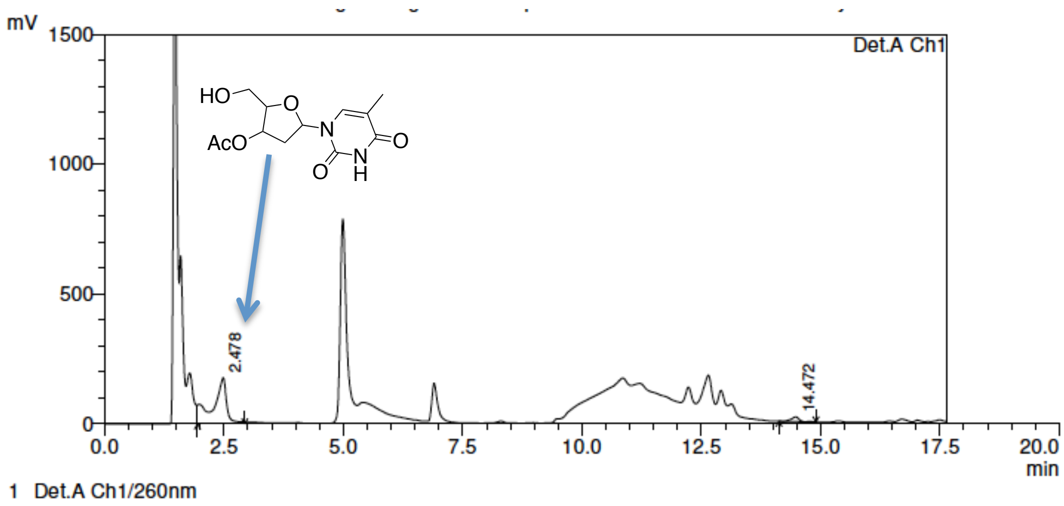

PeakTable

Detector A Ch1 260nm

Peak#	Ret. Time	Area	Height	Area %	Height %
1	2.478	3600364	179049	94.763	90.901
2	14.472	198988	17922	5.237	9.099
Total		3799352	196971	100.000	100.000

Figure 6.19 HPLC chromatogram of ether **45** (0.832 mM), triethylamine (0.108 M) and tris(bipyridine)ruthenium(II) chloride (2.11 mM) at t = 20 minutes.

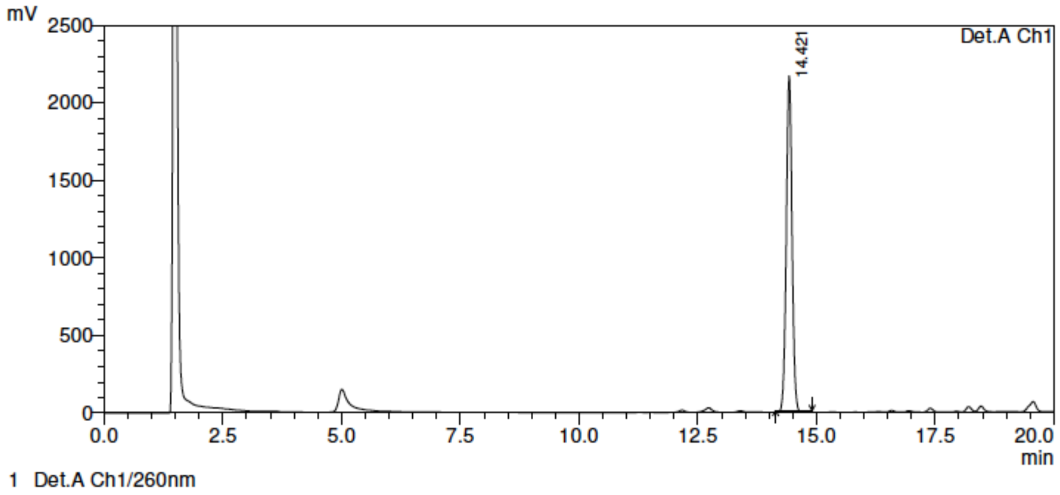

PeakTable

Detector A Ch1 260nm

Peak#	Ret. Time	Area	Height	Area %	Height %
1	14.421	17800873	2156108	100.000	100.000
Total		17800873	2156108	100.000	100.000

Figure 6.20 HPLC chromatogram of the same photolysis at t = 0 minutes, however no triethylamine was used in this photolysis.

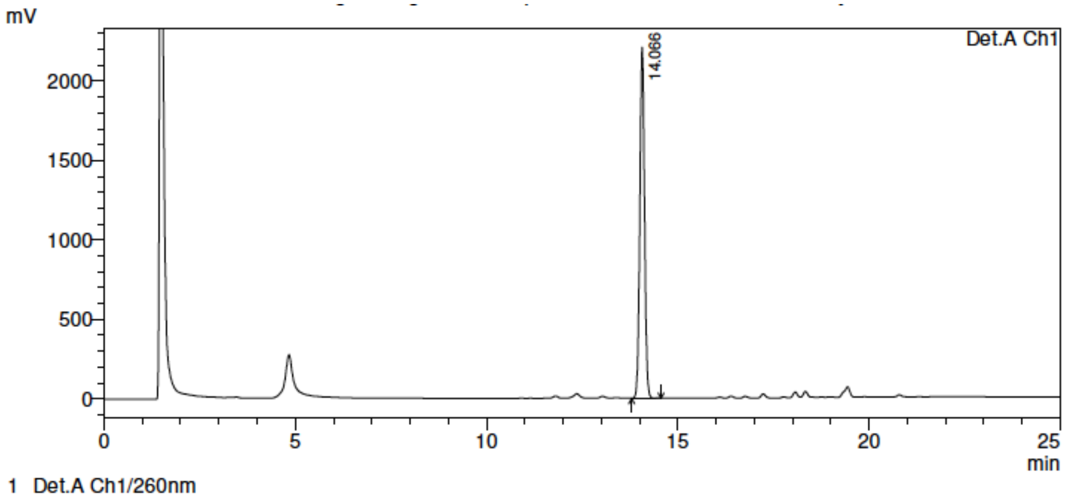

PeakTable

Detector A Ch1 260nm

Peak#	Ret. Time	Area	Height	Area %	Height %
1	14.066	18909224	2208297	100.000	100.000
Total		18909224	2208297	100.000	100.000

Figure 6.21 HPLC chromatogram at t = 20 minutes when no triethylamine was used in the photolysis. No conversion of the starting material ether and no yield of deprotected alcohol.

Below is the GC calibration curve for 4-(4’-methyoxyphenyl)-1-butanol and the subsequent photolysis time course for ether **47.** Using the same concentration of Ir(ppy)$_3$ as noted above, as well as the same 447 nm source the concentration of alcohol was monitored over time by GC. Starting concentration of **47** = 8.58 mM. Starting concentration of TEA was 47.3 mM. The solution was irradiated in MeCN in a sealed quartz cuvette at 20 degrees Celsius and purged under N_2 atmosphere. Approximately 200 microliters was taken out of the stock photolysis solution and subjected to GC analysis.

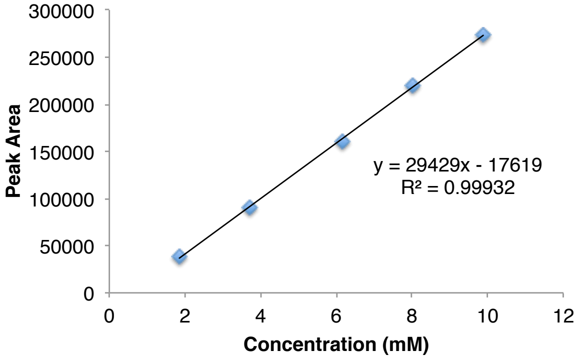

Figure 6.22 HPLC Calibration curve for 4-(4’-methyoxyphenyl)-1-butanol.

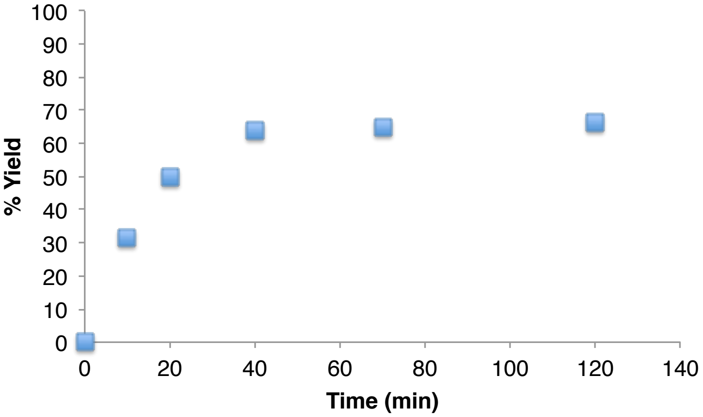

Figure 6.23 Photolysis time course for the analysis of 4-(4’-methyoxyphenyl)-1-butanol by GC as described above.

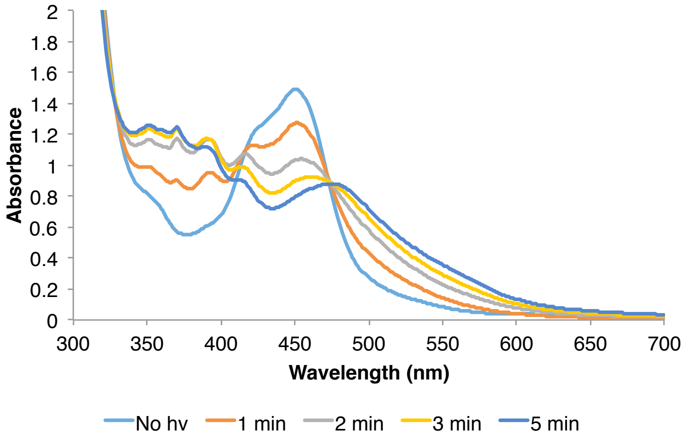

Figure 6.24 UV-Vis spectrum shown below is the result of a photolysis experiment consisting of $[Ru(bpy)_3]Cl_2$ (0.844 mM), octyl ether **44** (2.08 mM) and TEA (15.2 mM). A 2 mL solution was placed into a cuvette, capped and purged with N_2. The solution was irradiated using the 447 nm 1 W laser for short amounts of time and monitored by UV-Vis. The characteristic peak for the photocatalyst around 450 nm is diminished as the photolysis progresses.

E. Mass Spectrometry Analysis of 44

The following experiment was conducted on a JEOL AccuTOF-CS mass spectrometer using direct analysis in real time (DART) positive mode as the ionization source. Two samples were submitted for analysis. The first (top spectrum) consisted of 0.542 mM of ether **44** and 20 microliters of TEA in 2 mL of MeOH. The solution was placed into a small vial, capped with a septum and purged with N_2 and irradiated for 3 minutes under 350 nm light. The septum was removed and exposed to air for approximately 15 minutes and the screw cap was placed back on. More exposure to O_2 likely came from the MS analysis. The second (bottom spectrum) consisted of a photolysis equivalent to what was just mentioned above, however it was exposed to 30 minutes of 350 nm light. Exposure to air and further O_2 during MS analysis is also probable. The samples were not submitted for high-resolution MS.

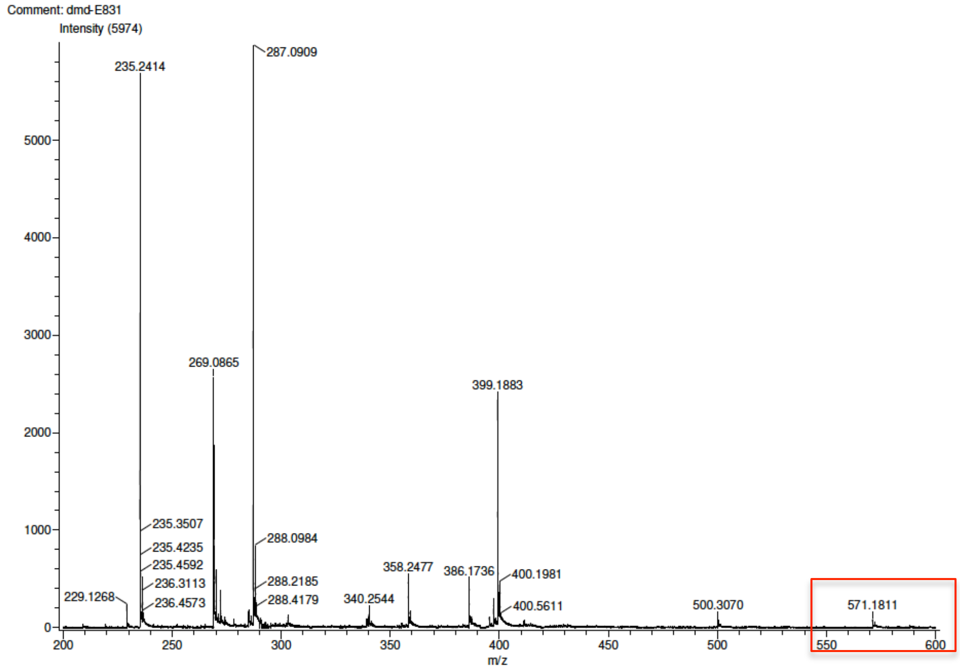

Figure 6.25 MS results of 0.542 mM of a 3 minute photolysis consisting of ether **44** and 20 microliters of TEA in 2 mL of MeOH.

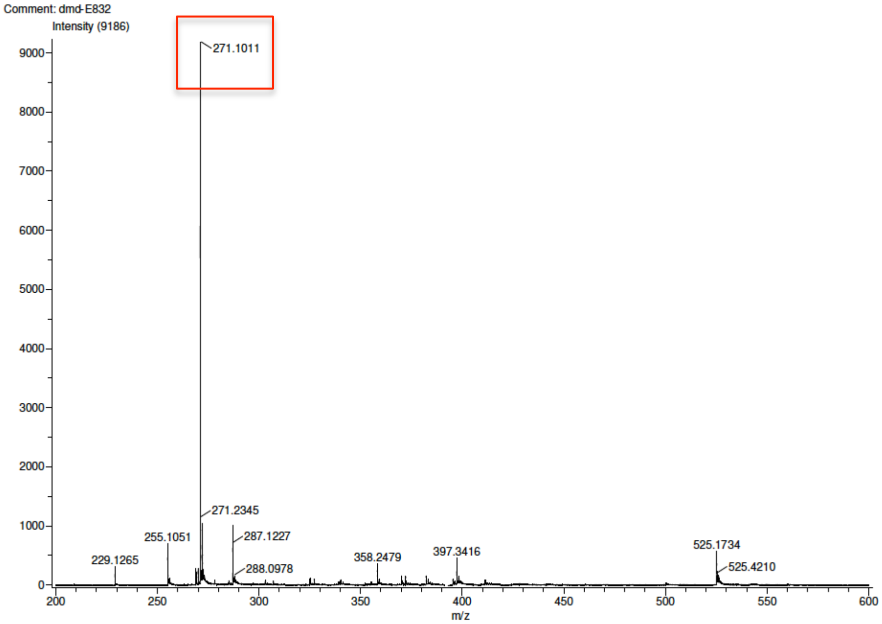

Figure 6.26 MS results of 0.542 mM of a 30 minute photolysis consisting of ether **44** and 20 microliters of TEA in 2 mL of MeOH.

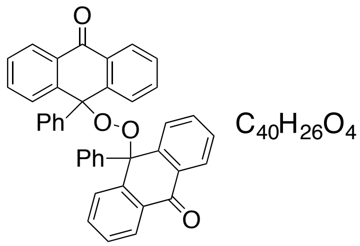

$C_{40}H_{26}O_6$ [M+H]$^+$: 571.1909, Found: 571.1811

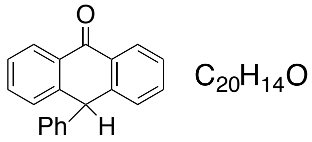

$C_{20}H_{14}O$ [M+H]$^+$: 271.1123, Found: 271.1011

6.4 Chapter 4 Experimental Results

A. Synthesis of 1,3-dimethylimidazolium-2-carboxylate (57)

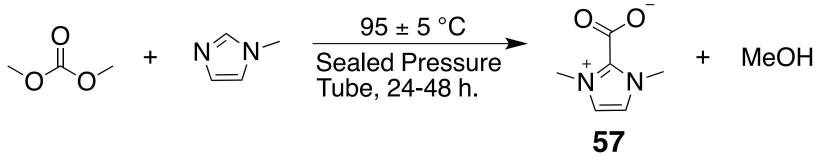

To a 30 mL screw top pressure tube, 1-methylimidazole (4.00 mL, 50.2 mmol) and dimethyl carbonate (6.00 mL, 71.2 mmol) were added. The tube was sealed and allowed to stir in an oil bath behind a blast shield for 48 hours at a temperature of 95 ± 5 °C. After the allotted time, the reaction was allowed to cool to room temperature and the screw cap was removed. The liquid was decanted off and the remaining white crystals were allowed to stir in diethyl ether for 30 minutes. The crystals were vacuum filtered and rinsed with generous portions of diethyl ether, acetone and acetonitrile. The remaining white crystals were transferred to a pre-weighed vial and allowed to dry under vacuum (2.14 g, 30.4%). Reported characterization data are consistent with previously reported results.[3] ^{1}H-NMR (400 MHz, D_2O), δ 7.37 (s, 2H), 3.99 (s, 6H). ^{13}C-NMR (400 MHz, D_2O), δ 158.71, 140.16, 123.45, 37.14. FT-IR (ATR): neat, 1642 cm^{-1}.

B. Kinetic Studies on the Decomposition of 57

Initial rate constants for the decomposition of **57** were measured by monitoring the decrease in absorbance at 240 nm over time by UV-Vis in a 1 cm quartz cuvette capped with a septum that was oven dried prior to use. HPLC grade water, methanol, and acetonitrile were used. The acetonitrile was distilled over CaH_2 and stored with 4 Å molecular sieves. Spectrophotometric grade 1,4-dioxane was used to minimize any absorbance overlap at 240 nm. The concentration of **57** in the kinetic studies ranged ca. 0.2-0.4 mM. Initial rate constants of decomposition are expressed in s^{-1} and the average of 3 runs where used to determine the reported rate constant.

Figure 6.27 Decomposition plots (below) as a function of water concentration in methanol, acetonitrile and 1,4-dioxane as well as with added salts.

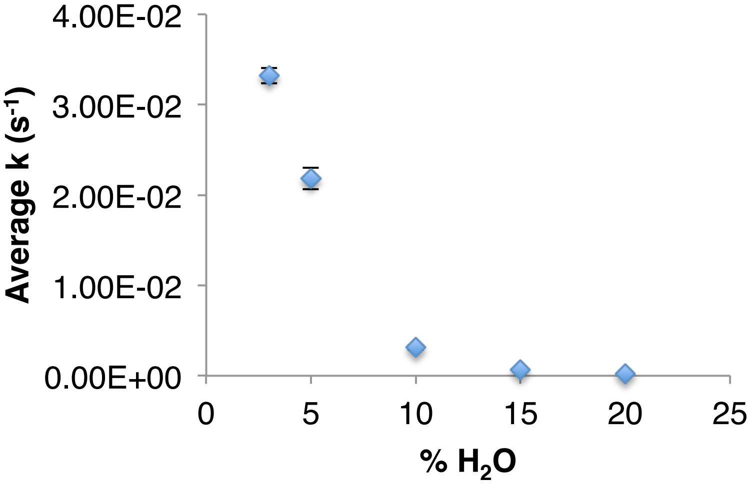

Decomposition of **57** in 1,4-dioxane/H_2O mixtures.

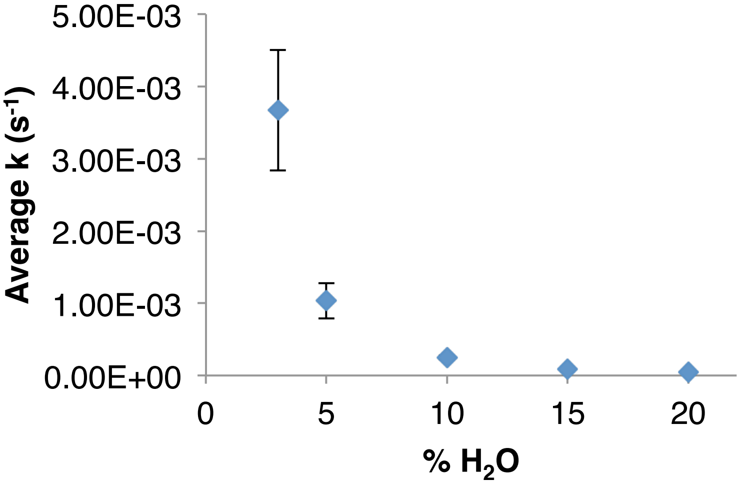

Decomposition of **57** in MeCN/H_2O mixtures.

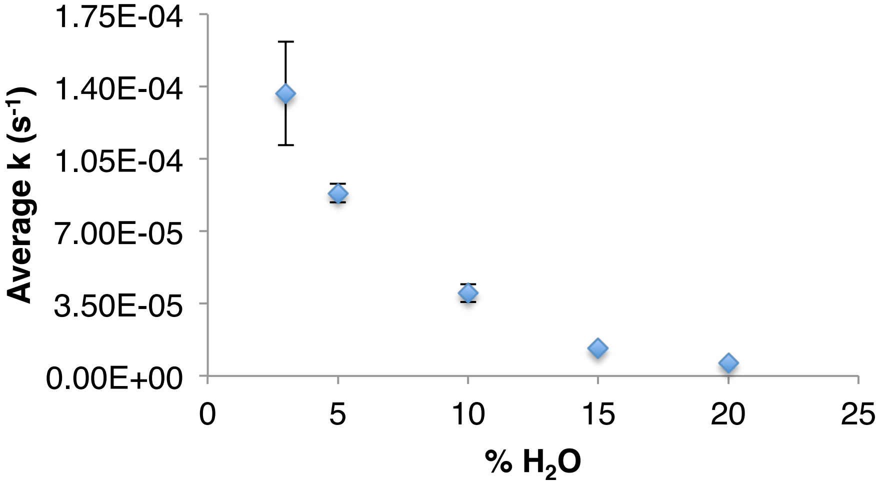

Decomposition of **57** in MeOH/H_2O mixtures.

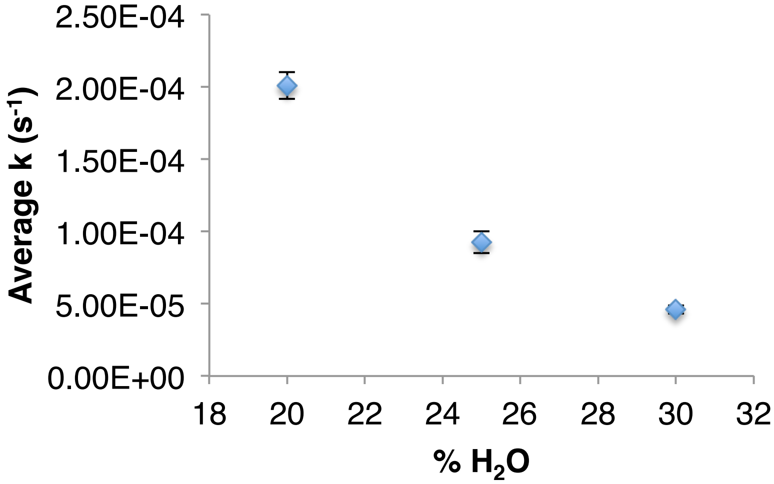

Decomposition of **57** in 1,4-dioxane/H_2O mixtures (Li^+ = 40.0 mM).

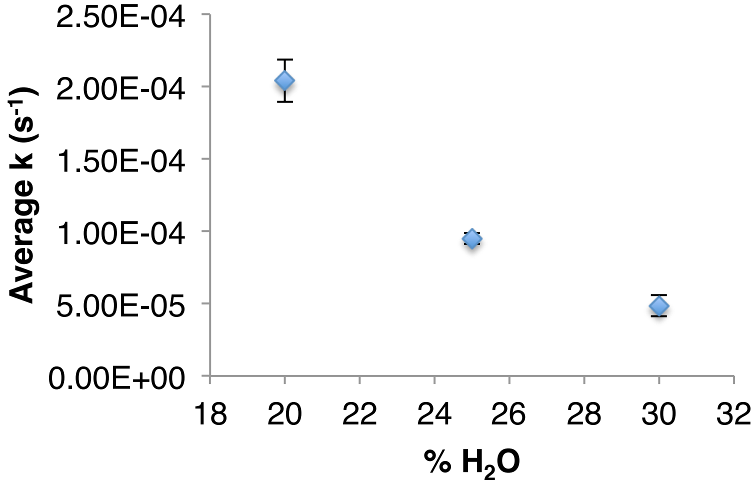

Decomposition of **57** in 1,4-dioxane/H_2O mixtures (Na^+ = 40.4 mM).

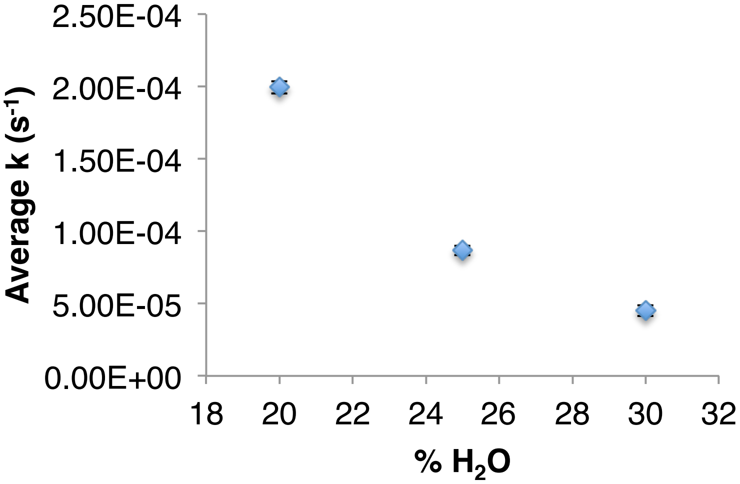

Decomposition of **57** in 1,4-dioxane/H_2O mixtures (K^+ = 39.8 mM).

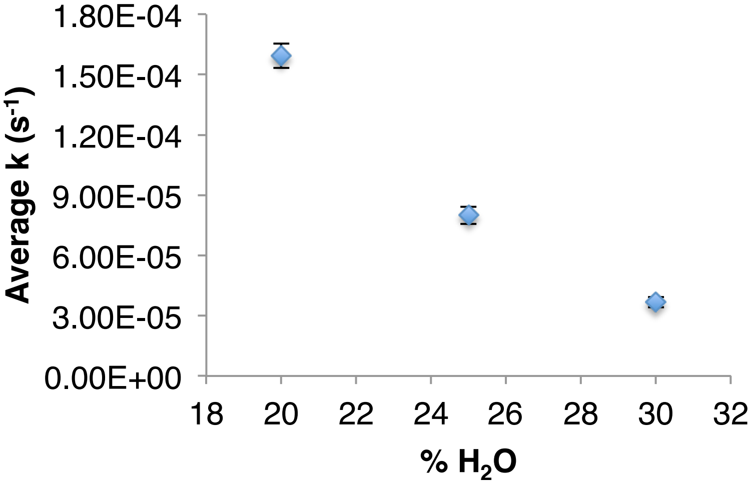

Decomposition of **57** in 1,4-dioxane/H_2O mixtures (Mg^{2+} = 39.9 mM).

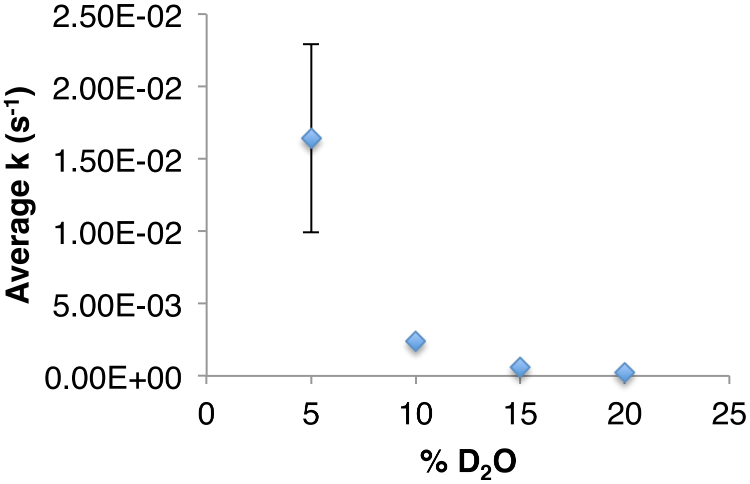

Decomposition of **57** in 1,4-dioxane/D_2O mixtures.

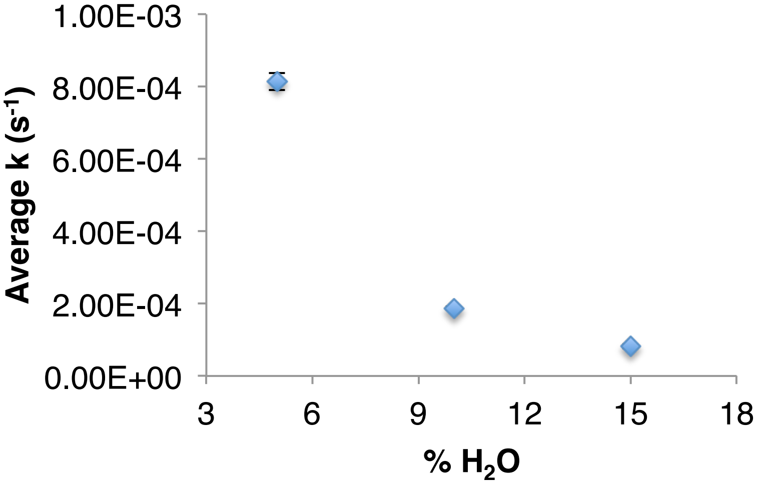

Decomposition of **57** in MeCN/H_2O mixtures purged with CO_2.

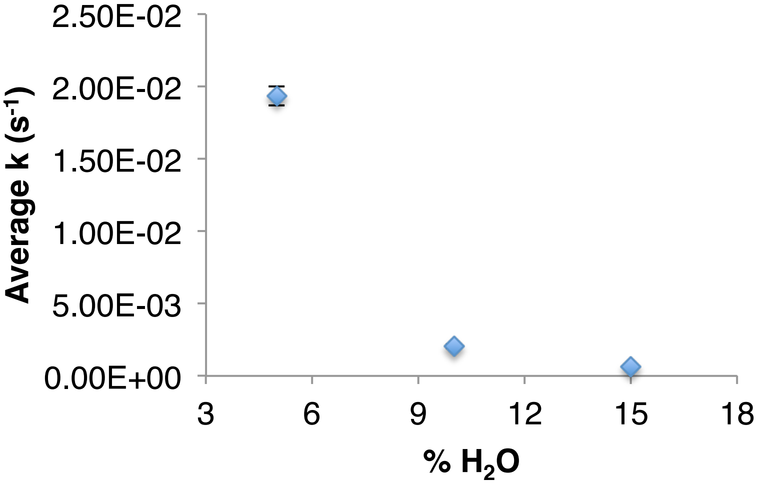

Decomposition of **57** in 1,4-dioxane/H_2O mixtures purged with CO_2.

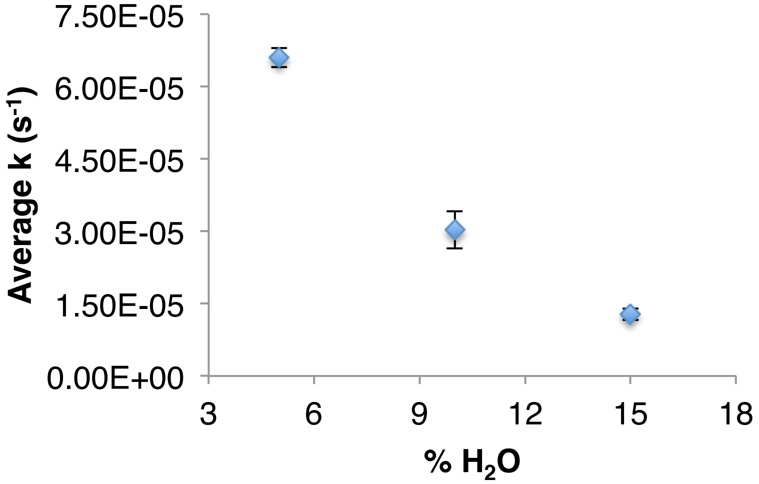

Decomposition of **57** in MeOH/H_2O mixtures purged with CO_2.

C. $^{13}CO_2$ ^{13}C NMR Experiment

A generous amount (due to necessity for ^{13}C NMR) of **57** was placed into CD_3CN and stirred for 30 minutes resulting in not all of **57** being solubilized. The solubilized portion of the mixture was separated into two vials capped with a septum. The top spectrum represents a solution of **57** purged with $^{12}CO_2$ for 20 minutes. The bottom spectrum represents a solution of **57** purged with $^{13}CO_2$ for 20 minutes. This is a reproduction of Figure 4.8.

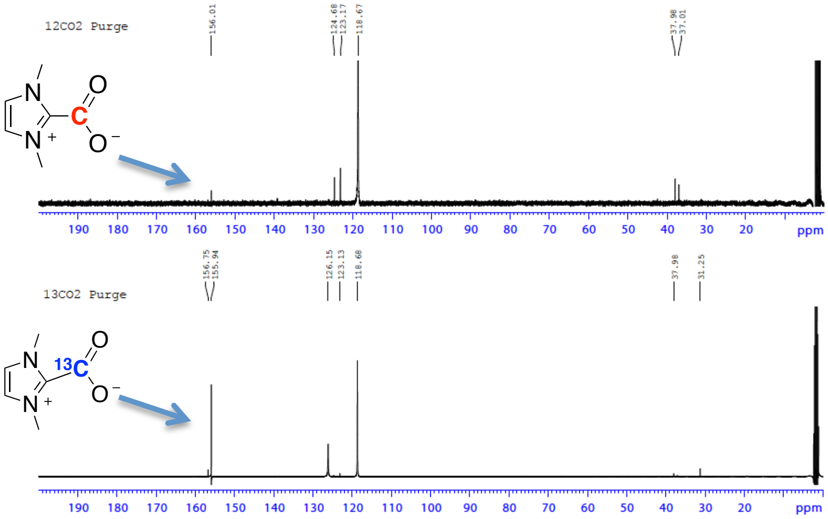

D. Experimental Free Energy of Activation

An Eyring plot was used to experimentally determine the free energy of activation for decarboxylation of **57** in water using a temperature controlled cuvette holder and monitoring the decrease in absorbance at 240 nm over time. A similar concentration range was used to that of the aforementioned kinetic studies in section B and the average of 3 runs where used to determine the rate constant at 353, 358, 363, 368 Kelvin.

Table 6.1 Eyring analysis for the decarboxylation of **57**.

Temperature (K)	Average k (s^{-1})
353	$5.59 \times 10^{-3} \pm 8.62 \times 10^{-4}$
358	$1.03 \times 10^{-2} \pm 5.80 \times 10^{-4}$
363	$1.76 \times 10^{-2} \pm 5.65 \times 10^{-4}$
368	$2.94 \times 10^{-2} \pm 3.93 \times 10^{-3}$

$\Delta H^{\ddagger} = 27.8$ kcal/mol
$\Delta G^{\ddagger} = 24.9$ kcal/mol

6.5 Chapter 5 Experimental Results

A. Synthesis of 1,3-dimethylimidazolium iodide

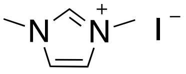

To a 100 mL round bottom flask, 50 mL of toluene was added. While stirring, 1-methylimidazole (1.50 mL, 18.8 mmol) and iodomethane (1.40 mL, 22.5) was added to the solution respectively. The flask was capped with a septa and allowed to stir overnight in an oil bath at a temperature of 45 ± 5 °C. The solution became cloudy shortly upon placing into the oil bath and over time white crystals can be seen accumulating on the bottom of the flask. The following day the toluene was decanted off and the remaining crystals were rinsed with diethyl ether, filtered and dried under vacuum. Slight yellow crystals were obtained (3.22 g, 76.5%). ^{1}H-NMR (400 MHz, D_2O) δ 8.69 (s, 1H, exchangeable), 7.44 (s, 2H), 3.92 (s, 6H). ^{13}C-NMR (400 MHz, CD_3CN) δ 138.11, 124.63, 37.49.

B. Synthesis of 1,3-dimethylimidazolium tetrafluoroborate

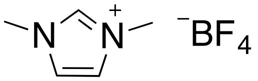

To a 50 mL round bottom flask, 1,3-dimethylimidazolium iodide (210.7 mg, 0.9404 mmol) and silver tetrafluoroborate (192.4 mg, 0.9883 mmol) was added. To that, 20 mL of acetone was added, capped and allowed to stir at room temperature for 3 hours. After the allotted time, the mixture was filtered and the acetone of the filtrate was removed under reduced pressure to yield a clear watery oil (0.1242 g, 71.8%). ^{1}H-NMR (400 MHz, acetone-d_6) δ 8.77 (s, 1H), 7.60 (d, 2H, J = 1.6 Hz), 3.96 (s, 6H). ^{13}C-NMR (400 MHz, acetone-d_6) δ 138.27, 124.61, 36.50.

C. UV-Vis and Fluorescence Quenching Data

The following UV-Vis data was conducted on a UV-1800 spectrophotometer supplied by Shimadzu using a 1 cm four-sided quartz cuvette. To avoid competing light absorption at 350 nm from 1,3-dimethylimidazolium iodide (ImI) due possible trace impurities of I_2, a metathesis reaction was conducted to acquire the 1,3-dimethylimidazolium tetrafluoroborate salt ($ImBF_4$). This ensured only excitation of the sensitizer.

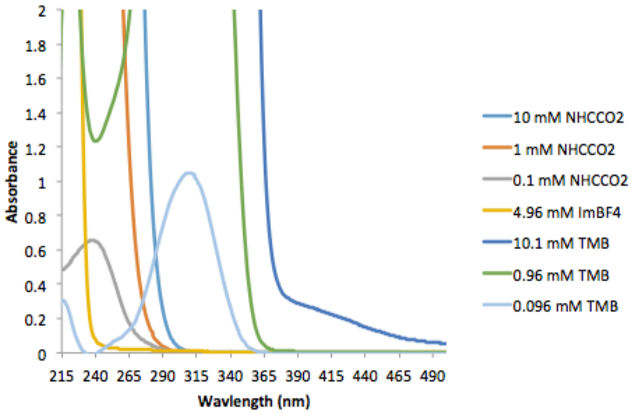

Figure 6.28 Absorption spectrum of *N,N,N',N'*-tetramethylbenzidine (TMB), 1,3-dimethylimidazolium tetrafluorobortate ($ImBF_4$), and NHC-CO_2 **57** at various concentrations. The latter two were taken in H_2O and the TMB spectrums were done in 1,4-dioxane.

Fluorescence quenching experiments were conducted on a Hitachi F-4500 fluorescence spectrophotometer. Solutions were purged with N_2 in a 4-sided, 1 cm path length, quartz cuvette capped with a septum for 5 minutes in the solution and 2 minutes for the head space. Unless otherwise stated the experiments were conducted with parameters consisting of Ex_{slit} = 2.5 nm, Em_{slit} = 5.0 nm, scan speed of 1200 nm/min, and a PMT voltage = 700 V. Experiments were conducted at room temperature and all concentrations expressed below are in mol/L. Also expressed below are the values (E_{ox} and E_{00}) used in determining the ΔG_{ET} for each of the six sensitizers. Fluorescence studies were conducted at high water ratios to ensure the stability of **57** over the time it took to conduct the experiments. Concentration of TMB used in each experiment was in the 10^{-5} M range so that the absorbance at the wavelength of excitation was around 0.2 absorbance units.

Table 6.2 Electrochemical and photophysical properties of selected donors.[4]

Sensitizer	E_{ox} (V)	E_{00} (kcal/mol)
TMB	0.43	83.0[5]
TMB	0.43	83.0
TMB	0.43	83.0
TMB	0.43	83.0
N-Methylcarbazole	1.03[6]	82.9
2-Aminoanthracene	0.44	63.1
Anthracene	1.09	76.2
Phenanthrene	1.50	82.5
9,10-Dibromoanthracene	1.28[6]	70.5

E_{00} denoted above represents the excited state singlet energy of the sensitizer.

Figure 6.29 Fluorescence quenching spectra and Stern–Volmer plots (below) for various donor in the presence of **57** at different water concentrations.

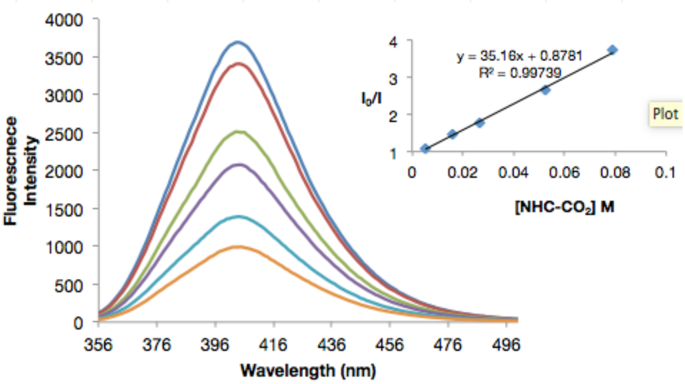

TMB in 40% H_2O (λ_{ex} = 346 nm, λ_{em} = 405 nm).

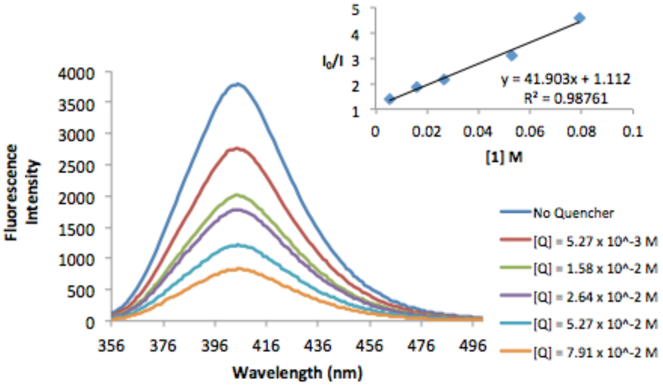

TMB in 50% H_2O (λ_{ex} = 346 nm, λ_{em} = 405 nm).

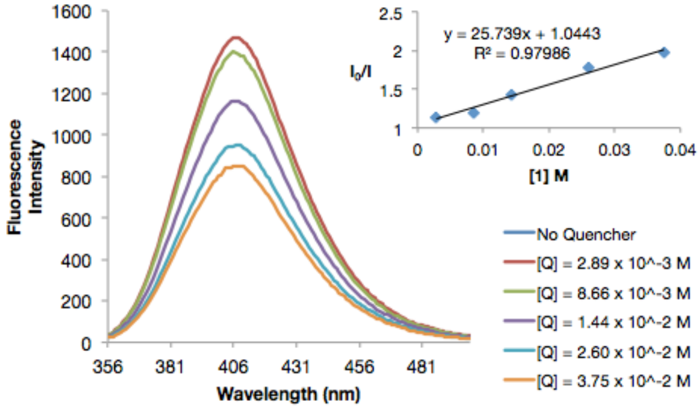

TMB in 70% H_2O (λ_{ex} = 346 nm, λ_{em} = 405 nm).

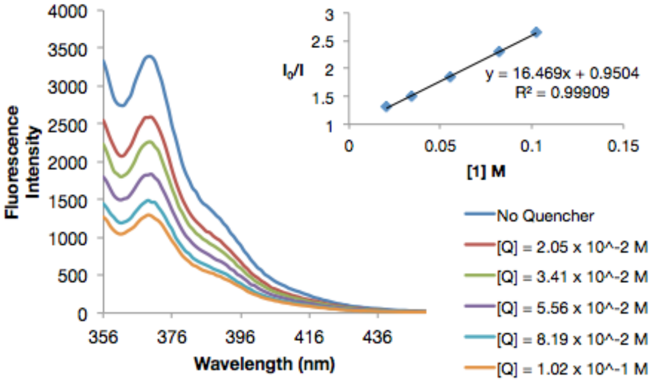

N-methylcarbazole in 50% H_2O (λ_{ex} = 346 nm, λ_{em} = 370 nm, Em_{slit} = 2.5 nm).

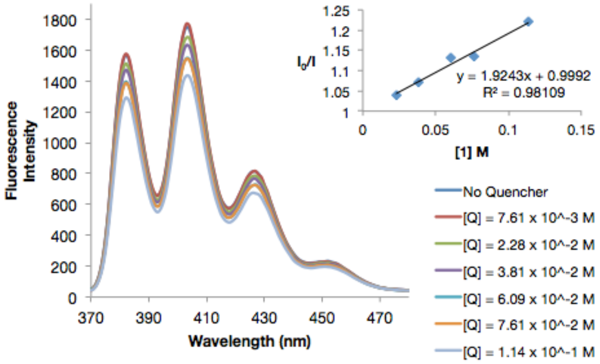

Anthracene in 50% H_2O (λ_{ex} = 360 nm, λ_{em} = 403 nm).

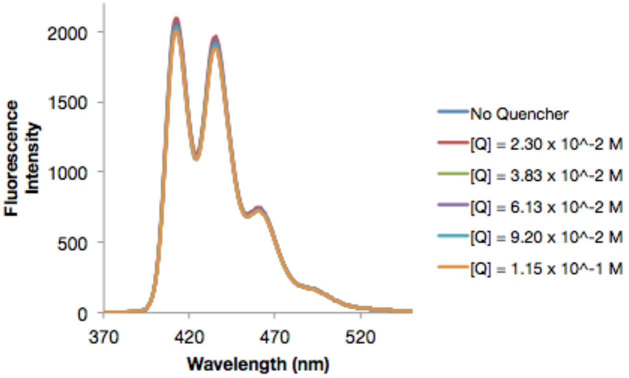

9,10-Dibromoanthracene in 50% H_2O (λ_{ex} = 360 nm, λ_{em} = 412 nm).

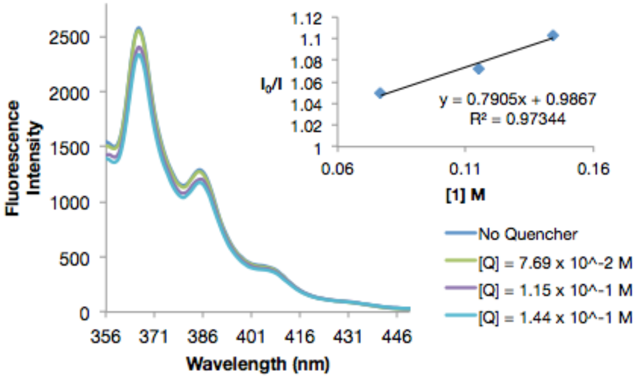

Phenanthrene in 50% H_2O (λ_{ex} = 346 nm, λ_{em} = 366 nm).

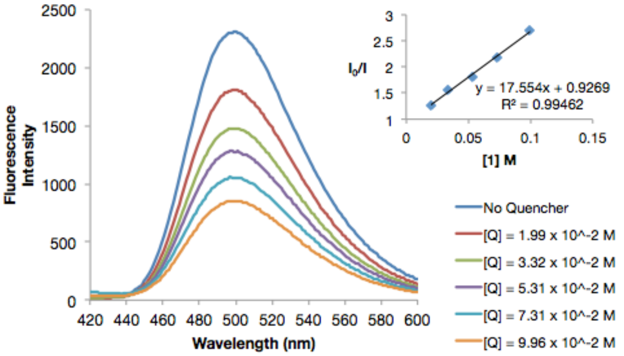

2-Aminoanthracene in 50% H_2O (λ_{ex} = 336 nm, λ_{em} = 500 nm).

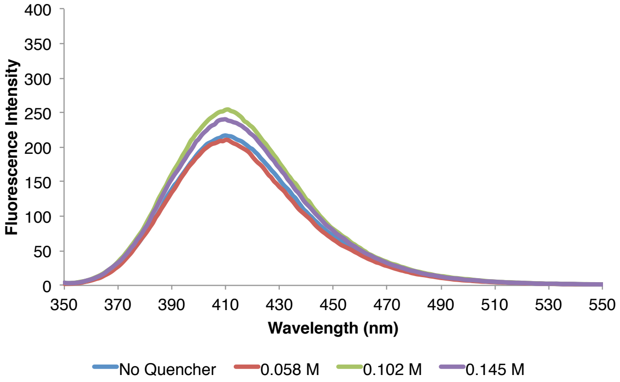

Figure 6.30 Fluorescence quenching experiment with $NaHCO_3$ as the quencher for TMB. The experiment was carried out in 40% H_2O in 1,4-dioxane (similar to the above experiments for TMB).

D. Formate Analysis by ^{1}H NMR

Solvents used:

Approximately 100 mL of spectroscopic grade 1,4-dioxane was place into an amber bottle with 4 Å molecular sieves. This was capped with a septum and purged with N_2 for 45 minutes. A stock of TMB in 10.0 mL spectroscopic grade 1,4-dioxane was put into an amber vial, capped with a septum and purged with N_2 for 30 minutes. HPLC grade H_2O was used and was not saturated with N_2. A stock of **57** in 2.0 mL of HPLC grade H_2O was put into a vial and was not purged with N_2. Preparative photolysis experiments were conducted at lower water ratios to ensure the solubility of the donor at the higher concentrations that were used.

Photolysis setup:

3 cuvettes were set up all the same, along with one dark control for each photolysis reaction. The appropriate amount of TMB stock, 1,4-dioxane, and H_2O was added to each cuvette and dark control. The cuvettes were each capped with a septum. Then, the appropriate amount of **57** stock was added to each cuvette and dark control yielding a total of 1.0 mL of photolysis solution (note: these samples were NOT further purged with N_2 to reduce the amount of time before being placed on the lamp and there was no stirring). The three cuvettes were then placed into the RMR-600 photoreactor spaced evenly throughout and irradiated at 350 nm for the selected amount of time.

Analysis:

After the conclusion of the irradiation time, the samples were each placed into a small vial and the solvents were removed under reduced pressure with heating. Each sample was dissolved in 1.0 mL of a stock of fumaric acid in D_2O (stock of fumaric acid in D_2O used a small amount of $NaHCO_3$ to aid in solvation). This mixture was drawn up into a 1 mL syringe through a 0.2 μm or 0.45 μm cellulose acetate filter tip to remove any insoluble material in the D_2O. The remaining filtered solution was transferred to an oven dried NMR tube. The T_1 for fumaric acid in D_2O is reported at 10.0 seconds,[7] therefore each sample was subjected to 32 scans with a $d_1 = 50$ seconds (5 x the T_1 of fumaric acid). For each sample, the singlet for formate and fumaric acid was integrated 5 times and the average (A_1) was recorded. Then the average (A_2) for each of the 3 photolysis samples (avg. of 3 $A_1 = A_2$) was taken to give the yield of formate. The same process was used for determining the standard deviation. The mass of formate can be calculated from the equation below[7] and thus used to determine the concentration and corresponding yield of formate.

$$m_x = P_{std} \cdot \frac{MW_x}{MW_{std}} \cdot \frac{nH_{std}}{nH_x} \cdot \frac{m_{std}}{P_x} \cdot \frac{A_x}{A_{std}}$$

(*x* = formate, *std* = fumaric acid)

m = mass (g)

P = purity (%)

MW = molecular weight (g/mol)

nH = number of protons associated with the peak (formate = 1, fumaric acid = 2)

A = area of the peak

The purity of fumaric acid and **57** used in the photolysis reactions and analyses was calculated using the above equation using spectrophotometric grade 2-propanol supplied by Alfa Aesar with a reported purity of 99.7%. The purity of fumaric acid was found to be 99.9 ± 1.8% and two separate stocks of **57** were used with purities of 74.6 ± 0.2% and 95.4 ± 0.7%.

Below are representative ^{1}H NMR spectrums for the analysis of a photolysis of **57** and TMB in 10% H_2O in 1,4-dioxane. [TMB] = 10.1 mM, [**57**] = 5.59 mM, [Fumaric standard] = 2.00 mM. The peak at 8.40 ppm represents formate (validated by spiking in authentic $NaHCO_2$) and the peak at 6.46 ppm represents fumaric acid in D_2O and the peak at 7.35 represents 1,3-dimethylimidazolium cation **58** (validated by spiking in independently synthesized cation).

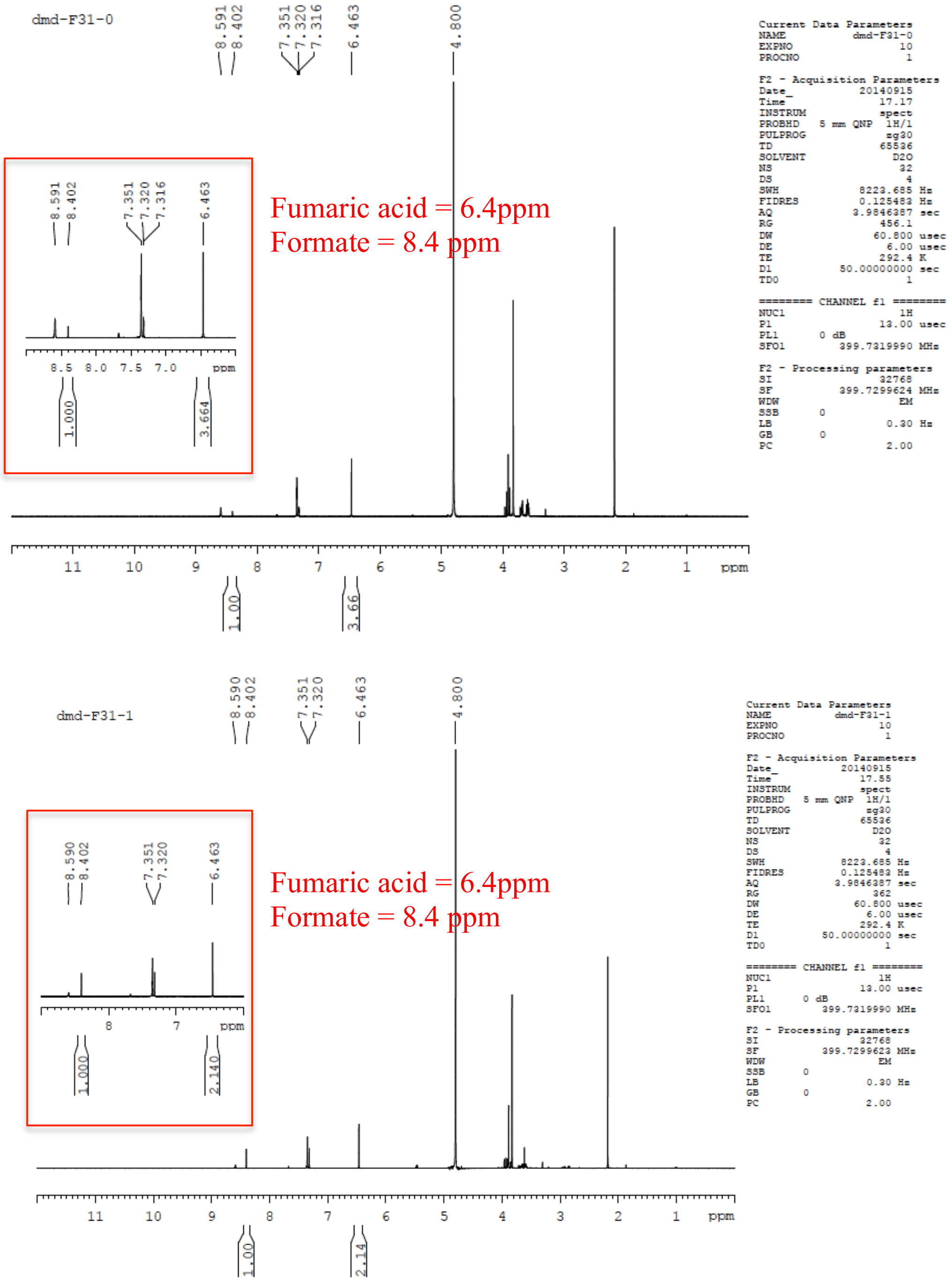

Figure 6.31 ^{1}H NMR spectra of the blank standard that was not irradiated (top) and one of the three photolyzed solutions for 60 minutes at 350 nm (bottom).

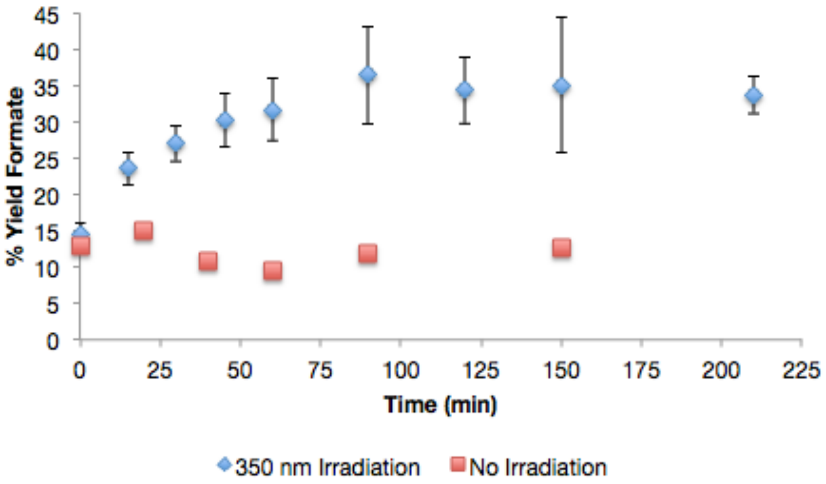

Figure 6.32 Time course of formate production that is shown in Figure 5.5 of the manuscript. 4.39 mM **57**, 10.2 mM TMB in 5.0% H_2O in 1,4-dioxane at 350 nm (represented by the diamonds). Squares indicate samples not irradiated at 350 nm (3.95 mM **57**, 10.8 mM TMB in 5% H_2O in 1,4-dioxane).

Purity of the NHC-CO_2 used for the dark control was 87.2% as measured against commercial 99.7% pure spectroscopic grade 2-propanol as the standard. Each time point in the time course was not done in triplicate, however averaging the 6 time points over the course of 150 minutes gives a formate yield of 12.2 ± 1.9%.

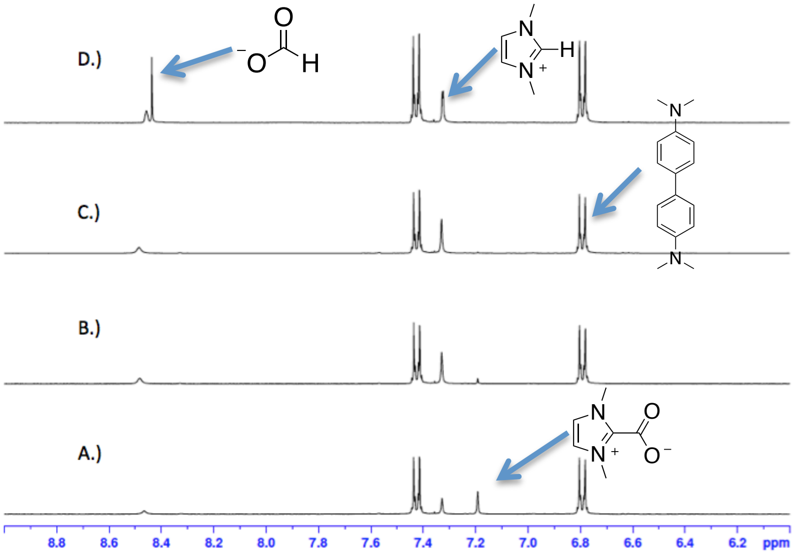

Figure 6.33 Time course of TMB (11.5 mM) and NHC-CO_2 (11.1 mM) in 5.88% H_2O in CD_3CN with no irradiation in an NMR tube. A.) = 6 minutes, B.) = 35 minutes, C.) = 68 minutes, D.) spiked with sodium formate. Formate is not observed over time under the following thermal conditions.

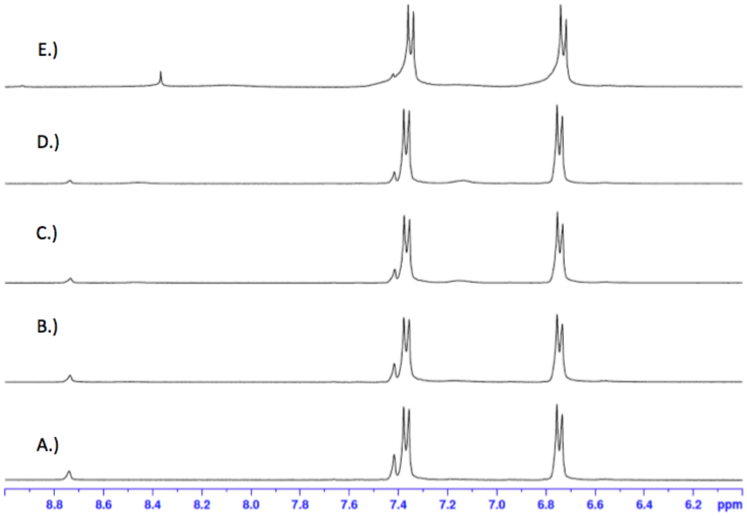

Figure 6.34 Time course of TMB (27.4 mM) and NHC-CO_2 (11.1 mM) in 5.88% H_2O in 1,4-dioxane-$_{d8}$ with no irradiation in an NMR tube. A.) = 7 minutes, B.) = 34 minutes, C.) = 68 minutes, D.) 107 minutes, E.) spiked with sodium formate. Formate is not observed over time under the following thermal conditions.

E. Colorimetric Detection of Formate Ion

Acetamide (2.5093 g, 44.8 mmol) and citric acid (0.1272 g, 0.662 mmol) were dissolved in 25.0 mL of spectrophotometric grade 2-propanol. Sodium acetate (1.4977 g, 18.3 mmol) was dissolved in 5.0 mL of HPLC grade H_2O. To test for formate, a solution was made up in a test tube containing 1.0 mL of the acetamide/citiric acid stock, 0.5 mL of the formate sample, 0.05 mL of the sodium acetate stock, and 3.5 mL of acetic anhydride. Each solution was briefly vortexed and allowed to sit for 2 hours.

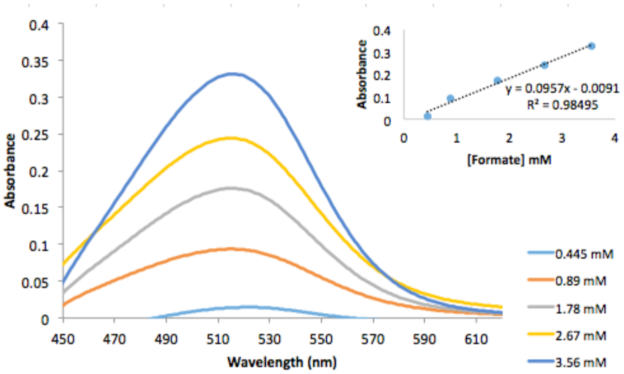

Figure 6.35 Colorimetric detection of formate calibration curve.

Three dark samples were prepared containing TMB (0.250 mL, 10.1 mM), 0.70 mL neat 1,4-dioxane, 0.04 mL H_2O and **57** (0.01 mL, 4.39 mM). The solvent was removed from each sample and dissolved in 1.0 mL H_2O and filtered through a 0.2 μm cellulose acetate filter tip. 0.5 mL of each sample was used to determine formate content. Three irradiated samples were prepared in the same manner as the dark controls stated above. These samples were irradiated for 60 minutes at 350 nm.

The following (below) is a test to see if formate is being produced under thermal conditions (i.e. by just letting the solutions sit over time without subjecting them to 350 nm and then working them up under the previous stated conditions.)

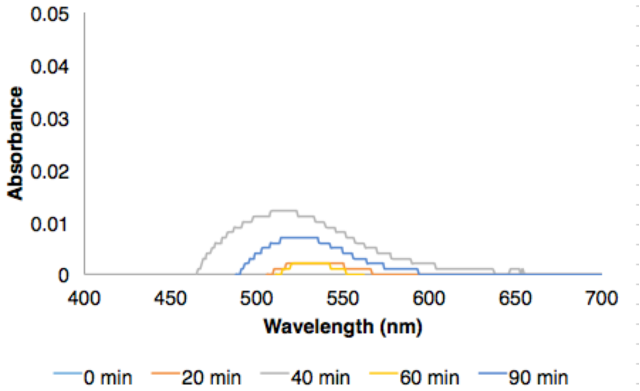

Figure 6.36 Colorimetric detection of formate in non-irradiated samples. [**57**] = 8.04 mM and [TMB] = 22.0 mM.

Above is the analysis of formate over time in separate solutions of TMB and NHC-CO_2 in 7% H_2O in 1,4-dioxane that were **NOT** irradiated at 350 nm. All samples were worked up in the same fashion as previously stated. The highest absorbance shown above is 0.012 at 510 nm at 40 minutes. This corresponds to a formate yield of 12.4% based on the aforementioned calibration curve.

F. MS of Irradiated TMB and 57

The following spectrums were recorded on a JEOL AccuTOF-CS mass spectrometer using electrospray ionization (ESI). A dark sample was prepared containing TMB (0.250 mL, 10.1 mM), 0.70 mL neat 1,4-dioxane, 0.04 mL H_2O and **57** (0.01 mL, 4.39 mM). The solvent was not removed and the solution was subjected to DART (+) analysis. The peak at 97 m/z corresponds to 1,3-dimethylimidazolium cation. The peak at 241 m/z corresponds to TMB M+1. Finally, the peak at 227 m/z represents *N,N,N'*-trimethylbenzidine M+1 (a product resulting from oxidation of TMB).

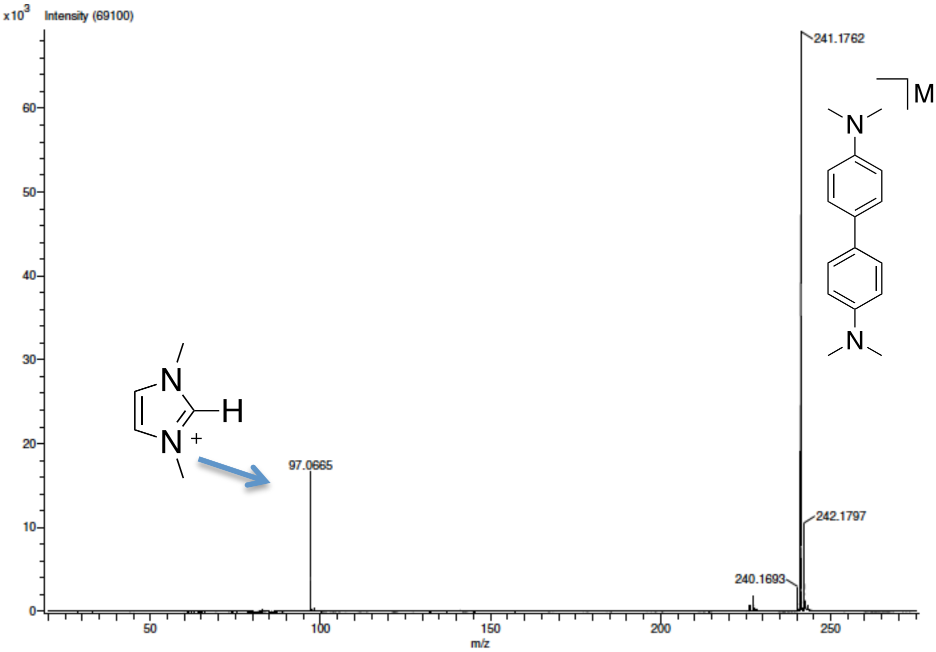

Figure 6.37 MS spectrum of a non-irradiated solution of **57** and TMB in 1,4-dioxane/H_2O.

An irradiated sample (60 min, 350 nm) was prepared containing TMB (0.250 mL, 10.1 mM), 0.70 mL neat 1,4-dioxane, 0.04 mL H_2O and **57** (0.01 mL, 4.39 mM). The solvent was not removed and the solution was subjected to DART (+) analysis. The peak at 97 m/z corresponds to 1,3-dimethylimidazolium cation. The peak at 241 m/z corresponds to TMB M+1. Finally, the peak at 227 m/z represents *N,N,N'*-

trimethylbenzidine M+1 (a product resulting from oxidation of TMB). The intensity of the peak at 227 m/z is more intense in the irradiated sample than the dark control.

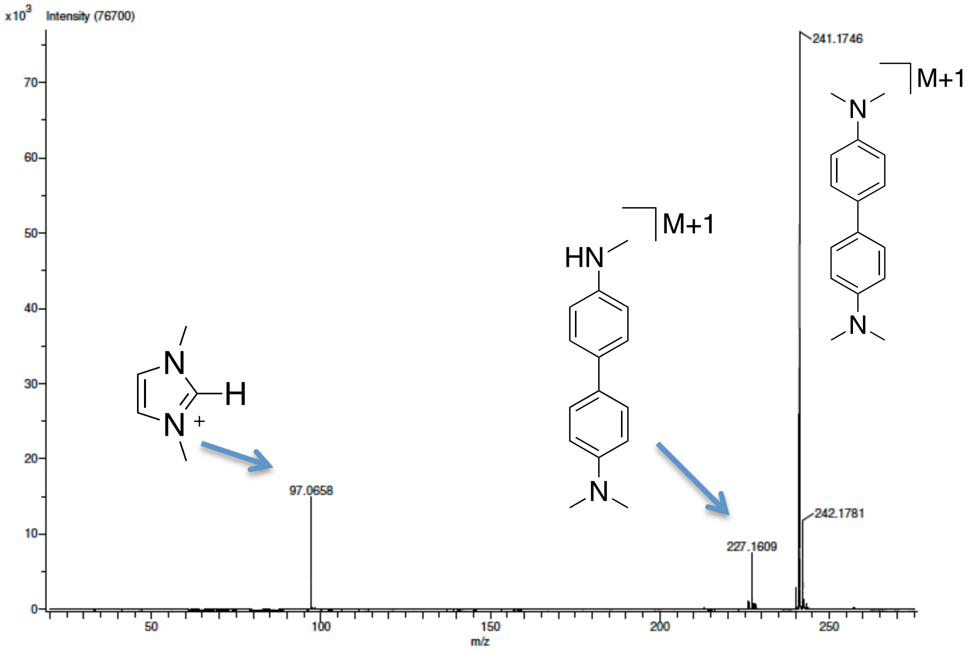

Figure 6.38 MS spectrum of an irradiated solution (60 min, 350 nm) of **57** and TMB in 1,4-dioxane/H_2O.

G. Laser Flash Photolysis Results

Laser flash photolysis results were conducted using a Nd:YAG laser (355 nm output) supplied by Continuum with pulses 4-6 ns in duration as the excitation source. The probe beam that was used was a 350 W Xe arc lamp that passed through a monochromator to a PMT detector. A 370 nm filter was used in front of the monochromator starting with detection at 400 nm to remove any 2nd order fluorescence. Solutions were made up in 40% H_2O in 1,4-dioxane in 4 sided quartz cuvettes capped with a septum. The solutions were purged with N_2 in the solution for a minimum of 10 minutes and headspace for a minimum for 3 minutes. For O_2 quenching, the septum was removed and exposed to the air for 20 minutes then shaken slightly. Laser studies were conducted under higher water ratios to ensure the stability of **57** for the time that was required to conduct the experiments. The following samples were prepared as stated:

- *N,N,N',N'*-tetramethylbenzidine = (1.23 mM, Abs @ 355 nm = 1.735) with/ NHC-CO_2 (0.142 M)
- *N*-methylcarbazole = (2.58 mM, Abs @ 355 nm = 0.766) with/ NHC-CO_2 (0.343 M)

N-methylcarbazole was excited at 355 nm in the presence of **57** as a quencher. Peaks around 690 nm and 770 nm are consistent with published reports of the cation radical.[8] Difficulties in recording measurements beyond 770 nm are the result as to why no points are presented beyond that wavelength.

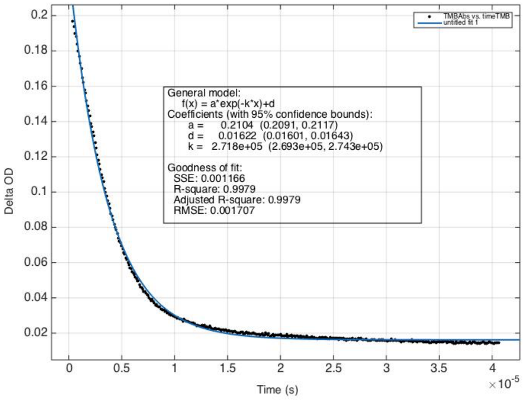

Figure 6.39 Decay of excited state triplet TMB in a N_2 degassed solution monitored at 470 nm. The decay constant (k) is 2.718 x 10^5 s^{-1}, which gives a mean lifetime of 3.68 μs.

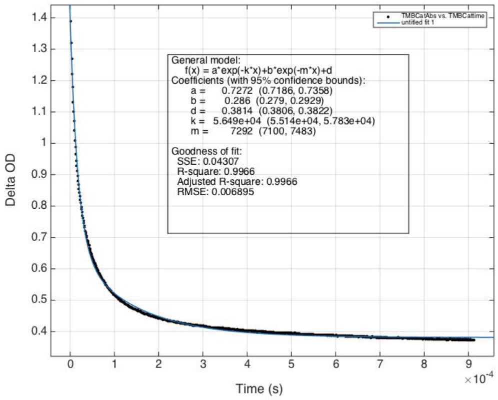

Figure 6.40 Decay of TMB cation radical generated by the quenching of excited state TMB by NHC-CO_2 **57** in a N_2 degassed solution monitored at 470 nm. The decay constant (k) is 5.649 x 10^4 s^{-1}, which gives a mean lifetime of greater than 17.7 μs.

H. HPLC Analysis of Oxalate

The following HPLC results were obtained using a Shimadzu Prominence instrument with an LC-20AT pump and SPD-20AV detector. Detection of oxalate was done at 214 nm. A 100 mM Na_2SO_4 buffer solution at a pH = 2.58 was used at a flow rate of 0.3 mL/min and an injection loop of 20 µL. The stationary phase was an Eclipse Plus C18 column (5 µm, 4.6 x 150 mm) supplied by Agilent. The retention times for the compounds of interest are as follows:

NHC-CO_2 **57** ~ 7.8 min.
1,3-dimethylimidazolium cation ~ 6.1 min.
Oxalate ~ 4.9 min.

Three (triplicate) photolysis reactions were analyzed by HPLC for possible oxalate formation. The photolysis reactions were conducted (60 minutes, 350 nm) and worked up in a similar fashion to that mentioned for ^{1}H NMR analysis. Maximum yield of oxalate would be 1.92 mM (half the starting concentration of NHC–CO_2).

10% H_2O in MeCN:
[TMB] = 7.38 mM [**57**] = 3.84 mM Oxalate yield = **5.21 ± 1.03%**

10% H_2O in 1,4-dioxane:
[TMB] = 7.45 mM [**57**] = 3.84 mM Oxalate yield = **2.64 ± 0.93%**

10% H_2O (pH ~ 14) in MeCN:
[TMB] = 7.38 mM [**57**] = 3.84 mM Oxalate yield = **7.54 ± 2.32%**

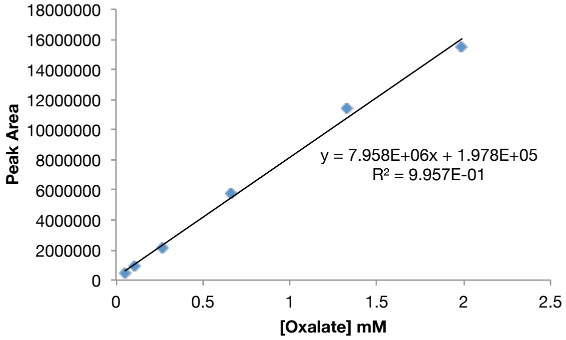

Figure 6.41 HPLC calibration curve for (bis-(tetramethylammonium) oxalate in water.

Figure 6.42 HPLC chromatograms (below) for the detection of oxalate from the photolysis of NHC–CO_2 and TMB in MeCN/H_2O and 1,4-dioxane/H_2O mixtures.

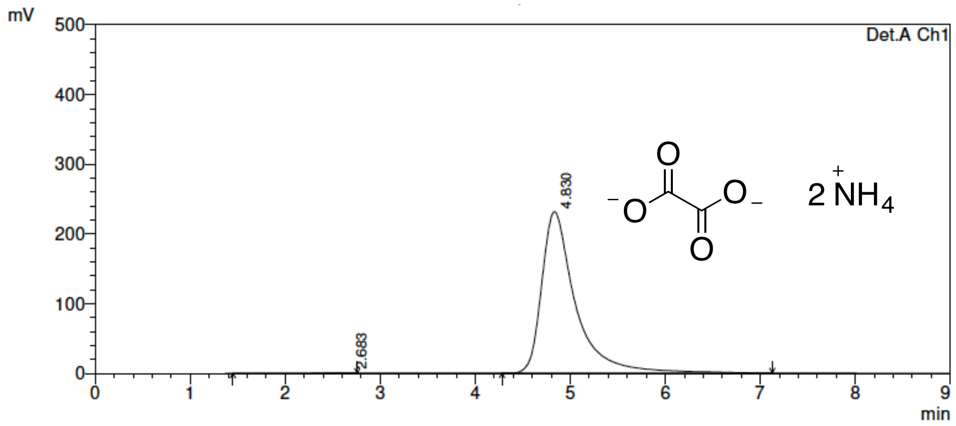

Chromatogram of bis-(tetramethylammonium) oxalate.

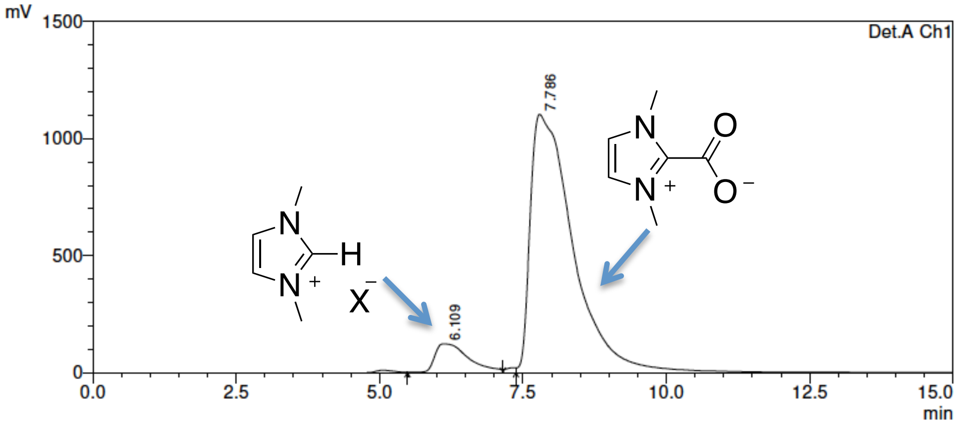

Chromatogram of NHC-CO_2 **57**.

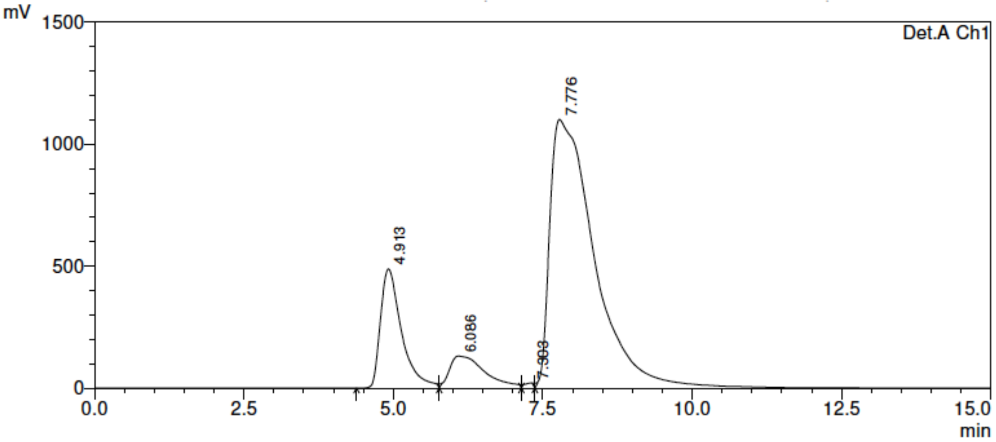

Chromatogram of NHC-CO_2 **57** with spiked in bis-(tetramethylammonium) oxalate.

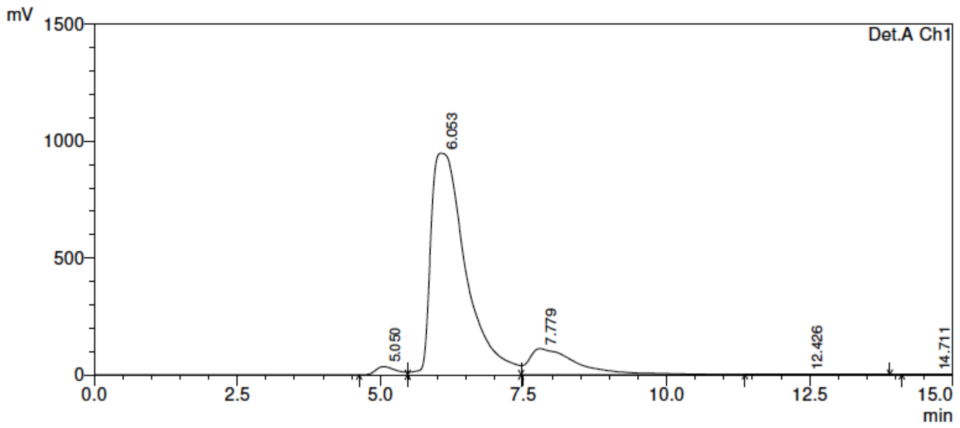

Chromatogram of one of the photolysis reactions of TMB and **57** in 10% H_2O in MeCN.

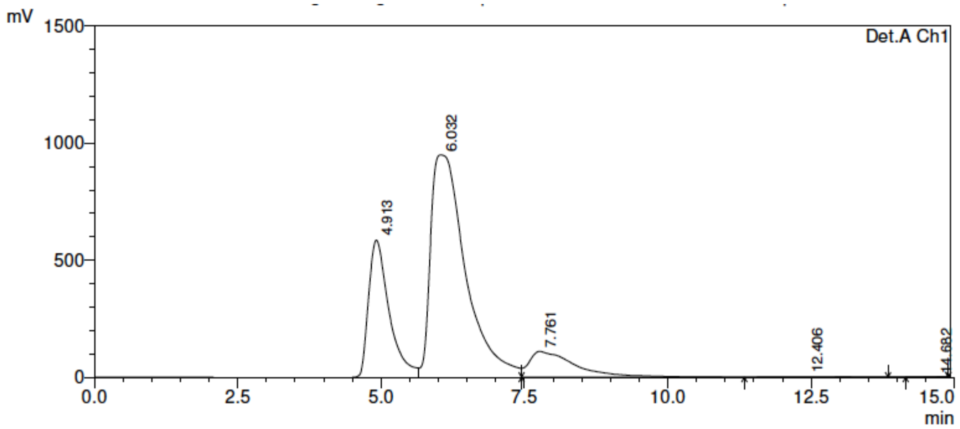

Chromatogram of one of the photolysis reactions of TMB and **57** in 10% H_2O in MeCN spiked with bis-(tetramethylammonium) oxalate.

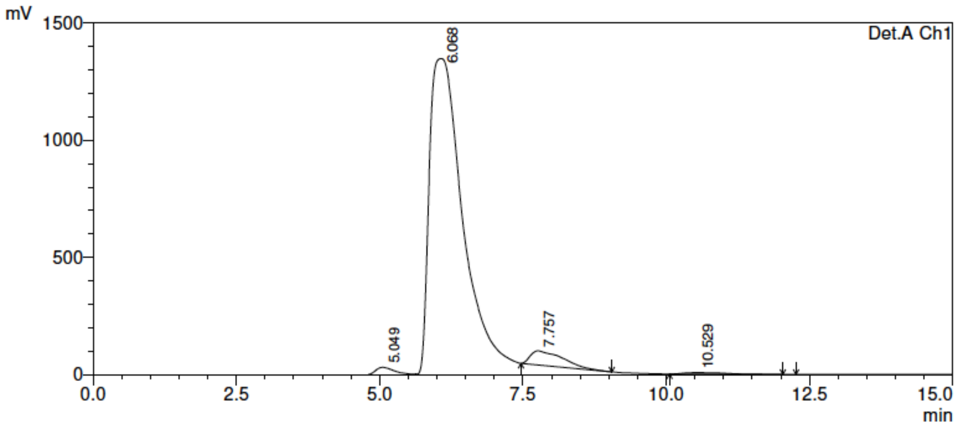

Chromatogram of one of the photolysis reactions of TMB and **57** in 10% H_2O in 1,4-dioxane.

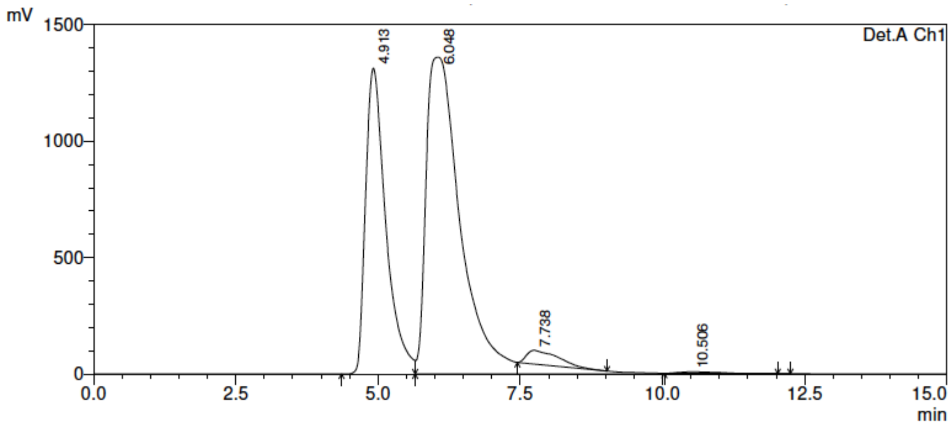

Chromatogram of one of the photolysis reactions of TMB and **57** in 10% H_2O in 1,4-dioxane spiked with bis-(tetramethylammonium) oxalate.

6.6 Computational Results

The following calculations on compound **57** were done using Gaussian 09[9] with the basis set B3LYP/6-31G(d,p) and the SMD implicit solvation model. Ground state geometries of **57** listed in Table 4.5 represent optimized minima. Transition state geometries were optimized by QST3 following a scan calculation of the C_{NHC}-CO_2 bond (30-40 scans in 0.05 Å increments). The free energy of activation was also calculated for **57** in water for three other implicit solvation models. Calculated energies and enthalpies represented in Hartrees.

Calculations performed on NHC-CO_2 **60–84** were performed in a similar fashion to **57** outlined above. Using the same B3LYP/6-31G(d,p) and the SMD implicit solvation model, all of the compounds were minimized to their ground state optimized geometry. The barriers for the 9 compounds should in Figure 4.14 were also optimized in a similar fashion described above.

A. Ground State Geometric Parameters of 57

The following computational data is presented on 1,3-dimethylimidazolium-2-carboxylate (**57**). Ground state optimization data is supplied for various implicit solvation models as indicated by the bold lettering above the structure shown.

Gas:

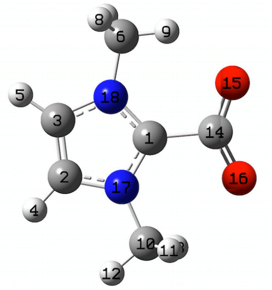

```
                          Standard orientation:
 ---------------------------------------------------------------------
 Center     Atomic      Atomic             Coordinates (Angstroms)
 Number     Number       Type             X           Y           Z
 ---------------------------------------------------------------------
    1          6           0       -0.042748    0.080880   -0.000007
    2          6           0        0.817928   -1.982430    0.000395
    3          6           0        1.855609   -1.103073   -0.000162
    4          1           0        0.807654   -3.060409    0.000779
    5          1           0        2.921273   -1.267168   -0.000407
    6          6           0        2.098880    1.403163   -0.001051
    7          1           0        2.730247    1.423428    0.890411
    8          1           0        2.725672    1.425545   -0.895698
    9          1           0        1.385518    2.228998    0.001601
   10          6           0       -1.692539   -1.828698    0.000709
   11          1           0       -2.240231   -1.497005   -0.878609
   12          1           0       -1.571065   -2.913569    0.004026
   13          1           0       -2.242115   -1.491805    0.876838
   14          6           0       -1.096741    1.252457    0.000022
   15          8           0       -0.599306    2.390883    0.002904
   16          8           0       -2.263240    0.826678   -0.002829
   17          7           0       -0.345326   -1.238914    0.000476
   18          7           0        1.308338    0.164301   -0.000329
 Sum of electronic and zero-point Energies=           -493.263930
 Sum of electronic and thermal Energies=              -493.254141
 Sum of electronic and thermal Enthalpies=            -493.253197
 Sum of electronic and thermal Free Energies=         -493.300704
```

1,4-Dioxane:

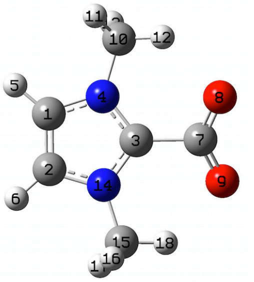

```
                    Standard orientation:
 ---------------------------------------------------------------------
 Center     Atomic      Atomic             Coordinates (Angstroms)
 Number     Number       Type             X           Y           Z
 ---------------------------------------------------------------------
    1          6           0        2.041186    0.678649    0.031318
    2          6           0        2.041139   -0.678796   -0.031297
    3          6           0       -0.088775    0.000002    0.000006
    4          7           0        0.720961    1.082744    0.043456
    5          1           0        2.854437    1.385796    0.071358
    6          1           0        2.854341   -1.385999   -0.071335
    7          6           0       -1.657113    0.000060   -0.000015
    8          8           0       -2.163182    1.036462   -0.467872
    9          8           0       -2.163279   -1.036306    0.467818
   10          6           0        0.299638    2.484472    0.138882
   11          1           0        0.859222    3.069665   -0.593824
   12          1           0       -0.766612    2.519351   -0.078125
   13          1           0        0.506081    2.860490    1.144066
   14          7           0        0.720884   -1.082796   -0.043434
   15          6           0        0.299460   -2.484493   -0.138862
   16          1           0        0.505806   -2.860507   -1.144067
   17          1           0        0.859058   -3.069735    0.593793
   18          1           0       -0.766778   -2.519304    0.078220
 Sum of electronic and zero-point Energies=           -493.280483
 Sum of electronic and thermal Energies=              -493.270690
 Sum of electronic and thermal Enthalpies=            -493.269746
 Sum of electronic and thermal Free Energies=         -493.316511
```

Tetrahydrofuran:

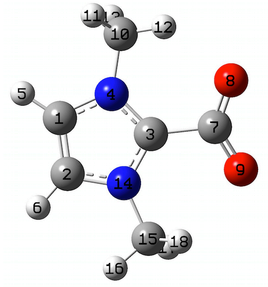

Standard orientation:

Center	Atomic	Atomic	Coordinates (Angstroms)		
Number	Number	Type	X	Y	Z
1	6	0	-2.014220	0.751497	0.021639
2	6	0	-1.151481	1.802287	-0.026050
3	6	0	0.061596	-0.072053	-0.004042
4	7	0	-1.251059	-0.396854	0.027003
5	1	0	-3.091869	0.719134	0.049155
6	1	0	-1.332361	2.864860	-0.057679
7	6	0	1.286074	-1.028126	0.001699
8	8	0	1.040043	-2.214961	-0.298103
9	8	0	2.355376	-0.462063	0.303195
10	6	0	-1.823854	-1.746219	0.096259
11	1	0	-2.616196	-1.827843	-0.650069
12	1	0	-1.021533	-2.452602	-0.105482
13	1	0	-2.242256	-1.910323	1.092500
14	7	0	0.124601	1.279412	-0.039042
15	6	0	1.333648	2.109574	-0.087367
16	1	0	1.024181	3.121287	-0.351542
17	1	0	1.828115	2.106420	0.883586
18	1	0	2.023194	1.715607	-0.829768

Sum of electronic and zero-point Energies= -493.291022
Sum of electronic and thermal Energies= -493.281367
Sum of electronic and thermal Enthalpies= -493.280423
Sum of electronic and thermal Free Energies= -493.327146

Dichloromethane:

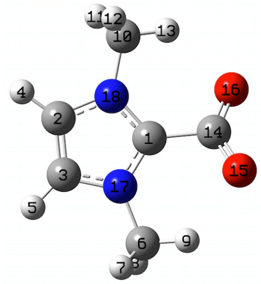

Standard orientation:

Center	Atomic	Atomic	Coordinates (Angstroms)		
Number	Number	Type	X	Y	Z
1	6	0	0.090900	-0.000112	-0.000007
2	6	0	-2.035844	0.681413	0.030187
3	6	0	-2.037377	-0.676834	-0.030499
4	1	0	-2.847085	1.391145	0.070399
5	1	0	-2.850213	-1.384734	-0.070812

6	6	0	-0.307581	-2.487704	-0.147741
7	1	0	-0.879325	-3.072807	0.574893
8	1	0	-0.513124	-2.850854	-1.157469
9	1	0	0.755433	-2.540812	0.074325
10	6	0	-0.301834	2.488322	0.148296
11	1	0	-0.877598	3.076216	-0.568809
12	1	0	-0.499540	2.849402	1.160360
13	1	0	0.759809	2.539924	-0.080608
14	6	0	1.645672	-0.001817	-0.000078
15	8	0	2.165603	-1.018981	0.503142
16	8	0	2.167778	1.014176	-0.503398
17	7	0	-0.718293	-1.083012	-0.041411
18	7	0	-0.715854	1.084634	0.041242

Sum of electronic and zero-point Energies= -493.293205
Sum of electronic and thermal Energies= -493.283330
Sum of electronic and thermal Enthalpies= -493.282385
Sum of electronic and thermal Free Energies= -493.329829

Acetonitrile:

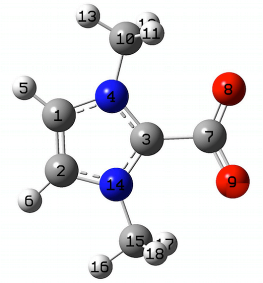

Standard orientation:

Center Number	Atomic Number	Atomic Type	Coordinates (Angstroms) X	Y	Z
1	6	0	0.680156	-2.030080	-0.017014
2	6	0	-0.681311	-2.029714	0.016470
3	6	0	0.000011	0.093766	0.000096
4	7	0	1.085293	-0.712785	-0.024603
5	1	0	1.388024	-2.843514	-0.037376
6	1	0	-1.389654	-2.842745	0.036401
7	6	0	0.000461	1.634466	-0.000111
8	8	0	1.123533	2.151772	0.180918
9	8	0	-1.122278	2.152428	-0.181304
10	6	0	2.492956	-0.298545	-0.054571
11	1	0	2.660585	0.383760	-0.885412
12	1	0	2.750814	0.208291	0.874101
13	1	0	3.095054	-1.199062	-0.175343
14	7	0	-1.085719	-0.712192	0.024441
15	6	0	-2.493126	-0.297123	0.055419

16	1	0	-3.095804	-1.197541	0.174004
17	1	0	-2.660382	0.383158	0.888031
18	1	0	-2.750586	0.212272	-0.871930

Sum of electronic and zero-point Energies= -493.294732
Sum of electronic and thermal Energies= -493.285022
Sum of electronic and thermal Enthalpies= -493.284078
Sum of electronic and thermal Free Energies= -493.330510

1-Decanol:

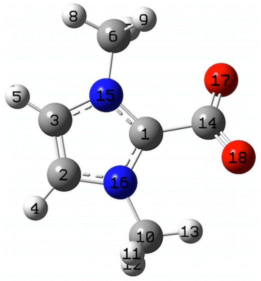

Standard orientation:

Center	Atomic	Atomic	Coordinates (Angstroms)		
Number	Number	Type	X	Y	Z
1	6	0	-0.063539	-0.069919	-0.005899
2	6	0	2.018499	0.725963	0.028446
3	6	0	1.169266	1.786911	-0.032129
4	1	0	3.095471	0.682023	0.066021
5	1	0	1.364819	2.846794	-0.067906
6	6	0	-1.314434	2.121988	-0.113889
7	1	0	-1.826548	2.120262	0.847944
8	1	0	-0.993511	3.132424	-0.367465
9	1	0	-1.992265	1.744775	-0.876931
10	6	0	1.806662	-1.766249	0.119534
11	1	0	2.473490	-1.924310	-0.730665
12	1	0	2.370701	-1.859675	1.050027
13	1	0	0.987790	-2.479383	0.088711
14	6	0	-1.285462	-1.004044	0.002849
15	7	0	-0.113132	1.280983	-0.048679
16	7	0	1.242887	-0.413608	0.037297
17	8	0	-2.340753	-0.462906	0.398732
18	8	0	-1.081020	-2.174899	-0.389173

Sum of electronic and zero-point Energies= -493.292178
Sum of electronic and thermal Energies= -493.282589
Sum of electronic and thermal Enthalpies= -493.281645
Sum of electronic and thermal Free Energies= -493.327909

Ethanol:

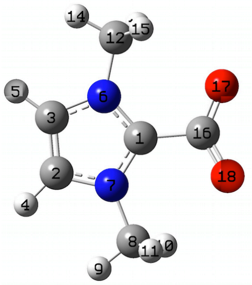

```
Standard orientation:
 ---------------------------------------------------------------------
Center     Atomic      Atomic             Coordinates (Angstroms)
 Number     Number       Type             X           Y           Z
 ---------------------------------------------------------------------
    1          6           0        0.003587   -0.093238   -0.000340
    2          6           0        0.595734    2.053213    0.024399
    3          6           0       -0.764463    1.996669   -0.018822
    4          1           0        1.268166    2.896057    0.052408
    5          1           0       -1.504582    2.780814   -0.044233
    6          7           0       -1.115466    0.665112   -0.030884
    7          7           0        1.055899    0.755224    0.031688
    8          6           0        2.480301    0.401612    0.074073
    9          1           0        3.040223    1.323724    0.227440
   10          1           0        2.667962   -0.289695    0.893692
   11          1           0        2.776749   -0.065217   -0.864589
   12          6           0       -2.505596    0.195642   -0.082048
   13          1           0       -2.770631   -0.292252    0.855218
   14          1           0       -3.138526    1.068381   -0.240825
   15          1           0       -2.630073   -0.509215   -0.902111
   16          6           0        0.067679   -1.619724    0.000621
   17          8           0       -1.012052   -2.199693    0.260127
   18          8           0        1.192582   -2.107807   -0.256367
Sum of electronic and zero-point Energies=          -493.299103
 Sum of electronic and thermal Energies=            -493.289725
 Sum of electronic and thermal Enthalpies=          -493.288781
Sum of electronic and thermal Free Energies=         -493.333900
```

Methanol:

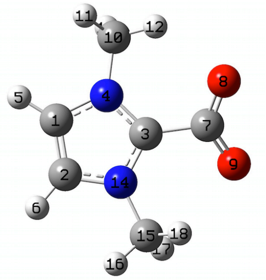

Standard orientation:

```
 ---------------------------------------------------------------------
 Center     Atomic      Atomic             Coordinates (Angstroms)
 Number     Number       Type             X           Y           Z
 ---------------------------------------------------------------------
      1          6           0       -2.126412    0.281437    0.022489
      2          6           0       -1.521706    1.498646   -0.048851
      3          6           0        0.074699   -0.052783   -0.007766
      4          7           0       -1.126723   -0.667906    0.037290
      5          1           0       -3.169331    0.008995    0.061351
      6          1           0       -1.935771    2.493136   -0.100475
      7          6           0        1.458869   -0.705146   -0.001953
      8          8           0        1.535025   -1.841585   -0.525386
      9          8           0        2.362998   -0.013340    0.520668
     10          6           0       -1.383382   -2.106739    0.171076
     11          1           0       -2.218689   -2.369771   -0.479188
     12          1           0       -0.488826   -2.647170   -0.125068
     13          1           0       -1.639928   -2.334568    1.208286
     14          7           0       -0.161097    1.276542   -0.060806
     15          6           0        0.839567    2.348669   -0.124438
     16          1           0        0.328477    3.257847   -0.439873
     17          1           0        1.290363    2.495583    0.857626
     18          1           0        1.614448    2.090398   -0.843653

 Sum of electronic and zero-point Energies=           -493.300006
 Sum of electronic and thermal Energies=              -493.290571
 Sum of electronic and thermal Enthalpies=            -493.289627
 Sum of electronic and thermal Free Energies=         -493.334682
```

Water:

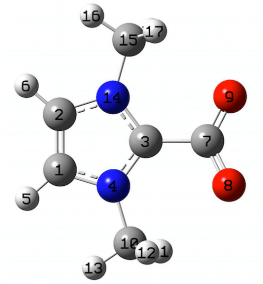

```
                         Standard orientation:
 ---------------------------------------------------------------------
 Center     Atomic      Atomic             Coordinates (Angstroms)
 Number     Number       Type             X           Y           Z
 ---------------------------------------------------------------------
      1          6           0       -0.679754   -2.025115    0.018751
      2          6           0        0.681288   -2.024613   -0.019206
      3          6           0       -0.000033    0.095147   -0.000236
      4          7           0       -1.087268   -0.709828    0.027138
      5          1           0       -1.386313   -2.839179    0.042588
```

6	1	0	1.388448	-2.838151	-0.042947
7	6	0	-0.000612	1.617060	-0.000138
8	8	0	-1.104388	2.159626	-0.252634
9	8	0	1.102693	2.160585	0.252397
10	6	0	-2.498690	-0.304757	0.078150
11	1	0	-2.658229	0.387688	0.902298
12	1	0	-2.785185	0.175129	-0.856514
13	1	0	-3.089810	-1.206760	0.230336
14	7	0	1.087803	-0.709016	-0.027458
15	6	0	2.498976	-0.302902	-0.077211
16	1	0	3.090938	-1.204316	-0.229568
17	1	0	2.658608	0.390273	-0.900724
18	1	0	2.784303	0.176616	0.858002

Sum of electronic and zero-point Energies= -493.297253
Sum of electronic and thermal Energies= -493.287949
Sum of electronic and thermal Enthalpies= -493.287005
Sum of electronic and thermal Free Energies= -493.332058

B. Ground State Geometric Parameters of 57 with a Lewis Acid (Cation)

The following computational data is presented on 1,3-dimethylimidazolium-2-carboxylate (**57**) with coordination to a metal cation. Ground state optimization data is supplied for various implicit solvation models (denoted in parentheses) and the metal cation as indicated by the bold lettering above the structure shown.

Lithium (Gas):

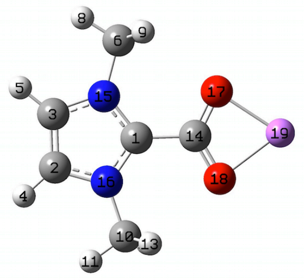

Standard orientation:

Center	Atomic	Atomic	Coordinates (Angstroms)		
Number	Number	Type	X	Y	Z
1	6	0	0.064342	0.000006	-0.000042
2	6	0	2.172486	-0.683869	0.000072
3	6	0	2.172868	0.682724	-0.000109
4	1	0	2.991686	-1.385045	-0.000174

5	1	0	2.992453	1.383448	0.000073
6	6	0	0.440314	2.506280	0.000028
7	1	0	-0.156724	2.711822	0.886690
8	1	0	1.343144	3.115436	-0.001146
9	1	0	-0.158964	2.711342	-0.885174
10	6	0	0.438770	-2.506427	0.000152
11	1	0	1.341227	-3.116159	0.000230
12	1	0	-0.159498	-2.711298	0.886096
13	1	0	-0.159568	-2.711335	-0.885745
14	6	0	-1.433983	0.000390	-0.000081
15	7	0	0.862498	1.092308	-0.000162
16	7	0	0.861909	-1.092731	0.000095
17	8	0	-2.024908	1.116250	0.000184
18	8	0	-2.025429	-1.115187	-0.000365
19	3	0	-3.610231	0.000542	0.000315

Sum of electronic and zero-point Energies= -500.685678
Sum of electronic and thermal Energies= -500.674807
Sum of electronic and thermal Enthalpies= -500.673863
Sum of electronic and thermal Free Energies= -500.722477

Lithium (Water):

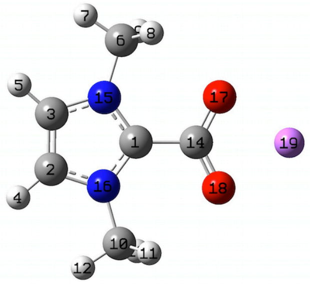

Standard orientation:

Center Number	Atomic Number	Atomic Type	Coordinates (Angstroms) X	Y	Z
1	6	0	0.065484	-0.000017	0.000008
2	6	0	2.178293	-0.682003	-0.000030
3	6	0	2.178147	0.682404	-0.000020
4	1	0	2.994873	-1.384888	-0.000075
5	1	0	2.994576	1.385465	0.000001
6	6	0	0.451702	2.501547	0.000034
7	1	0	1.357465	3.105508	-0.000102
8	1	0	-0.143262	2.709714	-0.886826
9	1	0	-0.143012	2.709755	0.887053
10	6	0	0.452181	-2.501491	0.000030
11	1	0	-0.141810	-2.710067	-0.887400
12	1	0	1.358050	-3.105294	0.000989
13	1	0	-0.143404	-2.709540	0.886491

```
 14        6          0       -1.442151   -0.000170   -0.000012
 15        7          0        0.866183    1.089828    0.000003
 16        7          0        0.866410   -1.089700    0.000010
 17        8          0       -2.015707    1.120289   -0.000043
 18        8          0       -2.015554   -1.120689   -0.000005
 19        3          0       -3.771160    0.000011    0.000032
Sum of electronic and zero-point Energies=          -500.792856
 Sum of electronic and thermal Energies=            -500.781769
 Sum of electronic and thermal Enthalpies=          -500.780825
Sum of electronic and thermal Free Energies=        -500.829978
```

Sodium (Water):

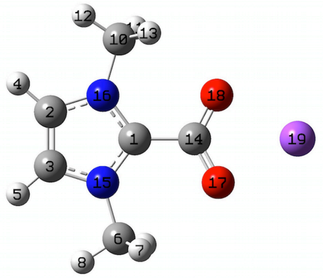

```
                       Standard orientation:
 ---------------------------------------------------------------------
 Center     Atomic      Atomic             Coordinates (Angstroms)
 Number     Number       Type             X           Y           Z
 ---------------------------------------------------------------------
  1        6          0       -0.449565   -0.000036   -0.000031
  2        6          0       -2.561498    0.681967    0.018234
  3        6          0       -2.561652   -0.681560   -0.017968
  4        1          0       -3.376082    1.387952    0.041762
  5        1          0       -3.376405   -1.387353   -0.041367
  6        6          0       -0.842349   -2.501803   -0.078259
  7        1          0       -0.371309   -2.789588    0.860608
  8        1          0       -1.742434   -3.092729   -0.239696
  9        1          0       -0.144700   -2.655000   -0.899429
 10        6          0       -0.841848    2.501850    0.078267
 11        1          0       -0.370932    2.789595   -0.860676
 12        1          0       -1.741795    3.092941    0.239889
 13        1          0       -0.144036    2.654923    0.899320
 14        6          0        1.051726   -0.000157   -0.000255
 15        7          0       -1.250258   -1.090026   -0.025363
 16        7          0       -1.250006    1.090144    0.025420
 17        8          0        1.626364   -1.095032    0.254166
 18        8          0        1.626451    1.094650   -0.254783
 19       11          0        3.634376   -0.000008    0.000382
Sum of electronic and zero-point Energies=          -655.535560
 Sum of electronic and thermal Energies=            -655.524348
 Sum of electronic and thermal Enthalpies=          -655.523403
```

Sum of electronic and thermal Free Energies= -655.573397

Potassium (Water):

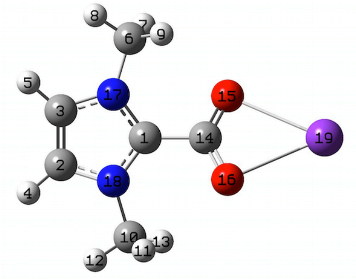

```
                    Standard orientation:
 ---------------------------------------------------------------------
 Center     Atomic      Atomic             Coordinates (Angstroms)
 Number     Number       Type             X           Y           Z
 ---------------------------------------------------------------------
    1          6           0       -0.848315   -0.000028    0.000065
    2          6           0       -2.962606   -0.680446   -0.031983
    3          6           0       -2.962532    0.680671    0.031504
    4          1           0       -3.775955   -1.387142   -0.072237
    5          1           0       -3.775810    1.387461    0.071533
    6          6           0       -1.231833    2.495248    0.121410
    7          1           0       -0.886102    2.836370   -0.854295
    8          1           0       -2.100452    3.075334    0.429735
    9          1           0       -0.433666    2.605419    0.852261
   10          6           0       -1.232124   -2.495270   -0.121210
   11          1           0       -0.888004   -2.836721    0.854960
   12          1           0       -2.100386   -3.075099   -0.431014
   13          1           0       -0.432826   -2.605384   -0.850812
   14          6           0        0.662237   -0.000051    0.000245
   15          8           0        1.219586    1.048236   -0.419283
   16          8           0        1.219542   -1.048324    0.419853
   17          7           0       -1.647763    1.088005    0.046598
   18          7           0       -1.647885   -1.087951   -0.046670
   19         19           0        3.652671   -0.000034   -0.000230
 Sum of electronic and zero-point Energies=          -1093.147995
 Sum of electronic and thermal Energies=             -1093.136080
 Sum of electronic and thermal Enthalpies=           -1093.135136
 Sum of electronic and thermal Free Energies=        -1093.188558
```

Magnesium (Water):

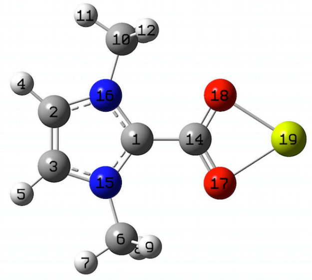

```
                         Standard orientation:
 ---------------------------------------------------------------------
 Center     Atomic      Atomic             Coordinates (Angstroms)
 Number     Number       Type             X           Y           Z
 ---------------------------------------------------------------------
    1          6           0       -0.464336   -0.000245    0.000275
    2          6           0       -2.565686    0.688476   -0.002631
    3          6           0       -2.568448   -0.680475    0.002033
    4          1           0       -3.381793    1.393209   -0.005444
    5          1           0       -3.387390   -1.381917    0.004164
    6          6           0       -0.859123   -2.507967    0.007584
    7          1           0       -1.767888   -3.103745    0.066016
    8          1           0       -0.319476   -2.740991   -0.909341
    9          1           0       -0.225998   -2.707098    0.870126
   10          6           0       -0.849124    2.509069   -0.007175
   11          1           0       -1.755699    3.108403   -0.063091
   12          1           0       -0.306567    2.739245    0.908744
   13          1           0       -0.217173    2.706486   -0.870971
   14          6           0        1.008179   -0.003260   -0.000011
   15          7           0       -1.265276   -1.092801    0.003632
   16          7           0       -1.260841    1.095528   -0.003406
   17          8           0        1.639363   -1.109353   -0.024923
   18          8           0        1.642838    1.101419    0.024898
   19         12           0        3.381535   -0.000234   -0.000169
 Sum of electronic and zero-point Energies=           -693.203458
 Sum of electronic and thermal Energies=              -693.192512
 Sum of electronic and thermal Enthalpies=            -693.191568
 Sum of electronic and thermal Free Energies=         -693.240614
```

C. Transition State Geometric Parameters of 57

The following computational data is presented on 1,3-dimethylimidazolium-2-carboxylate (**57**). Transition state optimization data is supplied for various implicit solvation models indicated in bold above the structure illustrated.

Water:

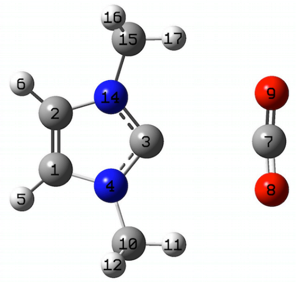

```
                    Standard orientation:
 ---------------------------------------------------------------------
 Center     Atomic      Atomic             Coordinates (Angstroms)
 Number     Number       Type             X           Y           Z
 ---------------------------------------------------------------------
      1          6           0       -2.394321   -0.678475    0.011841
      2          6           0       -2.394489    0.678002   -0.013219
      3          6           0       -0.197996    0.000068    0.000952
      4          7           0       -1.058657   -1.065814    0.019582
      5          1           0       -3.208930   -1.386943    0.023506
      6          1           0       -3.209286    1.386230   -0.026235
      7          6           0        2.762468    0.000165   -0.000384
      8          8           0        2.826233   -1.160655   -0.138377
      9          8           0        2.826145    1.160966    0.137835
     10          6           0       -0.628567   -2.458633    0.044682
     11          1           0        0.460283   -2.482712    0.049982
     12          1           0       -1.004648   -2.961818    0.939930
     13          1           0       -0.997065   -2.989932   -0.837473
     14          7           0       -1.058920    1.065714   -0.018999
     15          6           0       -0.629210    2.458659   -0.043827
     16          1           0       -0.998561    2.989929    0.837988
     17          1           0        0.459639    2.483083   -0.048283
     18          1           0       -1.004726    2.961652   -0.939421
 Sum of electronic and zero-point Energies=           -493.253216
 Sum of electronic and thermal Energies=              -493.242166
 Sum of electronic and thermal Enthalpies=            -493.241222
 Sum of electronic and thermal Free Energies=         -493.292016
```

Methanol:

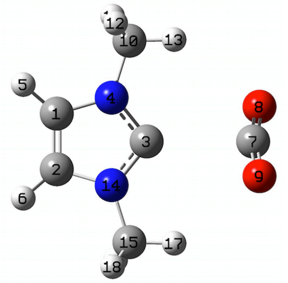

```
                    Standard orientation:
 ---------------------------------------------------------------------
 Center     Atomic      Atomic             Coordinates (Angstroms)
 Number     Number       Type             X           Y           Z
 ---------------------------------------------------------------------
      1          6           0       -2.301395    0.676959    0.048011
      2          6           0       -2.301463   -0.676845   -0.048155
      3          6           0       -0.114148   -0.000048    0.000027
      4          7           0       -0.966684    1.064437    0.074638
      5          1           0       -3.115868    1.384068    0.100164
      6          1           0       -3.116007   -1.383866   -0.100417
      7          6           0        2.477521   -0.000020   -0.000039
      8          8           0        2.632330    0.844990   -0.804323
      9          8           0        2.632382   -0.845033    0.804234
     10          6           0       -0.533592    2.451419    0.191203
     11          1           0       -0.941754    3.048671   -0.629314
     12          1           0       -0.868296    2.880777    1.140301
     13          1           0        0.554755    2.479374    0.149462
     14          7           0       -0.966794   -1.064438   -0.074670
     15          6           0       -0.533694   -2.451440   -0.190991
     16          1           0       -0.868326   -2.880980   -1.140033
     17          1           0        0.554654   -2.479279   -0.149168
     18          1           0       -0.941884   -3.048564    0.629607
 Sum of electronic and zero-point Energies=           -493.259560
 Sum of electronic and thermal Energies=              -493.249326
 Sum of electronic and thermal Enthalpies=            -493.248381
 Sum of electronic and thermal Free Energies=         -493.296832
```

Acetonitrile:

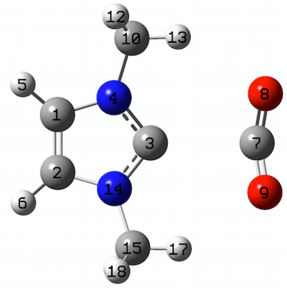

```
                    Standard orientation:
 ---------------------------------------------------------------------
 Center     Atomic      Atomic             Coordinates (Angstroms)
 Number     Number       Type             X           Y           Z
 ---------------------------------------------------------------------
      1          6           0       -2.282729    0.670742    0.071913
      2          6           0       -2.276713   -0.686683    0.053162
      3          6           0       -0.097519    0.003493   -0.065451
      4          7           0       -0.952884    1.066037   -0.000718
      5          1           0       -3.097827    1.376417    0.130110
```

6	1	0	-3.085392	-1.401100	0.091132
7	6	0	2.413495	0.003983	0.022949
8	8	0	2.609792	1.162689	-0.078606
9	8	0	2.596773	-1.155262	0.142417
10	6	0	-0.532907	2.462656	-0.017353
11	1	0	-0.930740	2.970039	-0.901240
12	1	0	-0.894499	2.978150	0.876979
13	1	0	0.554728	2.495393	-0.039858
14	7	0	-0.943496	-1.067957	-0.029730
15	6	0	-0.511512	-2.459822	-0.089175
16	1	0	-0.904535	-2.943319	-0.988431
17	1	0	0.576400	-2.482118	-0.111130
18	1	0	-0.868687	-3.005655	0.788810

Sum of electronic and zero-point Energies= -493.266548
Sum of electronic and thermal Energies= -493.256368
Sum of electronic and thermal Enthalpies= -493.255424
Sum of electronic and thermal Free Energies= -493.303486

1,4-Dioxane:

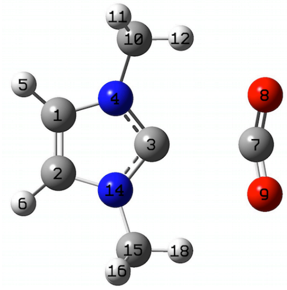

Standard orientation:

Center Number	Atomic Number	Atomic Type	Coordinates (Angstroms) X	Y	Z
1	6	0	-2.262946	0.683453	-0.036114
2	6	0	-2.266947	-0.672996	-0.014146
3	6	0	-0.082220	-0.000346	0.025735
4	7	0	-0.928756	1.068432	-0.011596
5	1	0	-3.075779	1.393074	-0.066599
6	1	0	-3.083997	-1.378378	-0.020680
7	6	0	2.355208	-0.004928	-0.008974
8	8	0	2.568689	1.150201	0.119703
9	8	0	2.559386	-1.160775	-0.145997
10	6	0	-0.490674	2.458028	-0.021036
11	1	0	-0.863094	2.982002	0.864722
12	1	0	0.597362	2.473681	-0.018719
13	1	0	-0.860829	2.968200	-0.915557
14	7	0	-0.935038	-1.064811	0.022876
15	6	0	-0.505114	-2.456351	0.065066

16	1	0	-0.877028	-2.944426	0.971299
17	1	0	-0.881316	-2.997845	-0.808255
18	1	0	0.582794	-2.478224	0.061984

Sum of electronic and zero-point Energies= -493.261634

Sum of electronic and thermal Energies= -493.251520

Sum of electronic and thermal Enthalpies= -493.250576

Sum of electronic and thermal Free Energies= -493.300181

Tetrahydrofuran:

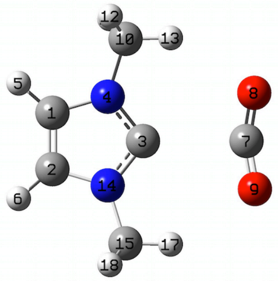

Standard orientation:

Center Number	Atomic Number	Atomic Type	Coordinates (Angstroms) X	Y	Z
1	6	0	-2.277197	0.679115	0.038765
2	6	0	-2.277663	-0.677981	0.060524
3	6	0	-0.094269	-0.001823	-0.050769
4	7	0	-0.944722	1.065778	-0.028197
5	1	0	-3.090065	1.389225	0.064143
6	1	0	-3.091079	-1.386220	0.109307
7	6	0	2.400128	0.001523	0.017942
8	8	0	2.587280	1.158965	0.152443
9	8	0	2.602791	-1.154934	-0.101343
10	6	0	-0.515493	2.457944	-0.084117
11	1	0	-0.902260	2.941114	-0.986457
12	1	0	-0.878975	3.003396	0.791754
13	1	0	0.572424	2.481116	-0.098298
14	7	0	-0.945399	-1.067557	0.005676
15	6	0	-0.516633	-2.460933	-0.002210
16	1	0	-0.897936	-2.972876	-0.890970
17	1	0	0.571372	-2.485201	-0.009849
18	1	0	-0.886443	-2.977416	0.888398

Sum of electronic and zero-point Energies= -493.266753

Sum of electronic and thermal Energies= -493.256631

Sum of electronic and thermal Enthalpies= -493.255687

Sum of electronic and thermal Free Energies= -493.303694

Gas:

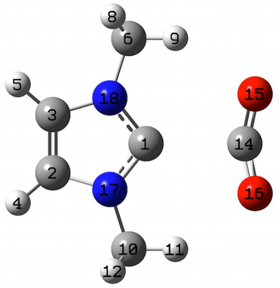

Standard orientation:

```
 ---------------------------------------------------------------------
 Center     Atomic      Atomic             Coordinates (Angstroms)
 Number     Number       Type             X           Y           Z
 ---------------------------------------------------------------------
   1          6           0       -0.056252    0.000019    0.001010
   2          6           0       -2.234860   -0.678410   -0.000967
   3          6           0       -2.234858    0.678476   -0.000968
   4          1           0       -3.050974   -1.384437   -0.001710
   5          1           0       -3.050965    1.384513   -0.001748
   6          6           0       -0.458029    2.458563    0.000672
   7          1           0       -0.828599    2.974833   -0.890088
   8          1           0       -0.830488    2.974896    0.890609
   9          1           0        0.629944    2.465635    0.001787
  10          6           0       -0.458106   -2.458552    0.001060
  11          1           0        0.629868   -2.465693    0.000064
  12          1           0       -0.828804   -2.974078    0.892205
  13          1           0       -0.830493   -2.975566   -0.888499
  14          6           0        2.254029   -0.000028   -0.000328
  15          8           0        2.494500    1.161492   -0.000042
  16          8           0        2.494304   -1.161589   -0.001040
  17          7           0       -0.901535   -1.068522    0.000203
  18          7           0       -0.901531    1.068559    0.000250
 Sum of electronic and zero-point Energies=           -493.253658
 Sum of electronic and thermal Energies=              -493.243632
 Sum of electronic and thermal Enthalpies=            -493.242688
 Sum of electronic and thermal Free Energies=         -493.290550
```

Dichloromethane:

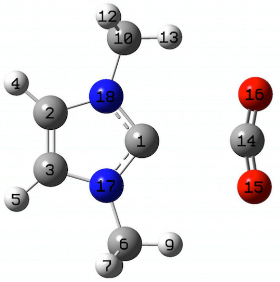

Standard orientation

```
 ---------------------------------------------------------------------
 Center     Atomic      Atomic             Coordinates (Angstroms)
 Number     Number       Type             X           Y           Z
 ---------------------------------------------------------------------
    1          6           0        0.099039    0.001260    0.021274
    2          6           0        2.284438    0.679390   -0.043712
    3          6           0        2.285253   -0.677204    0.004623
    4          1           0        3.097963    1.387989   -0.085495
    5          1           0        3.099652   -1.385947    0.016160
    6          6           0        0.519983   -2.455881    0.112687
    7          1           0        0.907348   -3.018022   -0.742089
    8          1           0        0.880104   -2.922652    1.034448
    9          1           0       -0.568246   -2.478529    0.096032
   10          6           0        0.516478    2.458547   -0.079467
   11          1           0        0.905941    3.009004    0.782099
   12          1           0        0.872892    2.938919   -0.995510
   13          1           0       -0.571724    2.479256   -0.058977
   14          6           0       -2.419670   -0.002585   -0.007525
   15          8           0       -2.596014   -1.127378   -0.314425
   16          8           0       -2.610219    1.121399    0.293637
   17          7           0        0.951568   -1.064966    0.042645
   18          7           0        0.950262    1.067345   -0.032309
 Sum of electronic and zero-point Energies=           -493.266480
 Sum of electronic and thermal Energies=              -493.256160
 Sum of electronic and thermal Enthalpies=            -493.255216
 Sum of electronic and thermal Free Energies=         -493.305386
```

1-Decanol:

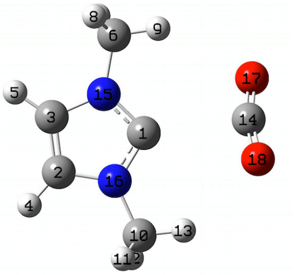

Standard orientation:

```
 ---------------------------------------------------------------------
 Center     Atomic      Atomic             Coordinates (Angstroms)
 Number     Number       Type             X           Y           Z
 ---------------------------------------------------------------------
    1          6           0        0.114173    0.000237    0.000217
    2          6           0        2.301678   -0.678380    0.039513
    3          6           0        2.302446    0.676308   -0.039387
    4          1           0        3.116273   -1.385867    0.082304
    5          1           0        3.117876    1.382832   -0.082095
    6          6           0        0.534697    2.452446   -0.157373
```

7	1	0	0.936842	3.036787	0.675589
8	1	0	0.874771	2.897865	-1.097334
9	1	0	-0.553545	2.477319	-0.120819
10	6	0	0.531849	-2.452450	0.156912
11	1	0	0.929784	-3.035963	-0.678673
12	1	0	0.874960	-2.899991	1.094738
13	1	0	-0.556561	-2.475526	0.124511
14	6	0	-2.477056	0.000756	-0.000006
15	7	0	0.968128	1.064526	-0.061026
16	7	0	0.966929	-1.065020	0.061424
17	8	0	-2.633102	1.034305	0.540349
18	8	0	-2.633463	-1.032742	-0.540381

Sum of electronic and zero-point Energies= -493.258337
Sum of electronic and thermal Energies= -493.248080
Sum of electronic and thermal Enthalpies= -493.247135
Sum of electronic and thermal Free Energies= -493.295585

Ethanol:

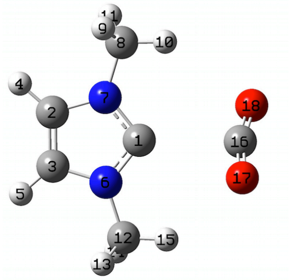

Standard orientation:

Center	Atomic	Atomic	Coordinates (Angstroms)		
Number	Number	Type	X	Y	Z
1	6	0	0.106163	-0.000095	-0.000437
2	6	0	2.291822	0.677535	-0.047417
3	6	0	2.292212	-0.676349	0.047839
4	1	0	3.106002	1.384932	-0.099313
5	1	0	3.106816	-1.383226	0.100151
6	7	0	0.957763	-1.064529	0.073593
7	7	0	0.957159	1.064853	-0.073961
8	6	0	0.523420	2.451622	-0.191434
9	1	0	0.852603	2.878271	-1.143662
10	1	0	-0.564504	2.479760	-0.142938
11	1	0	0.936731	3.050450	0.625276
12	6	0	0.525141	-2.451629	0.191255
13	1	0	0.940549	-3.050565	-0.624308
14	1	0	0.853156	-2.877282	1.144340
15	1	0	-0.562676	-2.481234	0.140961
16	6	0	-2.444900	-0.000431	0.000129

17	8	0	-2.614741	-0.839733	-0.809221
18	8	0	-2.614794	0.838821	0.809529

Sum of electronic and zero-point Energies= -493.261185
Sum of electronic and thermal Energies= -493.250868
Sum of electronic and thermal Enthalpies= -493.249924
Sum of electronic and thermal Free Energies= -493.298902

D. Dissociation Geometric Parameters of 57

The following computational data is presented on 1,3-dimethylimidazolium-2-carboxylate (**57**). A weakly dissociated complex was optimized and the data is supplied for various implicit solvation models as indicated by the bold lettering above the structure shown.

1,4-Dioxane:

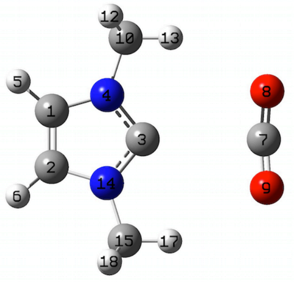

Standard orientation:

Center Number	Atomic Number	Atomic Type	Coordinates (Angstroms) X	Y	Z
1	6	0	-2.387876	0.685597	-0.040066
2	6	0	-2.393591	-0.670932	-0.027359
3	6	0	-0.195284	-0.001278	0.034176
4	7	0	-1.051482	1.065797	-0.002713
5	1	0	-3.200913	1.395334	-0.071844
6	1	0	-3.212693	-1.374130	-0.045343
7	6	0	2.735135	-0.005983	-0.012987
8	8	0	2.818400	1.159693	0.060121
9	8	0	2.809173	-1.171969	-0.089699
10	6	0	-0.605899	2.450168	0.003373
11	1	0	-0.959779	2.975273	-0.889755
12	1	0	-0.977422	2.974166	0.890127
13	1	0	0.483118	2.453662	0.014537
14	7	0	-1.060400	-1.061674	0.017021
15	6	0	-0.626603	-2.449421	0.052257
16	1	0	-0.996690	-2.993184	-0.822864

```
    17          1           0        0.462432   -2.462497    0.048730
    18          1           0       -0.990752   -2.948185    0.956522
 Sum of electronic and zero-point Energies=           -493.262626
 Sum of electronic and thermal Energies=              -493.251567
 Sum of electronic and thermal Enthalpies=            -493.250623
 Sum of electronic and thermal Free Energies=         -493.301752
```

Acetonitrile:

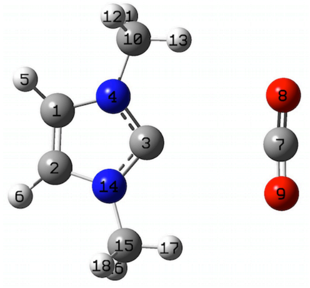

```
                         Standard orientation:
 ---------------------------------------------------------------------
 Center     Atomic      Atomic             Coordinates (Angstroms)
 Number     Number       Type             X           Y           Z
 ---------------------------------------------------------------------
      1          6           0       -2.389096    0.748953   -0.235201
      2          6           0       -2.447274   -0.607601   -0.219785
      3          6           0       -0.275863   -0.015638    0.250918
      4          7           0       -1.069780    1.081783    0.049687
      5          1           0       -3.153202    1.489217   -0.420062
      6          1           0       -3.271714   -1.284059   -0.389674
      7          6           0        2.899853   -0.054613   -0.084280
      8          8           0        2.963095    1.110112    0.003537
      9          8           0        2.919492   -1.219779   -0.183274
     10          6           0       -0.585858    2.452628    0.137353
     11          1           0       -0.779864    2.990419   -0.795623
     12          1           0       -1.075017    2.985935    0.958437
     13          1           0        0.488535    2.422649    0.316828
     14          7           0       -1.160802   -1.045407    0.073170
     15          6           0       -0.796321   -2.450385    0.191373
     16          1           0       -1.030913   -2.989042   -0.731724
     17          1           0        0.275727   -2.509231    0.377551
     18          1           0       -1.332822   -2.923249    1.019898
 Sum of electronic and zero-point Energies=           -493.267798
 Sum of electronic and thermal Energies=              -493.256642
 Sum of electronic and thermal Enthalpies=            -493.255698
 Sum of electronic and thermal Free Energies=         -493.307089
```

Methanol:

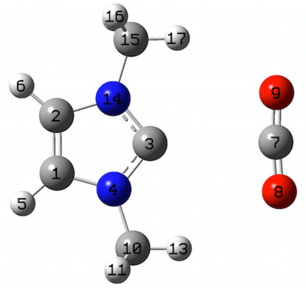

Standard orientation:

```
 ---------------------------------------------------------------------
 Center     Atomic      Atomic             Coordinates (Angstroms)
 Number     Number       Type             X           Y           Z
 ---------------------------------------------------------------------
    1          6           0        2.389008   -0.689469   -0.162956
    2          6           0        2.398519    0.667766   -0.143770
    3          6           0        0.222211   -0.000309    0.171656
    4          7           0        1.065631   -1.069663    0.028774
    5          1           0        3.190052   -1.401960   -0.294030
    6          1           0        3.209366    1.372520   -0.254988
    7          6           0       -2.798567    0.011826   -0.059540
    8          8           0       -2.863929   -1.151808    0.040871
    9          8           0       -2.836261    1.175769   -0.170114
   10          6           0        0.627956   -2.458058    0.078964
   11          1           0        0.860828   -2.972020   -0.858755
   12          1           0        1.118209   -2.988965    0.900759
   13          1           0       -0.450301   -2.473154    0.235890
   14          7           0        1.080435    1.060837    0.058515
   15          6           0        0.661879    2.453231    0.146497
   16          1           0        0.906685    2.990353   -0.775064
   17          1           0       -0.416785    2.479228    0.298687
   18          1           0        1.154954    2.954163    0.985325
 Sum of electronic and zero-point Energies=           -493.259845
 Sum of electronic and thermal Energies=              -493.248566
 Sum of electronic and thermal Enthalpies=            -493.247622
 Sum of electronic and thermal Free Energies=         -493.299328
```

Tetrahydrofuran:

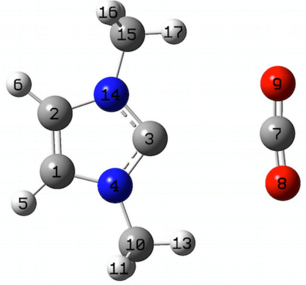

Standard orientation:

Center	Atomic	Atomic	Coordinates (Angstroms)		
Number	Number	Type	X	Y	Z
1	6	0	2.402727	-0.683585	-0.073049
2	6	0	2.406959	0.673717	-0.056621
3	6	0	0.212000	0.000253	0.066898
4	7	0	1.068418	-1.066044	0.001987
5	1	0	3.214177	-1.393745	-0.130908
6	1	0	3.222803	1.380029	-0.097161
7	6	0	-2.783678	0.005049	-0.024825
8	8	0	-2.857343	-1.159673	0.065221
9	8	0	-2.846520	1.169835	-0.120981
10	6	0	0.629515	-2.454054	0.022075
11	1	0	0.978353	-2.981833	-0.870885
12	1	0	1.014025	-2.969492	0.907926
13	1	0	-0.459612	-2.465135	0.044068
14	7	0	1.075029	1.062470	0.027201
15	6	0	0.644645	2.452239	0.082341
16	1	0	1.003811	3.002114	-0.792940
17	1	0	-0.444489	2.469177	0.095574
18	1	0	1.024702	2.940889	0.985175

Sum of electronic and zero-point Energies= -493.267727
Sum of electronic and thermal Energies= -493.256672
Sum of electronic and thermal Enthalpies= -493.255727
Sum of electronic and thermal Free Energies= -493.306413

Water:

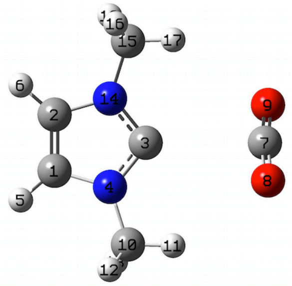

Standard orientation:

Center	Atomic	Atomic	Coordinates (Angstroms)		
Number	Number	Type	X	Y	Z
1	6	0	-2.372312	-0.676478	-0.046199
2	6	0	-2.371951	0.677330	0.045283
3	6	0	-0.176989	-0.000226	0.000604
4	7	0	-1.036632	-1.063897	-0.069589
5	1	0	-3.187482	-1.382539	-0.096799
6	1	0	-3.186696	1.383948	0.095078

7	6	0	2.697774	-0.000196	-0.000287
8	8	0	2.772845	-0.910114	0.733855
9	8	0	2.772015	0.909771	-0.734457
10	6	0	-0.602335	-2.450055	-0.188912
11	1	0	0.483590	-2.478396	-0.105280
12	1	0	-1.042411	-3.057875	0.606276
13	1	0	-0.899720	-2.868229	-1.155053
14	7	0	-1.036079	1.063948	0.069989
15	6	0	-0.601234	2.449886	0.189692
16	1	0	-0.899604	2.868271	1.155438
17	1	0	0.484799	2.477783	0.107325
18	1	0	-1.040097	3.057854	-0.606055

Sum of electronic and zero-point Energies=	-493.253815
Sum of electronic and thermal Energies=	-493.242575
Sum of electronic and thermal Enthalpies=	-493.241631
Sum of electronic and thermal Free Energies=	-493.293245

Gas:

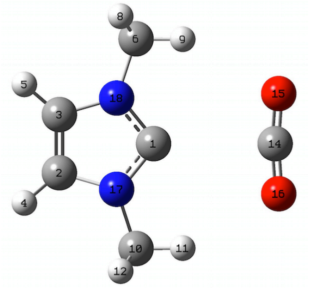

Standard orientation:

Center Number	Atomic Number	Atomic Type	Coordinates (Angstroms) X	Y	Z
1	6	0	-0.172025	0.000003	0.000032
2	6	0	-2.368877	-0.678367	-0.000037
3	6	0	-2.368891	0.678325	-0.000029
4	1	0	-3.186683	-1.382994	-0.000057
5	1	0	-3.186713	1.382932	-0.000051
6	6	0	-0.579700	2.446818	0.000007
7	1	0	-0.939115	2.973571	-0.890063
8	1	0	-0.939180	2.973584	0.890042
9	1	0	0.509064	2.436842	0.000045
10	6	0	-0.579631	-2.446819	0.000008
11	1	0	0.509132	-2.436793	0.000054
12	1	0	-0.939096	-2.973596	0.890043
13	1	0	-0.939026	-2.973584	-0.890062
14	6	0	2.665792	0.000017	-0.000047
15	8	0	2.749515	1.168593	0.000021
16	8	0	2.749519	-1.168558	0.000032

```
   17          7           0       -1.032893   -1.064275    0.000002
   18          7           0       -1.032915    1.064261    0.000002
 Sum of electronic and zero-point Energies=          -493.255441
 Sum of electronic and thermal Energies=             -493.244272
 Sum of electronic and thermal Enthalpies=           -493.243328
 Sum of electronic and thermal Free Energies=        -493.294601
```

1-Decanol:

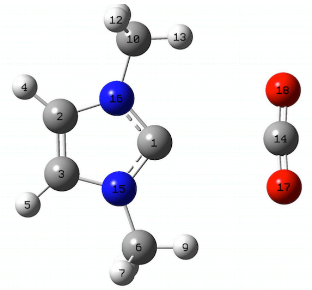

```
                        Standard orientation:
 ---------------------------------------------------------------------
 Center     Atomic      Atomic             Coordinates (Angstroms)
 Number     Number       Type             X           Y           Z
 ---------------------------------------------------------------------
    1          6           0        0.205508   -0.005074    0.072296
    2          6           0        2.384258    0.707677   -0.090414
    3          6           0        2.409201   -0.648094   -0.038842
    4          1           0        3.184720    1.428309   -0.169854
    5          1           0        3.236065   -1.342292   -0.064027
    6          6           0        0.675831   -2.450578    0.142949
    7          1           0        1.039309   -3.010928   -0.723934
    8          1           0        1.068552   -2.916299    1.052466
    9          1           0       -0.412847   -2.489866    0.162614
   10          6           0        0.587219    2.454375   -0.047112
   11          1           0        0.985842    3.009674    0.807757
   12          1           0        0.909402    2.949445   -0.968564
   13          1           0       -0.501284    2.456728   -0.000489
   14          6           0       -2.772076   -0.024815   -0.025985
   15          7           0        1.083463   -1.055456    0.058037
   16          7           0        1.044709    1.072471   -0.020804
   17          8           0       -2.819595   -1.153696   -0.330584
   18          8           0       -2.848731    1.103092    0.276341
 Sum of electronic and zero-point Energies=          -493.258490
 Sum of electronic and thermal Energies=             -493.247453
 Sum of electronic and thermal Enthalpies=           -493.246509
 Sum of electronic and thermal Free Energies=        -493.296994
```

Ethanol:

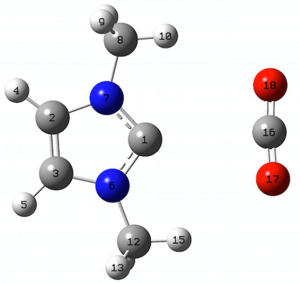

Standard orientation:

Center	Atomic	Atomic	Coordinates (Angstroms)		
Number	Number	Type	X	Y	Z
1	6	0	0.219148	0.001430	0.088789
2	6	0	2.403819	0.687240	-0.108065
3	6	0	2.412946	-0.668950	-0.053703
4	1	0	3.211312	1.398241	-0.202102
5	1	0	3.229841	-1.374444	-0.090886
6	7	0	1.084176	-1.059936	0.064292
7	7	0	1.069983	1.068833	-0.020060
8	6	0	0.630694	2.457749	-0.036346
9	1	0	0.965705	2.955814	-0.951184
10	1	0	-0.458147	2.474608	0.003477
11	1	0	1.031273	3.000097	0.825770
12	6	0	0.662072	-2.450899	0.160301
13	1	0	1.018370	-3.020664	-0.703147
14	1	0	1.051631	-2.913903	1.072332
15	1	0	-0.427018	-2.477779	0.181424
16	6	0	-2.810197	-0.011832	-0.032689
17	8	0	-2.847249	-1.137353	-0.349829
18	8	0	-2.879372	1.113268	0.280450

Sum of electronic and zero-point Energies= -493.261470
Sum of electronic and thermal Energies= -493.250328
Sum of electronic and thermal Enthalpies= -493.249384
Sum of electronic and thermal Free Energies= -493.300449

Dichloromethane:

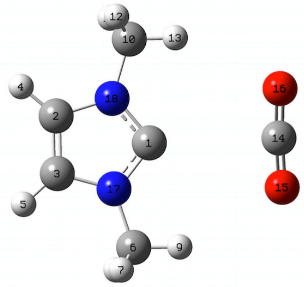

Standard orientation:

```
 ---------------------------------------------------------------------
 Center     Atomic      Atomic             Coordinates (Angstroms)
   Number     Number       Type             X           Y           Z
 ---------------------------------------------------------------------
   1         6           0        0.242951   -0.006240    0.190379
   2         6           0        2.395335    0.713308   -0.177997
   3         6           0        2.423500   -0.643941   -0.163217
   4         1           0        3.184399    1.436731   -0.319836
   5         1           0        3.241892   -1.337030   -0.289780
   6         6           0        0.711498   -2.450597    0.152141
   7         1           0        0.971371   -2.990054   -0.763970
   8         1           0        1.200789   -2.941028    0.999649
   9         1           0       -0.368490   -2.483205    0.292627
  10         6           0        0.609229    2.453780    0.096984
  11         1           0        1.091366    2.987952    0.921710
  12         1           0        0.830253    2.977887   -0.838161
  13         1           0       -0.468682    2.444054    0.255797
  14         6           0       -2.838095   -0.028462   -0.064372
  15         8           0       -2.872254   -1.193978   -0.158412
  16         8           0       -2.907390    1.136578    0.017258
  17         7           0        1.113993   -1.054445    0.059032
  18         7           0        1.069970    1.073989    0.036352
 Sum of electronic and zero-point Energies=           -493.267555
 Sum of electronic and thermal Energies=              -493.256276
 Sum of electronic and thermal Enthalpies=            -493.255332
 Sum of electronic and thermal Free Energies=         -493.307607
```

E. Ground and Transition State Geometric Parameters and Energies of Implicit Solvation Models

The following computational data was acquired for 1,3-dimethylimidazolium-2-carboxylate (**57**) using various implicit solvation models. Both the ground state and transition state of **57** were optimized (identified in parentheses) with the solvation model bolded.

CPCM (Ground State):

Standard orientation:

```
 ---------------------------------------------------------------------
 Center     Atomic      Atomic             Coordinates (Angstroms)
   Number     Number       Type             X           Y           Z
 ---------------------------------------------------------------------
   1         6           0        0.054581    0.077039   -0.003558
   2         6           0       -1.933563   -0.936788    0.016936
```

3	6	0	-0.975344	-1.901828	-0.027181
4	1	0	-3.008613	-1.009236	0.041431
5	1	0	-1.057824	-2.975926	-0.057642
6	6	0	-1.983925	1.568168	0.094627
7	1	0	-2.753435	1.588173	-0.678493
8	1	0	-2.450241	1.670443	1.076621
9	1	0	-1.246433	2.349387	-0.069037
10	6	0	1.530389	-1.975520	-0.078117
11	1	0	2.038598	-1.878709	0.879942
12	1	0	1.315832	-3.022251	-0.291118
13	1	0	2.162568	-1.550135	-0.853324
14	6	0	1.177218	1.138936	0.000633
15	7	0	0.246216	-1.262622	-0.036466
16	7	0	-1.283035	0.278554	0.025204
17	8	0	2.304892	0.681338	0.282198
18	8	0	0.825252	2.305746	-0.280896

Sum of electronic and zero-point Energies= -493.289241
Sum of electronic and thermal Energies= -493.279586
Sum of electronic and thermal Enthalpies= -493.278642
Sum of electronic and thermal Free Energies= -493.325029

CPCM (Transition State):

Standard orientation:

Center Number	Atomic Number	Atomic Type	Coordinates (Angstroms) X	Y	Z
1	6	0	-0.107410	-0.000084	0.000323
2	6	0	-2.296502	-0.677526	-0.020265
3	6	0	-2.295982	0.679136	0.019291
4	1	0	-3.112098	-1.383820	-0.042579
5	1	0	-3.111032	1.386081	0.040953
6	6	0	-0.524494	-2.456363	-0.079982
7	1	0	-0.919793	-3.011852	0.775146
8	1	0	-0.871154	-2.935152	-1.000327
9	1	0	0.563150	-2.470498	-0.050089
10	6	0	-0.522211	2.456382	0.080989
11	1	0	-0.918765	3.013268	-0.772622
12	1	0	-0.866310	2.934474	1.002674
13	1	0	0.565374	2.469045	0.048791
14	6	0	2.451533	-0.000627	-0.000224
15	7	0	-0.960938	1.066629	0.030568
16	7	0	-0.961749	-1.066129	-0.030406
17	8	0	2.619006	1.138037	-0.250756
18	8	0	2.618473	-1.139356	0.250273

Sum of electronic and zero-point Energies= -493.261523

```
 Sum of electronic and thermal Energies=            -493.251178
 Sum of electronic and thermal Enthalpies=          -493.250234
 Sum of electronic and thermal Free Energies=       -493.299416
```

IEF-PCM (Ground State):

```
                         Standard orientation:
 ---------------------------------------------------------------------
 Center     Atomic      Atomic             Coordinates (Angstroms)
 Number     Number       Type             X           Y           Z
 ---------------------------------------------------------------------
    1          6           0        0.054980    0.076543   -0.003711
    2          6           0       -1.941436   -0.920783    0.017369
    3          6           0       -0.991281   -1.893732   -0.027448
    4          1           0       -3.017020   -0.984273    0.042415
    5          1           0       -1.082685   -2.967106   -0.058393
    6          6           0        1.514101   -1.987460   -0.079958
    7          1           0        2.026256   -1.890288    0.875869
    8          1           0        1.290905   -3.033337   -0.288211
    9          1           0        2.147030   -1.570274   -0.859125
   10          6           0       -1.970203    1.584880    0.096238
   11          1           0       -2.745324    1.609047   -0.671101
   12          1           0       -2.428106    1.694620    1.081413
   13          1           0       -1.227238    2.359245   -0.075351
   14          7           0        0.235548   -1.264603   -0.036990
   15          7           0       -1.280847    0.289176    0.025553
   16          6           0        1.186578    1.128955    0.000726
   17          8           0        2.309019    0.662462    0.288330
   18          8           0        0.845587    2.297530   -0.286674
 Sum of electronic and zero-point Energies=         -493.289121
 Sum of electronic and thermal Energies=            -493.279457
 Sum of electronic and thermal Enthalpies=          -493.278513
 Sum of electronic and thermal Free Energies=       -493.324937
```

IEF-PCM (Transition State):

```
                         Standard orientation:
 ---------------------------------------------------------------------
 Center     Atomic      Atomic             Coordinates (Angstroms)
 Number     Number       Type             X           Y           Z
 ---------------------------------------------------------------------
    1          6           0       -0.107281   -0.000481    0.001350
    2          6           0       -2.295468    0.679997    0.018690
    3          6           0       -2.296763   -0.676655   -0.020866
    4          1           0       -3.110182    1.387362    0.039717
    5          1           0       -3.112816   -1.382415   -0.043666
    6          6           0       -0.525614   -2.456465   -0.079196
    7          1           0       -0.923027   -3.012020    0.774912
```

```
   8      1       0    -0.870529  -2.934769  -1.000468
   9      1       0     0.561968  -2.471251  -0.047031
  10      6       0    -0.521097   2.456379   0.080828
  11      1       0    -0.912022   3.011646  -0.776477
  12      1       0    -0.870848   2.936544   0.999290
  13      1       0     0.566683   2.468886   0.055411
  14      7       0    -0.962241  -1.066019  -0.030039
  15      7       0    -0.960213   1.066750   0.030878
  16      6       0     2.451486  -0.001148  -0.000444
  17      8       0     2.618516  -1.140173   0.248559
  18      8       0     2.618531   1.137814  -0.249776
 Sum of electronic and zero-point Energies=         -493.261482
 Sum of electronic and thermal Energies=            -493.251132
 Sum of electronic and thermal Enthalpies=          -493.250188
 Sum of electronic and thermal Free Energies=       -493.299431
```

PCM (Ground State):

```
                         Standard orientation:
 ---------------------------------------------------------------------
 Center     Atomic      Atomic             Coordinates (Angstroms)
 Number     Number       Type             X           Y           Z
 ---------------------------------------------------------------------
   1      6       0     0.054975   0.076569  -0.003672
   2      6       0    -1.941081  -0.921498   0.017310
   3      6       0    -0.990560  -1.894095  -0.027491
   4      1       0    -3.016644  -0.985443   0.042286
   5      1       0    -1.081583  -2.967501  -0.058450
   6      7       0     0.236038  -1.264515  -0.036982
   7      7       0    -1.280939   0.288696   0.025562
   8      6       0     1.514781  -1.987009  -0.079746
   9      1       0     2.026073  -1.891041   0.876693
  10      1       0     1.292017  -3.032694  -0.289451
  11      1       0     2.148295  -1.568645  -0.857773
  12      6       0    -1.970803   1.584139   0.096156
  13      1       0    -2.745352   1.608306  -0.671759
  14      1       0    -2.429522   1.693329   1.081014
  15      1       0    -1.227964   2.358814  -0.074570
  16      6       0     1.186180   1.129431   0.000694
  17      8       0     2.308912   0.663346   0.287802
  18      8       0     0.844592   2.297952  -0.286245
 Sum of electronic and zero-point Energies=         -493.289118
 Sum of electronic and thermal Energies=            -493.279456
 Sum of electronic and thermal Enthalpies=          -493.278512
 Sum of electronic and thermal Free Energies=       -493.324927
```

PCM (Transition State):

Standard orientation:

Center	Atomic	Atomic	Coordinates (Angstroms)		
Number	Number	Type	X	Y	Z
1	6	0	0.107304	0.000071	0.000341
2	6	0	2.296052	-0.678482	0.019699
3	6	0	2.296179	0.678174	-0.020235
4	1	0	3.111375	-1.385116	0.041571
5	1	0	3.111634	1.384639	-0.042603
6	7	0	0.961334	1.066375	-0.030662
7	7	0	0.961132	-1.066413	0.030838
8	6	0	0.523438	2.456399	-0.080604
9	1	0	0.918124	3.012233	0.774595
10	1	0	0.870137	2.935226	-1.000928
11	1	0	-0.564232	2.469931	-0.051101
12	6	0	0.523041	-2.456355	0.081243
13	1	0	0.918212	-3.012646	-0.773429
14	1	0	0.869123	-2.934764	1.002022
15	1	0	-0.564612	-2.469830	0.051073
16	6	0	-2.451393	0.000083	-0.000206
17	8	0	-2.618507	1.138589	0.251120
18	8	0	-2.618336	-1.138433	-0.251602

Sum of electronic and zero-point Energies= -493.261481
Sum of electronic and thermal Energies= -493.251132
Sum of electronic and thermal Enthalpies= -493.250188
Sum of electronic and thermal Free Energies= -493.299417

F. Ground State Calculations (gas phase) of NHC–CO_2 60-84

The following computational data is presented on N-heterocyclic carboxylates **60** - **84**. Ground state optimization data is supplied for the following compounds in the gas phase only. The NHC-CO_2 is indicted in bold heading above the corresponding structure.

NHC–CO_2 (60)

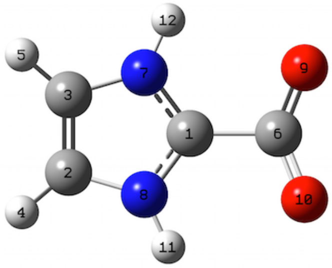

Standard orientation:

Center Number	Atomic Number	Atomic Type	Coordinates (Angstroms) X	Y	Z
1	6	0	0.032558	-0.000022	-0.000020
2	6	0	-2.087306	-0.680560	0.000073
3	6	0	-2.087284	0.680586	-0.000092
4	1	0	-2.904346	-1.382235	0.000558
5	1	0	-2.904303	1.382282	-0.000571
6	6	0	1.579896	-0.000004	-0.000082
7	7	0	-0.764768	1.067059	-0.000191
8	7	0	-0.764801	-1.067078	0.000233
9	8	0	2.038320	1.146925	0.000289
10	8	0	2.038370	-1.146909	-0.000243
11	1	0	-0.362582	-1.997312	-0.000096
12	1	0	-0.362493	1.997271	0.000165

Sum of electronic and zero-point Energies= -414.692734

Sum of electronic and thermal Energies= -414.686251

Sum of electronic and thermal Enthalpies= -414.685307

Sum of electronic and thermal Free Energies= -414.723880

NHC-CO$_2$ (61)

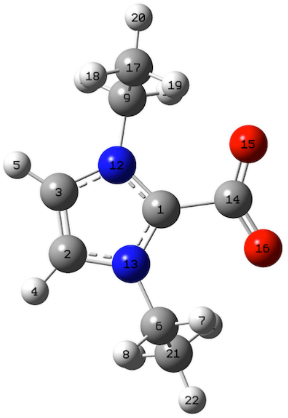

Standard orientation:

Center Number	Atomic Number	Atomic Type	Coordinates (Angstroms) X	Y	Z
1	6	0	-0.000045	0.125856	-0.000058
2	6	0	-0.650868	-1.992883	-0.191771
3	6	0	0.650697	-1.992892	0.191660
4	1	0	-1.324797	-2.808626	-0.394882

5	1	0	1.324627	-2.808642	0.394731
6	6	0	-2.402160	-0.260255	-0.670005
7	1	0	-2.320157	0.713582	-1.147519
8	1	0	-2.759434	-0.995862	-1.395745
9	6	0	2.402058	-0.260401	0.670018
10	1	0	2.759132	-0.996261	1.395633
11	1	0	2.320009	0.713199	1.147987
12	7	0	1.038173	-0.677997	0.304313
13	7	0	-1.038233	-0.677970	-0.304627
14	6	0	-0.000022	1.686468	-0.000036
15	8	0	1.133718	2.171917	-0.084105
16	8	0	-1.133693	2.172040	0.084067
17	6	0	3.316610	-0.172560	-0.540088
18	1	0	3.375579	-1.123908	-1.077008
19	1	0	2.959222	0.608112	-1.213040
20	1	0	4.324197	0.095243	-0.211491
21	6	0	-3.316321	-0.172649	0.540409
22	1	0	-4.324001	0.095431	0.212324
23	1	0	-3.375242	-1.124055	1.077250
24	1	0	-2.958615	0.607793	1.213485

Sum of electronic and zero-point Energies= -571.848530
Sum of electronic and thermal Energies= -571.836585
Sum of electronic and thermal Enthalpies= -571.835641
Sum of electronic and thermal Free Energies= -571.887041

NHC-CO$_2$ (62)

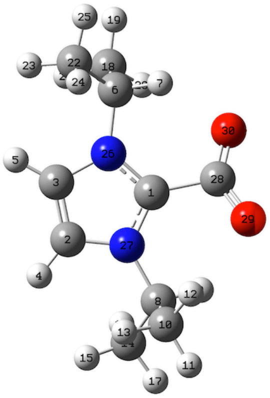

Standard orientation:

Center Number	Atomic Number	Atomic Type	Coordinates (Angstroms) X	Y	Z
1	6	0	-0.000050	0.324477	-0.000555
2	6	0	-0.677416	-1.794512	0.008472
3	6	0	0.677713	-1.794383	-0.006141
4	1	0	-1.373519	-2.615610	0.025740
5	1	0	1.373955	-2.615404	-0.021752

6	6	0	2.498456	-0.036611	-0.039026
7	1	0	2.435855	1.050285	0.031785
8	6	0	-2.498414	-0.036747	0.038165
9	1	0	-2.435764	1.049950	-0.035894
10	6	0	-3.237285	-0.565768	-1.184605
11	1	0	-4.255116	-0.168360	-1.188981
12	1	0	-2.745112	-0.241086	-2.103732
13	1	0	-3.307916	-1.658431	-1.187466
14	6	0	-3.141105	-0.446991	1.357647
15	1	0	-3.204800	-1.534956	1.464732
16	1	0	-2.584393	-0.046528	2.208145
17	1	0	-4.157791	-0.048990	1.403518
18	6	0	3.236918	-0.561838	1.185592
19	1	0	4.255022	-0.165114	1.188673
20	1	0	2.744797	-0.233657	2.103493
21	1	0	3.306806	-1.654539	1.192223
22	6	0	3.141488	-0.450895	-1.357092
23	1	0	3.205722	-1.539165	-1.460646
24	1	0	2.584680	-0.053442	-2.208952
25	1	0	4.157973	-0.052540	-1.404160
26	7	0	1.083199	-0.477987	-0.004045
27	7	0	-1.083127	-0.478170	0.004206
28	6	0	-0.000149	1.888882	-0.000971
29	8	0	-0.964009	2.379110	-0.600271
30	8	0	0.963779	2.379265	0.598176

Sum of electronic and zero-point Energies= -650.428327
Sum of electronic and thermal Energies= -650.413477
Sum of electronic and thermal Enthalpies= -650.412533
Sum of electronic and thermal Free Energies= -650.470224

NHC-CO$_2$ (63)

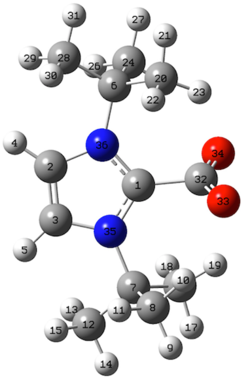

Standard orientation:

Center Atomic Atomic Coordinates (Angstroms)

```
 Number     Number       Type             X           Y            Z
 ---------------------------------------------------------------------
   1          6           0         0.000003    0.135974   -0.000137
   2          6           0         0.674920   -1.977491   -0.027300
   3          6           0        -0.674825   -1.977524    0.026782
   4          1           0         1.356323   -2.807025   -0.059632
   5          1           0        -1.356236   -2.807070    0.058559
   6          6           0         2.533699   -0.223380   -0.022886
   7          6           0        -2.533654   -0.223395    0.023075
   8          6           0        -2.882017    0.208616   -1.404263
   9          1           0        -3.928969    0.522647   -1.440596
  10          1           0        -2.249331    1.041443   -1.716612
  11          1           0        -2.751483   -0.623859   -2.102374
  12          6           0        -3.406328   -1.410678    0.438125
  13          1           0        -3.137425   -1.791347    1.427605
  14          1           0        -4.441791   -1.067882    0.483725
  15          1           0        -3.373543   -2.229485   -0.285463
  16          6           0        -2.749575    0.914255    1.024340
  17          1           0        -3.820291    1.127824    1.075177
  18          1           0        -2.408280    0.631107    2.023100
  19          1           0        -2.243601    1.832000    0.730311
  20          6           0         2.749848    0.914609   -1.023766
  21          1           0         3.820591    1.127997   -1.074558
  22          1           0         2.408483    0.631868   -2.022613
  23          1           0         2.244023    1.832308   -0.729304
  24          6           0         2.881647    0.208251    1.404656
  25          1           0         2.248869    1.041016    1.717008
  26          1           0         2.750962   -0.624384    2.102532
  27          1           0         3.928570    0.522342    1.441357
  28          6           0         3.406451   -1.410543   -0.438045
  29          1           0         3.373307   -2.229652    0.285192
  30          1           0         3.137948   -1.790817   -1.427789
  31          1           0         4.441970   -1.067823   -0.483090
  32          6           0        -0.000040    1.689257   -0.000168
  33          8           0        -0.404563    2.179617   -1.060580
  34          8           0         0.404419    2.179696    1.060264
  35          7           0        -1.090068   -0.659553    0.046312
  36          7           0         1.090109   -0.659507   -0.046669
 Sum of electronic and zero-point Energies=           -728.993888
 Sum of electronic and thermal Energies=              -728.976566
 Sum of electronic and thermal Enthalpies=            -728.975622
 Sum of electronic and thermal Free Energies=         -729.037903
```

NHC-CO_2 (64)

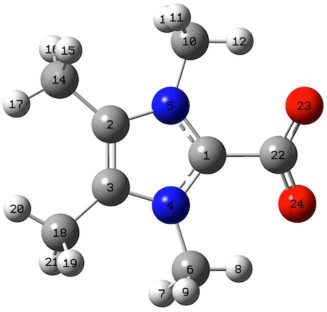

```
                     Standard orientation:
 ---------------------------------------------------------------------
 Center     Atomic      Atomic             Coordinates (Angstroms)
 Number     Number       Type             X           Y           Z
 ---------------------------------------------------------------------
    1          6           0        0.677192    0.000005   -0.000015
    2          6           0       -1.457628    0.681696   -0.025385
    3          6           0       -1.457621   -0.681711    0.025364
    4          7           0       -0.128147   -1.077709    0.031443
    5          7           0       -0.128160    1.077713   -0.031421
    6          6           0        0.311904   -2.467069    0.109545
    7          1           0       -0.222132   -3.055197   -0.638153
    8          1           0        1.381562   -2.479987   -0.098396
    9          1           0        0.104673   -2.865382    1.105399
   10          6           0        0.311868    2.467083   -0.109467
   11          1           0       -0.222180    3.055181    0.638246
   12          1           0        1.381525    2.480015    0.098477
   13          1           0        0.104635    2.865424   -1.105310
   14          6           0       -2.580325    1.653894   -0.072139
   15          1           0       -2.588319    2.307529    0.806053
   16          1           0       -2.525001    2.291857   -0.959649
   17          1           0       -3.534550    1.127199   -0.101947
   18          6           0       -2.580307   -1.653922    0.072112
   19          1           0       -2.524985   -2.291877    0.959627
   20          1           0       -3.534538   -1.127237    0.101904
   21          1           0       -2.588284   -2.307564   -0.806075
   22          6           0        2.242432    0.000009   -0.000026
   23          8           0        2.734789    1.015141    0.505480
   24          8           0        2.734792   -1.015128   -0.505513
 Sum of electronic and zero-point Energies=           -571.856644
 Sum of electronic and thermal Energies=              -571.843770
 Sum of electronic and thermal Enthalpies=            -571.842825
 Sum of electronic and thermal Free Energies=         -571.895622
```

NHC-CO_2 (65)

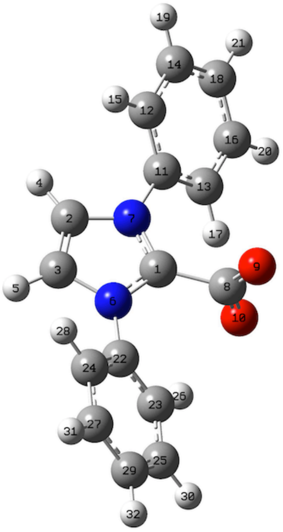

Standard orientation:

```
 ---------------------------------------------------------------------
 Center     Atomic      Atomic             Coordinates (Angstroms)
 Number     Number       Type             X           Y           Z
 ---------------------------------------------------------------------
      1          6           0        0.000125   -0.000704   -0.015415
      2          6           0        0.674705    2.030329   -0.662573
      3          6           0       -0.675323    2.030000   -0.662638
      4          1           0        1.381941    2.791173   -0.944646
      5          1           0       -1.382847    2.790610   -0.944664
      6          7           0       -1.081709    0.763849   -0.262769
      7          7           0        1.081575    0.764294   -0.262719
      8          6           0        0.000526   -1.467438    0.499092
      9          8           0        0.002013   -1.541363    1.724745
     10          8           0       -0.000789   -2.289102   -0.428966
     11          6           0        2.449081    0.361911   -0.124211
     12          6           0        3.335357    1.218166    0.523157
     13          6           0        2.871986   -0.854811   -0.649064
     14          6           0        4.672065    0.854891    0.633226
     15          1           0        2.978656    2.145756    0.957714
     16          6           0        4.209974   -1.210146   -0.519021
     17          1           0        2.158668   -1.515750   -1.129126
     18          6           0        5.110929   -0.358874    0.112791
     19          1           0        5.366208    1.515280    1.141523
     20          1           0        4.545835   -2.160880   -0.918189
     21          1           0        6.153201   -0.644052    0.207381
     22          6           0       -2.449176    0.361474   -0.124120
     23          6           0       -2.872619   -0.854706   -0.649758
     24          6           0       -3.335005    1.217480    0.524228
     25          6           0       -4.210730   -1.209612   -0.519631
     26          1           0       -2.159596   -1.515603   -1.130280
```

27	6	0	-4.671813	0.854624	0.634421
28	1	0	-2.977812	2.144589	0.959433
29	6	0	-5.111246	-0.358559	0.113074
30	1	0	-4.546987	-2.159938	-0.919456
31	1	0	-5.365546	1.514870	1.143457
32	1	0	-6.153585	-0.643482	0.207674

Sum of electronic and zero-point Energies= -876.633248
Sum of electronic and thermal Energies= -876.617453
Sum of electronic and thermal Enthalpies= -876.616508
Sum of electronic and thermal Free Energies= -876.678200

NHC-CO$_2$ (66)

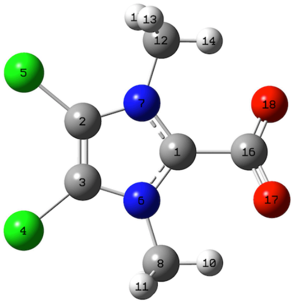

Standard orientation:

Center Number	Atomic Number	Atomic Type	Coordinates (Angstroms) X	Y	Z
1	6	0	1.102478	-0.000019	-0.000041
2	6	0	-1.016120	0.679926	0.018460
3	6	0	-1.016134	-0.679853	-0.018463
4	17	0	-2.328798	-1.754874	-0.068390
5	17	0	-2.328731	1.754948	0.068388
6	7	0	0.301878	-1.085436	-0.021900
7	7	0	0.301973	1.085457	0.021746
8	6	0	0.735029	-2.482365	-0.077692
9	1	0	0.492148	-2.897518	-1.057115
10	1	0	1.809352	-2.486961	0.101416
11	1	0	0.216891	-3.043018	0.700475
12	6	0	0.735195	2.482338	0.077815
13	1	0	0.494400	2.896683	1.058113
14	1	0	1.809216	2.487086	-0.103240
15	1	0	0.215411	3.043619	-0.698771
16	6	0	2.681478	-0.000042	-0.000035
17	8	0	3.161308	-1.016020	0.506893
18	8	0	3.161450	1.015870	-0.506895

Sum of electronic and zero-point Energies= -1412.453052
Sum of electronic and thermal Energies= -1412.440925
Sum of electronic and thermal Enthalpies= -1412.439980

Sum of electronic and thermal Free Energies= -1412.492496

NHC-CO$_2$ (67)

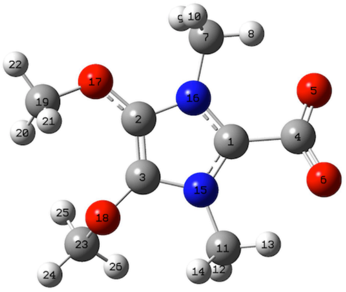

Standard orientation:

Center	Atomic	Atomic	Coordinates (Angstroms)		
Number	Number	Type	X	Y	Z
1	6	0	-1.216595	-0.005373	-0.011044
2	6	0	0.873239	0.797404	-0.125284
3	6	0	0.945772	-0.565405	-0.200613
4	6	0	-2.784472	-0.089188	0.068015
5	8	0	-3.321751	1.003479	0.207099
6	8	0	-3.212895	-1.233577	-0.028500
7	6	0	-0.965193	2.496238	0.159242
8	1	0	-1.807421	2.448259	0.848735
9	1	0	-0.168767	3.116070	0.575440
10	1	0	-1.257014	2.891782	-0.815960
11	6	0	-0.716471	-2.463100	-0.221297
12	1	0	-0.498922	-2.953265	0.731177
13	1	0	-1.782836	-2.501005	-0.445581
14	1	0	-0.123655	-2.927751	-1.009991
15	7	0	-0.357806	-1.041897	-0.143151
16	7	0	-0.470063	1.123428	0.002520
17	8	0	1.834016	1.743183	-0.111136
18	8	0	1.999826	-1.391189	-0.362942
19	6	0	3.181472	1.245235	-0.254638
20	1	0	3.394826	0.481151	0.498276
21	1	0	3.334374	0.829499	-1.255883
22	1	0	3.835481	2.105093	-0.107792
23	6	0	2.876076	-1.491538	0.780198
24	1	0	3.722161	-2.098514	0.456980
25	1	0	3.223647	-0.501391	1.089034
26	1	0	2.366663	-1.981450	1.616338

Sum of electronic and zero-point Energies= -722.236877
Sum of electronic and thermal Energies= -722.221397
Sum of electronic and thermal Enthalpies= -722.220453
Sum of electronic and thermal Free Energies= -722.280741

NHC-CO_2 (68)

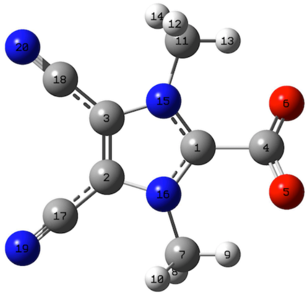

```
                 Standard orientation:
 ---------------------------------------------------------------------
 Center     Atomic      Atomic             Coordinates (Angstroms)
 Number     Number       Type             X           Y           Z
 ---------------------------------------------------------------------
      1          6           0        0.975885   -0.000142   -0.000159
      2          6           0       -1.141821   -0.686868   -0.025291
      3          6           0       -1.141738    0.686883    0.025276
      4          6           0        2.557140   -0.000074    0.000162
      5          8           0        3.023834   -0.950460    0.626789
      6          8           0        3.024351    0.950273   -0.625853
      7          6           0        0.627852   -2.478931   -0.089739
      8          1           0        0.601708   -2.823385   -1.124814
      9          1           0        1.645823   -2.501264    0.298105
     10          1           0       -0.040117   -3.085554    0.520968
     11          6           0        0.628057    2.478830    0.088638
     12          1           0        0.600601    2.824220    1.123335
     13          1           0        1.646315    2.500941   -0.298356
     14          1           0       -0.039224    3.084897   -0.523419
     15          7           0        0.178454    1.084567    0.028838
     16          7           0        0.178263   -1.084746   -0.029168
     17          6           0       -2.229225   -1.582077   -0.067331
     18          6           0       -2.228916    1.582314    0.067890
     19          7           0       -3.113176   -2.325250   -0.101313
     20          7           0       -3.112682    2.325720    0.101647
 Sum of electronic and zero-point Energies=           -677.730349
 Sum of electronic and thermal Energies=              -677.716812
 Sum of electronic and thermal Enthalpies=            -677.715868
 Sum of electronic and thermal Free Energies=         -677.771257
```

NHC-CO$_2$ (69)

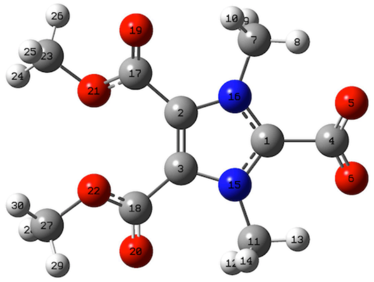

Standard orientation:

Center Number	Atomic Number	Atomic Type	Coordinates (Angstroms) X	Y	Z
1	6	0	1.914478	-0.000090	0.000051
2	6	0	-0.202129	0.685131	0.029683
3	6	0	-0.202331	-0.684685	-0.029823
4	6	0	3.485408	-0.000333	0.000086
5	8	0	3.962671	0.812352	0.795329
6	8	0	3.962358	-0.813199	-0.795189
7	6	0	1.610134	2.465666	0.087114
8	1	0	2.645216	2.424903	0.423449
9	1	0	1.547437	2.887860	-0.917768
10	1	0	0.995687	3.044108	0.771498
11	6	0	1.609349	-2.465766	-0.087043
12	1	0	0.995136	-3.043890	-0.771917
13	1	0	2.644625	-2.425325	-0.422820
14	1	0	1.545887	-2.888108	0.917730
15	7	0	1.118620	-1.082946	-0.066364
16	7	0	1.118941	1.083004	0.066369
17	6	0	-1.327872	1.649417	0.038782
18	6	0	-1.328209	-1.648859	-0.039162
19	8	0	-1.329680	2.678680	0.666308
20	8	0	-1.330481	-2.677359	-0.667932
21	8	0	-2.318689	1.241748	-0.755542
22	8	0	-2.318358	-1.242162	0.756449
23	6	0	-3.482700	2.083229	-0.772288
24	1	0	-4.177565	1.601316	-1.456451
25	1	0	-3.910908	2.156557	0.228676
26	1	0	-3.222862	3.081248	-1.128076
27	6	0	-3.482411	-2.083596	0.772994
28	1	0	-3.910384	-2.157042	-0.228055
29	1	0	-3.222665	-3.081581	1.128964
30	1	0	-4.177403	-1.601618	1.456982

Sum of electronic and zero-point Energies= -948.926178

Sum of electronic and thermal Energies= -948.907184

Sum of electronic and thermal Enthalpies= -948.906240
Sum of electronic and thermal Free Energies= -948.975091

NHC-CO_2 (70)

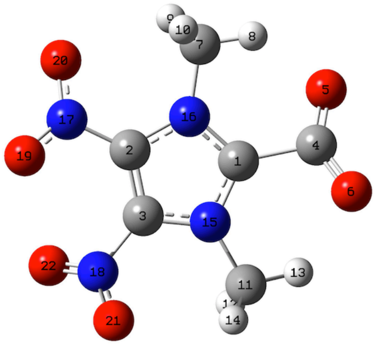

Standard orientation:

Center Number	Atomic Number	Atomic Type	X	Y	Z
1	6	0	-1.365798	-0.029549	0.011306
2	6	0	0.706614	0.747788	-0.028056
3	6	0	0.763868	-0.611819	0.030471
4	6	0	-2.949628	-0.133701	0.008605
5	8	0	-3.481879	0.748906	0.676511
6	8	0	-3.341613	-1.084647	-0.666296
7	6	0	-1.200794	2.451486	-0.108946
8	1	0	-2.273768	2.337357	0.032959
9	1	0	-0.772461	3.061442	0.681708
10	1	0	-0.963289	2.886326	-1.079338
11	6	0	-0.902366	-2.498263	0.133763
12	1	0	-0.743774	-2.849228	1.154547
13	1	0	-1.955212	-2.548058	-0.140990
14	1	0	-0.297021	-3.070433	-0.567068
15	7	0	-0.512674	-1.083472	0.043443
16	7	0	-0.630107	1.094838	-0.031500
17	7	0	1.819934	1.654674	-0.126999
18	7	0	1.914756	-1.508972	0.107670
19	8	0	2.900290	1.139905	-0.344363
20	8	0	1.597900	2.842149	0.016322
21	8	0	2.068895	-2.250787	-0.840164
22	8	0	2.575256	-1.454591	1.118869

Sum of electronic and zero-point Energies= -902.209026
Sum of electronic and thermal Energies= -902.193981
Sum of electronic and thermal Enthalpies= -902.193037
Sum of electronic and thermal Free Energies= -902.253625

NHC-CO$_2$ (71)

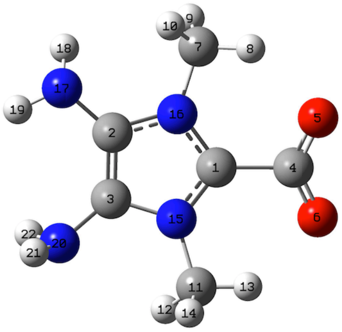

Standard orientation:

Center	Atomic	Atomic	Coordinates (Angstroms)		
Number	Number	Type	X	Y	Z
1	6	0	0.663464	-0.017828	0.004017
2	6	0	-1.455567	0.692980	-0.033184
3	6	0	-1.481418	-0.673465	0.021715
4	6	0	2.227770	-0.020085	-0.011212
5	8	0	2.725637	1.007180	0.466683
6	8	0	2.714934	-1.044583	-0.499848
7	6	0	0.303755	2.470303	-0.071695
8	1	0	1.358012	2.481303	0.206002
9	1	0	0.176311	2.876340	-1.079115
10	1	0	-0.293814	3.043725	0.639041
11	6	0	0.273364	-2.477886	0.128826
12	1	0	-0.441821	-3.082047	-0.426843
13	1	0	1.278509	-2.542920	-0.284427
14	1	0	0.276599	-2.796624	1.173629
15	7	0	-0.144336	-1.081897	0.041683
16	7	0	-0.134459	1.079465	-0.031168
17	7	0	-2.484773	1.617964	0.003823
18	1	0	-2.429303	2.345416	-0.697747
19	1	0	-3.397647	1.184731	-0.000986
20	7	0	-2.529969	-1.588455	0.039741
21	1	0	-3.055911	-1.652659	0.900091
22	1	0	-3.128944	-1.591687	-0.773685

Sum of electronic and zero-point Energies= -603.940956
Sum of electronic and thermal Energies= -603.928057
Sum of electronic and thermal Enthalpies= -603.927113
Sum of electronic and thermal Free Energies= -603.980130

NHC-CO$_2$ (72)

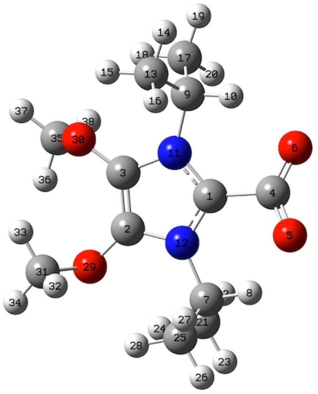

Standard orientation:

```
 ---------------------------------------------------------------------
 Center     Atomic      Atomic             Coordinates (Angstroms)
 Number     Number       Type             X           Y           Z
 ---------------------------------------------------------------------
    1          6           0       -0.000192   -1.072017   -0.000081
    2          6           0       -0.680935    1.046664   -0.032695
    3          6           0        0.681062    1.046496    0.032716
    4          6           0       -0.000408   -2.637832   -0.000167
    5          8           0       -0.962367   -3.128483    0.602351
    6          8           0        0.961434   -3.128676   -0.602722
    7          6           0       -2.484864   -0.754805   -0.229917
    8          1           0       -2.382816   -1.839703   -0.189293
    9          6           0        2.484525   -0.755492    0.230013
   10          1           0        2.382183   -1.840351    0.189076
   11          7           0        1.087678   -0.277438    0.059919
   12          7           0       -1.087860   -0.277157   -0.060050
   13          6           0        3.031169   -0.326324    1.586779
   14          1           0        4.021438   -0.767530    1.727121
   15          1           0        3.126861    0.759376    1.663750
   16          1           0        2.390004   -0.683328    2.396689
   17          6           0        3.354356   -0.326326   -0.945001
   18          1           0        3.528836    0.751855   -0.959017
   19          1           0        4.325662   -0.820711   -0.862874
   20          1           0        2.904003   -0.637893   -1.890102
   21          6           0       -3.031771   -0.325162   -1.586440
   22          1           0       -2.390791   -0.681962   -2.396588
   23          1           0       -4.022089   -0.766273   -1.726718
   24          1           0       -3.127387    0.760565   -1.663045
   25          6           0       -3.354227   -0.325741    0.945466
   26          1           0       -4.325774   -0.819664    0.863346
   27          1           0       -2.903769   -0.637879    1.890324
   28          1           0       -3.528259    0.752509    0.959956
   29          8           0       -1.542760    2.074688   -0.114137
```

30	8	0	1.543062	2.074380	0.114276
31	6	0	-1.586822	2.916660	1.049091
32	1	0	-1.911849	2.344960	1.922839
33	1	0	-0.608550	3.363337	1.244071
34	1	0	-2.312959	3.697653	0.826616
35	6	0	1.588483	2.915536	-1.049482
36	1	0	0.610634	3.362734	-1.245399
37	1	0	2.314980	3.696207	-0.827038
38	1	0	1.913719	2.343061	-1.922640

Sum of electronic and zero-point Energies= -879.396406
Sum of electronic and thermal Energies= -879.375716
Sum of electronic and thermal Enthalpies= -879.374771
Sum of electronic and thermal Free Energies= -879.445566

NHC-CO_2 (73)

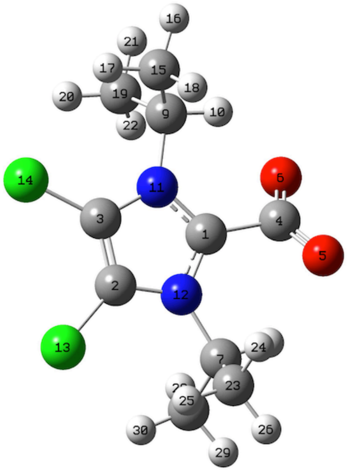

Standard orientation:

Center Number	Atomic Number	Atomic Type	Coordinates (Angstroms)		
			X	Y	Z
1	6	0	-0.000038	0.998954	0.000038
2	6	0	-0.680500	-1.107640	0.010125
3	6	0	0.680615	-1.107604	-0.010191
4	6	0	-0.000120	2.570047	-0.000107
5	8	0	-0.813780	3.049772	-0.794307
6	8	0	0.813373	3.050160	0.794000
7	6	0	-2.490362	0.733603	0.039267
8	1	0	-2.341818	1.812606	-0.006343
9	6	0	2.490359	0.733780	-0.038793
10	1	0	2.341756	1.812751	0.007390
11	7	0	1.093598	0.210762	-0.009372
12	7	0	-1.093576	0.210671	0.009388
13	17	0	-1.701657	-2.468905	0.048531

14	17	0	1.701902	-2.468743	-0.048968
15	6	0	3.183965	0.370088	-1.346303
16	1	0	4.140909	0.896190	-1.388866
17	1	0	3.386440	-0.699048	-1.435702
18	1	0	2.590486	0.689625	-2.206344
19	6	0	3.251762	0.328608	1.217325
20	1	0	3.447435	-0.744059	1.269932
21	1	0	4.214543	0.845697	1.219163
22	1	0	2.706439	0.640548	2.110405
23	6	0	-3.251990	0.329089	-1.216934
24	1	0	-2.706744	0.641303	-2.109967
25	1	0	-3.447856	-0.743517	-1.269894
26	1	0	-4.214651	0.846410	-1.218410
27	6	0	-3.183808	0.369185	1.346654
28	1	0	-2.590129	0.687898	2.206862
29	1	0	-4.140646	0.895441	1.389830
30	1	0	-3.386533	-0.699973	1.435228

Sum of electronic and zero-point Energies= -1569.609270
Sum of electronic and thermal Energies= -1569.591713
Sum of electronic and thermal Enthalpies= -1569.590769
Sum of electronic and thermal Free Energies= -1569.654880

NHC-CO$_2$ (74)

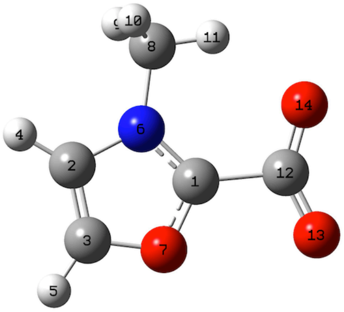

Standard orientation:

Center Number	Atomic Number	Atomic Type	Coordinates (Angstroms) X	Y	Z
1	6	0	-0.091135	-0.276299	-0.026622
2	6	0	2.095626	0.053362	0.018449
3	6	0	1.856391	-1.264190	-0.081270
4	1	0	3.015745	0.610771	0.071924
5	1	0	2.481831	-2.137534	-0.145449
6	7	0	0.846353	0.662988	0.045834
7	8	0	0.508291	-1.455148	-0.103705
8	6	0	0.618748	2.105538	0.147922
9	1	0	0.906719	2.443629	1.144656
10	1	0	1.222505	2.608583	-0.608150

11	1	0	-0.445003	2.270255	-0.029063
12	6	0	-1.672991	-0.147703	-0.014340
13	8	0	-2.215744	-1.194913	0.301671
14	8	0	-2.035810	0.992452	-0.325415

Sum of electronic and zero-point Energies= -473.821808
Sum of electronic and thermal Energies= -473.813701
Sum of electronic and thermal Enthalpies= -473.812757
Sum of electronic and thermal Free Energies= -473.855781

NHC-CO_2 (75)

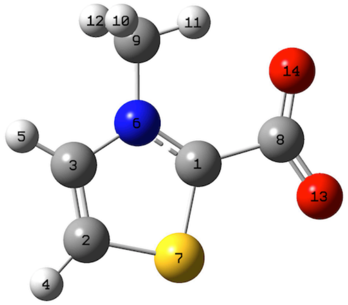

Standard orientation:

Center Number	Atomic Number	Atomic Type	Coordinates (Angstroms) X	Y	Z
1	6	0	-0.182974	-0.085410	0.000433
2	6	0	2.226495	-0.540097	-0.000233
3	6	0	1.929758	0.778345	-0.000108
4	1	0	3.209115	-0.986861	-0.000345
5	1	0	2.612625	1.616168	-0.000503
6	7	0	0.566718	1.015198	-0.000127
7	16	0	0.782856	-1.488017	0.000050
8	6	0	-1.750824	-0.270957	0.000003
9	6	0	0.016290	2.378797	0.000313
10	1	0	0.364903	2.897933	-0.893698
11	1	0	-1.071164	2.285750	-0.000083
12	1	0	0.364559	2.897025	0.894962
13	8	0	-2.023282	-1.472501	0.000139
14	8	0	-2.402370	0.775976	-0.000476

Sum of electronic and zero-point Energies= -796.806707
Sum of electronic and thermal Energies= -796.798369
Sum of electronic and thermal Enthalpies= -796.797425
Sum of electronic and thermal Free Energies= -796.840502

NHC-CO$_2$ (76)

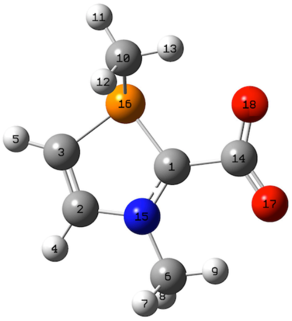

Standard orientation:

Center	Atomic	Atomic	Coordinates (Angstroms)		
Number	Number	Type	X	Y	Z
1	6	0	-0.317487	-0.086691	-0.098397
2	6	0	0.237033	2.144543	0.062488
3	6	0	1.498510	1.680165	-0.052532
4	1	0	-0.089687	3.173845	0.140077
5	1	0	2.369213	2.320096	-0.087356
6	6	0	-2.175445	1.529624	0.152014
7	1	0	-2.297983	2.182476	1.018001
8	1	0	-2.469884	2.060893	-0.755602
9	1	0	-2.748028	0.607886	0.265329
10	6	0	2.346358	-1.124677	0.704142
11	1	0	3.402381	-1.116306	0.430930
12	1	0	2.216180	-0.796664	1.734776
13	1	0	1.928172	-2.122933	0.564227
14	6	0	-1.107349	-1.427728	-0.069854
15	7	0	-0.759795	1.153615	0.048093
16	15	0	1.419116	-0.055067	-0.466620
17	8	0	-2.309464	-1.360535	0.206946
18	8	0	-0.336568	-2.370716	-0.311310

Sum of electronic and zero-point Energies= -779.837514
Sum of electronic and thermal Energies= -779.826924
Sum of electronic and thermal Enthalpies= -779.825980
Sum of electronic and thermal Free Energies= -779.874270

NHC-CO_2 (77)

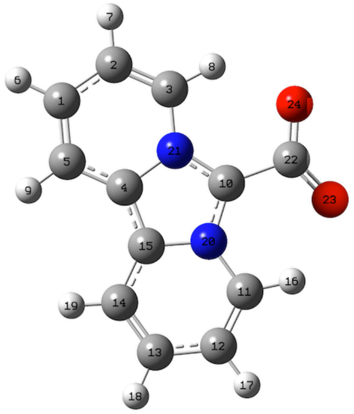

```
                      Standard orientation:
 ---------------------------------------------------------------------
 Center     Atomic      Atomic             Coordinates (Angstroms)
 Number     Number       Type             X           Y           Z
 ---------------------------------------------------------------------
   1          6           0        2.999726   -1.844643    0.000018
   2          6           0        3.358392   -0.469895    0.000018
   3          6           0        2.418399    0.511148    0.000016
   4          6           0        0.698640   -1.194617    0.000010
   5          6           0        1.679056   -2.201482    0.000014
   6          1           0        3.772372   -2.604142    0.000020
   7          1           0        4.401230   -0.177243    0.000017
   8          1           0        2.575798    1.584068    0.000012
   9          1           0        1.368888   -3.239403    0.000012
  10          6           0        0.000019    0.974058    0.000020
  11          6           0       -2.418400    0.511273    0.000011
  12          6           0       -3.358441   -0.469728   -0.000004
  13          6           0       -2.999845   -1.844492   -0.000017
  14          6           0       -1.679194   -2.201394   -0.000013
  15          6           0       -0.698727   -1.194577    0.000004
  16          1           0       -2.575747    1.584199    0.000025
  17          1           0       -4.401265   -0.177025   -0.000004
  18          1           0       -3.772528   -2.603954   -0.000029
  19          1           0       -1.369076   -3.239331   -0.000021
  20          7           0       -1.082379    0.148760    0.000013
  21          7           0        1.082363    0.148698    0.000015
  22          6           0        0.000099    2.518196    0.000029
  23          8           0       -1.135197    3.014295   -0.000128
  24          8           0        1.135459    3.014148    0.000020
 Sum of electronic and zero-point Energies=           -721.861039
 Sum of electronic and thermal Energies=              -721.849659
 Sum of electronic and thermal Enthalpies=            -721.848714
 Sum of electronic and thermal Free Energies=         -721.898693
```

NHC-CO$_2$ (78)

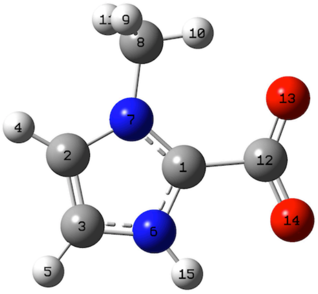

Standard orientation:

Center Number	Atomic Number	Atomic Type	Coordinates (Angstroms) X	Y	Z
1	6	0	0.107031	-0.225400	0.000015
2	6	0	-2.101464	0.002428	0.000041
3	6	0	-1.827606	-1.330053	-0.000218
4	1	0	-3.043723	0.525380	0.000139
5	1	0	-2.484374	-2.183462	-0.000190
6	7	0	-0.460617	-1.433495	0.000064
7	7	0	-0.890909	0.669373	0.000107
8	6	0	-0.718810	2.120779	0.000030
9	1	0	-1.184145	2.539765	0.893657
10	1	0	0.355308	2.313193	-0.000038
11	1	0	-1.184441	2.539743	-0.893415
12	6	0	1.661190	-0.084349	0.000070
13	8	0	2.081205	1.075320	-0.000237
14	8	0	2.185179	-1.205313	0.000136
15	1	0	0.148939	-2.246251	-0.000175

Sum of electronic and zero-point Energies= -453.981786
Sum of electronic and thermal Energies= -453.973874
Sum of electronic and thermal Enthalpies= -453.972930
Sum of electronic and thermal Free Energies= -454.014588

NHC-CO$_2$ (79)

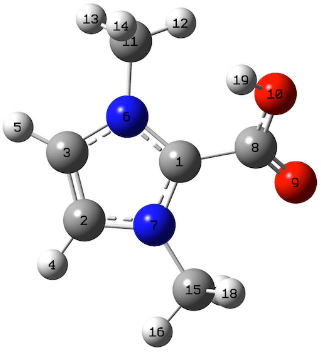

Standard orientation:

Center Number	Atomic Number	Atomic Type	Coordinates (Angstroms) X	Y	Z
1	6	0	0.047737	-0.011414	0.032800
2	6	0	-2.132112	-0.339169	0.064753
3	6	0	-1.913553	1.001185	-0.039020
4	1	0	-3.053880	-0.895664	0.116537
5	1	0	-2.608478	1.822293	-0.110454
6	7	0	-0.555698	1.190377	-0.057952
7	7	0	-0.909172	-0.952386	0.098195
8	6	0	1.510999	-0.332423	-0.058306
9	8	0	1.868607	-1.281179	-0.687319
10	8	0	2.360366	0.490474	0.560118
11	6	0	0.091024	2.499812	-0.206988
12	1	0	1.039828	2.389641	-0.728936
13	1	0	-0.562252	3.136787	-0.800938
14	1	0	0.243802	2.958747	0.772018
15	6	0	-0.703528	-2.406755	0.161708
16	1	0	-1.652968	-2.863568	0.433504
17	1	0	-0.368693	-2.769511	-0.808960
18	1	0	0.044426	-2.643123	0.916464
19	1	0	1.937122	1.056677	1.216998

Sum of electronic and zero-point Energies= -493.634533
Sum of electronic and thermal Energies= -493.624584
Sum of electronic and thermal Enthalpies= -493.623640
Sum of electronic and thermal Free Energies= -493.669962

NHC-CO$_2$ (80)

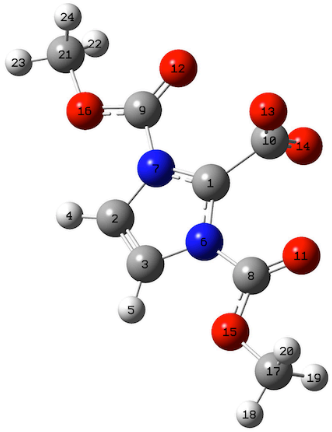

Standard orientation:

Center Number	Atomic Number	Atomic Type	Coordinates (Angstroms) X	Y	Z
1	6	0	-0.000055	0.309746	0.000066

```
   2        6         0      0.669988   -1.855265    0.000731
   3        6         0     -0.670220   -1.855222    0.000908
   4        1         0      1.382048   -2.660584    0.001083
   5        1         0     -1.382364   -2.660467    0.001192
   6        7         0     -1.076578   -0.514248    0.000478
   7        7         0      1.076436   -0.514328    0.000193
   8        6         0     -2.432610   -0.058870    0.000251
   9        6         0      2.432472   -0.059032   -0.000242
  10        6         0      0.000238    1.880825    0.000008
  11        8         0     -2.748636    1.086224    0.001057
  12        8         0      2.748580    1.086042   -0.000546
  13        8         0     -0.000392    2.323495   -1.142942
  14        8         0      0.001074    2.322878    1.143253
  15        8         0     -3.234634   -1.121961   -0.000858
  16        8         0      3.234482   -1.122158   -0.000248
  17        6         0     -4.640826   -0.811854   -0.001001
  18        1         0     -5.146297   -1.774714    0.000052
  19        1         0     -4.896840   -0.237674    0.889978
  20        1         0     -4.896996   -0.239638   -0.893212
  21        6         0      4.640670   -0.812060   -0.000621
  22        1         0      4.897224   -0.239934    0.891536
  23        1         0      5.146142   -1.774922   -0.002002
  24        1         0      4.896335   -0.237789   -0.891644
 Sum of electronic and zero-point Energies=           -870.326563
 Sum of electronic and thermal Energies=              -870.311358
 Sum of electronic and thermal Enthalpies=            -870.310414
 Sum of electronic and thermal Free Energies=         -870.370929
```

NHC-CO$_2$ (81)

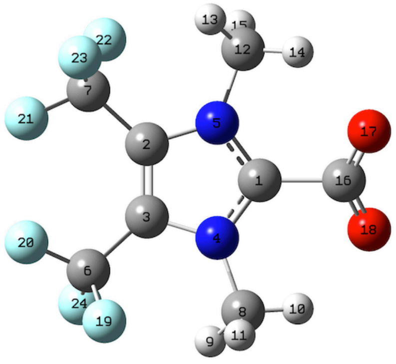

```
                         Standard orientation:
 ---------------------------------------------------------------------
 Center     Atomic      Atomic             Coordinates (Angstroms)
 Number     Number       Type             X           Y           Z
 ---------------------------------------------------------------------
      1          6           0        1.683155    0.000300    0.000327
      2          6           0       -0.433386    0.683689   -0.014143
```

3	6	0	-0.433180	-0.683425	0.013917
4	7	0	0.888286	-1.083975	-0.010788
5	7	0	0.888135	1.084420	0.011108
6	6	0	-1.563188	-1.672611	0.096357
7	6	0	-1.563936	1.672342	-0.096567
8	6	0	1.394747	-2.462636	-0.072426
9	1	0	0.767084	-3.043804	-0.745203
10	1	0	2.410199	-2.398909	-0.462540
11	1	0	1.385438	-2.904834	0.923164
12	6	0	1.394929	2.463010	0.073580
13	1	0	0.768472	3.043489	0.748082
14	1	0	2.410989	2.398551	0.461988
15	1	0	1.384019	2.906411	-0.921446
16	6	0	3.257003	0.000281	-0.000295
17	8	0	3.728948	0.805019	0.803732
18	8	0	3.727882	-0.804570	-0.804863
19	9	0	-1.220814	-2.709575	0.880263
20	9	0	-2.661261	-1.128675	0.617415
21	9	0	-2.659663	1.129578	-0.623853
22	9	0	-1.219907	2.712881	-0.874822
23	9	0	-1.879348	2.165235	1.112689
24	9	0	-1.873746	-2.170922	-1.111886

Sum of electronic and zero-point Energies=	-1167.304340
Sum of electronic and thermal Energies=	-1167.287755
Sum of electronic and thermal Enthalpies=	-1167.286811
Sum of electronic and thermal Free Energies=	-1167.349951

NHC-CO_2 (82)

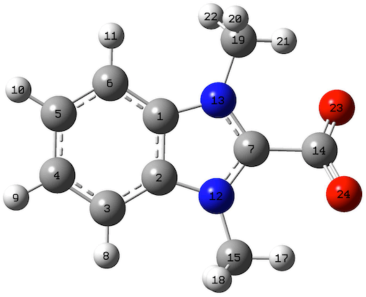

Standard orientation:

Center	Atomic	Atomic	Coordinates (Angstroms)		
Number	Number	Type	X	Y	Z
1	6	0	1.011268	0.698464	-0.038962
2	6	0	1.011183	-0.698522	0.038843
3	6	0	2.196228	-1.425192	0.086864
4	6	0	3.379711	-0.699977	0.043115
5	6	0	3.379764	0.699909	-0.043211

6	6	0	2.196291	1.425145	-0.086935
7	6	0	-1.106271	0.000101	0.000021
8	1	0	2.199586	-2.506537	0.154582
9	1	0	4.326008	-1.228285	0.075636
10	1	0	4.326103	1.228137	-0.075732
11	1	0	2.199550	2.506490	-0.154643
12	7	0	-0.318572	-1.091449	0.049288
13	7	0	-0.318478	1.091530	-0.049327
14	6	0	-2.670530	-0.000007	-0.000053
15	6	0	-0.770922	-2.475050	0.124730
16	1	0	-0.585195	-2.871191	1.125606
17	1	0	-1.834568	-2.487847	-0.109166
18	1	0	-0.224892	-3.065230	-0.613379
19	6	0	-0.770795	2.475198	-0.124128
20	1	0	-0.584835	2.871891	-1.124743
21	1	0	-1.834498	2.487925	0.109470
22	1	0	-0.224886	3.064958	0.614406
23	8	0	-3.152685	0.928831	0.655099
24	8	0	-3.152139	-0.928994	-0.655532

Sum of electronic and zero-point Energies=	-646.871597
Sum of electronic and thermal Energies=	-646.859438
Sum of electronic and thermal Enthalpies=	-646.858494
Sum of electronic and thermal Free Energies=	-646.910035

NHC-CO$_2$ (83)

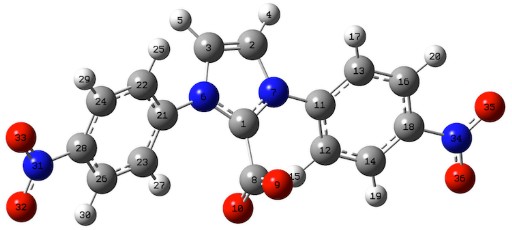

Standard orientation:

Center Number	Atomic Number	Atomic Type	Coordinates (Angstroms) X	Y	Z
1	6	0	0.000002	0.202892	-0.097177
2	6	0	0.674370	2.226139	-0.779277
3	6	0	-0.674148	2.226216	-0.779302
4	1	0	1.379258	2.982462	-1.079284
5	1	0	-1.378984	2.982519	-1.079481
6	7	0	-1.081179	0.964681	-0.357867
7	7	0	1.081270	0.964580	-0.357785
8	6	0	-0.000271	-1.248817	0.461326
9	8	0	-0.001282	-1.277584	1.687269
10	8	0	0.000339	-2.095744	-0.442419

11	6	0	2.443486	0.562198	-0.205353
12	6	0	2.854188	-0.687138	-0.663284
13	6	0	3.338134	1.450326	0.388962
14	6	0	4.186779	-1.048837	-0.525207
15	1	0	2.137131	-1.370159	-1.105449
16	6	0	4.671316	1.093348	0.515303
17	1	0	2.992143	2.402639	0.774101
18	6	0	5.073333	-0.152105	0.053195
19	1	0	4.542975	-2.012293	-0.866437
20	1	0	5.393932	1.754010	0.976397
21	6	0	-2.443410	0.562311	-0.205476
22	6	0	-3.338080	1.450452	0.388787
23	6	0	-2.854055	-0.687061	-0.663322
24	6	0	-4.671243	1.093442	0.515157
25	1	0	-2.992103	2.402799	0.773852
26	6	0	-4.186641	-1.048802	-0.525206
27	1	0	-2.137003	-1.370113	-1.105469
28	6	0	-5.073216	-0.152058	0.053123
29	1	0	-5.393873	1.754106	0.976224
30	1	0	-4.542817	-2.012286	-0.866378
31	7	0	-6.493688	-0.533018	0.184731
32	8	0	-6.820528	-1.629313	-0.229646
33	8	0	-7.245128	0.277746	0.696649
34	7	0	6.493816	-0.533017	0.184786
35	8	0	7.245188	0.277682	0.696897
36	8	0	6.820730	-1.629200	-0.229828

Sum of electronic and zero-point Energies= -1285.620911
Sum of electronic and thermal Energies= -1285.599931
Sum of electronic and thermal Enthalpies= -1285.598987
Sum of electronic and thermal Free Energies= -1285.674247

NHC-CO$_2$ (84)

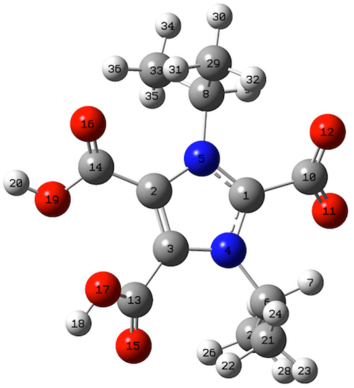

Standard orientation:

\---

Center	Atomic	Atomic	Coordinates (Angstroms)		
Number	Number	Type	X	Y	Z

```
---------------------------------------------------------------------
  1     6     0     0.220017  -1.219067   0.035951
  2     6     0    -0.782058   0.752339   0.019295
  3     6     0     0.572991   0.967478  -0.031875
  4     7     0     1.178443  -0.285943  -0.013676
  5     7     0    -0.981868  -0.606638   0.055857
  6     6     0     2.624452  -0.670981  -0.066157
  7     1     0     2.573817  -1.758227  -0.127187
  8     6     0    -2.264041  -1.370017   0.112521
  9     1     0    -1.941429  -2.376814   0.378586
 10     6     0     0.426635  -2.763302   0.058265
 11     8     0     1.052388  -3.150780   1.048204
 12     8     0    -0.083513  -3.315108  -0.921468
 13     6     0     1.260496   2.265669  -0.112984
 14     6     0    -1.888439   1.757308   0.022027
 15     8     0     2.413449   2.483473   0.158464
 16     8     0    -2.704942   1.863299  -0.851809
 17     8     0     0.418117   3.223553  -0.545395
 18     1     0     0.903188   4.060395  -0.518337
 19     8     0    -1.865316   2.506521   1.130879
 20     1     0    -2.574829   3.161789   1.051256
 21     6     0     3.300589  -0.148995  -1.327322
 22     1     0     3.453252   0.929925  -1.303482
 23     1     0     4.281769  -0.623439  -1.409213
 24     1     0     2.728438  -0.418422  -2.218908
 25     6     0     3.331996  -0.326797   1.237537
 26     1     0     3.406380   0.749496   1.390470
 27     1     0     2.814334  -0.791800   2.079049
 28     1     0     4.342890  -0.741348   1.200183
 29     6     0    -2.908020  -1.432442  -1.266753
 30     1     0    -3.802707  -2.057896  -1.208472
 31     1     0    -3.198977  -0.442251  -1.621905
 32     1     0    -2.219141  -1.895595  -1.975271
 33     6     0    -3.178805  -0.848111   1.212988
 34     1     0    -3.986046  -1.570367   1.355368
 35     1     0    -2.648431  -0.749201   2.163152
 36     1     0    -3.644888   0.105656   0.957486
 Sum of electronic and zero-point Energies=         -1027.524113
 Sum of electronic and thermal Energies=            -1027.504332
 Sum of electronic and thermal Enthalpies=          -1027.503388
 Sum of electronic and thermal Free Energies=       -1027.571369
```

G. Transition State Calculations (gas phase) of selected NHC–CO_2

The following computational data is presented on NHC-CO_2 **61, 63, 66, 67, 68, 74, 75, 77, 81**. Transition state optimization data is supplied for the gas phase only and the NHC-CO_2 is identified in bold above the respective structure.

Table 6.3 Free energy activation barriers for selected NHC–CO_2.

NHC–CO_2	**Bond Length (Å)**	**$\Delta G^{\ddagger}$ (kcal/mol)**
61	1.570	6.02
63	1.564	6.42
66	1.598	3.35
67	1.579	6.00
68	1.604	1.47
74	1.613	1.05
75	1.585	2.62
77	1.553	7.86
81	1.592	2.42

NHC-CO_2 (61)

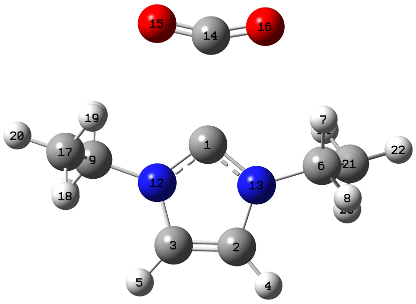

Standard orientation:

```
 ---------------------------------------------------------------------
 Center     Atomic      Atomic             Coordinates (Angstroms)
 Number     Number       Type             X           Y           Z
```

1	6	0	0.000006	0.004323	0.000074
2	6	0	0.652663	2.181515	-0.185763
3	6	0	-0.653141	2.181415	0.185523
4	1	0	1.332036	2.997992	-0.376354
5	1	0	-1.332701	2.997774	0.375975
6	6	0	2.381827	0.392006	-0.625913
7	1	0	2.281210	-0.581452	-1.105392
8	1	0	2.800687	1.095350	-1.353212
9	6	0	-2.381864	0.391533	0.626028
10	1	0	-2.800769	1.094615	1.353559
11	1	0	-2.280953	-0.582012	1.105264
12	7	0	-1.026645	0.847332	0.298278
13	7	0	1.026484	0.847495	-0.298293
14	6	0	0.000294	-2.315588	-0.000078
15	8	0	-1.136955	-2.548504	0.241306
16	8	0	1.137613	-2.548147	-0.241491
17	6	0	-3.276696	0.281980	-0.607627
18	1	0	-3.366502	1.242233	-1.125803
19	1	0	-2.866968	-0.453993	-1.303977
20	1	0	-4.279682	-0.044018	-0.314939
21	6	0	3.276451	0.282399	0.607896
22	1	0	4.279554	-0.043335	0.315332
23	1	0	3.365944	1.242574	1.126272
24	1	0	2.866755	-0.453803	1.304024

Sum of electronic and zero-point Energies= -571.835846
Sum of electronic and thermal Energies= -571.823150
Sum of electronic and thermal Enthalpies= -571.822206
Sum of electronic and thermal Free Energies= -571.877446

NHC-CO$_2$ (63)

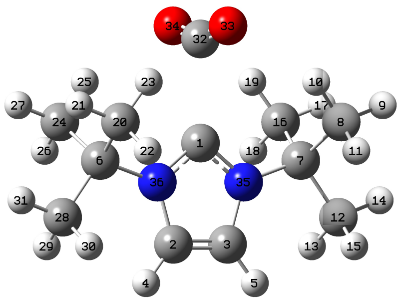

Standard orientation:

Center Atomic Atomic Coordinates (Angstroms)

```
 Number     Number      Type             X              Y              Z
 ---------------------------------------------------------------------
   1          6           0        -0.000013      0.053302     -0.000024
   2          6           0        -0.676696     -2.113944     -0.000653
   3          6           0         0.676819     -2.113931     -0.000769
   4          1           0        -1.359160     -2.945098     -0.000783
   5          1           0         1.359344     -2.945049     -0.001241
   6          6           0        -2.507838     -0.318476      0.000081
   7          6           0         2.507791     -0.318459      0.000194
   8          6           0         2.761448      0.505986      1.274440
   9          1           0         3.795779      0.864114      1.280657
  10          1           0         2.095163      1.365630      1.344383
  11          1           0         2.609184     -0.112409      2.164967
  12          6           0         3.447529     -1.534364      0.000346
  13          1           0         3.315890     -2.155547     -0.890843
  14          1           0         4.479028     -1.173201      0.000455
  15          1           0         3.315711     -2.155538      0.891502
  16          6           0         2.762421      0.506666     -1.273444
  17          1           0         3.796772      0.864882     -1.278843
  18          1           0         2.610811     -0.111243     -2.164384
  19          1           0         2.096222      1.366373     -1.343496
  20          6           0        -2.761900      0.506092      1.274127
  21          1           0        -3.796357      0.863946      1.280165
  22          1           0        -2.609637     -0.112080      2.164776
  23          1           0        -2.095963      1.366014      1.344117
  24          6           0        -2.762098      0.506504     -1.273741
  25          1           0        -2.095860      1.366215     -1.343561
  26          1           0        -2.610113     -0.111504     -2.164572
  27          1           0        -3.796461      0.864635     -1.279538
  28          6           0        -3.447477     -1.534413      0.000165
  29          1           0        -3.316096     -2.155435     -0.891171
  30          1           0        -3.315474     -2.155731      0.891211
  31          1           0        -4.478948     -1.173209      0.000552
  32          6           0         0.000038      2.267741     -0.000222
  33          8           0        -0.000530      2.553792      1.157799
  34          8           0         0.000516      2.553467     -1.158343
  35          7           0         1.079096     -0.782130     -0.000337
  36          7           0        -1.079078     -0.782164     -0.000092
 Sum of electronic and zero-point Energies=           -728.983709
 Sum of electronic and thermal Energies=              -728.966498
 Sum of electronic and thermal Enthalpies=            -728.965554
 Sum of electronic and thermal Free Energies=         -729.027680
```

NHC-CO_2 (66)

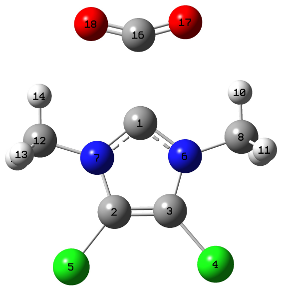

```
                    Standard orientation:
 ---------------------------------------------------------------------
 Center     Atomic      Atomic             Coordinates (Angstroms)
 Number     Number       Type             X           Y           Z
 ---------------------------------------------------------------------
    1          6           0        1.040490    0.000711    0.000080
    2          6           0       -1.119117   -0.681025    0.000098
    3          6           0       -1.119579    0.680796    0.000182
    4         17           0       -2.444554    1.771070   -0.000251
    5         17           0       -2.443504   -1.772048   -0.000049
    6          7           0        0.209742    1.078243    0.000089
    7          7           0        0.210546   -1.077507   -0.000052
    8          6           0        0.657348    2.471810    0.000626
    9          1           0        0.281938    2.982678    0.890518
   10          1           0        1.744801    2.463060    0.001075
   11          1           0        0.283031    2.983094   -0.889505
   12          6           0        0.658410   -2.470959    0.000144
   13          1           0        0.284536   -2.981769   -0.890435
   14          1           0        1.745844   -2.462172    0.001400
   15          1           0        0.282476   -2.982146    0.889615
   16          6           0        3.188650    0.000119   -0.000186
   17          8           0        3.481405    1.157147   -0.000566
   18          8           0        3.480488   -1.157145    0.000129
 Sum of electronic and zero-point Energies=          -1412.446633
 Sum of electronic and thermal Energies=             -1412.434386
 Sum of electronic and thermal Enthalpies=           -1412.433442
 Sum of electronic and thermal Free Energies=        -1412.487164
```

NHC-CO_2 (67)

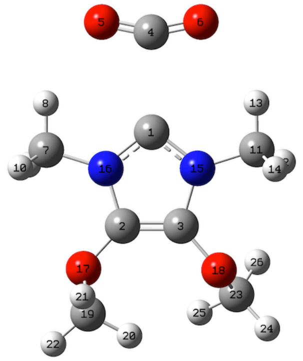

Standard orientation:

Center Number	Atomic Number	Atomic Type	Coordinates (Angstroms) X	Y	Z
1	6	0	1.081444	-0.015178	-0.008563
2	6	0	-1.078889	-0.744020	0.071582
3	6	0	-1.112425	0.606782	-0.116029
4	6	0	3.360114	0.036311	0.000645
5	8	0	3.638817	-1.100572	0.202419
6	8	0	3.587342	1.185182	-0.199002
7	6	0	0.727601	-2.465146	0.348286
8	1	0	1.815111	-2.447723	0.332544
9	1	0	0.372896	-2.843220	1.310803
10	1	0	0.349990	-3.118202	-0.442952
11	6	0	0.623513	2.405885	-0.403620
12	1	0	0.299735	3.047178	0.421952
13	1	0	1.708957	2.423847	-0.474085
14	1	0	0.177286	2.776466	-1.329913
15	7	0	0.219083	1.024010	-0.170598
16	7	0	0.263071	-1.097830	0.138091
17	8	0	-2.049491	-1.675145	0.218754
18	8	0	-2.157303	1.457176	-0.286367
19	6	0	-3.081271	-1.644566	-0.781211
20	1	0	-3.617101	-0.690984	-0.767438
21	1	0	-2.658049	-1.805082	-1.778871
22	1	0	-3.764264	-2.458077	-0.533497
23	6	0	-2.760605	1.916006	0.937442
24	1	0	-3.564117	2.594218	0.645690
25	1	0	-3.172397	1.076243	1.507294
26	1	0	-2.034933	2.452499	1.558399

Sum of electronic and zero-point Energies= -722.225380
Sum of electronic and thermal Energies= -722.209422
Sum of electronic and thermal Enthalpies= -722.208478
Sum of electronic and thermal Free Energies= -722.271175

NHC-CO_2 (68)

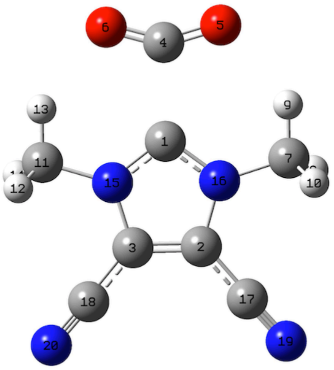

Standard orientation:

Center Number	Atomic Number	Atomic Type	Coordinates (Angstroms) X	Y	Z
1	6	0	-0.925439	-0.000013	-0.000423
2	6	0	1.229926	-0.688785	-0.000014
3	6	0	1.229918	0.688786	-0.000014
4	6	0	-2.929197	-0.000004	0.000221
5	8	0	-3.265872	-1.153146	0.000276
6	8	0	-3.265854	1.153142	0.000416
7	6	0	-0.540583	-2.481501	-0.000338
8	1	0	-0.155895	-2.981217	0.891266
9	1	0	-1.628221	-2.482034	-0.001151
10	1	0	-0.154398	-2.981561	-0.891089
11	6	0	-0.540611	2.481481	-0.000339
12	1	0	-0.154646	2.981480	-0.891224
13	1	0	-1.628248	2.482003	-0.000906
14	1	0	-0.155713	2.981264	0.891132
15	7	0	-0.103148	1.078362	-0.000257
16	7	0	-0.103134	-1.078378	-0.000270
17	6	0	2.315060	-1.596347	0.000166
18	6	0	2.315040	1.596362	0.000137
19	7	0	3.189327	-2.364127	0.000299
20	7	0	3.189276	2.364176	0.000237

Sum of electronic and zero-point Energies= -677.727097
Sum of electronic and thermal Energies= -677.713658
Sum of electronic and thermal Enthalpies= -677.712714
Sum of electronic and thermal Free Energies= -677.768916

NHC-CO$_2$ (74)

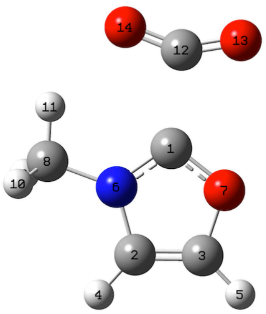

```
                    Standard orientation:
 ---------------------------------------------------------------------
 Center     Atomic      Atomic             Coordinates (Angstroms)
 Number     Number       Type             X           Y           Z
 ---------------------------------------------------------------------
      1          6           0        0.025031   -0.280467   -0.000642
      2          6           0        2.252459    0.072081    0.000481
      3          6           0        2.030452   -1.254100    0.000491
      4          1           0        3.165432    0.645485    0.001247
      5          1           0        2.670092   -2.120836    0.000620
      6          7           0        0.981330    0.658834   -0.000254
      7          8           0        0.669985   -1.461528   -0.000326
      8          6           0        0.711066    2.096976   -0.000533
      9          1           0        1.145030    2.555300    0.891642
     10          1           0        1.146089    2.555272   -0.892180
     11          1           0       -0.369981    2.227918   -0.000792
     12          6           0       -2.070213   -0.134905    0.000147
     13          8           0       -2.432245   -1.266206   -0.000317
     14          8           0       -2.277583    1.043673    0.000840
 Sum of electronic and zero-point Energies=           -473.819995
 Sum of electronic and thermal Energies=              -473.811968
 Sum of electronic and thermal Enthalpies=            -473.811024
 Sum of electronic and thermal Free Energies=         -473.854107
```

NHC-CO$_2$ (75)

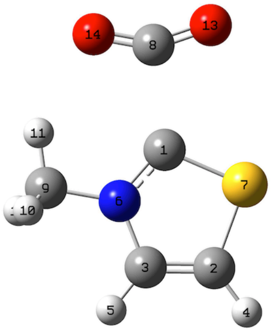

Standard orientation:

Center Number	Atomic Number	Atomic Type	Coordinates (Angstroms) X	Y	Z
1	6	0	-0.101882	-0.073914	-0.000009
2	6	0	2.355813	-0.630745	-0.000193
3	6	0	2.102620	0.696814	-0.000058
4	1	0	3.322202	-1.113246	-0.000286
5	1	0	2.813688	1.512335	-0.000016
6	7	0	0.733092	0.973727	0.000060
7	16	0	0.848780	-1.510894	-0.000205
8	6	0	-2.181876	-0.217502	0.000107
9	6	0	0.228876	2.357290	0.000237
10	1	0	0.586746	2.877307	-0.891993
11	1	0	-0.859001	2.313625	0.000281
12	1	0	0.586824	2.877112	0.892550
13	8	0	-2.361334	-1.397256	-0.000045
14	8	0	-2.586652	0.909685	0.000272

Sum of electronic and zero-point Energies= -796.801489
Sum of electronic and thermal Energies= -796.793015
Sum of electronic and thermal Enthalpies= -796.792071
Sum of electronic and thermal Free Energies= -796.836319

NHC-CO$_2$ (77)

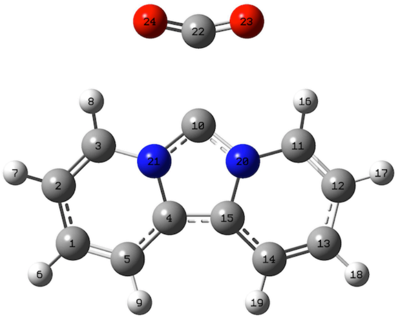

Standard orientation:

Center Number	Atomic Number	Atomic Type	Coordinates (Angstroms) X	Y	Z
1	6	0	-3.021323	-1.946788	-0.000014
2	6	0	-3.363859	-0.556599	-0.000014
3	6	0	-2.401827	0.404151	-0.000008
4	6	0	-0.696611	-1.335184	-0.000002
5	6	0	-1.704840	-2.326380	-0.000008
6	1	0	-3.807653	-2.693354	-0.000019
7	1	0	-4.403967	-0.251241	-0.000019
8	1	0	-2.573646	1.472237	-0.000009

9	1	0	-1.415862	-3.372113	-0.000009
10	6	0	0.000087	0.889300	0.000005
11	6	0	2.401885	0.403575	0.000016
12	6	0	3.363686	-0.557406	0.000018
13	6	0	3.020816	-1.947512	0.000013
14	6	0	1.704242	-2.326789	0.000005
15	6	0	0.696252	-1.335351	0.000003
16	1	0	2.573960	1.471618	0.000019
17	1	0	4.403867	-0.252297	0.000024
18	1	0	3.806967	-2.694266	0.000015
19	1	0	1.415013	-3.372453	0.000002
20	7	0	1.064955	0.031151	0.000008
21	7	0	-1.064987	0.031406	-0.000002
22	6	0	0.000446	3.141916	-0.000004
23	8	0	1.162323	3.388074	-0.000013
24	8	0	-1.161346	3.388473	0.000001

Sum of electronic and zero-point Energies= -721.846893
Sum of electronic and thermal Energies= -721.835128
Sum of electronic and thermal Enthalpies= -721.834183
Sum of electronic and thermal Free Energies= -721.886175

NHC-CO$_2$ (81)

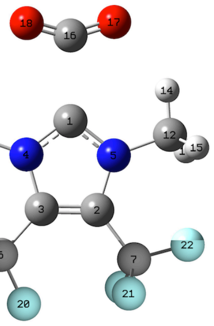

Standard orientation:

Center Number	Atomic Number	Atomic Type	Coordinates (Angstroms)		
			X	Y	Z
1	6	0	-1.634735	0.000000	0.000006
2	6	0	0.527943	-0.684791	-0.015305
3	6	0	0.527938	0.684802	0.015309
4	7	0	-0.807345	1.073888	0.001650
5	7	0	-0.807337	-1.073884	-0.001641
6	6	0	1.625971	1.710424	0.046250
7	6	0	1.625990	-1.710402	-0.046250
8	6	0	-1.295297	2.462130	-0.016253
9	1	0	-0.752875	3.025983	-0.775992
10	1	0	-2.355769	2.423988	-0.252634

11	1	0	-1.140807	2.926673	0.958396
12	6	0	-1.295270	-2.462131	0.016256
13	1	0	-0.752850	-3.025975	0.776005
14	1	0	-2.355745	-2.424003	0.252621
15	1	0	-1.140757	-2.926672	-0.958390
16	6	0	-3.726959	-0.000017	0.000001
17	8	0	-4.037453	-1.102908	0.344677
18	8	0	-4.037467	1.102866	-0.344690
19	9	0	1.349920	2.661954	0.967902
20	9	0	2.818265	1.192661	0.355577
21	9	0	2.818279	-1.192650	-0.355623
22	9	0	1.349929	-2.661966	-0.967859
23	9	0	1.735577	-2.337106	1.146617
24	9	0	1.735525	2.337132	-1.146622

Sum of electronic and zero-point Energies= -1167.299367
Sum of electronic and thermal Energies= -1167.282657
Sum of electronic and thermal Enthalpies= -1167.281713
Sum of electronic and thermal Free Energies= -1167.346096

REFERENCES

Chapter 1.

(1) Meyers, A. I.; Temple Jr., D. L. *J. Am. Chem. Soc.*, **1970**, *92*, 6644–6646.

(2) Meyers, A. I.; Temple Jr., D. L. *J. Am. Chem. Soc.*, **1970**, *92*, 6646–6647.

(3) Wuts, P. G. M.; Greene, T. W. *Greene's Protective Groups in Organic Synthesis*; 4th ed.; John Wiley & Sons, Inc.: Hoboken, NJ, 2007.

(4) Schelhaas, M.; Waldmann, H. *Angew. Chem. Int. Ed. Engl.*, **1996**, *35*, 2056–2083.

(5) Hayward, C. M.; Yohannes, D.; Danishefski, S. J. *J. Am. Chem. Soc.*, **1993**, *115*, 9345–9346.

(6) Ellison, R. A.; Lukenbach, E. R.; Chiu, C. W. *Tetrahedron Lett.*, **1975**, 499–502.

(7) Wong, C-H.; Ye, X-S.; Zhang, Z. *J. Am. Chem. Soc.*, **1998**, *120*, 7137.

(8) Bochet, C. G. *Angew. Chem. Int. Ed.*, **2001**, *40*, 2071–2073.

(9) Klán, P.; Šolomek, T.; Bochet, C. G.; Blanc, A.; Givens, R.; Rubina, M.; Popik, V.; Kostikov, A.; Wirz, J. *Chem. Rev.*, **2013**, *113*, 119–191.

(10) Reiser, A. *Photoreactive Polymers: The Science and Technology of Resists*; John Wiley & Sons, Inc.: New York, 1989; 226–251.

(11) Bochet, C. G. *J. Chem. Soc., Perkin Trans. 1*, **2002**, 125–142.

(12) Pelliccioli, A. P.; Wirz, J. *Photochem. Photobiol. Sci.,* **2002**, *1*, 441–458.

(13) Barltrop, J. A.; Schofield, P. *Tetrahedron Lett.*, **1962**, 697–699.

(14) Barltrop, J. A.; Plant, P. J.; Schofield, P. *Chem. Commun.*, **1966**, 822–823.

(15) Kaplan. J. H.; Forbush III, B.; Hoffman, J. F. *Biochemistry*, **1978**, *17*, 1929–1935.

(16) Walker, J. W.; Reid, G. P.; McCray, J. A.; Trentham, D. R. *J. Am. Chem. Soc.*, **1988**, *110*, 7170–7177.

(17) Barth, A.; Hauser, K.; Maentele, W.; Corrie, J. E. T.; Trentham, D. R. *J. Am. Chem. Soc.*, **1995**, *117*, 10311–10316.

(18) Il'ichev, Y. V.; Schwoerer, M. A.; Wirz, J. *J. Am. Chem. Soc.*, **2004**, *126*, 4581–4595.

(19) Klan, P.; Wirz, J. *Photochemistry of organic compounds: From concepts to practice*; Wiley: Chichester, U.K., 2009.

(20) Warren, J. A.; Bernstein, E. R. *J. Chem. Phys.*, **1986**, *85*, 2365–2367.

(21) Park, S. T.; Feenstra, J. S.; Zewail, A. H. *J. Chem. Phys.*, **2006**, *124*, 174707–174723.

(22) Silva, C. R.; Reilly, J. P. *J. Phys. Chem.*, **1996**, *100*, 17111–17123.

(23) Itoh, T.; Baba, H.; Takemura, T. *Bull. Chem. Soc. Jpn.*, **1978**, *51*, 2841–2846.

(24) Fang, W. H.; Phillips, D. L. *ChemPhysChem,* **2002**, *3*, 889–892.

(25) Sheehan, J. C.; Umezawa, K. *J. Org. Chem.*, **1973**, *38*, 3771–3774.

(26) Anderson, J. C.; Reese, C. B. *Tetrahedron Lett.*, **1962**, 1–4.

(27) Givens, R. S.; Athey, P. S.; Matuszewski, B.; Kueper, L.W.; Xue, J.; Fisher, T. *J. Am. Chem. Soc.*, **1993**, *115*, 6001–6012.

(28) Givens, R. S.; Heger, D.; Hellrung, B.; Kamdzhilov, Y.; Mac, M.; Conrad, P. G.; Cope, E.; Lee, J. I.; Mata-Segreda, J. F.; Schowen, R. L.; Wirz, J. *J. Am. Chem. Soc.*, **2008**, *130*, 3307–3309.

(29) Stensrud, K. F.; Heger, D.; Sebej, P.; Wirz, J.; Givens, R. S. Photochem. Photobiol. Sci. **2008**, *7*, 614–624.

(30) Balachandran Kammath, V.; Šolomek, T.; Ngoy, B. P.; Heger, D.; Klan, P.; Rubina, M.; Givens, R. S. *J. Org. Chem*., **2013**, *78*, 1718–1729.

(31) Givens, R. S.; Matuszewski, B. *J. Am. Chem. Soc*., **1984**, *106*, 6860–6863.

(32) Zimmerman, H. E.; Sandel, V. R. *J. Am. Chem. Soc*., **1963**, *85*, 915–922.

(33) Zimmerman, H. E. *J. Am. Chem. Soc*., **1995**, *117*, 8988–8991.

(34) Schade, B.; Hagen, V.; Schmidt, R.; Herbrich, R.; Krause, E.; Eckardt, T.; Bendig, J. *J. Org. Chem*., **1999***, 64*, 9109–9117.

(35) Rossi, F. M.; Kao, J. P. Y. *J. Biol. Chem*., **1997**, *272*, 3266–3271.

(36) Rossi, F. M.; Margulis, M.; Tang, C. M.; Kao, J. P. Y. *J. Biol. Chem*. **1997**, *272*, 32933–32929.

(37) Skwarczynski, M.; Noguchi, M.; Hirota, S.; Sohma, Y.; Kimura, T.; Hayashi, Y.; Kiso, Y. *Bioorg. Med. Chem. Lett*., **2006**, *16*, 4492–4496.

(38) Goswami, P. P.; Syed, A. S.; Beck, C. L.; Albright, T. R.; Mahoney, K. M.; Unash, R.; Smith, E. A.; Winter, A. H. *J. Am. Chem. Soc,*. **2015**, *137*, 3783–3786.

(39) Šebej, P.; Wintner, J.; Müeller, P.; Slanina, T.; Anshori, J. A.; Antony, L. A. P.; Klán, P.; Wirz, J. *J. Org. Chem*., **2013**, *78*, 1833–1843.

(40) Gorka, A. P.; Nani, R. R.; Zhu, J.; Mackem, S.; Schnermann, M. J. *J. Am. Chem. Soc*., **2014**, *136*, 14153–14159.

Chapter 2.

(1) de Wit, C. A. *Chemosphere,* **2002**, *46*, 583–624.

(2) Haeggblom, M. M.; Bossert, I. D. *Dehalogenation,* **2003**, 3–29.

(3) Alaee, M.; Arias, P.; Sjodin, A.; Bergman, A. *Environ. Int.,* **2003**, *29*, 683–689.

(4) Monroe, B. M.; Weed, G. C. *Chem. Rev*., **1993**, *93*, 435–448.

(5) Gannon, T.; McGimpsey, W. G. *J. Org. Chem*., 1993, **58**, 913–916.

(6) Barra, M.; Redmond, R. W.; Allen, M. T.; Calabrese, G. S.; Sinta, R.; Scaiano, J. C. *Macromolecules,* **1991**, *24*, 4972–4977.

(7) Scaiano, J. C.; Barra, M.; Calabrese, G. S.; Sinta, R. *J. Chem. Soc., Chem. Commun.*, **1992**, 1418–1419.

(8) McCloskey, C. M.; Bond, J. *Ind. Eng. Chem.*, **1955**, 47, 2125–2128.

(9) Galli, C.; Gentili, P.; Guarnieri, A.; Kobayashi, S.; Rappoport, Z. *J. Org. Chem.*, **1998**, *63*, 9292–9299.

(10) Wagner, P. J.; Sedon, J.; Waite, C.; Gudmunsdottir, A. *J. Am. Chem. Soc.*, **1994**, *116*, 10284–10285.

(11) Wender, P. A.; Jeon, R. *Org. Lett.*, **1999**, *1*, 2117–2120.

(12) van Dorp, J. W. J.; Lodder, G. *J. Org. Chem.*, **2008**, *73*, 5416–5428.

(13) Krijnen, E. S.; Zuilhof, H.; Lodder, G. *J. Org. Chem.*, **1994**, *59*, 8139–8150.

(14) Moorthy, J. N.; Samanta, S. *J. Org. Chem.,* **2007**, *72*, 9786–9789.

(15) Kasafirek, E. *Tetrahedron Lett.*, **1972**, *20*, 2021–2024.

(16) Semmelhack, M. F; Heinsohn, G. E. *J. Am. Chem. Soc.*, **1972**, *94*, 5139–5140.

(17) Engels, J. *Angew. Chem.*, **1979**, *91*, 155–156.

(18) Engels, J. *Liebigs Ann. Chem.*, **1980**, *4*, 557–563.

(19) Kropp, P. J.; Poindexter, G. S.; Pienta, N. J.; Hamimlton, D. C. *J. Am. Chem. Soc.*, **1976**, *98*, 8135–8144.

(20) Kropp, P. J.; Pienta, G. S. *J. Org. Chem.*, **1983**, *48*, 2084–2090.

(21) Moret, E.; Jones, C. R.; Grant, B. *J. Org. Chem.*, **1983**, *48*, 2090–2092.

(22) Kropp, P. J. *Acc. Chem. Res.*, **1984**, *17*, 131–137.

(23) Kropp, P. J.; Adkins, R. L. *J. Am. Chem. Soc.*, **1991**, *113*, 2709–2717.

(24) Huang, H-Y.; Chuang, W-T.; Sharma, R. C.; Hsu, C-Y.; Lin, C-H. *J. Chem. Phys.*, **2004**, *121*, 5253–5260.

(25) Kwok, W. M.; Zhao, C.; Li, Y-L.; Guan, X.; Phillips, D. L. *J. Chem. Phys.*, **2004**, *120*, 3323–3332.

(26) Kwok, W. M.; Zhao, C.; Li, Y-L.; Guan, X.; Wang, D.; Phillip, D. L. *J. Am. Chem. Soc.*, **2004**, *126*, 3119–3131.

(27) Carrier, S. L.; Preston, T. J.; Dutta, M.; Crowther, A. C.; Crim, F. F. *J. Phys. Chem. A*. **2010**, *114*, 1548–1555.

(28) Kalume, A.; George, L.; Reid, S. A. *J. Phys. Chem. Lett*., **2010**, *1*, 3090-3095.

(29) George, L.; Kalume, A.; Esselman, B. J.; Wagner, J.; McMahon, R. J.; Reid, S. A. *J. Chem. Phys*., **2011**, *135*, 1245031–1245038.

(30) Perrotta, R, R.; Winter, A. H.; Falvey, D. E. *Org. Lett*., **2011**, *13*, 212–215.

(31) Dawson, W. R.; Windsor, M. W. *J. Phys. Chem*., **1968**, *72*, 3251–3260.

(32) Tanner, D. D.; Chen, J. J.; Chen, L.; Luelo, C. *J. Am. Chem. Soc*., **1991**, *113*, 8074–8081.

(33) Sundararajan, C.; Falvey, D. E. *Photochem. Photobiol. Sci*., **2006**, *5*, 116–121.

(34) Borak, J. B.; Falvey, D. E. *J. Org. Chem*., **2009**, *74*, 3894–3899.

(35) Luo, Y-R. *Tabulated BDE's of C-H Bonds: Handbook of Bond Dissociation Energies in Organic Compounds*; CRC Press: Boca Raton, FL, 2003; pp 57, 76.

(36) Fleming, I. *Frontier Orbitals and Organic Chemical Reactions*; John Wiley & Sons: Chichester, U.K.; 1985; pp 182–188.

(37) Russell, G. A. *Free Radicals*; Kochi, J. K., Ed.; Wiley: New York, 1973; Vol. 1; pp 293–298.

(38) Ringshaw, D. J.; Smith, H. J. *J. Chem. Soc*., **1964**, 1559–1562.

Chapter 3.

(1) Givens, R. S.; Rubina, M.; Wirz, J. *Photochem. Photobiol. Sci*., **2012**, *11*, 472–488.

(2) Hagen, V.; Kilic, F.; Schaal, J.; Dekowski, B.; Schmidt, R.; Kotzur, N. *J. Org. Chem*., **2010**, *75*, 2790–2797.

(3) Suzuki, A. Z.; Watanabe, T.; Kawamoto, M.; Nishiyama, K.; Yamashita, H.; Ishii, M.; Iwamura, M.; Furuta, T. *Org. Lett*., **2003**, *5*, 4867–4870.

(4) Pirrung, M. C.; Fallon, L.; Zhu, J.; Lee, Y. R. *J. Am. Chem. Soc*., **2001**, *123*, 3638–3643.

(5) Duan, X.-Y.; Zhai, B.-C.; Song, Q.-H. *Photochem. Photobiol. Sci*., **2012**, *11*, 593–598.

(6) Konosonoks, A.; Wright, P. J.; Tsao, M.-L.; Pika, J.; Novak, K.;Mandel, S. M.; Bauer, J. A. K.; Bohne, C.; Gudmundsdottir. *J. Org. Chem*., **2005**, *70*, 2763–2770.

(7) Kulikov, A.; Arumugam, S.; Popik, V. V. *J. Org. Chem*., **2008**, *73*, 7611–7615.

(8) Zhou, L.; Yang, H.; Wang, P. *J. Org. Chem*., **2011**, *76*, 5873–5881.

(9) Yang, H.; Zhou, L.; Wang, P. *Photochem. Photobiol*., Sci. **2012**, *11*, 514–517.

(10) McGrath, N. A.; Brichacek, M.; Njardarson, J. *J. Chem. Educ*., **2010**, *87*, 1348–1349.

(11) Barnett, W. E.; Needham, L. L.; Powell, R. W. *Tetrahedron*, **1972**, *28*, 419–424.

(12) Barnett, W. E.; Needham, L. L. *J. Chem. Soc. D.,* **1971**, 170–171.

(13) Iverson, B. L.; Cameron, K. E.; Jahangiri, G. K.; Pasternak, D. S. *J. Am. Chem. Soc.,* **1990**, *112*, 5320–5323.

(14) Sieber, P.; Riniker, B. *Tetrahedron Lett.* **1987**, *28*, 6031–6034.

(15) Shchepinov, M. S.; Korshun, V. A. *Chem. Soc. Rev.,* **2003**, *32*, 170–180.

(16) van der Stouwe, C.; Schäfer, H. J. *Tetrahedron Lett*., **1979**, *20*, 2643–2646.

(17) Edson, J. B.; Spencer, L. P.; Boncella, J. M. *Org. Lett*., **2011**, *13*, 6156–6159.

(18) Borak, J. B.; Lee, H. Y.; Raghavan, S. R.; Falvey, D. E. *Chem. Commun*., **2010**, *46*, 8983–8985.

(19) Banerjee, A.; Falvey, D. E. *J. Org. Chem*., **1997**, *62*, 6245–6251

(20) Wöll, D.; Walbert, S.; Stengele, K. P.; Albert, T. J.; Richmond, T.; Norton, J.; Singer, M.; Green, R. D.; Pfleiderer, W.; Steiner, U. E. *Helv. Chim. Acta.,* **2004**, *87*, 28–45.

(21) Tu, W.; Floreancig, P. E. *Org. Lett*., **2007**, *9*, 2389–2392.

(22) Jaffe, H. H.; Miller, A. L. *J. Chem. Educ.*, **1966**, *43*, 469–473.

(23) Priestley, E. B.; Haug, A. *J. Chem. Phys*., **1968**, *49*, 622–629.

(24) Banerjee, A.; Lee, K.; Yu, Q.; Fang, A. G.; Falvey, D. E. *Tetrahedron Lett.*, **1998**, *39*, 4635–4638.

(25) Sundararajan, C.; Falvey, D. E. *Photochem. Photobiol. Sci.*, **2006**, *5*, 116–121.

(26) Borak, J. B.; Falvey, D. E. *J. Org. Chem.*, **2009**, *74*, 3894–3899.

(27) Schaap, A. P.; Zaklika, K. A.; Kaskar, B.; Fung, L. W-M. *J. Am. Chem. Soc.,* **1980**, *102*, 389–391.

(28) Lepley, A. R.; Closs, G. L. *Chemically Induced Magnetic Polarization*; John Wiley & Sons, Inc.: New York, 1973.

(29) Marcus, R. A. *J. Chem. Phys.,* **1956**, *24*, 966–978.

(30) Marcus, R. A. *Annu. Rev. Phys. Chem.*, **1964**, *15*, 155–196.

(31) Marcus, R. A. *Pure & Appl. Chem.*, **1997**, *69*, 13–29.

(32) Weller, A. *Pure Appl. Chem.*, **1968**, *16*, 115–123.

(33) Rehm, D.; Weller, A. *Isr. J. Chem.*, **1970**, *8*, 259–271.

(34) Miller, J. R.; Beitz, J. V.; Huddleson, R. K. *J. Am. Chem. Soc.*, **1984**, *106*, 5057–5068.

(35) Smitha, M. A.; Prasad, E.; Gopidas, K. R. *J. Am. Chem. Soc.*, **2001**, *123*, 1159–1165.

(36) Gould, I. R.; Young, R. H.; Moody, R. E.; Farid, S. *J. Phys. Chem.*, **1991**, *95*, 2068–2080.

(37) Arnold, B. R.; Noukakis, D.; Farid, S.; Goodman, J. L.; Gould. I. R. *J. Am. Chem. Soc.*, **1995**, *117*, 4399–4400.

(38) Niwa, T.; Kikuchi, K.; Matsusita, N.; Hayashi, M.; Katagiri, T.; Takahasi, Y.; Miyashi, T. *J. Phys. Chem.*, **1993**, *97*, 11960–11964.

(39) Meites, L.; Zuman, P. *CRC Handbook Series in Organic Electrochemistry*, Vols. I-V; CRC Press, Inc.: Boca Raton, FL, 1977–1982.

(40) Leigh, W. J.; Arnold, D. R. *J. Chem. Soc., Chem. Commun.*, **1980**, 406–408.

(41) Nguyen, J. D.; D'Amato, E. M.; Narayanam, J. M. R.; Stephenson, R. *J. Nat. Chem.*, **2012**, *4*, 854–859.

(42) Prier, C. K.; Rankic, D. A.; MacMillan, D. W. C. *Chem. Rev.*, **2013**, *113*, 5322–5363.

(43) Porter, G.; Topp. M. R. *Proc. R. Soc. London, Ser. A*, **1970**, 315, 173–184.

(44) Das, P. K. *Chem. Rev.*, **1993**, *93*, 119–144.

(45) Beckett, A.; Porter, G. *Trans. Faraday Soc.*, **1963**, *59*, 2038–2050.

(46) Bell, J. A.; Linschitz, H. *J. Am. Chem. Soc.*, **1963**, *85*, 528–533.

(47) Buettner, A. V.; Dedinas, J. *J. Phys. Chem.*, **1971**, *75*, 187–191.

(48) Inbar, S.; Linschitz, H.; Cohen, S. G. *J. Am. Chem. Soc.*, **1981**, *103*, 1048–1054.

(49) Devadoss, C.; Fessenden, R. W. *J. Phys. Chem.*, **1990**, *94*, 4540–4549.

(50) Faria, J. L.; Steenken, S. *J. Am. Chem. Soc.*, **1990**, *112*, 1277–1279.

(51) Bromberg, A.; Schmidt, K. H.; Meisel, D. *J. Am. Chem. Soc.*, **1985**, *107*, 83–91.

(52) Kunsberg, D. J.; Kipping, A. H.; Falvey, D. E. *Org. Lett.*, **2015**, *17*, 3454–3457.

Chapter 4.

(1) Quadrelli, R.; Peterson, S. *Energy Policy,* **2007**, *35*, 5938–5952.

(2) Tans, P. NOAA/ESRL. *www.esrl.noaa.gov/gmd/ccgg/trends/* (accessed January 2016).

(3) Keeling, R. Scripps Institution of Oceanography. *scrippsco2.ucsd.edu/* (accessed January 2016).

(4) Stauffer, P. H.; Keating, G. N.; Middleton, R. S.; Viswanathan, H.S.; Berchtold, K. A.; Singh, R. P.; Pawar, R. J.; Mancino, A. *Environ. Sci. Technol.*, **2011**, *45*, 8597−8604.

(5) Markewitz, P.; Kuckshinrichs, W.; Leitner, W.; Linssen, J.; Zapp, P.; Bongartz, R.; Schreiber, A.; Müller, T. E. *Energy Environ. Sci.*, **2012**, *5*, 7281−7305.

(6) Rochelle, G. T. *Science,* **2009**, *325*, 1652–1654.

(7) da Silva, E. F.; Svendsen, H. F. *Int. J. Greenhouse Gas Control,* **2007**, *1*, 151–157.

(8) Peeters, A. N. M.; Faaij, A. P. C; Turkenburg, W. C. Int. *J. Greenhouse Gas Control,* **2007**, *1*, 396–417.

(9) Sumida, K.; Rogow, D. L.; Mason, J. A.; McDonald, T. M.; Bloch, E. D.; Herm, Z. R.; Bae, T.-H.; Long, J. R. *Chem. Rev.,* **2012**, *112*, 724−728.

(10) Millward, A. R.; Yaghi, O. M. *J. Am. Chem. Soc*., **2005**, *127*, 17998–17999.

(11) An, J.; Rosi, N. L. *J. Am. Chem. Soc.,* **2010**, *132*, 5578–5579.

(12) Ashley, A. E.; Thompson, A. L.; O'Hare, D. *Angew. Chem., Int. Ed*., **2009**, *48*, 9839–9843.

(13) Mömming, C. M.; Otten, E.; Kehr, G.; Fröhlick, R.; Grimme, S.;Stephan, D. W.; Erker, G. *Angew. Chem., Int. Ed.* **2009**, *48*, 6643−6646.

(14) Ménard, G.; Stephan, D. W. *J. Am. Chem. Soc.,* **2010**, *132*, 1796−1797.

(15) Jutz, F.; Andanson, J.-M.; Baiker, A. *Chem. Rev*., **2011**, *111*, 322−353.

(16) Tang, J.; Sun, W.; Tang, H.; Radosz, M.; Shen, Y. *Macromolecules,* **2005**, *38*, 2037–2039.

(17) Muldoon, M. J.; Aki, S. N. V. K.; Anderson, J. L.; Dixon, J. K.; Brennecke, J. F. *J. Phys. Chem. B,* **2007**, *111*, 9001–9009.

(18) Bates, E. D.; Mayton, R. D.; Ntai, I.; Davis, Jr. J. H. *J. Am. Chem. Soc.,* **2002**, *124*, 926–927.

(19) Schuster, G. B. *Adv. Phys. Org. Chem*., **1986**, *22*, 311–315.

(20) Gleiter, R.; Hoffmann, R. *J. Am. Chem. Soc*., **1968**, *90*, 1475–1485.

(21) Bourissou, D.; Guerret, O.; Gabbaï, F. P.; Bertrand, G. *Chem. Rev.,* **2000**, *100*, 39–91.

(22) Sulzbach, H. M.; Bolton, E.; Lenoir, D.; Schleyer, P. v. R.; Schaefer III, H. F. *J. Am. Chem. Soc.,* **1996**, *118*, 9908–9914.

(23) Gano, J. E.; Wettach, R. H.; Platz, M. S.; Senthilnathan, V. P. *J. Am. Chem. Soc.,* **1982**, *104*, 2326–2327.

(24) Moss, R. A.; Platz, M. S.; Jones, Jr., M. *Reactive Intermediate Chemistry*, Wiley and Sons, In.c: Hoboken, New Jersey, **2004**, pp 273–454.

(25) Bernheim, R. A.; Bernard, H. W.; Wang, P. S.; Wood, L. S.; Skell, P. S. *J. Chem. Phys.,* **1970**, *53*, 1280–1281.

(26) Trozzolo, A. M.; Wasserman, E.; Yager, W. A. *J. Am. Chem. Soc.,* **1965**, *87*, 129–130.

(27) Moritani, I.; Murahashi, S-I.; Ashitaka, H.; Kimura, K.; Tsubomura, H. *J. Am. Chem. Soc.,* **1968**, *90*, 5918–5919.

(28) Moritani, I.; Murahashi, S-I.; Nishino, M.; Kimura, K.; Tsubomura, H. *Tetrahedron Lett.,* **1966**, *7*, 373–378.

(29) Arduengo III, A. J.; Harlow, R. L.; Kline, M. *J. Am. Chem. Soc.,* **1991**, *113*, 361–363.

(30) Wanzlick, H. W.; Schönherr, H. J. *Liebigs Ann. Chem*., **1970**, *731*, 176–179.

(31) Schönherr, H. J.; Wanzlick, H. W. *Chem. Ber*., **1970**, *103*, 1037–1046.

(32) Hopkinson, M. N.; Richter, C.; Schedler, M.; Glorius, F. *Nature,* **2014**, *510*, 485–496.

(33) Arduengo III, A. J.; Rasika Dias, H. V.; Harlow, R. L.; Kline, M. *J. Am. Chem. Soc.,* **1992**, *114*, 5530–5534.

(34) Arduengo III, A. J.; Davidson, F.; Dias, H. V. R.; Goerlich, J. R.; Khasnis, D.; Marshall, W. J.; Prakasha, T. K. *J. Am. Chem. Soc.,* **1997**, *119*, 12742–12749.

(35) Amyes, T. L.; Diver, S. T.; Richard, J. P.; Rivas, F. M.; Toth, K. *J. Am. Chem. Soc*., **2004**, *126*, 4366–4374.

(36) Chu, Y.; Deng, H.; Cheng, J.-P. *J. Org. Chem.,* **2007**, *72*, 7790–7793.

(37) Dröge, T.; Glorius, F. *Angew. Chem. Int. Ed.,* **2010**, *49*, 6940–6952.

(38) Benhamou, L.; Chardon, E.; Lavigne, G.; Bellemin-Laponnaz, S.; César, V. *Chem. Rev.,* **2011**, *111*, 2705–2733.

(39) Díez-González, S.; Marion, N.; Nolan, S. P. *Chem. Rev.,* **2009**, *109*, 3612–3676.

(40) Samojlowicz, C.; Bieniek, M.; Grela, K. *Chem. Rev.,* **2009**, *109*, 3708–3742.

(41) Flanigan, D. F.; Romanov-Michailidis, F.; White, N. A.; Rovis, T. *Chem. Rev.,* **2015**, *115*, 9307–9387.

(42) Pesch, J.; Harms, K.; Bach, T. *Eur. J. Org. Chem*., **2004**, 2025−2035.

(43) Enders, D.; Kallfass, U. *Angew. Chem., Int. Ed*., **2002**, *41*, 1743−1745.

(44) Piel, I.; Pawelczyk, M. D.; Hirano, K.; Fröhlich, R.; Glorius, F. *Eur. J. Org. Chem.*, **2011**, 5475−5484.

(45) Kerr, M. S.; Read de Alaniz, J.; Rovis, T. *J. Am. Chem. Soc.*, **2002**, *124*, 10298−10299.

(46) Read de Alaniz, J.; Kerr, M. S.; Moore, J. L.; Rovis, T. *J. Org. Chem.*, **2008**, *73*, 2033−2040.

(47) Kaeobamrung, J.; Mahatthananchai, J.; Zheng, P.; Bode, J. *J. Am. Chem. Soc.*, **2010**, *132*, 8810−8812.

(48) Phillips, E. M.; Riedrich, M.; Scheidt, K. A. *J. Am. Chem. Soc.*, **2010**, *132*, 13179–13181.

(49) Connor, E. F.; Nyce, G. W.; Myers, M.; Möck, A.; Hedrick, J. L. *J. Am. Chem. Soc.*, **2002**, *124*, 914−915.

(50) Lee, K-S.; Zhugralin, A. R.; Hoveyda, A. H. *J. Am. Chem. Soc.*, **2009**, *131*, 7253−7255.

(51) O'Brien, J. M.; Hoveyda, A. M. *J. Am. Chem. Soc.*, **2011**, *133*, 7712−7715.

(52) Kuhn, N.; Niquet, E.; Steimann, M.; Walker, I. *Z. Naturforsch., B* **1999**, *54*, 427–433.

(53) Holbrey, J. D.; Reichert, W. M.; Tkatchenko, I.; Bouajila, E.; Walter, O.; Tommasi, I.; Rogers, R. D. *Chem. Commun.*, **2003**, 28−29.

(54) Kayaki, Y.; Yamamoto, M.; Ikariya, T. *Angew. Chem.*, **2009**, *121*, 4258–4261.

(55) Tommasi, I.; Sorrentino, F. *Tetrahedron Lett.*, **2005**, *46*, 2141–2145.

(56) Tommasi, I.; Sorrentino, F. *Tetrahedron Lett.*, **2009**, *50*, 104–107.

(57) Hans, M.; Delaude, L.; Rodriguez, J.; Coquerel, Y. *J. Org. Chem.,* **2014**, *79*, 2758–2764.

(58) Kayaki, Y.; Yamamoto, M.; Ikariya, T. *Angew. Chem., Int. Ed.*, **2009**, *48*, 4194–4197.

(59) Zhou, H.; Zhang, W.; Liu, C.; Qu, J.; Lu, Z. *J. Org. Chem.*, **2008**, *73*, 8039–8044.

(60) Voutchkova, A. M.; Appelhans, L. H.; Chianese, A. R.; Crabtree, R. H. *J. Am. Chem. Soc.,* **2005**, *127*, 17624–17625.

(61) Voutchkova, A. M.; Feliz, M.; Clot, E.; Eisenstein, O.; Crabtree, R. H. *J. Am. Chem. Soc*., **2007**, *129*, 12834–12846.

(62) Tudose, A.; Demonceau, A.; Delaude, L. *J. Organomet. Chem*., **2006**, *691*, 5356–5365.

(63) Fèvre, M.; Pinaud, J.; Leteneur, A.; Gnanou, Y.; Vignolle, J.; Taton, D. *J. Am. Chem. Soc.,* **2012**, *134*, 6776–6784.

(64) Fevre, M.; Coupillaud, P.; Miqueu, K.; Sotiropoulous, J-M.;Vignolle, J.; Taton, D. *J. Org. Chem*., **2012**, *77*, 10135–10144.

(65) Ajitha, M. J.; Suresh, C. H. *J. Org. Chem*., **2012**, *77*, 1087–1094.

(66) Van Ausdall, B. R.; Glass, J. L.; Wiggins, K. M.; Aarif, A. M.; Louie, J. *J. Org. Chem*., **2009**, *74*, 7935–7942.

(67) Van Ausdall, B. R.; Poth, N. F.; Kincaid, V. A.; Arif, A. M.; Louie, J. *J. Org. Chem*., **2011**, *76*, 8413−8420.

(68) Becke, A. D. *J. Phys. Chem*., **1993**, *98*, 1372–1377.

(69) Lee, C.; Yang, W.; Parr, R. G. *Phys. Rev. B* **1988**, *37*, 785–789.

(70) Marenich, A. V.; Cramer, C. J.; Truhlar, D. G. *J. Phys. Chem. B* **2009**, *113*, 6378-6396.

(71) Klamt, A.; Schüürmann, G. *J. Chem. Soc., Perkin Trans. 2* **1993**, 799–805.

(72) Andzelm, J.; Kölmel, C.; Klamt, A. *J. Chem. Phys*., **1995**, *103*, 9312–9320.

(73) Cancès, E.; Mennucci, B.; Tomasi, J. *J. Chem. Phys*., **1997**, *8*, 3032–3042.

(74) Miertus, S.; Scrocco, E.; Tomasi, *J. Chem. Phys*., **1981**, *55*, 117–129.

(75) Barone, V.; Cammi, R.; Tomasi, *J. Chem. Phys. Lett*., **1996**, *255*, 327–335.

(76) Dimroth, K.; Reichardt, C.; Siepmann, T.; Bohlmann, F. *Liebigs Ann. Chem*., **1963**, *661*, 1–37.

(77) Reichardt, C. *Liebigs Ann. Chem*., **1971**, *752*, 64–67.

Chapter 5.

(1) Aresta, M.; Dibenedetto, A.; Angelini, A. *J. CO_2 Util.,* **2013**, *3-4*, 65–73.

(2) Duraccio, V.; Gnoni, M. G.; Elia, V. *J. CO_2 Util.,* **2015**, *10*, 2329.

(3) Cokoja, M.; Bruckmeier, C.; Rieger, B.; Herrmann, W. A.; Kühn, F. E. *Angew. Chem. Int. Ed.,* **2011**, *50,* 8510−8537.

(4) Sakakura, T.; Choi, J. C.; Yasuda, H. *Chem. Rev*., **2007**, *107*, 2365−2387.

(5) Gibson, D. H. *Chem. Rev*., **1996**, *96*, 2063–2095.

(6) Finn, C.; Schnittger, S.; Yellowlees, L. J.; Love, J. B. *Chem. Commun*., **2012**, *48*, 1392−1399.

(7) Lu, Q.; Rosen, J.; Zhou, Y.; Hutchings, G. S.; Kimmel, Y. C.; Chen, J. G.; Jiao, F. *Nat. Commun.,* **2014**, *5*, 1–6.

(8) Zhang, S.; Kang, P.; Meyer, T. J. *J. Am. Chem. Soc*., **2014**, *136*, 1734−1737.

(9) Benson, E. E.; Kubiak, C. P.; Sathrum, A. J.; Smieja, J. M. *Chem. Soc. Rev*., **2009**, *38*, 89−99.

(10) Tamura, M.; Honda, M.; Nakagawa, Y.; Tomishige, K. *J. Chem. Technol. Biotechnol.,* **2014**, *89*, 19−33.

(11) Saeidi, S.; Amin, N. A. S.; Rahimpour, M. R. *J. CO_2 Util*., **2014**, *5*, 66−81.

(12) Yu, B.; Diao, Z.-F.; Guo, C.-X.; He, L.-N. *J. CO_2 Util*., **2013**, *1*, 60−68.

(13) Tlili, A.; Frogneux, X.; Blondiaux, E.; Cantat, T. *Angew. Chem. Int. Ed*., **2014**, *53*, 2543−2545.

(14) Tlili, A.; Blondiaux, E.; Frogneux, X.; Cantat, T. *Green Chem*., **2015**, *17*, 157−168.

(15) Rahim, M. A.; Matsui, Y.; Matsuyama, T.; Kosugi, Y. *Bull. Chem. Soc. Jpn*., **2003**, *76*, 2191–2195.

(16) Kosugi, Y.; Imaoka, Y.; Gotoh, F.; Rahim, M. A.; Matsui, Y.; Sakanishi, K. *Org. Biomol. Chem.,* **2003**, *1*, 817–821.

(17) Lindsey, A. S.; Jeskey, H. *Chem. Rev.,* **1957**, *57*, 583–620.

(18) Kumar, P.; Chauhan, R. K.; Sain, B.; Jain, S. L. *Dalton Trans*., **2015**, *44*, 4546−4553.

(19) Doherty, M. D.; Grills, D. C.; Muckerman, J.T.; Polyansky, D. E.; Fujita, E. Coord. *Chem. Rev*., **2010**, *254*, 2472−2482.

(20) Morris, A. J.; Meyer, G. J.; Fujita, E. *Acc. Chem. Res.*, **2009**, *42*, 1983−1994.

(21) Fujita, E.; Braunschwig, B. S.; Ogata, T.; Yanagida, S. *Coord. Chem. Rev.*, **1994**, *132*, 195−200.

(22) Ahmed, N.; Morikawa, M.; Izumi, Y. *Catal. Today.,* **2012**, *185*, 263−269.

(23) Kawamura, S.; Puscasu, M. C.; Yoshida, Y.; Izumi, Y.; Carja, G. *Appl. Catal. A.*, **2015**, *504*, 238–247.

(24) Sato, S.; Arai, T.; Morikawa, T. Inorg. Chem. **2015**, *54*, 5105−5113.

(25) Barton, E. E.; Rampulla, D. M.; Bocarsly, A. B. *J. Am. Chem. Soc.*, **2008**, *130*, 6342−6344.

(26) Kamimura, S.; Murakami, N.; Tsubota, T.; Ohno, T. *Appl. Catal. B.*, **2015**, *174-175*, 471−476.

(27) Oh, Y.; Hu, X. *Chem. Soc. Rev.*, **2013**, *42*, 2253−2261.

(28) Mao, X.; Hatton, A. *Ind. Eng. Chem. Res.*, **2015**, *54*, 4033−4042.

(29) Gennaro, A.; Isse, A. A.; Saveant, J. M.; Severin, M. G.; Vianello, E. *J. Am. Chem. Soc.*, **1996**, *118*, 7190−7196.

(30) Matsuoka, S.; Kohzuki, T.; Pac, C.; Ishida, A.; Takamuku, S.; Kusaba, M.; Nakashima, N.; Yanagida, S. *J. Phys. Chem.*, **1992**, *96*, 4437−4442.

(31) Matsuoka, S.; Kohzuki, T.; Pac, C. J.; Yanagida, S. *Chem. Lett.*, **1990**, 2047−2048.

(32) Taniguchi, I.; Aurianblajeni, B.; Bockris, J. O. *J. Electroanal. Chem. Interfacial Electrochem.*, **1984**, *161*, 385−388.

(33) Boston, D. J.; Xu, C.; Armstrong, D. W.; Macdonnell, F. M. *J. Am. Chem. Soc.*, **2013**, *135*, 16252−16255.

(34) Cole-Barton, E.; Lakkaraju, P. S.; Rampulla, D. M.; Morris, A. J.; Abelev, E.; Bocarsly, A. B. *J. Am. Chem. Soc.*, **2010**, *132*, 11539−11551.

(35) Seshadri, G.; Lin, C.; Bocarsly, A. B. *J. Electroanal. Chem.*, **1994**, *372*, 145−50.

(36) Tommasi, I.; Sorrentino, F. *Tetrahedron Lett.*, **2005**, *46*, 2141−2145.

(37) Tommasi, I.; Sorrentino, F. *Tetrahedron Lett.*, **2009**, *50*, 104−107.

(38) Kayaki, Y.; Yamamoto, M.; Ikariya, T. *Angew. Chem.*, **2009**, *121*, 4258−4261.

(39) Riduan, S. N.; Zhang, Y.; Ying, J. Y. *Angew. Chem*., **2009**, *121*, 3372−3375.

(40) Luca, O. R.; McCrory, C. L.; Dalleska, N. F.; Koval, C. A. *J. Electrochem. Soc.,* **2015**, *162*, H473–H476.

(41) de Robillard, G.; Devillers, C. H.; Kunz, D.; Cattey, H.; Digard, E.; Andrieu, *J. Org. Lett*., **2013**, *15*, 4410−4413.

(42) Murov, S. L.; Carmichael, I.; Hug, G. L. *Handbook of Photochemistry*, Marcel Dekker Inc., New York, pp 4–53 and 269–273.

(43) Kavarnos, G. J.; Turro, N. J. *Chem. Rev*., 1986, **86**, 401–449.

(44) Bonesi, S. M.; Erra-Balsells, R. *J. Chem. Soc., Perkin Trans 2*., **2000**, 1583–1595.

(45) Guichard, V.; Poizat, O. *J. Phys. Chem*., **1989**, *93*, 4436−4441.

(46) Alkaitis, S. A.; Grätzel, M. *J. Am. Chem. Soc*., **1976**, *98*, 3549−3554.

(47) Sundararajan, C.; Falvey, D. E. *J. Org. Chem*., **2004**, *69*, 5547–5554.

(48) Sleat, R.; Mah, R. *Appl. Environ. Microb*., **1984**, *47*, 884−885.

(49) Feroci, M.; Orsini, M.; Rossi, L.; Sotgiu, G.; Inesi, A. *J. Org. Chem*., **2007**, *72*, 200−203.

(50) Barrosse-Antle, L. E.; Compton, R. G. *Chem. Commun*., **2009**, 3744−3746.

(51) Martindale, B. C. M.; Compton, R. G. *Chem. Commun*., **2012**, *48*, 6487−6489.

(52) Skarpeli-Liati, M.; Pati, S. G.; Bolotin, J.; Eustis, S. N.; Hofstetter, T. B. *Environ. Sci. Technol*., **2012**, *46*, 7189−7198.

(53) Vernois, M.; Friedmann, G.; Brini, M.; Federlin, P. *Bull. Soc. Chim. Fr*., **1973**, *5*, 1793−1796.

(54) Zhang, X.; Yeh, S.; Hong, S.; Freccero, M.; Albini, A.; Falvey, D.E.; Mariano, P. S. *J. Am. Chem. Soc.,* **1994**, *116*, 4211−4220.

(55) Luo, Y. *Tabulated BDE's of C-H Bonds: Handbook of Bond Dissociation Energies in Organic Compounds*; CRC Press: Boca Raton, FL, 2003.

(56) Flyunt, R.; Schuchmann, M. N.; Sonntag, C. V. *Chem. Eur. J*., 2001, *7*, 796−799.

Chapter 6.

(1) Ringshaw, D. J.; Smith, H. J. *J. Chem. Soc*. **1964**, 1559−1562.

(2) Flamigni, L.; Barbieri, A.; Sabatini, C.; Ventura, B.; Barigelletti, F. *Top. Curr. Chem.,* **2007**, *281*, 143–203.

(3) Holbrey, J. D.; Reichert, W. M.; Tkatchenko, I.; Bouajila, E.; Walter, O.; Tommasi, I.; Rogers, R. D. *Chem. Commun.,* **2003**, 28–29.

(4) Murov, S. L.; Carmichael, I.; Hug, G. L. *Handbook of Photochemistry*, Marcel Dekker Inc., New York, pp 4–53 and 269–273.

(5) Kavarnos, G. J.; N. J. Turro, N. J. *Chem. Rev*., **1986**, *86*, 401–449.

(6) Bonesi, S. M.; Erra-Balsells, R. *J. Chem. Soc., Perkin Trans 2.*, **2000**, 1583–1595.

(7) Rundlöf, T.; Mathiasson, M.; Bekiroglu, S.; Hakkarainen, B.; Bowden, T.; Arvidsson, T. *J. Pharm. Biomed. Anal.*, **2010**, *52*, 645–651.

(8) Sundararajan, C.; Falvey, D. E. *J. Org. Chem*., **2004**, *69*, 5547–5554.

(9) Gaussian 09, Revision D.01, Frisch, M. J.; Trucks, G. W.; Schlegel, H. B.; Scuseria, G. E.; Robb, M. A.; Cheeseman, J. R.; Scalmani, G.; Barone, V.; Mennucci, B.; Petersson, G. A.; Nakatsuji, H.; Caricato, M.; Li, X.; Hratchian, H. P.; Izmaylov, A. F.; Bloino, J.; Zheng, G.; Sonnenberg, J. L.; Hada, M.; Ehara, M.; Toyota, K.; Fukuda, R.; Hasegawa, J.; Ishida, M.; Nakajima, T.; Honda, Y.; Kitao, O.; Nakai, H.; Vreven, T.; Montgomery, J. A., Jr.; Peralta, J. E.; Ogliaro, F.; Bearpark, M.; Heyd, J. J.; Brothers, E.; Kudin, K. N.; Staroverov, V. N.; Kobayashi, R.; Normand, J.; Raghavachari, K.; Rendell, A.; Burant, J. C.; Iyengar, S. S.; Tomasi, J.; Cossi, M.; Rega, N.; Millam, N. J.; Klene, M.; Knox, J. E.; Cross, J. B.; Bakken, V.; Adamo, C.; Jaramillo, J.; Gomperts, R.; Stratmann, R. E.; Yazyev, O.; Austin, A. J.; Cammi, R.; Pomelli, C.; Ochterski, J. W.; Martin, R. L.; Morokuma, K.; Zakrzewski, V. G.; Voth, G. A.; Salvador, P.; Dannenberg, J. J.; Dapprich, S.; Daniels, A. D.; Farkas, Ö.; Foresman, J. B.; Ortiz, J. V.; Cioslowski, J.; Fox, D. J. Gaussian, Inc., Wallingford, CT, 2009.